2012

# Impact of Design Parameters on Detached-Die Tapered Resin Injection Pultrusion

Sudip Ranjit

# IMPACT OF DESIGN PARAMETERS ON DETACHED-DIE TAPERED RESIN INJECTION PULTRUSION

**A Thesis**

**Submitted to the Graduate School**

**in partial fulfillment of the requirements for the**

**Degree of Master of Science in Engineering Science**

**The University of Mississippi**

**SUDIP RANJIT**

**July, 2012**

## ABSTRACT

Injection pultrusion is an efficient process for manufacturing composites of continuous lengths with constant cross-section area. The main objective of this study is to compare the performances of the detached-die with the attached-die resin injection chamber configurations. In this work the impact of various geometric design parameters (the length of the injection chamber, slot width, multiple injection slot locations, and part thickness) on the performances and complete wetout of the composite parts for both the attached-die and detached-die configurations is investigated with various chamber lengths and compression ratios. A 3-D finite volume technique is employed to simulate the liquid resin flow through the fiber reinforcement and to predict the liquid resin flow front. A minimum injection pressure for a complete wetout of the composite parts in both the attached-die and detached-die configuration is determined along with the associated maximum interior chamber wall pressure. Feasible manufacturing solutions are determined from the results. The detached-die resin injection configuration was always better than attached-die configuration. Shorter injection chamber lengths at higher compression ratios were found to yield better performance and more feasible manufacturing solutions.

## ACKNOWLEDGEMENTS

I express my hearty thanks to my advisor Dr. Jeffrey A. Roux, who has guided me throughout my study and thesis and helped me to accomplish my Master's degree.

It is my pleasure to thank my friends Mr. Dinesh Raj Palikhel and Neerad Shakya for their help and support throughout this work. I would like to express my sincere gratitude to Dr Arunachalam M. Rajendran, Head of Department of Mechanical Engineering for his support. I would like to thank committee members, Dr. Jagadish P.Sharma, and Dr. Ajit Sadana for their help. Lastly, I would also thank The University of Mississippi for financial support for my Master's degree.

## TABLE OF CONTENTS

## LIST OF FIGURES

## LIST OF TABLES

## NOMENCLATURE

| | |
|---|---|
| $x$……. | Axial coordinate, in the longitudinal direction of fiber, m |
| $y$……. | Vertical coordinate, in the transverse (height) direction of fiber, m |
| $z$……. | Coordinate along the width dimension of fiber, m |
| $x_{IS}$…….. | Injection slot location |
| $L_{IC}$……. | Tapered length, m (Fig. 2-3) |
| $L_D$…….. | Exit length, m (Fig. 2-3) |
| $L_T$…….. | Total length, m (Fig. 2-3) |
| $K_{11}$……. | Permeability in $x$ (axial direction), $m^2$ |
| $K_{22}$……. | Permeability in $y$ (transverse), $m^2$ |
| $K_{33}$……. | Permeability in $z$ (transverse), $m^2$ |
| $P$…… | Pressure, Pa |
| $\varphi$…… | Porosity |
| $U$……... | Fiber velocity in $x$ (axial) direction, m/s |
| $V$……... | Fiber velocity in $y$ (transverse) direction, m/s |
| $u$…… | Resin velocity in $x$ (axial) direction, m/s |
| $v$…… | Resin velocity in $y$ (transverse) direction, m/s |
| $w$……... | Resin velocity in $z$ (transverse) direction, m/s |
| $\mu$..... | Viscosity of liquid resin, Pa•S |
| $V_{f0}$……. | Fiber volume fraction of the finished product |

$V_f$……... Local fiber volume fraction, $V_f(x)$

$\rho$…… Density of the liquid resin, kg/m$^3$

$F_{i,j,k}$..... Fill factor for a specific control volume

# CHAPTER 1

# INTRODUCTION

## *1.1 Composite Materials*

Composite materials are materials made by combining two or more materials to give better mechanical properties than the properties of the individual constituent materials. However, the constituents retain their characteristics. Generally, most composites are comprised of fibers in a matrix resin (polymeric composite). The fiber reinforcement provides strength and stiffness, while the resin acts as a binder. Resin may be of thermosetting or thermoplastic types.

Composites have many advantages, such as high strength, high stiffness, high fatigue strength, corrosion resistance and lightweight as compared with metals, ceramics and polymers. Composites have design flexibility, the part count can be significantly reduced eliminating joints, and reduced manufacturing cost and time. So, composites have many applications such as structural, civil, mechanical, thermal, electrochemical, electronic, environmental and biomedical applications. Automotive and aviation industry are the major users of composites because of composites having lighter weight, high specific strength and high stiffness.

There are many methods to manufacture composites; they are extrusion, open molding, vacuum bag molding, pressure bag molding, autoclave molding, resin transfer molding (RTM), thermoplastic molding, structural reaction molding (SRIM), press molding, compression molding, transfer molding, filament winding, casting and pultrusion. Selection of a manufacturing process depends on the application needs and requirements. By choosing an

appropriate combination of reinforcement and matrix material, manufacturers can produce properties that closely fit the requirements of a particular structure for a particular purpose using a particular method.

### *1.2 Pultrusion Process*

Pultrusion manufacturing is a composite manufacturing method used to manufacture fiber-reinforced polymeric composite materials with a constant cross section shaped profile. The pultrusion process consists of pulling/drawing continuous reinforcements through a resin impregnation system. The reinforcement is commonly fiberglass and a common resin is polyester resin. Epoxy resin and vinyl esters are also used for higher temperature and corrosion applications.

A pultrusion machine (Fig. 1-1) consists of the following components: creel, forming plates, resin wetout station or impregnator, heated metal die, puller or pulling mechanism, and cutoff saw. A number of continuous rovings and/or mats from a creel are pulled through the preform plates to the resin impregnator; plates align the fiber reinforcement. After the fiber is impregnated with resin, it is pulled through a performing fixture where excess resin and trapped air are removed. The coated fiber is then passed through a heated die and cured to produce the desired final part. After curing, the profile laminate is finally cut to the desired length with a cut-off saw. Various selections of solid and hollow profiles can be pultruded, and the process can be customized to fit specific applications. According to the method of impregnation to achieve fiber reinforcement wetout, pultrusion process can be divided into two categories: open bath pultrusion (Fig. 1-1) and resin injection (Fig. 1-2).

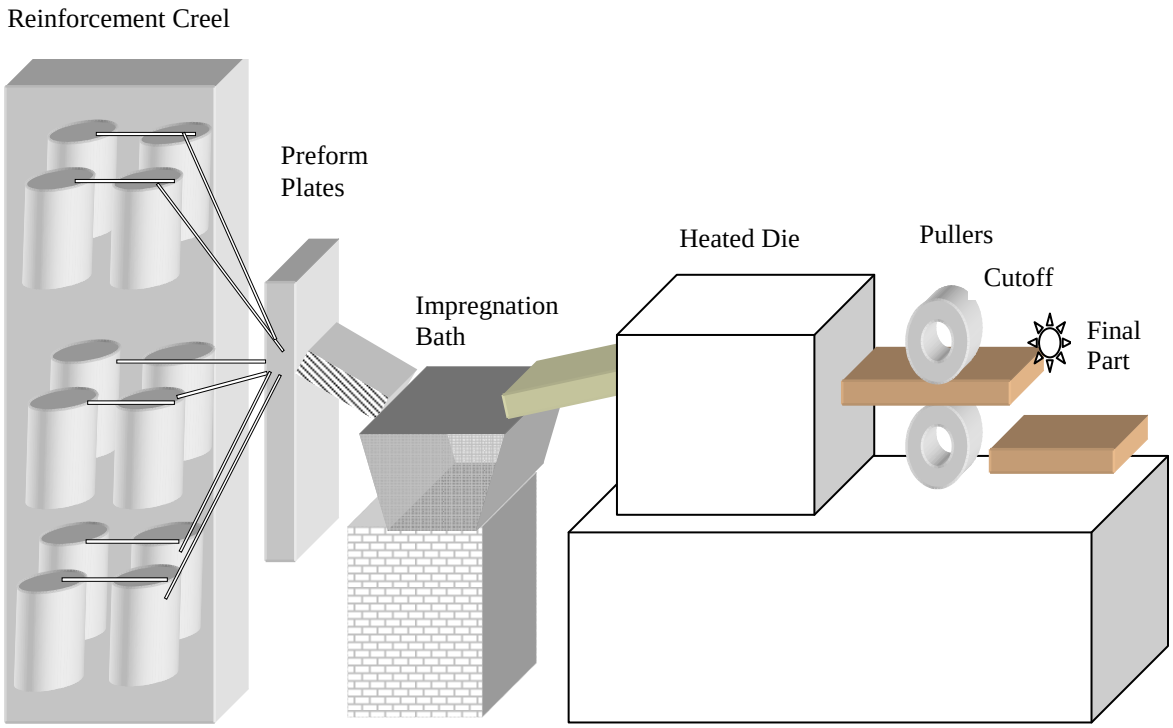


**Fig. 1-1. Schematic of Open Bath Pultrusion.**

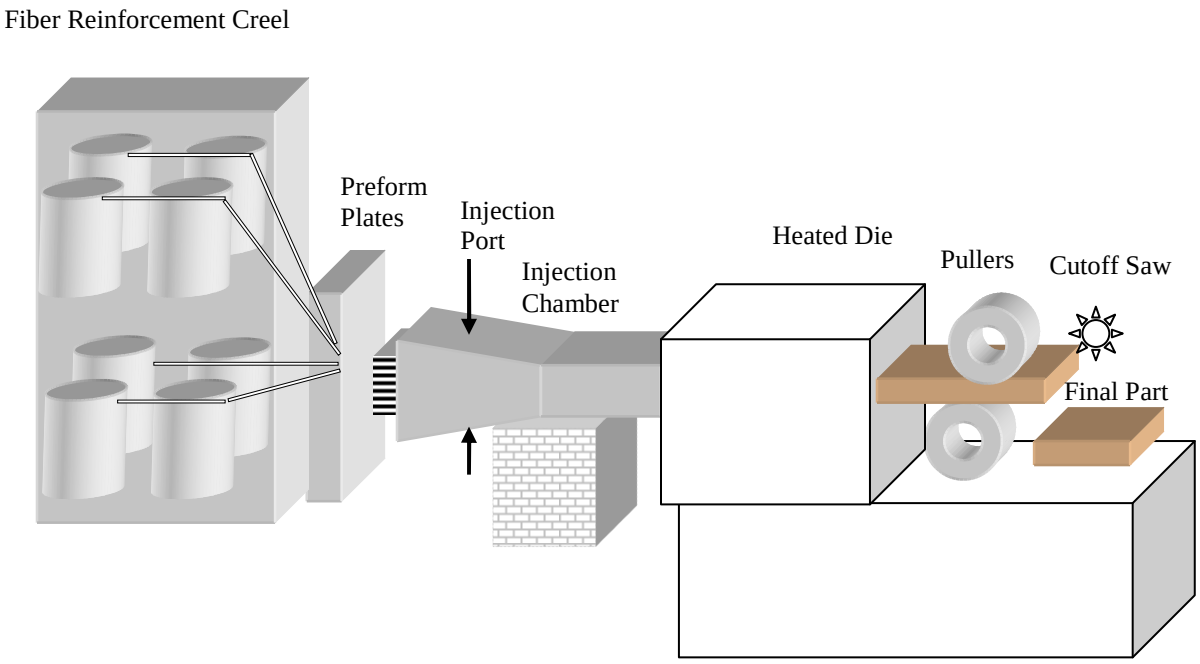


**Fig. 1-2. Schematic of Resin Injection Pultrusion (Attached-Die Configuration).**

Open bath pultrusion is a conventional pultrusion process in which wetout of fiber reinforcement is achieved by immerging it into the liquid resin which then adheres to the fiber reinforcement as the fibers are pulled through wetout resin bath. This process is quite simple and inexpensive but resins with very high or very low viscosities can be difficult to use because impregnation resin may not adhere properly to the surface of the fiber. Since the wetout tank is opened to the environment, workers may be potentially harmed by the emissions of volatile organic compounds (VOC) to the surroundings.

Resin injection or closed bath pultrusion is a modification of the resin impregnation process in which the fiber reinforcement is pulled through an injection chamber where the resin is injected under pressure through top and/or bottom injection ports in order to achieve complete wetout of the fiber reinforcement. Then un-cured, the wetted fiber is passed through the heated die, where the resin undergoes polymerization. Closed bath pultrusion has many advantages compared to the open bath pultrusion. It is a highly automated and efficient continuous process, an efficient process for high-quality, low-cost, high-volume manufacturing of fiber reinforced composites such as beams rod stocks, channels, and tubing. Since it is closed bath the emission of volatile resin components is either reduced greatly or eliminated.

### *1.3 Previous Work*

Significant research work has been done on experimental and numerical analysis of the injected pultrusion process by researchers at the University of Mississippi [1, 2, 3, 4, 5, 6], Washington University [7, 8], University of Minnesota [9] and Ohio State University [10, 11]. Table 1.1 summarizes and compares the important work done by these researchers and the scope of the present work.

Rahetekar and Roux [3] developed a 2-D finite volume method to predict resin pressure field, resin velocity field and resin moving flow front location. They modeled and analyzed the slot injection port system developed from the 2-D model. The study was focused on the effect of pull speed, fiber volume fraction, resin viscosity and compression ratio of the injection chamber on composites. The injection pressure, location of the liquid resin flow front were predicted for a wide variety of process variables to achieve complete wetout.

Jeswani and Roux [4] developed a numerical model that incorporates resin injection slots as well as discrete resin injection ports to identify the sensitivity and range of design parameters for manufacturing of polyester resin/glass roving composites associated with high pull speeds to achieve high product yield. They also explored a variety of geometrical design parameters for the pultrusion process like composite thickness, injection slot width, injection slot location and location of multiple injection ports. They suggested that for the high pull speed resin injection pultrusion manufacturing of a polyester/glass roving composite, the slot injection configuration is favorable to the discrete port configuration. They studied two injection chamber configurations (a) attached-die and (b) detached-die. The attached-die configuration means the resin injection chamber is rigidly attached to the entrance of the heated die. The detached-die configuration means there is a gap between the resin injection chamber exit and the entrance of the heated die; this gap acts as a pressure release mechanism to release mechanism to realize the resin pressure which builds up within the resin injection chamber. Their study corresponded to an injection chamber length of 0.30 m; their work [4] did not consider the impact of the injection chamber length as an important geometric parameter.

Ranga [5] used 3-D finite volume technique to simulate the resin flow through the fiber reinforcement in the injection pultrusion process. He considered an attached die configuration

and modeled the impact of the tapering of the walls of the injection chamber on the minimum injection pressure necessary to achieve complete wetout by varying the length of the injection chamber and the processing parameters. His work showed that high compression ratios and short injection chamber lengths were desirable to achieve complete wetout at reasonable resin injection pressures with reasonable injection chamber interior pressures, and with high pull speeds, high resin viscosity, and high fiber volume fractions.

Li et. al. [10, 11] built a device to measure the friction coefficient of fibers impregnated with liquid and partially cured resin. They suggested that the friction coefficient varies with respect to the temperature and has less impact on resin conversion when the temperature is high. They also suggested that the dies can be made longer without causing a significant increase in the pulling force. They concluded that the viscous drag force in the injection die is much smaller than the compaction force and the friction force; hence it may be neglected in modeling the resistance force in the injection die. They conducted experimental and theoretical analysis of pulling force in resin injection pultrusion process with a tapered injection chamber, but they did not show chamber resin pressure results with respect to the change in the length of injection chamber.

Srinivasagupta et. al. [7, 8] developed an integrated procedure for a model-based economic design of the injected pultrusion process with controllability, economic, environmental and quality considerations. Likewise, they provided a brief description of the 3D-mathematical model of the resin injected pultrusion process for their bench scale process unit. They were able to determine favorable values of the processing conditions and parameters like heating zone temperatures, resin injection pressure, and temperature as well as equipment design

specifications. They also compared the process model predictions with the experimental data to the dynamic simulation model.

Mustafa, Khomami, Kardos, and Kommu [12, 13] developed a 3-D flow simulation model for injected pultrusion process to determine the effect of fiber pull speed, reinforcement anisotropy, and taper of the die on the product quality of the product. They showed that with the aid of the simulation model the die geometry (die length, location of the injection port, shape of the injection section) can be designed and optimize the operating conditions (injection pressure, fiber pull speed, wall temperature). Though they considered high taper angles in the injection chamber, they considered no source terms in the pressure equation due to the injection chamber tapered walls or considered the impact of chamber length.

Liu [14, 15] developed a finite element/nodal volume technique to simulate the resin flow through the fiber reinforcement during the injection pultrusion processes. He developed transient and iterative methods to predict the steady-state flow fronts for one-, two-, and three-dimensional problems and numerical performance from these models was investigated for pull speed, injection pressure and variation of permeability. He suggested that the iterative model is more efficient than the transient model, using generally less than one-tenth of the computer time required by the transient model to reach the converged steady-state solutions. He also suggested that constant injection pressure employed should be significantly larger than that required to maintain the quasi-steady-state for the good flow pattern in injection pultrusion process. He considered a non-tapered resin injection chamber.

Mitlapalli and Roux [6] employed a 3-D finite volume technique to simulate the liquid resin flow through the fiber reinforcement and to predict the liquid resin flow front. Their work dealt with the impact of design parameters, tapering of the walls, and the injection chamber

length on minimum injection pressure required to achieve complete wet out and associated chamber interior pressure. The design parameters analyzed were: location of the injection slots, slot width, part thickness and the multiple injection slots. They demonstrated that tapering of the injection chamber wall and injection chamber length have significant effects on minimum injection pressure as well as the associated chamber interior pressure. They suggested shorter injection chamber lengths with more tapering of the wall for safe minimum injection pressures and associated exit pressure to operate industrial pultrusion manufacturing process. Their work was for an attached-die resin injection chamber configuration.

None of the above works considered the impact of resin injection chamber length on pultrusion manufacturing for various geometric design parameters for a detached-die configuration.

### *1.4 Present Work*

The main objective of the present work is to investigate the minimum resin injection pressure needed to achieve wetout for both an attached-die and a detached-die resin injection chamber configuration. The study also focuses on determining the corresponding maximum resin injection chamber interior pressure, to predict the liquid resin flow front location for different design parameters such as: location of the single injection slot, width of the injection slot, location of multiple injection slots and composites thickness in a resin injection pultrusion process for different taper angles (compression ratios) and chamber lengths. Results will compare the performances of “attached-die” and “detached-die” resin injection chamber configurations. The overall objective is to determine the tapered injection chamber length where the overall performance of the pultrusion process is most favorable.

Various numerical laws and models are used to create 3-D numerical modeling of the injection pultrusion process. Here the resin is considered as an incompressible fluid propagating through a porous medium. Hence, Darcy's law [16] of flow through porous media is used to stimulate resin flow through a fiber matrix. The Gutowski model [17] is employed to predict the permeability of the fiber matrix. The governing pressure equation is obtained by substituting the equations from Darcy's law into the continuity equation. The governing pressure equation is then discretized, and the pressure field is determined by using the line-by-line TDMA (Tridiagonal Matrix Algorithm) solution technique. Then the velocity field is obtained by finite differentiation of Darcy's equations. The main emphasis of the present work is to investigate various geometric design parameters for different tapered injection chamber "lengths" to obtain the minimum resin injection pressures to achieve complete reinforcement wetout along with reasonable interior injection chamber resin pressures for both the attached and the detached die configurations. Hence favorable manufacturing conditions are determined corresponding to minimum injection pressure and reduce chamber wall interior pressure. Table 1.1 compares the key features of the present work compared with the previous studies of the other researchers. This work is unique since it describes how the design parameters are affected with the change in the injection chamber length for various taper angles (compression ratios); none of the previous works [2-15] addressed the conditions and geometric parameters considered in thi study. Next, Chapter 2 contains a detailed physical statement of problem for the present study.

**Table 1.1 Comparisons of Previous Works and Present Work**

| **Researches** | | **[3]** | **[5]** | **[6]** | **[7, 8]** | **[12, 13]** | **[14, 15]** | **Ranjit (Present Work)** |
|---|---|---|---|---|---|---|---|---|
| **Model** | | 3D | 3D | 3D | 3D | 2D/3D | 3D | 3D |
| **Numerical Method** | | FVM | FVM | FVM | FE/CV | FE/CV | FE/NV | FVM |
| **Permeability Model** | A* | Yes | Yes | Yes | No | Yes | No | Yes |
| | D* | Yes | No | No | No | No | No | Yes |
| **Multiple Injection Port/Slot** | A* | Yes | Yes | Yes | No | No | Yes | Yes |
| | D* | Yes | No | No | No | No | No | Yes |
| **Fiber Pull Speed Variation** | A* | Yes | Yes | Yes | Yes | Yes | No | Yes |
| | D* | Yes | Yes | No | No | No | No | Yes |
| **Taper Allowed in Injection Chamber** | A* | Yes | Yes | Yes | Yes | Yes | No | Yes |
| | D* | Yes | No | No | No | No | No | Yes |
| **Injection Chamber Length Variation** | A* | No | Yes | Yes | No | No | No | Yes |
| | D* | No | No | No | No | No | No | Yes |

A* = Attached

B* = Detachhed

# CHAPTER 2
# STATEMENT OF THE PROBLEM

## *2.1 Definition of the Problem*

The main objective of the present work is to investigate and compare the minimum resin injection pressure needed to achieve complete wetout and the associated interior chamber pressure for both an attached-die and a detached-die resin injection chamber configurations. The present work explores the impact of different injection chamber taper angles (compression ratios) and chamber lengths on fiber wetout, minimum resin injection pressure, corresponding maximum resin injection chamber interior pressure and resin flow front profile for various geometric design parameters such as: location of the single injection slot, width of the injection slot, location of multiple injection slots and composite thickness in a resin injection pultrusion process. Nominal values are considered for the processing parameters of pull speed, fiber volume fraction and resin viscosity. The overall objective is to compare the performances of "attached-die" and "detached-die" resin injection chamber configurations.

Complete wetout of the fibers is an important aspect in the resin injection pultrusion process because composites properties depend upon complete wetout being achieved before curing begins during the pultrusion process. Complete wetout is essential for the manufacture of good quality composites with good mechanical and chemical properties. Complete wetout can be achieved by selecting proper design parameters and processing parameters. For the injection pressure to achieve complete wetout to be favorable and applicable, it must be within the resin pressure limits of reasonable manufacturing conditions.

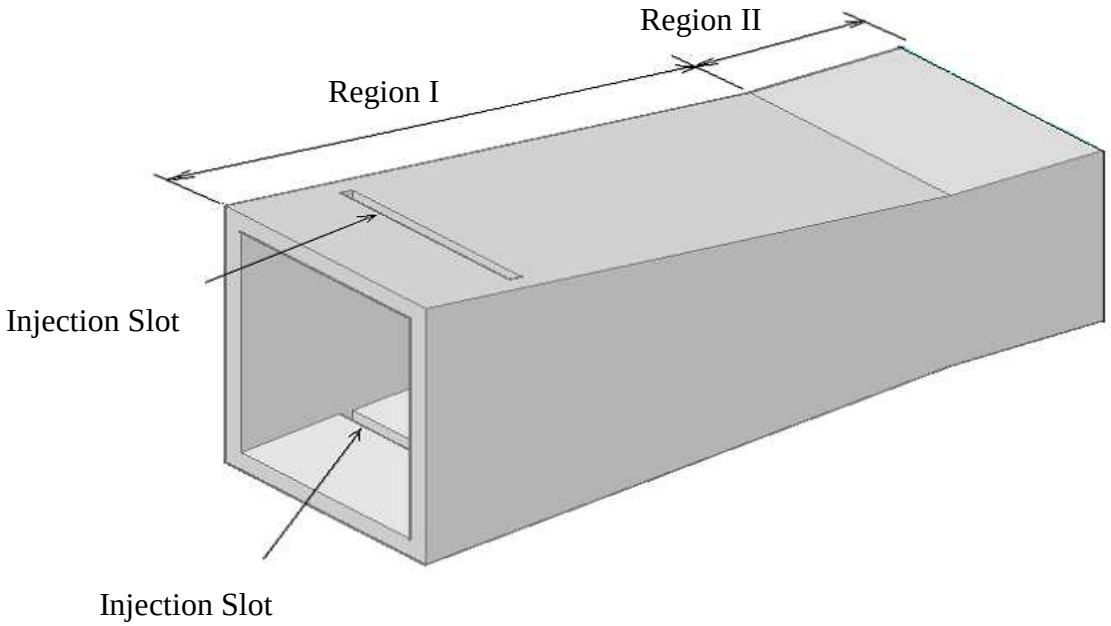


**(a) Attached-Die Configuration.**

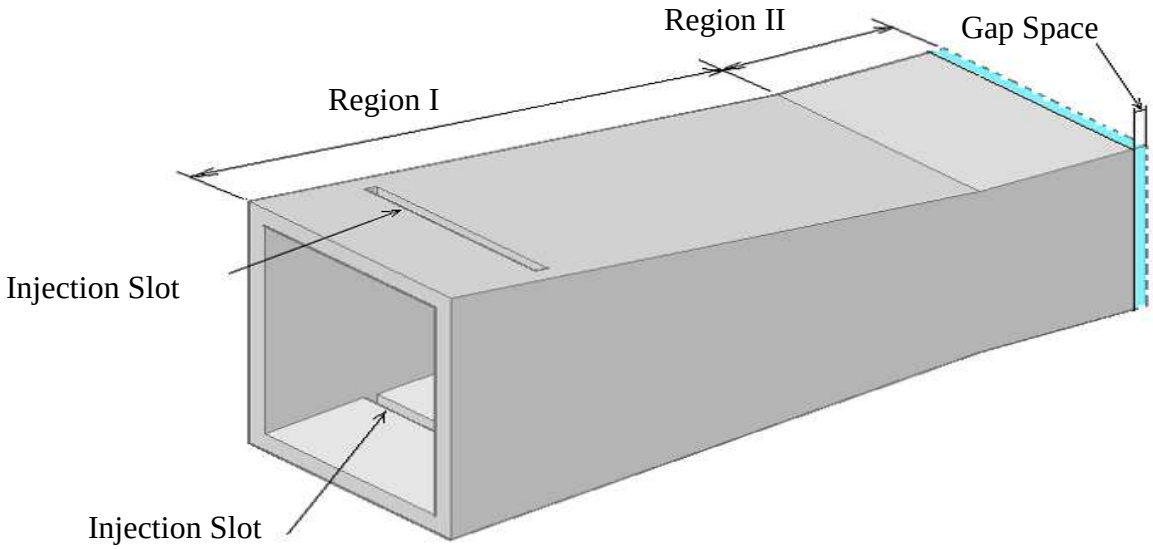


**(b) Detached-Die Configuration.**

**Figure 2-1. Physical Description of Tapered Injection Chamber.**

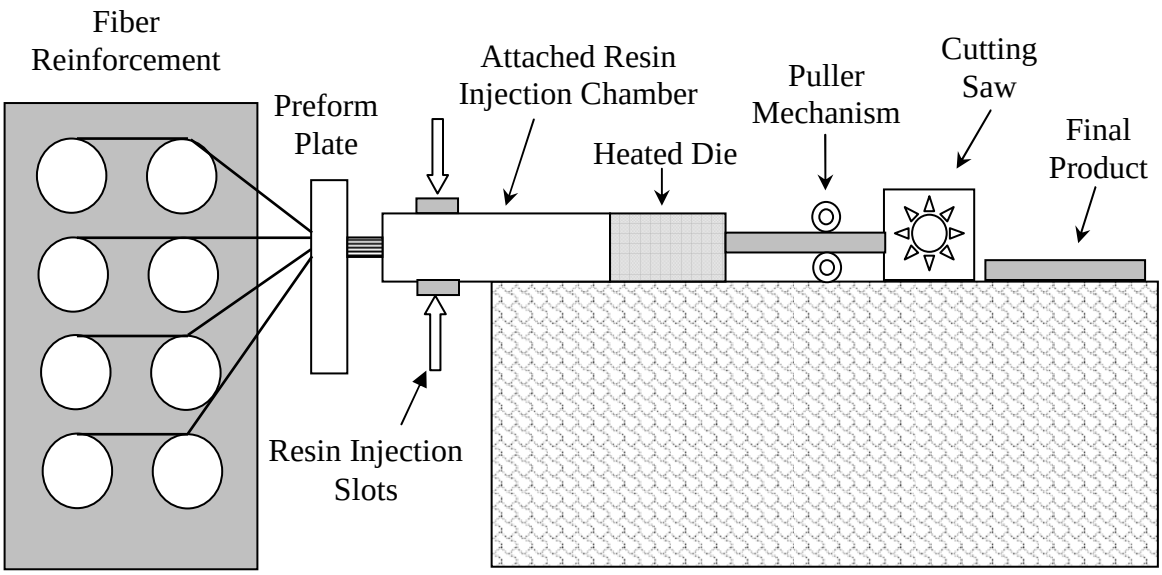


**(a) Attached-Die Configuration.**

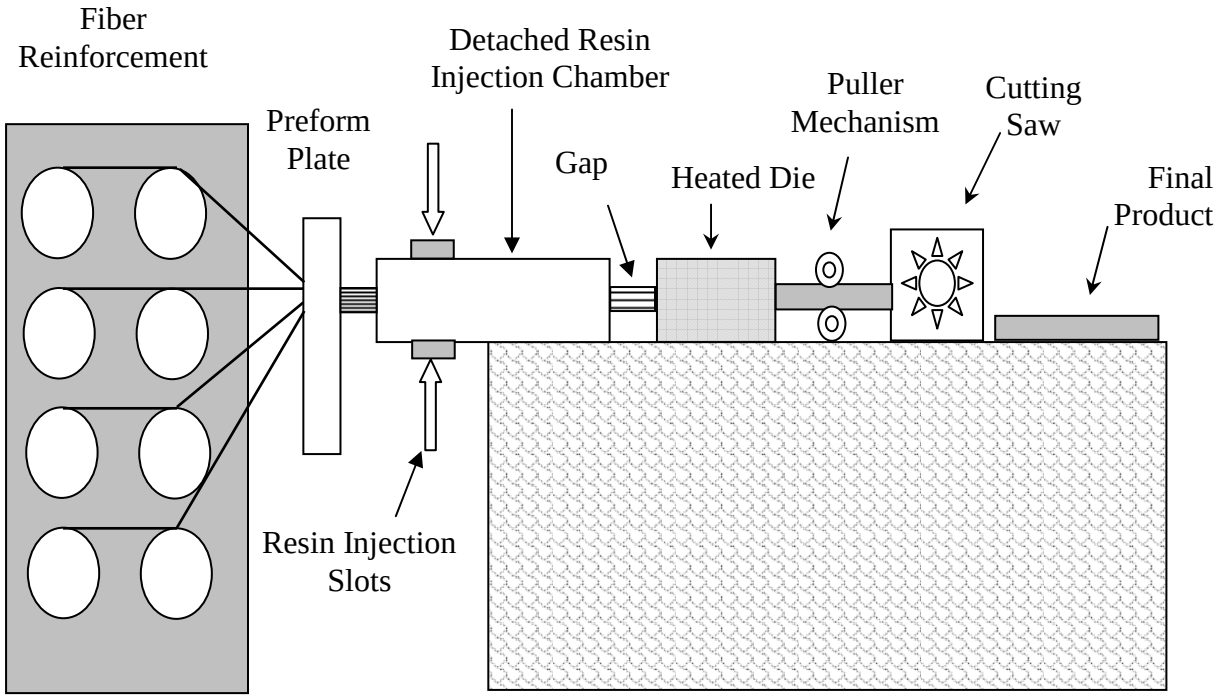


**(b) Detached-Die Configuration.**

**Fig. 2-2. Schematic of Resin Injection Pultrusion Process.**

This work focuses on the impact of the geometric design parameters on the pultrusion process for different tapered lengths ($L_{IC}$) of the injection chamber for both an attached-die and a detached-die configurations shown in the Fig. 2-1 and Fig. 2-2. As the fiber reinforcement is passed through the tapered injection chamber it is impregnated with resin and then compressed which results in a change in the fiber volume fraction and the permeabilities and the pressure fields of the fiber matrix as it progresses along the chamber longitudinal ($x$) direction. Hence, the length ($L_{IC}$) of the tapered injection chamber has a significant effect on the wetout process. In the attached-die configuration there is no gap between the injection chamber and the heated die inlet, but in the detached-die configuration there is a small gap set between the injection chamber and the heated die inlet. This gap in the detached-die configuration acts as a pressure release mechanism as the fiber/resin system is subjected to atmospheric pressure at the exit of the injection chamber.

### *2.2 Description of the Injection Chamber*

The regions and geometry of the resin injection chamber are shown in Fig. 2-1 and Fig. 2-2. The injection chamber is divided into two regions; Region I and Region II. In Region I, the injection chamber walls are tapered along the longitudinal ($x$) direction while Region II is of constant cross section (non-tapered). Injection slots on the top and on the bottom in pairs are located in Region I proportional to the length ($L_{IC}$) of the tapered region of the injection chamber as measured from the injection chamber front face. Fiber reinforcement enters into Region I; resin is injected through these dual injection slots into the fiber reinforcement with the help of a feed pump. As it passes along Region I the fiber/resin system is compressed since the walls are tapered in the Region I. Hence, there is change in the local fiber volume fraction and

permeabilities as the wetted fibers move along the longitudinal ($x$) direction. Location of the injection slot also has an effect on the injection pressure needed to achieve complete wetout, as well as the maximum interior pressure within the injection chamber. If the slot is located near the inlet of injection chamber, then the interior chamber pressure may be high which is undesirable. Multiple longitudinal slots may be used for obtaining good wetout with a reduction in injection pressure.

In this study, the total lengths of injection chambers ($L_T$) considered are 0.15 m, 0.20 m and 0.30 m. The effect of geometric design parameters on the resin injection pultrusion process is explored by varying the tapered length ($L_{IC}$), Region I, of the injection chamber for an attached and a detached die configuration, while Region II is set to a constant length of 0.05 m. In the attached die configuration the resin injection chamber is attached to the heated pultrusion die as shown in the Fig. 2-2 (a). In the detached die configuration there is gap of length 0.005 m between the Region II exit and the heated die entrance as shown in Fig. 2-2 (b). Jeswani [4] showed that due to the detached configuration gap at the exit of the injection chamber, the fiber/resin system is subjected to atmospheric pressure so that the pressure developed internally within the injection chamber is somewhat released (reduced) as compared to the attached die configuration.

### *2.3 Computational Domain*

The schematic computational domain of the tapered resin injection chamber for an attached and a detached die configuration is shown in Fig. 2-3 and Fig. 2-4. The domain is divided into two regions Region I and Region II. The walls of the injection chamber in the Region I are tapered, whereas the cross-sectional area of Region II is constant (non-tapered).

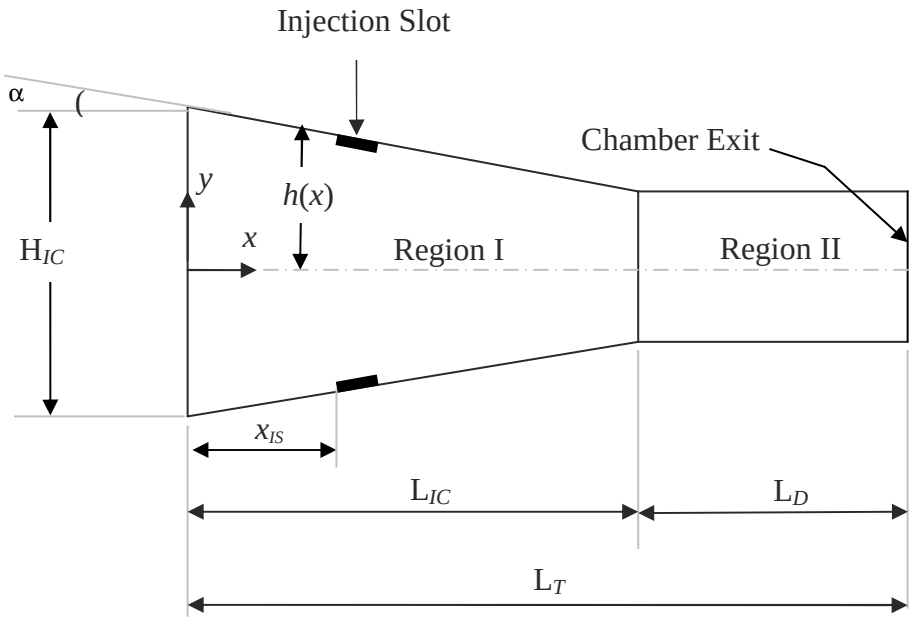


**a) In *xy* Plane (Side View).**

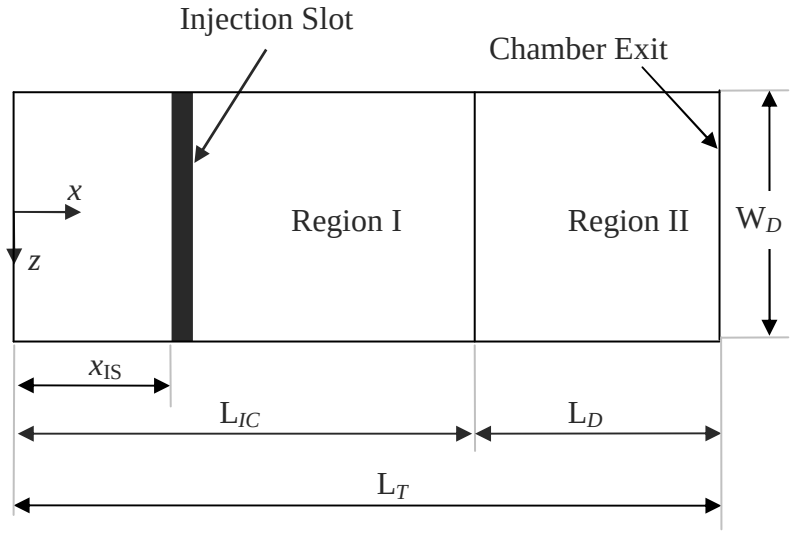


**b) In *xz* Plane (Top View).**

**Fig. 2-3. Sketch of the Computational Domain for the Attached-Die Injection Chamber (Not to Scale).**

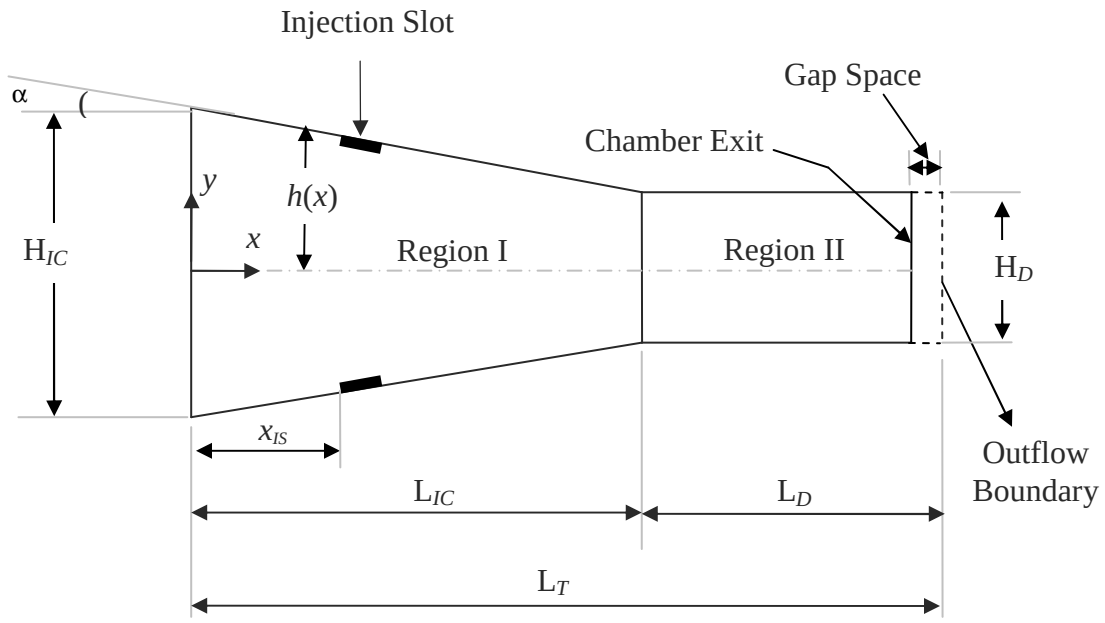


**a) In *xy* Plane (Side View).**

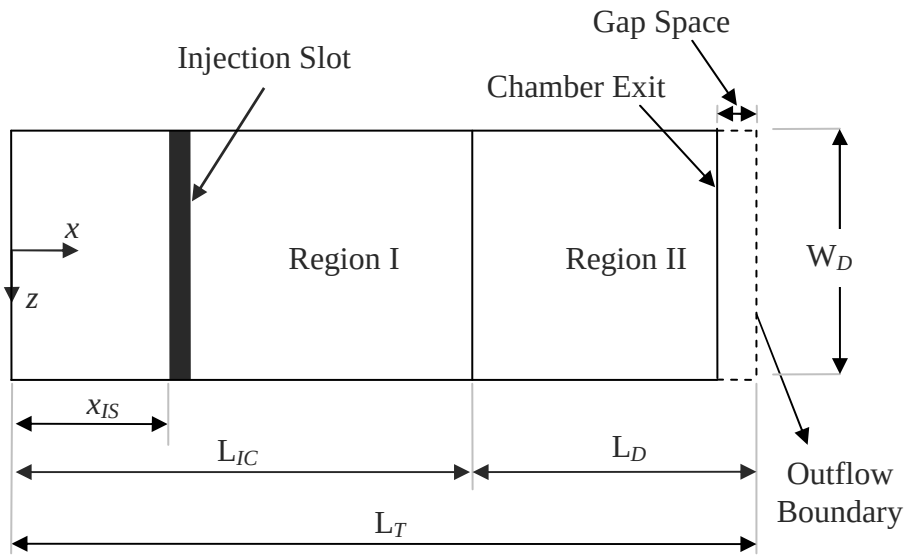


**b) In *xz* Plane (Top View).**

**Fig. 2-4. Sketch of the Computational Domain for the Detached Die Injection Chamber (Not to Scale).**

Figures 2-3 and 2-4 illustrate the top view and the side view of the tapered injection chamber, axes of the domain, height and width of the front and outflow boundaries, injection slot location ($x_{IS}$) and the lengths of Region I ($L_{IC}$) and Region II ($L_D$) considered for the analysis. $H_{IC}$ represents the height of the injection chamber at the inlet of Region I, whereas $H_D$ is the height of the injection chamber in Region II. $W_D$ represents the width of the composite. Hence $H_D$ and $W_D$ represent the thickness and width of the final composite. The walls of the injection chamber are tapered by angle α in Region I as shown in the Fig. 2-3 (a) and Fig. 2-4 (a). A slight change in the taper of the injection chamber may result in a significant impact on the minimum resin injection pressure required to achieve complete wetout and also on the resin injection chamber interior pressure. A gap space of 0.005 m at the end of Region II of the computational domain between the resin chamber exit and the heated die entrance is shown in Fig. 2-4. Compression ratio, CR, is defined as the ratio of the height of the injection chamber at the front boundary in Region I to the height of the injection chamber at the outflow boundary in Region II; CR is defined mathematically as

$$CR = H_{IC}/H_D \tag{2.1}$$

When $H_{IC}$ and $H_D$ are equal then the CR is equal to 1 which is a non-tapered injection chamber. Since tapered injection chambers are considered for this study, $H_{IC}$ is greater than $H_D$, and hence the value of CR is greater than 1 which means that the top and bottom walls of the injection chamber are tapered by a small angle ($\alpha > 0$) which can be calculated from the following equation

$$\tan\alpha = \frac{H_D}{2L_{IC}}[CR - 1] \tag{2.2}$$

The values for CR chosen for this study are 2.0, 3.0 and 4.0, whereas the values for the tapered lengths ($L_{IC}$) of the injection chamber for Region I are 0.10 m, 0.15 m and 0.25 m and with the length of Region II ($L_D$) of 0.05 m. From Eq. (2.2) the taper angle (α) varies with a change in CR as well as the tapered length ($L_{IC}$) of the injection chamber and the thickness ($H_D$) of the composite as shown via Eq. (2.2) in Table 2-1. The sketch of different lengths of tapered injection chamber and CR's are shown in the Fig. 2-5.

**Table 2-1. Taper Angles (α)* in Degree for different CR and $L_T$ with $H_D$ = 0.003175 m Considered for the Computational Domain.**

| Length ($L_T$) / CR | 0.15 m | 0.20 m | 0.30 m |
|---|---|---|---|
| **2** | 0.607˚ | 0.455˚ | 0.303˚ |
| **3** | 1.214˚ | 0.911˚ | 0.607˚ |
| **4** | 1.821˚ | 1.366˚ | 0.911˚ |

* α is given in degrees (˚)

### *2.4 Features of Numerical Model*

The Finite Volume Method (FVM) is a discretization method for the approximation of a system of partial differential equation expressing a conservation principle. This method is used in the numerical model to compute the pressure field, the flow field, and the location of flow front. Darcy's law [16] for flow through porous media was used to simulate the flow of liquid resin through the fiber reinforcement. The governing pressure equation is obtained by substituting the

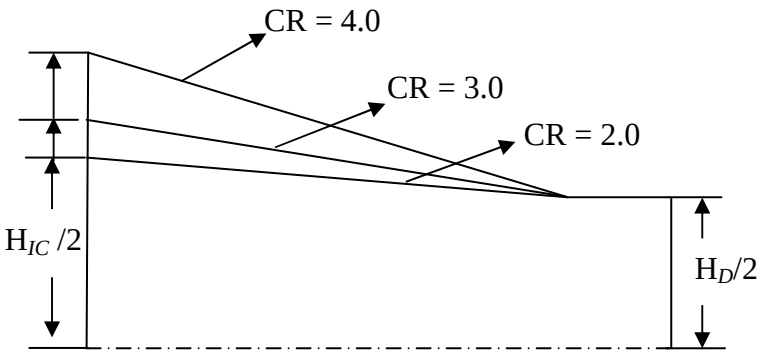


**a) Fixed $L_{IC}$ with varying CR.**

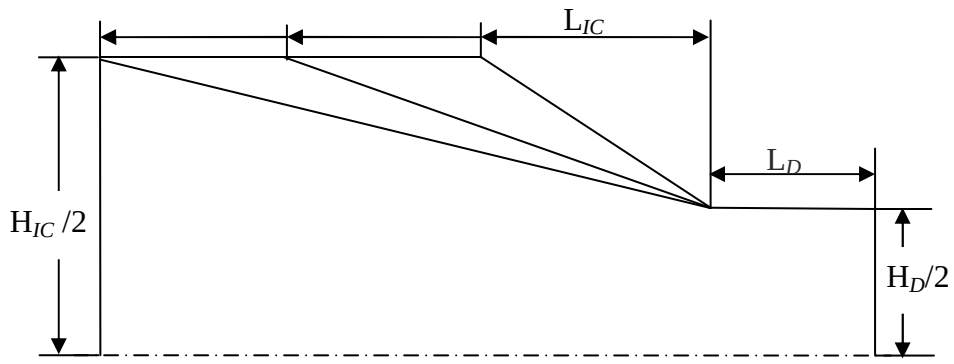


**b) Fixed CR with varying $L_{IC}$.**

**Fig. 2-5. Sketch of Different Lengths of Tapered Injection Chamber and Different CR's (Not to scale).**

Darcy momentum equations into the continuity equation. For solving the pressure equations all boundary conditions are converted into pressure boundary conditions. Then, the TDMA (Tri-Diagonal Matrix Algorithm) technique was used to solve the pressure field for the entire computational domain. The computational domain is symmetric about the centerline planes; so, only a quarter of the computational domain is modeled. This reduces the modeling time of the domain. This practice also reduces the storage space and runtime of the model by about 75%.

The features and capabilities of numerical model in this study are as follows:

- **Different fiber/resin systems:** glass or carbon fibers/polyester or epoxy resin
- **Permeability model:** Gutowski model
- **Different processing parameters:** pull speed or line speed, fiber volume fraction, and resin viscosity
- **Different geometric parameters:** location of injection slots, width of the injection slots, thickness of the final composite, and multiple injection slots and their location
- **Type of resin injection:** Dual slot (one slot on top and one slot on bottom) injection and multiple slot injection configurations
- **Type of injection chamber configuration:** attached-die and detached-die configuration

The model was developed in FORTRAN 90 language and was executed on a personal computer (Dell Optiplex GX620, Pentium 4, 3.8 GHz, 2 GB RAM). The program allows the user to choose different processing parameters, geometric parameters to study their impact on the pultrusion process. The output of the program is saved in a data file, and plotting routines are used to visualize the data. The transient solution of the program provides the location of the

liquid resin flow front at different time instances and determines the total simulated time for the flow front to reach steady state. Next, a detailed mathematical description of the governing equations is presented in Chapter 3.

# CHAPTER 3

# ANALYSIS

The simulation of the flow of liquid resin through the fiber reinforcement process in resin injection pultrusion is presented using the 3-D finite volume technique. This chapter contains presentation of the permeability model, the governing equations for two regions (Region I and Region II) of the injection chamber, the boundary conditions, the solution method and the discretization equations.

## *3.1 Assumptions*

Assumptions made for the mathematical modeling of the resin injection pultrusion process are as follows:

- The resin is an incompressible fluid.
- The flow of the fluid resin through the fiber reinforcement is simulated using Darcy's law [16] of flow through porous media.
- Since the flow of the liquid resin is basically isothermal inside the injection chamber, the resin viscosity remains constant.
- For Region I of the injection chamber, the cross-sectional area varies as a function of $x$. Therefore, the local fiber volume fraction ($V_f(x)$) and local permeabilities ($K_{11}$, $K_{22}$, *and* $K_{33}$) are functions of $x$.

- The fiber volume fraction and the permeability are constant in Region II since the cross-sectional area in this region is constant.
- The numerical model is based on the 3-D Cartesian coordinate system.
- To compute the three components of the permeability in the longitudinal and transverse directions, the Gutowski permeability model [17] is used which depicts anisotropic permeability behavior.
- Atmospheric pressure (101.325 kPa) is assumed at the inlet and exit of the detached-die injection chamber configuration.

### *3.2 Mathematical Model*

The flow of the resin through the fiber reinforcement is similar to the flow of liquid through porous medium. Therefore, Darcy's law for the flow through a porous medium is used to simulate this model. As per the Darcy's law, volumetric flow rate ($Q$) through a specimen is proportional to the cross section area ($A$), the pressure difference across the specimen ($\Delta P$) and inversely proportional to the length in the stream-wise direction of the specimen ($L$) and the viscosity ($\mu$) which is mathematically expressed as

$$Q = K \frac{A}{\mu} \frac{\Delta P}{L} \tag{3.1}$$

where the constant $K$ is called permeability (the unit of permeability is $m^2$).

#### *3.2.1 Permeability Models*

Permeability for composite materials is a measure of the ease of flow of liquid resin through the fiber matrix. Higher the permeability, lower is the resistance to flow and vice versa. Since composite materials are highly anisotropic in nature, the permeabilities of composite

materials are higher in the longitudinal direction as compared to the transverse direction. Here, the Gutowski permeability model is used. The permeability in the longitudinal ($x$) direction proposed by Gutowski [17] is the same as the Kozeny-Carman [18] equation as defined by the equation

$$K_{11} = \frac{R_f^{\,2}}{4k} \frac{\left(1 - V_f\right)^3}{V_f^{\,2}} \tag{3.2}$$

whereas, the permeabilities in the transverse directions ($y$, $z$) are expressed as

$$K_{22} = K_{33} = \frac{R_f^{\,2}}{4k'} \frac{\left(\sqrt{\frac{V_a'}{V_f}} - 1\right)^3}{\left(\frac{V_a'}{V_f} + 1\right)} \tag{3.3}$$

where $K_{11}$, $K_{22,}$ $K_{33}$ are the components of permeability in the $x$, $y$, and $z$ directions, respectively, $k$ ($k$ = 1.4) is the Kozeny constant, $R_f$ is fiber radius, $V_f$ is the local fiber volume fraction, $V'_a$ and $k'$ are empirical parameters; values for different fiber arrangements are given in the Table 3-1.

**Table 3-1. Empirical Parameters for Gutowski Model.**

| **Fiber Packing Arrangement** | $V'_a$ | $k'$ |
|---|---|---|
| Quadratic | 0.760 | 0.20 |
| Hexagonal | 0.907 | 0.20 |

A mean fiber diameter of 30 microns (glass) was determined at the University of Mississippi Composite Materials Research Laboratory (CMRG).

### *3.2.2 Fiber Volume Fraction and Porosity*

The fiber volume fraction ($V_{fo}$) of the composite material is the volume fraction of the fiber in the final composite and porosity ($\varphi$) is the fraction of the non-fiber volume in the final composites. At every point, the sum of the fiber volume fraction and the porosity is always equal to unity which is mathematically,

$$\varphi(x) = 1 - V_f(x) \tag{3.4}$$

Both of these parameters mainly depend upon the "compression ratio (CR)" as defined in the Eq. (2.1). For CR = 1, the fiber volume fraction and the porosity remain constant throughout the injection chamber. For CR > 1, i.e. for a tapered injection chamber, the local fiber volume fraction ($V_f$) increases with respect increasing axial direction $x$. The local fiber volume fraction is minimum at the inlet of the injection chamber, it increases with the increasing longitudinal ($x$) coordinate in Region I, attains its maximum value at the end of the Region I and then remains constant throughout Region II, since there is no tapering of the walls of the injection chamber in Region II. For Region I, the local fiber volume fraction $V_f(x)$ is a function of $x$ and mathematically given as

$$V_f(x) = V_{fo}\left(\frac{H_D}{2h(x)}\right) \tag{3.5}$$

where $h(x)$ is shown in Fig. 2.3 and Fig. 2.4 and will be defined in Eq. (3.12) and the value of $V_f(x)$ in Eq. (3.5) are used in Eqs. (3.2) and (3.3) above to determine $K_{11}$, $K_{22}$, $K_{33}$ as functions of $x$ in Region I.

### *3.2.3 Governing Equations for Region I*

The walls of the injection chamber are tapered in Region I, therefore, the fiber volume fraction ($V_f(x)$), porosity ($\varphi$) and components of the permeability tensor ($K_{11}, K_{22}, K_{33}$) are functions of distance ($x$) along the longitudinal direction. For flow of resin through the reinforcement, the continuity equation is expressed as

$$\frac{\partial(u\varphi)}{\partial x}+\frac{\partial(v\varphi)}{\partial y}+\frac{\partial(w\varphi)}{\partial z}=0 \tag{3.6}$$

For Region I, the total velocity of resin movement, **u,** referenced to a stationary coordinate system is defined by

$$\mathbf{u} = \{u\ v\ w\}^{\mathrm{T}} \tag{3.7}$$

where $u$, $v$, and $w$ are the components of resin velocity in the three coordinate ($x$, $y$, $z$) directions. They are defined as follows

$$\begin{aligned} u &= U-\frac{K_{11}}{\mu\varphi}\frac{\partial \mathrm{P}}{\partial x} \\ v &= V-\frac{K_{22}}{\mu\varphi}\frac{\partial P}{\partial y} \\ w &= -\frac{K_{33}}{\mu\varphi}\frac{\partial P}{\partial z} \end{aligned} \tag{3-8}$$

where $\varphi$ is the porosity, $U$ and $V$ are the two velocity components of the fiber reinforcement in the $x$ and $y$ directions respectively, $K_{11}, K_{22}, K_{33}$ are the components of the permeability tensor and $\mu$ is the viscosity of the resin and $-\frac{K_{11}}{\mu\varphi}\frac{\partial P}{\partial x}$, $-\frac{K_{22}}{\mu\varphi}\frac{\partial P}{\partial y}$, and $-\frac{K_{33}}{\mu\varphi}\frac{\partial P}{\partial z}$ are the three components of the liquid resin velocity relative to the reinforcement. Equation (3.8) are the Darcy momentum equations in $x$, $y$ and $z$ directions for Region I, respectively. For Region I,

substituting Eq. (3.8) (the *x*, *y*, *z* momentum equations) into the continuity equation, Eq. (3.6), yields

$$\frac{\partial}{\partial x}\left(U\varphi-\frac{K_{11}}{\mu\varphi}\frac{\partial P}{\partial x}\varphi\right)+\frac{\partial}{\partial y}\left(V\varphi-\frac{K_{22}}{\mu\varphi}\frac{\partial P}{\partial y}\varphi\right)+\frac{\partial}{\partial z}\left(-\frac{K_{33}}{\mu\varphi}\frac{\partial P}{\partial z}\varphi\right)=0 \tag{3.9}$$

On simplification of Eq. (3-9), the pressure equation becomes

$$\frac{\partial}{\partial x}\left(\frac{K_{11}}{\mu}\frac{\partial P}{\partial x}\right)+\frac{\partial}{\partial y}\left(\frac{K_{22}}{\mu}\frac{\partial P}{\partial y}\right)+\frac{\partial}{\partial z}\left(\frac{K_{33}}{\mu}\frac{\partial P}{\partial z}\right)=\frac{\partial(U\varphi)}{\partial x}+\frac{\partial(V\varphi)}{\partial y} \tag{3.10}$$

Equation (3.11) below expresses the relationship between fiber velocity in the *y* direction (*V*) in terms of taper angle ($\alpha$), fiber velocity (*U*) in *x* direction, and position in the *y* direction as

$$V=-U\left(\frac{y}{h(x)}\right)\tan\alpha \tag{3.11}$$

where the vertical distance *y* varies according (see Figs. 2-3 and 2-4) to the relation $-h(x)\le y\le h(x)$ where

$$h(x)=-\left(\frac{H_{IC}-H_D}{2L_{IC}}\right)(x-L_{IC})+\frac{H_D}{2} \tag{3.12}$$

Substituting the fiber velocity *V* from Eq. (3.11) into Eq. (3.10) results in the following equation

$$\frac{\partial}{\partial x}\left(\frac{K_{11}}{\mu}\frac{\partial P}{\partial x}\right)+\frac{\partial}{\partial y}\left(\frac{K_{22}}{\mu}\frac{\partial P}{\partial y}\right)+\frac{\partial}{\partial z}\left(\frac{K_{33}}{\mu}\frac{\partial P}{\partial z}\right)=\frac{\partial}{\partial x}(U\varphi)+\frac{\partial}{\partial y}\left(-U\left(\frac{y}{h(x)}\right)\tan\alpha\,\varphi\right) \tag{3.13}$$

Simplification of Eq. (3.13) yields

$$\frac{\partial}{\partial x}\left(\frac{K_{11}}{\mu}\frac{\partial P}{\partial x}\right)+\frac{\partial}{\partial y}\left(\frac{K_{22}}{\mu}\frac{\partial P}{\partial y}\right)+\frac{\partial}{\partial z}\left(\frac{K_{33}}{\mu}\frac{\partial P}{\partial z}\right)=\mathrm{U}\left\{\frac{\partial\varphi}{\partial x}-\frac{\varphi}{h(x)}\tan\alpha\right\} \tag{3.14}$$

Equation (3.14) is the represents the governing pressure equation for Region I. As the walls of the injection chamber in Region I are tapered, the right hand side of this equation acts like a pressure source, i.e. it produces a rise in pressure. In the case where the walls of the

injection chamber are not tapered in Region I, then ($\alpha$ = 0) and Eq. (3.14) would reduce to Eq. (3.19) below.

### *3.2.4 Governing Equations for Region II*

The continuity equation for the flow of resin through the fiber reinforcement is represented as

$$\frac{\partial(u\varphi)}{\partial x}+\frac{\partial(v\varphi)}{\partial y}+\frac{\partial(w\varphi)}{\partial z}=0 \tag{3.15}$$

In the injection pultrusion process, the resin velocity components in the three coordinate directions *u*, *v*, and *w* are defined as

$$\begin{aligned} u &= U-\frac{K_{11}}{\mu\varphi}\frac{\partial P}{\partial x} \\ v &= -\frac{K_{22}}{\mu\phi}\frac{\partial P}{\partial y} \\ w &= -\frac{K_{33}}{\mu\phi}\frac{\partial P}{\partial z} \end{aligned} \tag{3.16}$$

where, $\varphi$ is the porosity, *U* is the velocity of the fiber reinforcement in the longitudinal direction, *P* is resin pressure, $K_{11}, K_{22}, K_{33}$ are the components of permeability in the *x*, *y*, and *z* directions, respectively, and $\mu$ is the viscosity of the liquid resin and $-\frac{K_{11}}{\mu\varphi}\frac{\partial P}{\partial x}$, $-\frac{K_{22}}{\mu\varphi}\frac{\partial P}{\partial y}$, $-\frac{K_{33}}{\mu\varphi}\frac{\partial P}{\partial z}$ are the velocity components of the liquid resin relative to the reinforcement in the longitudinal direction. The three expressions in Eq. (3.16) are the Darcy momentum equations in *x*, *y* and *z* directions, respectively. By substituting these momentum equations in Eq. (3.15) one obtains the governing pressure equation as

$$\frac{\partial}{\partial x}\left(U\varphi-\frac{K_{11}}{\mu\varphi}\frac{\partial P}{\partial x}\varphi\right)+\frac{\partial}{\partial y}\left(-\frac{K_{22}}{\mu\varphi}\frac{\partial P}{\partial y}\varphi\right)+\frac{\partial}{\partial z}\left(-\frac{K_{33}}{\mu\varphi}\frac{\partial P}{\partial z}\varphi\right)=0 \qquad (3.17)$$

further simplification yeilds,

$$\frac{\partial}{\partial x}\left(\frac{K_{11}}{\mu}\frac{\partial P}{\partial x}\right)+\frac{\partial}{\partial y}\left(\frac{K_{22}}{\mu}\frac{\partial P}{\partial y}\right)+\frac{\partial}{\partial z}\left(\frac{K_{33}}{\mu}\frac{\partial P}{\partial z}\right)=\frac{\partial}{\partial x}(U\varphi)=0 \qquad (3.18)$$

Since $U$ and $\varphi$ are constant in Region II, then $\frac{\partial}{\partial x}(U\varphi)$ =0 and Eq. (3.18) simplifies to,

$$\frac{\partial}{\partial x}\left(\frac{K_{11}}{\mu}\frac{\partial P}{\partial x}\right)+\frac{\partial}{\partial y}\left(\frac{K_{22}}{\mu}\frac{\partial P}{\partial y}\right)+\frac{\partial}{\partial z}\left(\frac{K_{33}}{\mu}\frac{\partial P}{\partial z}\right)=0 \qquad (3.19)$$

which is the governing pressure equation for Region II.

### *3.2.5 Boundary Conditions for Attached-Die Configuration*

The governing pressure equations, Eq. (3.14) and Eq. (3.19) are second order partial differential equations. So six spatial boundary conditions, two in each coordinate direction are required for solution for the pressure field. Equations (3.20a) through (3.20k) describe the boundary conditions in terms of pressure and velocity for the "attached" die configuration.

$P = P_{atm}$ at $x = 0$ (3.20a)

$P = P_{Inj}$ at injection slot (3.20b)

$\tan\alpha = \frac{-v}{u}$ at $y = h(x)$ (Region I) (3.20c)

$\tan\alpha = \frac{v}{u}$ at $y = -h(x)$ (Region I) (3.20d)

$w = 0$ at $z = W_D/2$ (Region I) (3.20e)

$w = 0$ at $z = -W_D/2$ (Region I) (3.20f)

$v = 0$ at $y = h(x)$ (Region II) (3.20g)

$v = 0$ at $y = -h(x)$ (Region II) (3.20h)

$w = 0$ at $z = W_D/2$ (Region II) (3.20i)

$w = 0$ at $z = -W_D/2$ (Region II) (3.20j)

$u = U$ at $x$ = length of injection chamber (3.20k)

At $x = 0$, i.e. the front of the computational domain, dry fiber reinforcement enters the injection chamber where the fluid pressure is assumed to at one atmospheric pressure (101.3 kPa). The injection slot has the injection pressure (input to the program). Since a slip boundary condition is possible along the chamber walls in both the regions, Eq. (3.20c) through Eq. (3.20j) are obtained setting the normal to the wall component of the resin resultant velocity to zero. This means there is no penetration of resin into the wall of the injection chamber. At the exit of the injection chamber, the resin impregnated fibers enter the "attached-die". At the outlet, it is assumed that the velocity of the resin in the $x$-direction is equal to the fiber velocity in the same direction ($u = U$). To solve the Eqs. (3.14) and (3.19), all the boundary conditions are recast in terms of pressure so the resin velocities are substituted in Eq. (3.20c) through Eq. (3.20j) which yield

$P = P_{atm}$ at $x = 0$ (3.21a)

$P = P_{Inj}$ at injection slot (3.21b)

$$\frac{K_{11}}{\mu\varphi}\frac{\partial P}{\partial x}sin\alpha + \frac{K_{22}}{\mu\varphi}\frac{\partial P}{\partial y}cos\alpha = 0$$ at $y = h(x)$ ( Region I ) (3.21c)

$$\frac{K_{11}}{\mu\varphi}\frac{\partial P}{\partial x}sin\alpha - \frac{K_{22}}{\mu\varphi}\frac{\partial P}{\partial y}cos\alpha = 0$$ at $y = -h(x)$ ( Region I ) (3.21d)

$$\frac{\partial P}{\partial z} = 0$$ at $z = W_D/2$ ( Region I ) (3.21e)

$$\frac{\partial P}{\partial z} = 0 \qquad \text{at } z = -W_D/2 \quad (\text{Region I}) \qquad (3.21f)$$

$$\frac{\partial P}{\partial y} = 0 \qquad \text{at } y = H_D/2 \quad (\text{Region II}) \qquad (3.21g)$$

$$\frac{\partial P}{\partial y} = 0 \qquad \text{at } y = -H_D/2 \quad (\text{Region II}) \qquad (3.21h)$$

$$\frac{\partial P}{\partial z} = 0 \qquad \text{at } z = W_D/2 \quad (\text{Region II}) \qquad (3.21i)$$

$$\frac{\partial P}{\partial z} = 0 \qquad \text{at } z = -W_D/2 \quad (\text{Region II}) \qquad (3.21j)$$

$$\frac{\partial P}{\partial x} = 0 \qquad \text{at } x = \text{length of injection chamber} \qquad (3.21k)$$

Since the computational domain is symmetric about the *xy* and *xz* planes, only a quarter of the computational domain is modeled. For this, the boundary conditions have to be suitably modified for the simulation of the resin flow in a quarter of the computational domain. The modified (quarter domain) boundary conditions for the "attached-die" configuration are as follows,

$$P = P_{atm} \qquad \text{at } x = 0 \qquad (3.22a)$$

$$P = P_{Inj} \qquad \text{at injection slot} \qquad (3.22b)$$

$$\frac{K_{11}}{\mu\varphi}\frac{\partial P}{\partial x}\sin\alpha + \frac{K_{22}}{\mu\varphi}\frac{\partial P}{\partial y}\cos\alpha = 0 \qquad \text{at } y = h(x) \quad (\text{Region I}) \qquad (3.22c)$$

$$\frac{\partial P}{\partial y} = 0 \qquad \text{at } y = 0 \quad (\text{Region I}) \qquad (3.22d)$$

$$\frac{\partial P}{\partial z} = 0 \qquad \text{at } z = W_D/2 \quad (\text{Region I}) \qquad (3.22e)$$

$$\frac{\partial P}{\partial z} = 0 \qquad \text{at } z = 0 \qquad \text{( Region I )} \qquad (3.22f)$$

$$\frac{\partial P}{\partial y} = 0 \qquad \text{at } y = H_D/2 \qquad \text{( Region II )} \qquad (3.22g)$$

$$\frac{\partial P}{\partial y} = 0 \qquad \text{at } y = 0 \qquad \text{( Region II )} \qquad (3.22h)$$

$$\frac{\partial P}{\partial z} = 0 \qquad \text{at } z = W_D/2 \qquad \text{( Region II )} \qquad (3.22i)$$

$$\frac{\partial P}{\partial z} = 0 \qquad \text{at } z = 0 \qquad \text{( Region II )} \qquad (3.22j)$$

$$\frac{\partial P}{\partial x} = 0 \qquad \text{at } x = \text{length of injection chamber} \qquad (3.22k)$$

### *3.2.6 Boundary Conditions for Detached-Die Configuration*

In the detached injection chamber configuration, there is a gap of 0.005 m between the exit of the resin injection chamber and the heated die inlet; thus the circumferential surface area of the resin/matrix system in this gap space is subjected to the atmospheric pressure boundary condition between $L_T - 0.005 \text{ m} < x \leq L_T$ (see Eq. (3.23h) and Eq. (3.23i). Equations (3.23a) through (3.23i) express the boundary conditions for the detached configuration in terms of pressure and velocity.

$$P = P_{atm} \qquad \text{at } x = 0 \qquad (3.23a)$$

$$P = P_{Inj} \qquad \text{at injection slot} \qquad (3.23b)$$

$$\tan \alpha = \frac{-v}{u} \qquad \text{at } y = h(x) \qquad \text{(Region I)} \qquad (3.23c)$$

$$\tan \alpha = \frac{v}{u} \qquad \text{at } y = -h(x) \qquad \text{(Region I)} \qquad (3.23d)$$

$w = 0$ at $z = W_D/2$ (Region I) (3.23e)

$w = 0$ at $z = -W_D/2$ (Region I) (3.23f)

$v = 0$ at $y = \pm H_D/2$ and $L_{IC} \leq x \leq L_T$ - 0.005 m (Region II) (3.23g)

$w = 0$ at $z = \pm W_D/2$ and $L_{IC} \leq x \leq L_T$ - 0.005 m (Region II) (3.23h)

$u = U$ at $x = L_T$ (3.23i)

$P = P_{atm}$ at $y = \pm H_D/2$ and $L_T - 0.005$ m $< x \leq L_T$ (Region II) (3.23h)

$P = P_{atm}$ at $z = \pm W_D/2$ and $L_T - 0.005$ m $< x \leq L_T$ (Region II) (3.23i)

Boundary conditions in term of pressure obtained by substituting resin velocities into Eqs. (3.24a) to (3.24k) are given as

$P = P_{atm}$ at $x = 0$ (3.24a)

$P = P_{Inj}$ at injection slot (3.24b)

$\frac{K_{11}}{\mu\varphi}\frac{\partial P}{\partial x}\sin\alpha + \frac{K_{22}}{\mu\varphi}\frac{\partial P}{\partial y}\cos\alpha = 0$ at $y = h(x)$ (Region I) (3.24c)

$\frac{K_{11}}{\mu\varphi}\frac{\partial P}{\partial x}\sin\alpha - \frac{K_{22}}{\mu\varphi}\frac{\partial P}{\partial y}\cos\alpha = 0$ at $y = -h(x)$ (Region I) (3.24d)

$\frac{\partial P}{\partial z} = 0$ at $z = W_D/2$ (Region I) (3.24e)

$\frac{\partial P}{\partial z} = 0$ at $z = -W_D/2$ (Region I) (3.24f)

$\frac{\partial P}{\partial y} = 0$ at $y = \pm H_D/2$ and $L_{IC} \leq x \leq L_T - 0.005$ m (Region II) (3.24g)

$\frac{\partial P}{\partial z} = 0$ at $z = \pm W_D/2$ and $L_{IC} \leq x \leq L_T - 0.005$ m (Region II) (3.24h)

$\frac{\partial P}{\partial x} = 0$ at $x = L_T$ (3.24i)

$P = P_{atm}$ at $y = \pm H_D/2$ and $L_T - 0.005$ m $< x \leq L_T$ (Region II) (3.24j)

$P = P_{atm}$ at $z = \pm W_D/2$ and $L_T - 0.005$ m $< x \leq L_T$ (Region II) (3.24k)

Since the computational domain is symmetric about the *xy* and *xz* planes, only a quarter of the computational domain is modeled. For this, the boundary conditions have to be suitably modified for the simulation of the resin flow in a quarter of the computational domain. The modified (quarter domain) boundary conditions for the "detached-die" configuration are as follows,

$P = P_{atm}$ at $x = 0$ (3.25a)

$P = P_{Inj}$ at injection slot (3.25b)

$\frac{K_{11}}{\mu\phi}\frac{\partial P}{\partial x}\sin\alpha + \frac{K_{22}}{\mu\phi}\frac{\partial P}{\partial y}\cos\alpha = 0$ at $y = h(x)$ (Region I) (3.25c)

$\frac{\partial P}{\partial y} = 0$ at $y = 0$ (Region I) (3.25d)

$\frac{\partial P}{\partial z} = 0$ at $z = W_D/2$ (Region I) (3.25e)

$\frac{\partial P}{\partial z} = 0$ at $z = 0$ (Region I) (3.25f)

$\frac{\partial P}{\partial y} = 0$ at $y = H_D/2$ and $L_{IC} \leq x \leq L_T - 0.005$ m (Region II) (3.25g)

$P = P_{atm}$ at $y = H_D/2$ and $L_T - 0.005$ m $< x \leq L_T$ (Region II) (3.25h)

$\frac{\partial P}{\partial y} = 0$ at $y = 0$ ( Region II ) (3.25i)

$\frac{\partial P}{\partial z} = 0$ at $z = W_D/2$ and $L_{IC} \leq x \leq L_T - 0.005$ m (Region II) (3.25h)

$P = P_{atm}$ at z = $W_D/2$ and $L_T - 0.005$ m $< x \leq L_T$ (Region II) (3.25i)

$$\frac{\partial P}{\partial z} = 0 \qquad \text{at } z = 0 \text{ ( Region II )} \tag{3.25j}$$

$$\frac{\partial P}{\partial x} = 0 \qquad \text{at } x = \text{length of injection chamber} \tag{3.25k}$$

### *3.3 Finite Volume Method*

The finite volume method is a representation and evaluation technique of the partial differential equation as a system of algebraic equations. Finite volume basically means a small volume surrounding nodal points in mesh domain. Here, this method is utilized to calculate the pressure field, velocity field and the location of the liquid resin flow front in the computational domain. In this method, the computational domain is distributed into touching but non-overlapping finite control volumes which fill the domain with one node associated with each control volume as in Fig 3-1. It estimates the partial differential equation over a finite control volume surrounding the grid node. Employing the finite volume approach, discretization equations are obtained by integration of the partial differential equation over each control volume surrounding each grid node. To evaluate the required integrals, linear interpolation functions expressing the variation of the pressure between the grid points are used.

### *3.4 Discretization Equations*

#### *3.4.1 Discretization Equation for Region I*

The general discretization equation for Region I is represented as

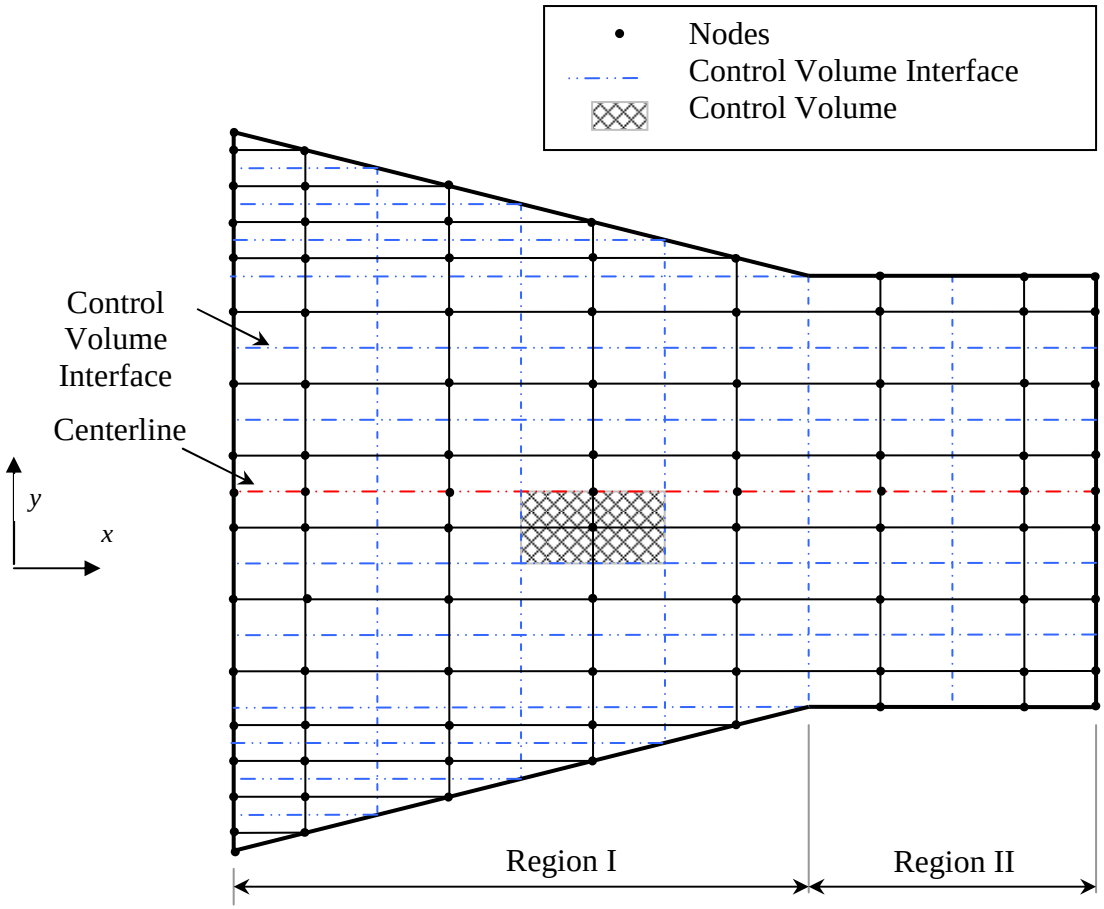


**Fig. 3-1. Schematic Diagram of the Computational Domain with the Grid.**

$$P_P\left\{\left.\frac{K_{11}}{\mu}\right|_e \frac{\Delta y\,\Delta z}{(\delta x)_e}+\left.\frac{K_{11}}{\mu}\right|_w \frac{\Delta y\,\Delta z}{(\delta x)_w}+\left.\frac{K_{22}}{\mu}\right|_n \frac{\Delta x\,\Delta z}{(\delta y)_n}+\left.\frac{K_{22}}{\mu}\right|_s \frac{\Delta x\,\Delta z}{(\delta y)_s}+\left.\frac{K_{33}}{\mu}\right|_t \frac{\Delta x\,\Delta y}{(\delta z)_t}+\left.\frac{K_{33}}{\mu}\right|_b \frac{\Delta x\,\Delta y}{(\delta z)_b}\right\}$$
$$= P_E\left\{\left.\frac{K_{11}}{\mu}\right|_e \frac{\Delta y\,\Delta z}{(\delta x)_e}\right\}+P_W\left\{\left.\frac{K_{11}}{\mu}\right|_w \frac{\Delta y\,\Delta z}{(\delta x)_w}\right\}+P_N\left\{\left.\frac{K_{22}}{\mu}\right|_n \frac{\Delta x\,\Delta z}{(\delta y)_n}\right\}+P_S\left\{\left.\frac{K_{22}}{\mu}\right|_s \frac{\Delta x\,\Delta z}{(\delta y)_s}\right\}+$$
$$P_T\left\{\left.\frac{K_{33}}{\mu}\right|_t \frac{\Delta x\,\Delta y}{(\delta z)_t}\right\}+P_B\left\{\left.\frac{K_{33}}{\mu}\right|_b \frac{\Delta x\,\Delta y}{(\delta z)_b}\right\}-U\left(\left(\varphi_e-\varphi_w\right)\right)\Delta y\,\Delta z+U\frac{\tan\alpha_P}{h(x_P)}\varphi_P\Delta x\,\Delta y\,\Delta z \tag{3.26}$$

This equation for 3-D has the linear form as

$$a_P P_P = a_E P_E + a_W P_W + a_N P_N + a_S P_S + a_T P_T + a_B P_B + S_p \tag{3.27}$$

where $a_P$, $a_E$, $a_W$, $a_N$, $a_S$, $a_T$, $a_B$ are the coefficients of the pressures at the given node and its neighboring nodes, respectively and $S_p$ is the Source term. This expresses a relation between a node and its neighbors. The coefficients are defined below in Eq. (3.30).

### *3.4.2 Discretization Equation for Region II*

The general pressure discretization equation for Region II is represented as,

$$P_P\left\{\left.\frac{K_{11}}{\mu}\right|_e \frac{\Delta y\Delta z}{(\delta x)_e}+\left.\frac{K_{11}}{\mu}\right|_w \frac{\Delta y\Delta z}{(\delta x)_w}+\left.\frac{K_{22}}{\mu}\right|_n \frac{\Delta x\Delta z}{(\delta y)_n}+\left.\frac{K_{22}}{\mu}\right|_s \frac{\Delta x\Delta z}{(\delta y)_s}+\left.\frac{K_{33}}{\mu}\right|_t \frac{\Delta x\Delta y}{(\delta z)_t}+\left.\frac{K_{33}}{\mu}\right|_b \frac{\Delta x\Delta y}{(\delta z)_b}\right\}$$
$$= P_E\left\{\left.\frac{K_{11}}{\mu}\right|_e \frac{\Delta y\Delta z}{(\delta x)_e}\right\}+P_W\left\{\left.\frac{K_{11}}{\mu}\right|_w \frac{\Delta y\Delta z}{(\delta x)_w}\right\}+P_N\left\{\left.\frac{K_{22}}{\mu}\right|_n \frac{\Delta x\Delta z}{(\delta y)_n}\right\}+P_S\left\{\left.\frac{K_{22}}{\mu}\right|_s \frac{\Delta x\Delta z}{(\delta y)_s}\right\}+ \tag{3.28}$$
$$P_T\left\{\left.\frac{K_{33}}{\mu}\right|_t \frac{\Delta x\Delta y}{(\delta z)_t}\right\}+P_B\left\{\left.\frac{K_{33}}{\mu}\right|_b \frac{\Delta x\Delta y}{(\delta z)_b}\right\}$$

This equation has the linear form

$$a_P P_P = a_E P_E + a_W P_W + a_N P_N + a_S P_S + a_T P_T + a_B P_B \tag{3.29}$$

where $a_P$, $a_E$, $a_W$, $a_N$, $a_S$, $a_T$, $a_B$ are the coefficients of the pressures at the given node and its neighboring nodes, respectively. Equation (3.29) expresses a relation between a pressure node and its neighbors. The coefficients for Eq. (3.27) and Eq. (3.29) are represented as follow

$$a_E = \left.\frac{K_{11}}{\mu}\right|_e \frac{\Delta y\ \Delta z}{(\delta x)_e} \tag{3.30a}$$

$$a_W = \left.\frac{K_{11}}{\mu}\right|_w \frac{\Delta y\ \Delta z}{(\delta x)_w} \tag{3.30b}$$

$$a_N = \left.\frac{K_{22}}{\mu}\right|_n \frac{\Delta x\ \Delta z}{(\delta y)_n} \tag{3.30c}$$

$$a_S = \left.\frac{K_{22}}{\mu}\right|_s \frac{\Delta x\ \Delta z}{(\delta y)_s} \tag{3.30d}$$

$$a_T = \left.\frac{K_{33}}{\mu}\right|_t \frac{\Delta x\ \Delta y}{(\delta z)_t} \tag{3.30e}$$

$$a_B = \left.\frac{K_{33}}{\mu}\right|_b \frac{\Delta x\ \Delta y}{(\delta z)_b} \tag{3.30f}$$

$$S_p = U\left(\left(\ \varphi_e - \varphi_w\ \right)\right)\Delta y\ \Delta z + U\frac{\tan\alpha_P}{h(x_P)}\varphi_P \Delta x\ \Delta y\ \Delta z \tag{3.30g}$$

$$a_P = a_E + a_W + a_N + a_S + a_T + a_B + S_P \tag{3.30h}$$

### *3.5 Solution of the Algebraic Equations by TDMA*

To solve the system of discretized linear algebraic equations, the current solution technique utilizes the line-by-line Tridiagonal Matrix Algorithm (TDMA) [18]. Basically, there are two methods to solve the system of descretization equations, namely, direct methods and iterative methods. Direct methods which do not require iterations are somewhat complicated and

require larger computational space and time. Whereas iterative methods start from a guessed field of the dependent variable and utilize algebraic equations for gradually improved field results. Repetitive algorithm eventually gives a solution which is very close to the correct solution of the algebraic equation. Also, iterative methods require smaller memory storage and are especially suitable for handling nonlinearities. The line-by-line method converges to the solution very fast as the boundary condition information is transmitted rapidly to the interior of the domain. TDMA is a very effective equation solver and unlike general direct methods (matrix).

### *3.6 Time Marching Scheme*

The fraction of the control volume occupied by the resin liquid at a given instant of time relative to the maximum resin liquid the control volume can hold is called the fill factor $F_{i,j,k}$. Numerically, $F_{i,j,k}$ is related to the fractional amount of resin in the control volume. For a control volume completely filled with liquid the fill factor is unity (resin saturated reinforcement) and for an empty control volume it is zero (dry reinforcement). If a control volume is fully saturated with liquid the pressure is computed at the control volume node, otherwise it is assigned as atmospheric pressure.

The components of the resin velocities at the interface of the control volume are illustrated by Fig. 3-2. The node is represented by the solid dot and the control volume is represented by the bounded dashed lines. The figure also shows the fill factors and porosities of the control neighboring volumes. The net mass flow rate of liquid resin into and out of the control volume is computed using the following equations.

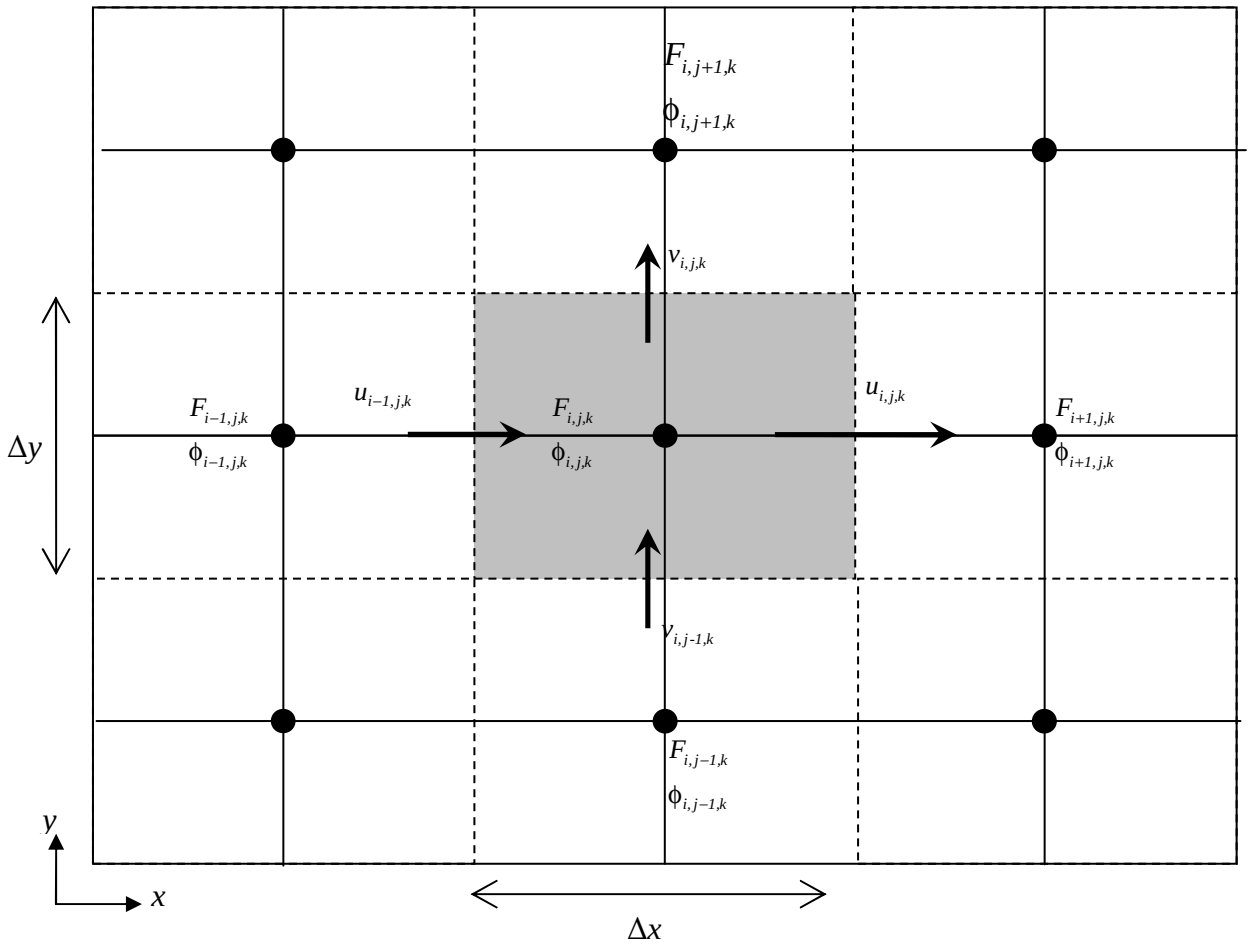


**Fig. 3-2. Schematic for Net Mass Flow Rate Calculations.**

$$(Net\,MassFlowRate)_{in} = \rho\{u_{i-1,j,k}\left(\frac{\phi_{i-1,j,k}+\phi_{i,j,k}}{2}\right)\Delta y\Delta z\left[\frac{u_{i-1,j,k}}{abs(u_{i-1,j,k})}F_{i-1,j,k},\frac{-u_{i-1,j,k}}{abs(u_{i-1,j,k})}F_{i,j,k}\right]$$
$$+v_{i,j-1,k}\phi_{i,j,k}\Delta x\Delta z\left[\frac{v_{i,j-1,k}}{abs(v_{i,j-1,k})}F_{i,j-1,k},\frac{-v_{i,j-1,k}}{abs(v_{i,j-1,k})}F_{i,j,k}\right]+ \quad (3.31)$$
$$w_{i,j,k-1}\phi_{i,j,k}\Delta x\Delta y\left[\frac{w_{i,j,k-1}}{abs(w_{i,j,k-1})}F_{i,j,k-1},\frac{-w_{i,j,k-1}}{abs(w_{i,j,k-1})}F_{i,j,k}\right]\}$$

$$(NetMassFlowRate)_{out} = \rho\{u_{i,j,k}\left(\frac{\phi_{i,j,k}+\phi_{i+1,j,k}}{2}\right)\Delta y\Delta z\left[\frac{u_{i,j,k}}{abs(u_{i,j,k})}F_{i,j,k},\frac{-u_{i,j,k}}{abs(u_{i,j,k})}F_{i+1,j,k}\right]$$
$$+v_{i,j,k}\phi_{i,j,k}\Delta x\Delta z\left[\frac{v_{i,j,k}}{abs(v_{i,j,k})}F_{i,j,k},\frac{-v_{i,j,k}}{abs(v_{i,j,k})}F_{i,j+1,k}\right]+$$
$$w_{i,j,k}\phi_{i,j,k}\Delta x\Delta y\left[\frac{w_{i,j,k}}{abs(w_{i,j,k})}F_{i,j,k},\frac{-w_{i,j,k}}{abs(w_{i,j,k})}F_{i,j,k+1}\right]\} \quad (3.32)$$

The terms $\left(\frac{\phi_{i-1,j,k}+\phi_{i,j,k}}{2}\right)$ and $\left(\frac{\phi_{i,j,k}+\phi_{i+1,j,k}}{2}\right)$ represent the average values of porosity at the interface of a control volume in the longitudinal direction. If the component of the resin velocity is positive, the mass flow rate is computed using the first term in the square bracket; whereas, if the velocity component is negative, the second term is used instead. The time taken to fill a yet unfilled control volume is represented as

$$(1-F_{i,j,k})\,\rho\,\Delta x\,\Delta y\,\Delta z\,\phi_{i,j,k} = [(Mass\ Flow\ Rate)_{in} - (Mass\ Flow\ Rate)_{out}]\,\Delta t \quad (3.33)$$

Equation (3.30) can be simplified to express the time to fill a specific control volume as

$$\Delta t = \frac{(1-F_{i,j,k})\,\rho\,\Delta x\,\Delta y\,\Delta z\,\phi_{i,j,k}}{[(Net\,Mass\ Flow\ Rate)_{in} - (Net\ Mass\ Flow\ Rate)_{out}]} \quad (3.34)$$

The net flow rate across the interface of the control volume approaches zero and $\Delta t$ defined by Eq. (3.34) approaches infinity as the resin flow front approaches steady state. To overcome this problem and maintain the numerical stability of the algorithm, the pultruded part is restricted

from travelling more than the length of the nodal control volume in the pull direction during a given time step, which means

$$0 < \Delta t_{min} < \frac{L_{min}}{U} \tag{3.35}$$

where $L_{min}$ is minimum length of the control volume in the pull speed direction and $U$ is the fiber pull speed in longitudinal direction. This condition is checked at every step and only one control volume is allowed to be newly filled ($F_{i,j,k}$ = 1) at that time step. If the calculated value of minimum time step from Eq. (3.34) is greater than as defined by Eq. (3.35) at any given time step, the value of minimum time step from Eq. (3.35) is used, otherwise the value of minimum time step from Eq. (3.34) is used.

The minimum value of the time step, calculated for all the unfilled control volumes from Eq. (3.35), is the amount of time required to fill the next quickest to fill-the control volume which has resin in it but neither completely filled nor overfilling any other control volume. As the flow front is advanced using this minimum time step, it is ensured that only one control volume is filled in one time step and no control volume is overfilled as time advances forward. All the unfilled or not completely filled control volumes (where $0 \le F < 1$) fill factors are updated at the end of each time step utilizing the minimum time step calculated from Eq. (3.34) or Eq. (3.35) employing the following equations.

$$\Delta F_{i,j,k} = \left[ \left( Mass\ Flow\ Rate \right)_{in} - \left( Mass\ Flow\ Rate \right)_{out} \right] \frac{\Delta t_{min}}{\rho \Delta x \Delta y \Delta z \phi_{i,j,k}} \tag{3.36}$$

$$F_{i,j,k} = F^{o}{}_{i,j,k} + \Delta F_{i,j,k} \tag{3.37}$$

where $\Delta F_{i,j,k}$ is the change in fill factor and $F^{o}{}_{i,j,k}$ is the fill factor at the end of the previous time step. The detailed analysis, the governing equations for tapered Region I and constant area

Region II, the permeability model, the boundary conditions and the pressure discretization equations have been explained in Chapter 3. Next the results and detailed discussion will be presented in Chapter 4.

# CHAPTER 4

# RESULTS AND DISCUSSION

In this chapter, the impact of different chamber lengths coupled with the geometric parameters are presented for various compression ratios by simulating the liquid resin flow through fiber reinforcement using a 3-D finite volume technique. For a given minimum resin injection pressure to achieve complete fiber reinforcement wetout, the corresponding maximum resin pressure inside the injection chamber for both the attached-die and detached-die configurations is presented and compared for CR values of 2, 3 and 4. The geometric design parameters used to study the effect on the minimum resin injection pressure required to achieve complete resin wetout and the associated maximum resin pressure within the injection chamber are as follows:

- Axial location of the single injection slot
- Width of the single injection slot
- Multiple injection slots and their axial locations
- Final composite thickness

Each of these design geometric parameters were studied at different injection chamber lengths ($L_T$) of 0.15 m, 0.20 m and 0.30 m, with the axial location of dual injection slots (one on top and one on bottom; see Fig. 2-1) at 0.40 $L_I$, 0.60 $L_I$ and 0.80 $L_I$ along the tapered length (Region I; see Fig. 2-1) for different CR values of 2, 3 and 4. For total length of the injection

chamber ($L_T$) 0.15 m, 0.20 m and 0.30 m, the length of the tapered Region ($L_I$) are 0.10 m, 0.15 m, and 0.25 m respectively. The cases are compared for the pull speed $U$ = 0.0254 m/s (60 in/min) or 0.0508 m/s (120 in/min). For a particular simulation the other parameters are held at their nominal values. The nominal values of processing and design parameters selected were:

- Nominal width of the injection slot = 0.01 m
- Nominal thickness of the final composite, $H_D$ = 0.00318 m and width, $W_D$ = 0.00635 m
- Nominal pull speed, $U$ = 0.0254 m/s (60 in/min) or 0.0508 m/s (120 in/min)
- Nominal fiber volume fraction, $V_{fo}$ = 0.68
- Nominal resin viscosity, $\mu$ = 0.75 Pa·s; this viscosity value corresponds to a polyester resin system.

The simulations correspond to a composite consisting of fiberglass reinforcement with a polyester resin system.

### *4.1 Axial Location of Single Injection Slot*

The effect of the axial location of the injection slot for different injection chamber lengths was studied for the attached-die and detached-die configurations in this section. Axial location of the injection slot has a significant impact on the minimum resin injection pressure needed to achieve complete wetout of the fiber reinforcement as well as the corresponding maximum resin pressure inside the injection chamber for both the attached-die and detached-die configurations. The location of the single injection slot was varied as 0.40 $L_I$, 0.60 $L_I$ and 0.80 $L_I$ of the tapered length of Region I. The study was carried out for the total injection chamber lengths ($L_T$) of 0.15

m, 0.20 m and 0.30 at different compression ratios of 2, 3 and 4 and compared at two different pull speeds, 0.0254 m/s and 0.0508 m/s. For a particular length of injection chamber and compression ratio Tables 4-1 and 4-2 show the impact of the location of single injection slot for the pull speeds 0.0254 m/s (Table 4-1) and 0.0508 m/s (Table 4-2) respectively. The minimum injection pressure (column 5) required for the complete wetout of the reinforcement fiber and the corresponding maximum chamber wall pressure (columns 6 and 7) of the attached-die and detached-die configurations are shown in Tables 4-1 and 4-2. The minimum injection pressure to achieve complete wetout was the same value for both the attached-die and detached-die configurations, hence one column (column 5) for the minimum injection pressure is shown in all the tables of the results section. The maximum interior pressure for the attached-die configuration is achieved in Region II except for some cases; whereas, for the detached-die configuration, the maximum pressure is achieved inside Region I of injection chamber. For maximum interior pressure, only chamber wall pressure has been shown and discussed.

When the injection slot is located near the inlet of the injection chamber, the minimum injection pressure needed to achieve complete fiber wetout in both the attached-die and detached-die configurations is low because the local fiber volume fraction at the far upstream axial location of injection slot is low; however, the maximum resin pressure inside the injection chamber is high because of the pressure rise due to the longer compression distance along the tapered injection chamber walls. And when the injection slot is located near the end of Region I of the injection chamber, the injection pressure necessary to achieve complete wetout increases because the local fiber volume fraction is higher at this downstream axial injection slot location of the injection chamber; however, the corresponding maximum resin pressure inside the injection chamber decreases due to the shorter axial distance over which the resin is compressed.

**Table 4-1. Single Slot Minimum Injection Pressure Required for Complete Wetout for Different Axial Locations and Different Compression Ratios for $U$ = 0.0254 m/s, $V_{fo}$ = 0.68, $\mu$ = 0.75 Pa·s, $H_D$ = 0.003175 m, $W_D$ = 0.0635 m, Slot Width= 0.10 m.**

| Case* | CR | Location of Injection Slot ($x_{IS}$) (m) | Injection Chamber Length ($L_T$) (m) | Minimum Injection Pressure (Gauge) (MPa) | Maximum Pressure (Gauge) (MPa) | Maximum Pressure (Gauge) (MPa) |
|---|---|---|---|---|---|---|
| | | | | | Attached | Detached |
| A1 | 2 | 0.04 | 0.15 | 0.002 | 0.93 | 0.76 |
| A2 | 2 | 0.06 | 0.15 | 0.077 | 0.70 | 0.58 |
| A3 | 2 | 0.08 | 0.15 | 0.263 | 0.42 | 0.37 |
| A4 | 3 | 0.04 | 0.15 | 0.002 | 0.69 | 0.59 |
| A5 | 3 | 0.06 | 0.15 | 0.002 | 0.55 | 0.48 |
| A6 | 3 | 0.08 | 0.15 | 0.078 | 0.35 | 0.19 |
| A7 | 4 | 0.04 | 0.15 | 0.002 | 0.53 | 0.45 |
| A8 | 4 | 0.06 | 0.15 | 0.002 | 0.45 | 0.38 |
| A9 | 4 | 0.08 | 0.15 | 0.009 | 0.30 | 0.23 |
| A10 | 2 | 0.06 | 0.2 | 0.016 | 1.15 | 0.87 |
| A11 | 2 | 0.09 | 0.2 | 0.085 | 0.81 | 0.62 |
| A12 | 2 | 0.12 | 0.2 | 0.243 | 0.24 | 0.24 |
| A13 | 3 | 0.06 | 0.2 | 0.002 | 0.77 | 0.64 |
| A14 | 3 | 0.09 | 0.2 | 0.002 | 0.59 | 0.49 |
| A15 | 3 | 0.12 | 0.2 | 0.113 | 0.33 | 0.28 |
| A16 | 4 | 0.06 | 0.2 | 0.002 | 0.55 | 0.47 |
| A17 | 4 | 0.09 | 0.2 | 0.002 | 0.44 | 0.38 |
| A18 | 4 | 0.12 | 0.2 | 0.064 | 0.11 | 0.11 |
| A20 | 2 | 0.10 | 0.3 | 0.002 | **2.36** | 1.58 |
| A21 | 2 | 0.15 | 0.3 | 0.051 | 1.74 | 1.19 |
| A22 | 2 | 0.20 | 0.3 | 0.202 | 0.90 | 0.65 |
| A24 | 3 | 0.10 | 0.3 | 0.002 | 1.74 | 1.35 |
| A25 | 3 | 0.15 | 0.3 | 0.002 | 1.42 | 1.10 |
| A26 | 3 | 0.20 | 0.3 | 0.037 | 0.18 | 0.13 |
| A28 | 4 | 0.10 | 0.3 | 0.002 | 1.34 | 1.11 |
| A29 | 4 | 0.15 | 0.3 | 0.002 | 1.16 | 0.96 |
| A30 | 4 | 0.20 | 0.3 | 0.002 | 0.77 | 0.65 |

* Bold font indicates non-acceptable manufacturing solutions for an injection pressure ≥ 0.42 MPa (60 psi) and/or with an associated maximum pressure for attached or detached ≥ 2.07 MPa (300 psi).

**Table 4-2 Single Slot Minimum Injection Pressure Required for Complete Wetout for Different Axial Locations and Different Compression Ratios for U = 0.0508 m/s, $V_{fo}$ = 0.68, $\mu$ = 0.75 Pa·s, $H_D$ = 0.003175 m, $W_D$ = 0.0635 m, Slot Width= 0.10 m**

| Case* | CR | Location of Injection Slot ($x_{IS}$) (m) | Total Length ($L_T$) (m) | Minimum Injection Pressure (Gauge) (MPa) | Maximum Pressure (Gauge) (MPa) | Maximum Pressure (Gauge) (MPa) |
|---|---|---|---|---|---|---|
| | | | | | Attached | Detached |
| B1 | 2 | 0.04 | 0.15 | 0.002 | 1.87 | 1.48 |
| B2 | 2 | 0.06 | 0.15 | 0.161 | 1.40 | 1.15 |
| B3 | 2 | 0.08 | 0.15 | **0.526** | 0.84 | 0.73 |
| B4 | 3 | 0.04 | 0.15 | 0.002 | 1.37 | 1.19 |
| B5 | 3 | 0.06 | 0.15 | 0.002 | 1.11 | 0.95 |
| B6 | 3 | 0.08 | 0.15 | 0.154 | 0.70 | 0.37 |
| B7 | 4 | 0.04 | 0.15 | 0.002 | 1.05 | 0.89 |
| B8 | 4 | 0.06 | 0.15 | 0.002 | 0.90 | 0.76 |
| B9 | 4 | 0.08 | 0.15 | 0.0228 | 0.60 | 0.50 |
| B10 | 2 | 0.06 | 0.20 | 0.03 | **2.30** | 1.78 |
| B11 | 2 | 0.09 | 0.20 | 0.168 | 1.61 | 1.24 |
| B12 | 2 | 0.12 | 0.20 | 0.451 | 0.45 | 0.45 |
| B13 | 3 | 0.06 | 0.20 | 0.002 | 1.54 | 1.28 |
| B14 | 3 | 0.09 | 0.20 | 0.002 | 1.17 | 0.98 |
| B15 | 3 | 0.12 | 0.20 | 0.223 | 0.65 | 0.56 |
| B16 | 4 | 0.06 | 0.20 | 0.002 | 1.10 | 0.94 |
| B17 | 4 | 0.09 | 0.20 | 0.002 | 0.89 | 0.76 |
| B18 | 4 | 0.12 | 0.20 | 0.106 | 0.23 | 0.22 |
| B19 | 2 | 0.10 | 0.30 | 0.002 | **4.71** | **3.17** |
| B20 | 2 | 0.15 | 0.30 | 0.099 | **3.47** | **2.37** |
| B21 | 2 | 0.20 | 0.30 | 0.416 | 1.80 | 1.30 |
| B22 | 3 | 0.10 | 0.30 | 0.002 | **3.49** | **2.70** |
| B23 | 3 | 0.15 | 0.30 | 0.002 | **2.84** | **2.20** |
| B24 | 3 | 0.20 | 0.30 | 0.071 | 0.32 | 0.27 |
| B25 | 4 | 0.10 | 0.30 | 0.002 | **2.68** | **2.22** |
| B26 | 4 | 0.15 | 0.30 | 0.002 | **2.31** | **1.86** |
| B27 | 4 | 0.20 | 0.30 | 0.002 | 1.55 | 0.65 |

* Bold font indicates non-acceptable manufacturing solutions for an injection pressure ≥ 0.42 MPa (60 psi) with an associated maximum pressure for attached or detached ≥ 2.07 MPa (300 psi).

$V_f(x)$ is minimum at the front inlet of the injection chamber and is a maximum at the end of the Region I of injection chamber and remains constant ($V_{fo}$) throughout Region II of the injection chamber. When the single injection slot is located downstream in the injection chamber, with an increase in the $x_{IS}$ location for the tapered injection chamber, the increased local fiber volume fraction, ($V_f$ $(x)$), in turn offers higher resistance to the flow of liquid resin through the fiber matrix and therefore there requires an increase in the injection pressure to achieve complete wetout. For design and safety considerations, the location of the injection slot should be selected in a manner such that the injection pressure and maximum interior pressure are both within reasonable and desirable limits. High maximum chamber wall pressure can cause the leakage of resin and damage the injection chamber. The feasible manufacturing pressure range was taken as the resin injection pressure not greater than 0.42 MPa (60 psi) and for the resin maximum chamber pressure not greater than 2.07 MPa (300 psi). In Table 4-1 and Table 4-2 the bold cases are unsuitable for commercial pultrusion manufacturing process since these cases do not satisfy the above stated pressure feasibility requirements.

From Tables 4-1 and 4-2 it is observed that when the location of the injection slot ($x_{IS}$) moves downstream for all other parameters fixed, the injection pressure increases and the corresponding maximum pressure inside the injection chamber of both the attached-die and detached-die configurations decreases. For all cases the maximum pressure for the detached-die configuration is significantly lower than the corresponding attached-die configuration because the detached-die configuration has an exit gap (see Fig. 2-2) at atmospheric pressure between the resin injection chamber and heated die inlet, which acts as a pressure release mechanism to lower the internal chamber pressure. It is seen from Eqs. 3-20j and 3-20k that the atmospheric boundary condition applied at the circumference of the injection chamber exit of detached-die

configuration acts to relieve the resin pressure within the resin injection chamber before entering the heated pultrusion die.

It is also observed from Table 4-1 and Table 4-2 that for the particular length of injection chamber, at the same axial injection location of the injection slot ($x_{IS}$), the minimum injection pressure necessary to achieve complete wetout decreases with an increase of tapering of the injection chamber (increasing CR values). At the same axial location of the injection slot, the minimum pressure required for the complete wetout is higher for CR values of 2 than that required for CR = 3 or 4; for CR = 3 or 4 the injection pressure is only slightly greater than the atmospheric pressure. This is because the local fiber volume fraction at the injection slot for CR value of 2 is greater, which causes more resistance to the resin flow and thus a higher injection pressure is required to push the resin through the fiber to achieve complete wetout. As the CR value of the injection chamber increases the local fiber volume fraction at that injection slot location decreases causing less resistance to the flow of liquid resin through the fiber matrix. Thus, a lower minimum resin injection pressure is required to achieve complete wetout as CR increases.

From Table 4-1 ($U$ = 0.0254 m/s) and Table 4-2 ($U$ = 0.0508 m/s), the impact of pull speed on the minimum resin injection pressure necessary to achieve complete wetout along with the associated maximum resin pressure inside the injection chamber of the attached-die and detached-die configurations can be observed and compared. The pull speed has a significant impact on the injection pressure and maximum interior pressure of attached-die and detached-die configurations. When the pull speed is doubled from 0.0254 m/s to 0.0508 m/s, the minimum resin injection pressure and the corresponding maximum interior pressure for both the attached-die and detached-die configurations are essentially doubled. The maximum chamber wall

pressure increases when the pull speed is increased because the increased pull speed compresses rapidly the liquid resin by rapidly increasing the fiber volume fraction along the chamber length. The injection pressure required for complete wetout increases with pull speed because the resin is more rapidly swept downstream by fibers; thus, a higher injection pressure is needed to force the resin to the centerline. But for those injection pressures that are near to atmospheric pressure at different combinations of injection chamber length ($L_I$), location of injection slot ($x_{IS}$) and CR values the resin injection pressure remains about the same even when the pull speed is doubled. For the injection chamber length $L_T$ = 0.15 m, in cases A1, A4, A5, A7, and A8 and for the injection chamber length $L_T$ = 0.2 m, in cases A13, A14, A16, and A17, the injection pressure remains just above atmospheric pressure. Similarly, for the injection chamber length $L_T$ = 0.30 m, in cases A20, A24, A25, A28, A29, and A30, the injection pressure remains just above atmospheric pressure. For all the above cases the injection pressure is not impacted even when the pull speed is doubled; however, the associated maximum pressure for both the attached-die and detached-die configurations are approximately doubled when the pull speed is doubled for all cases as observed in in Table 4-2. However, for case A12, even though the maximum pressures for both the attached-die and detached-die configurations are the same as the injection pressure, they are doubled when the pull speed is doubled as observed in case B12 of Table 4-2. In case A30, the maximum interior pressure for the attached-die configuration doubled when the pull speed is doubled; however, the maximum pressure for the detached-die configuration remains approximately the same value as observed in case B30 of Table 4-2.

Figures 4-1 through 4-6 show the impact of injection slot location ($x_{IS}$) for different chamber lengths ($L_T$) on the minimum injection pressure required to achieve complete wetout along with the associated maximum interior chamber resin pressure of the attached-die and

detached-die configurations. Figures 4-1, 4-2 and 4-3 are for a pull speed of 0.0254 m/s at CR values 2, 3 and 4 respectively and Fig. 4-4, Fig. 4-5 and Fig. 4.6 are for a pull speed of 0.0508 m/s at CR values 2, 3 and 4 respectively. In these figures the gauge pressures are non-dimensionalized by taking atmospheric pressure $P_o$ = 0.1013 MPa as a reference pressure. The lower horizontal line corresponds to $P$ = 0.42 MPa and the upper horizontal line corresponds to $P$ = 2.07 MPa represent the limits for the acceptable manufacturing solutions for the resin injection pressure and maximum chamber wall pressure. To be an acceptable pultrusion manufacturing solution, both the maximum chamber wall pressure must be below the upper horizontal line and the minimum injection pressure to achieve complete wetout must be below the lower horizontal line simultaneously.

From Figs. 4-1 through 4-6, it can be seen that for the particular value of CR, the maximum pressure for the attached-die and detached-die configurations decreases when the injection slot is moved downstream from $x_{IS}$ = 0.40 $L_I$ to 0.80 $L_I$. The injection pressure generally increases when the injection slot is moved downstream in the injection chamber; for an injection slot located at upstream and for higher CR values the injection pressure values are approximately 0.002 MPa which is just above atmospheric gauge pressure and hence difficult to see in the figures. From Figs 4-1 through 4-6, the maximum chamber wall pressure between the attached-die and detached-die configurations can also be compared. It is observed that the maximum interior chamber wall pressure for the attached-die configuration is always higher than the detached-die configuration.

In Figs. 4-1 and 4-4, for CR value 2 and pull speeds of 0.0254 m/s and 0.0508 m/s, respectively, it can be observed that the injection pressure remains essentially same at the same

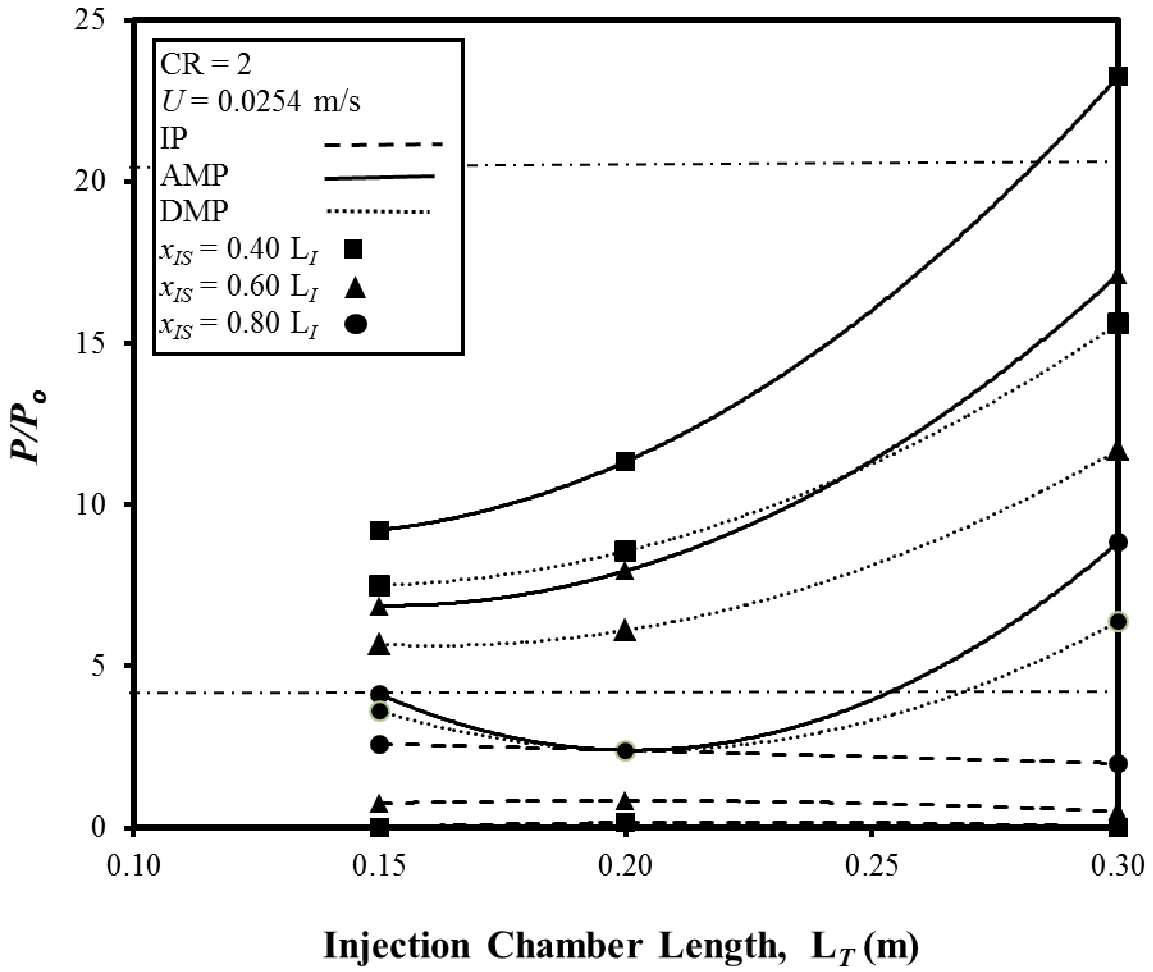


**Figure 4-1. Injection Pressure (IP) and Attached Maximum Pressure (AMP) and Detached Maximum Pressure (DMP) for Different Injection Chamber Lengths and Different Injection Slot Locations at CR = 2, $U$ = 0.0254 m/s, $H_D$ = 0.003175 m, $W_D$ = 0.0635 m, $V_{fo}$ = 0.68, $\mu$ = 0.75 Pa·s.**

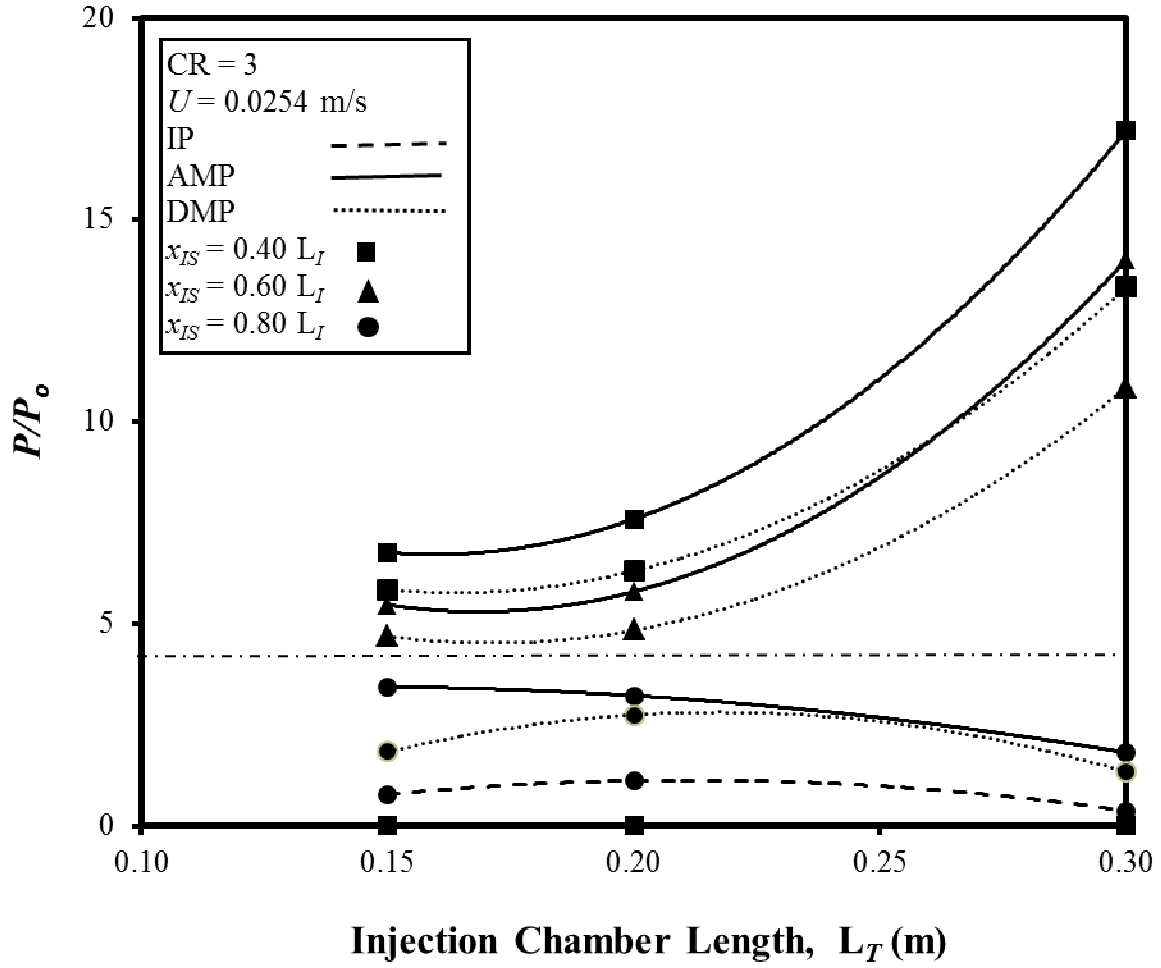


**Figure 4-2. Injection Pressure (IP) and Attached Maximum Pressure (AMP) and Detached Maximum Pressure (DMP) for Different Injection Chamber Lengths and Different Injection Slot Locations at CR = 3, $U$ = 0.0254 m/s, $H_D$ = 0.003175 m, $W_D$ = 0.0635 m, $V_{fo}$ = 0.68, $\mu$ = 0.75 Pa·s.**

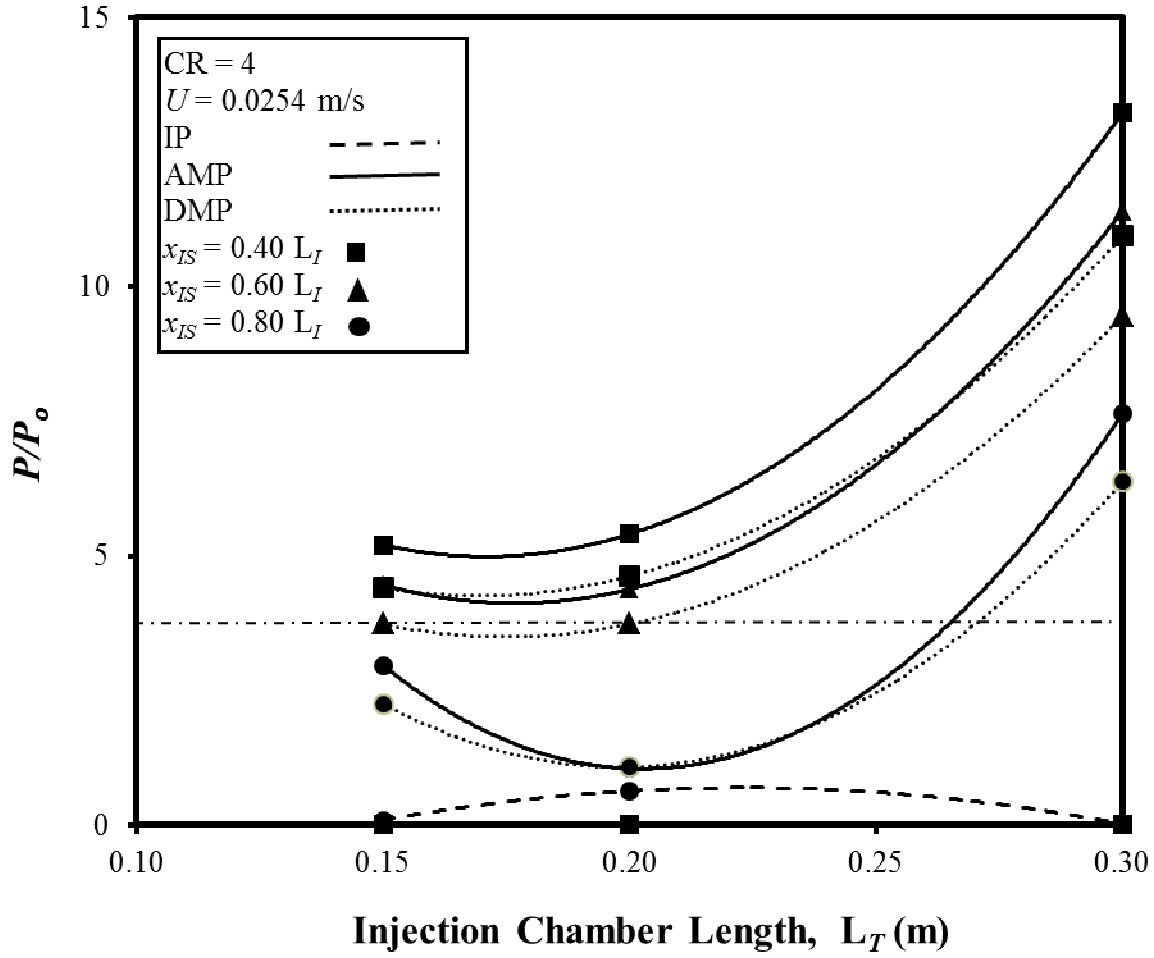


**Figure 4-3. Injection Pressure (IP) and Attached Maximum Pressure (AMP) and Detached Maximum Pressure (DMP) for Different Injection Chamber Lengths and Different Injection Slot Locations at CR = 4, $U$ = 0.0254 m/s, $H_D$ = 0.003175 m, $W_D$ = 0.0635 m, $V_{fo}$ = 0.68, $\mu$ = 0.75 Pa·s.**

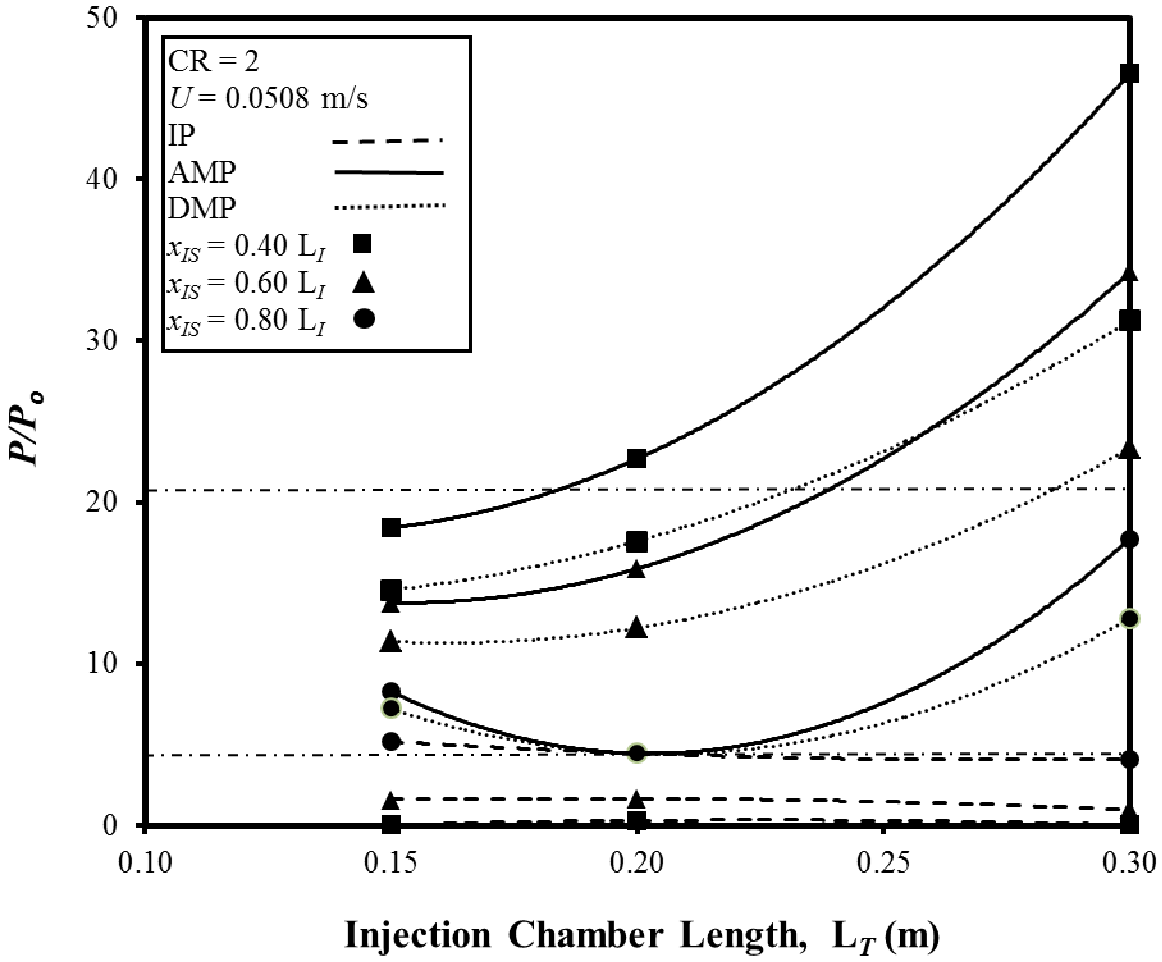


**Figure 4-4. Injection Pressure (IP) and Attached Maximum Pressure (AMP) and Detached Maximum Pressure (DMP) for Different Injection Chamber Lengths and Different Injection Slot Locations at CR = 2, $U$ = 0.0508 m/s, $H_D$ = 0.003175 m, $W_D$ = 0.0635 m, $V_{fo}$ = 0.68, $\mu$ = 0.75 Pa·s.**

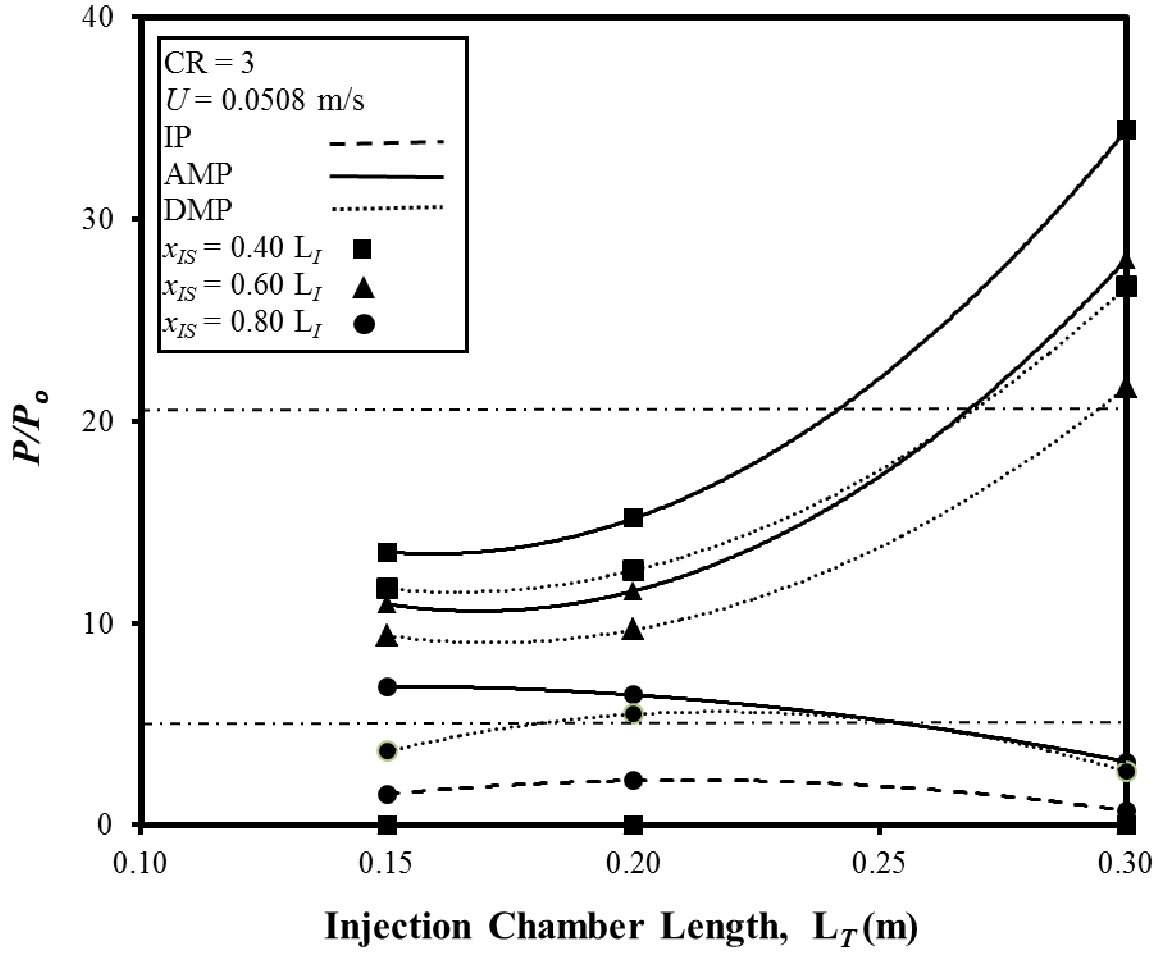


**Figure 4-5. Injection Pressure (IP) and Attached Maximum Pressure (AMP) and Detached Maximum Pressure (DMP) for Different Injection Chamber Lengths and Different Injection Slot Locations at CR = 3, $U$ = 0.0508 m/s, $H_D$ = 0.003175 m, $W_D$ = 0.0635 m, $V_{fo}$ = 0.68, $\mu$ = 0.75 Pa·s.**

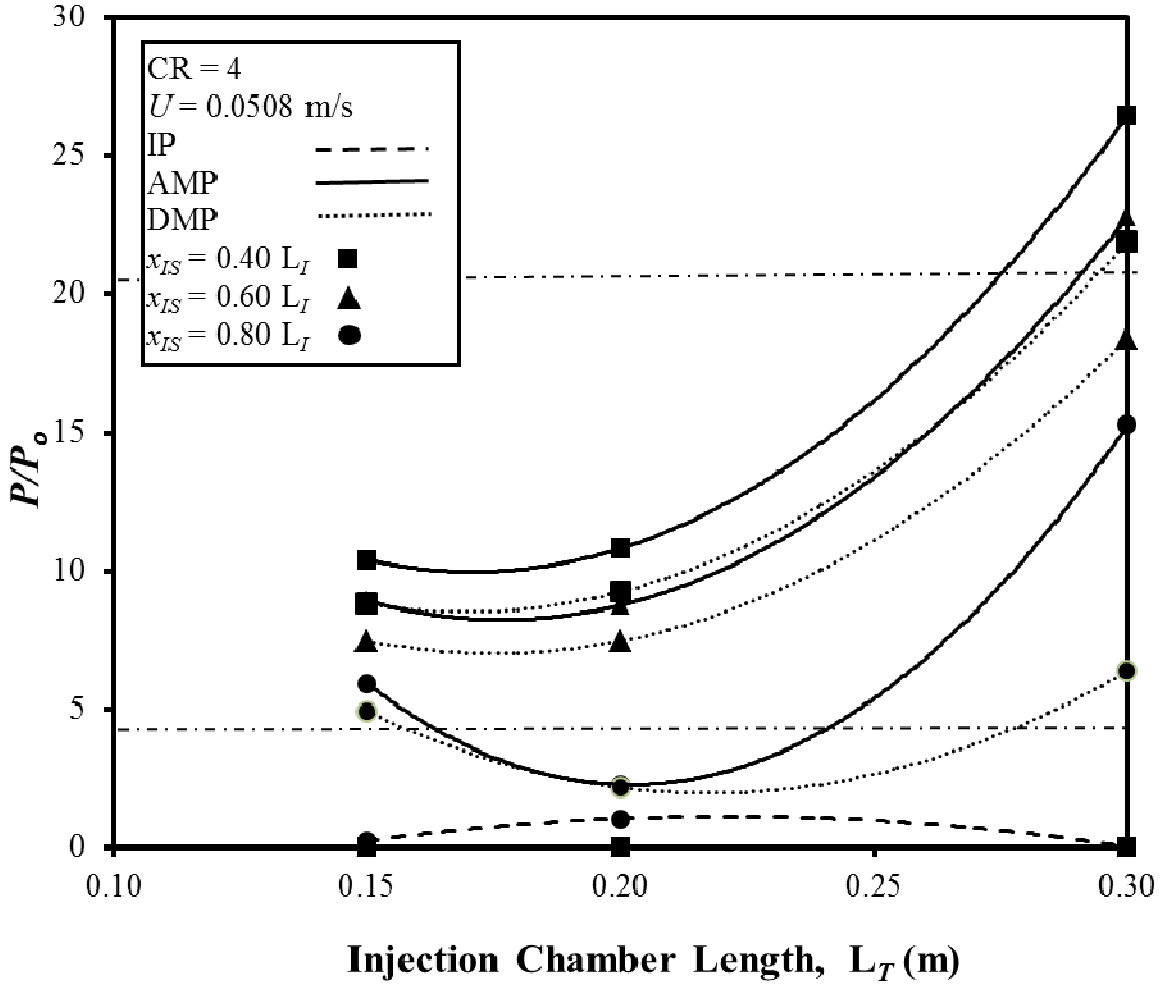


**Figure 4-6. Injection Pressure (IP), Attached Maximum Pressure (AMP) and Detached Maximum Pressure (DMP) for Different Injection Chamber Lengths and Different Injection Slot Locations at CR = 4, $U$ = 0.0508 m/s, $H_D$ = 0.003175 m, $W_D$ = 0.0635 m, $V_{fo}$ = 0.68, $\mu$ = 0.75 Pa·s.**

proportional location of the injection slot ($x_{IS}$) in the injection chamber even though the length of the injection chamber ($L_T$) is increased. The maximum interior pressure for both the attached-die and detached-die configurations increases with an increase of the injection chamber length ($L_T$) for the injection slot location at 0.40 $L_I$ and 0.60 $L_I$; whereas, for injection slot at location 0.80 $L_I$, the maximum pressure for both the attached-die and detached-die configurations first decreases when the length of the injection chamber ($L_T$) increases from 0.15 m to 0.20 m and then again increases when the length is increased from 0.20 m to 0.30 m. In Fig. 4-2 and 4-5, for CR value 3 and pull speeds of 0.0254 m/s and 0.0508 m/s, respectively, and in Figs. 4-3 and 4-6, for CR value 4 and pull speeds of 0.0254 m/s and 0.0508 m/s, respectively, the maximum interior chamber wall pressure behavior for both the attached-die and detached-die configurations, for the location of injection slot ($x_{IS}$) at 0.40 $L_I$ and 0.60 $L_I$, remain almost the same when the length of the injection chamber ($L_T$) increases from 0.15 m to 0.20 m and then both increase when the length of the injection chamber is increased from 0.20 m to 0.30 m. For an injection slot location $x_{IS}$ = 0.80 $L_I$, as observed in Fig. 4-2 and 4-5, for CR = 3, the maximum interior pressure for the attached-die configuration decreases when the length of the injection chamber increases; whereas the maximum pressure for the detached-die configuration increases when the length of the injection chamber ($L_T$) increases from 0.15 m to 0.20 m and then decreases when the length of the injection chamber is increased to 0.30 m. However, when the location of injection slot ($x_{IS}$) is at 0.80 $L_I$ for CR value 4 (Fig. 4-3 and Fig 4-6), the maximum interior chamber wall pressure for the both configurations follows the same trend as observed in Fig. 4-1 and 4-3, in which the maximum chamber wall pressure decreases with increase of the chamber length ($L_T$) from 0.15 m to 0.20 m and then increases with an increase of the chamber length ($L_T$) from 0.20 m to 0.30 m. The injection pressures in Figs. 4-2, 4-3, 4-5 and 4-6 follow

the same behavior; in which the injection pressures for the location of the injection slot ($x_{IS}$) at 0.40 $L_I$ and 0.60 $L_I$ are slightly above atmospheric pressure; whereas, for the location of the injection slot ($x_{IS}$) at 0.80 $L_I$, the injection pressure tends to increase slightly when the length of the injection chamber ($L_T$) is 0.20 m and again decreases when the length of the injection chamber ($L_T$) is increased to 0.30 m; which is more discernable in Figs. 4-3 and 4-6. Hence from Figs 4-1 through 4-6 it can be observed that for the particular value of CR, location of injection slot ($x_{IS}$), and length of the injection chamber ($L_T$), the general behavior of the injection pressure and maximum chamber wall pressure of both the attached-die and detached-configurations remain same even when the speed is doubled from 0.0254 m/s to 0.0508 m/s. However, it can be observed from Figs. 4-4, 4-5 and 4-6 that, with the pull speed doubled at large chamber lengths ($L_T$), the chamber wall pressure rises into the non-feasible region above the upper horizontal line corresponding to 2.07 MPa.

Figures 4-7, 4-8, 4-9 ($U$ = 0.0254 m/s) through 4-10, 4-11, 4-12 ($U$ = 0.0508m/s) through 4-12 are presented to show the chamber wall resin pressure profiles inside the injection chamber of both the attached-die and detached-die configurations for different axial locations of the injection slot ($x_{IS}$ = 0.40 $L_I$, 0.60 $L_I$ and 0.80 $L_I$) for the various lengths ($L_T$ = 0.15 m, 0.20 m and 0.30 m) of the injection chamber with CR = 3. Figures 4-7 to 4-8 are for the pull speed of 0.0254 m/s and Figs. 4-10 to 4-12 are for the pull speed of 0.0508 m/s. These figures illustrate the differences in the chamber wall pressure profile progression inside the chamber for both the attached-die and the detached-die configuration. From Figs. 4-7 through 4-12, it can observed that, for a given axial location of the injection slot ($x_{IS}$), the chamber wall pressure of the attached-die configuration rises at the location of the injection slot and continues to rise and reaches a maximum gauge pressure value at the beginning of Region II and remains level to the

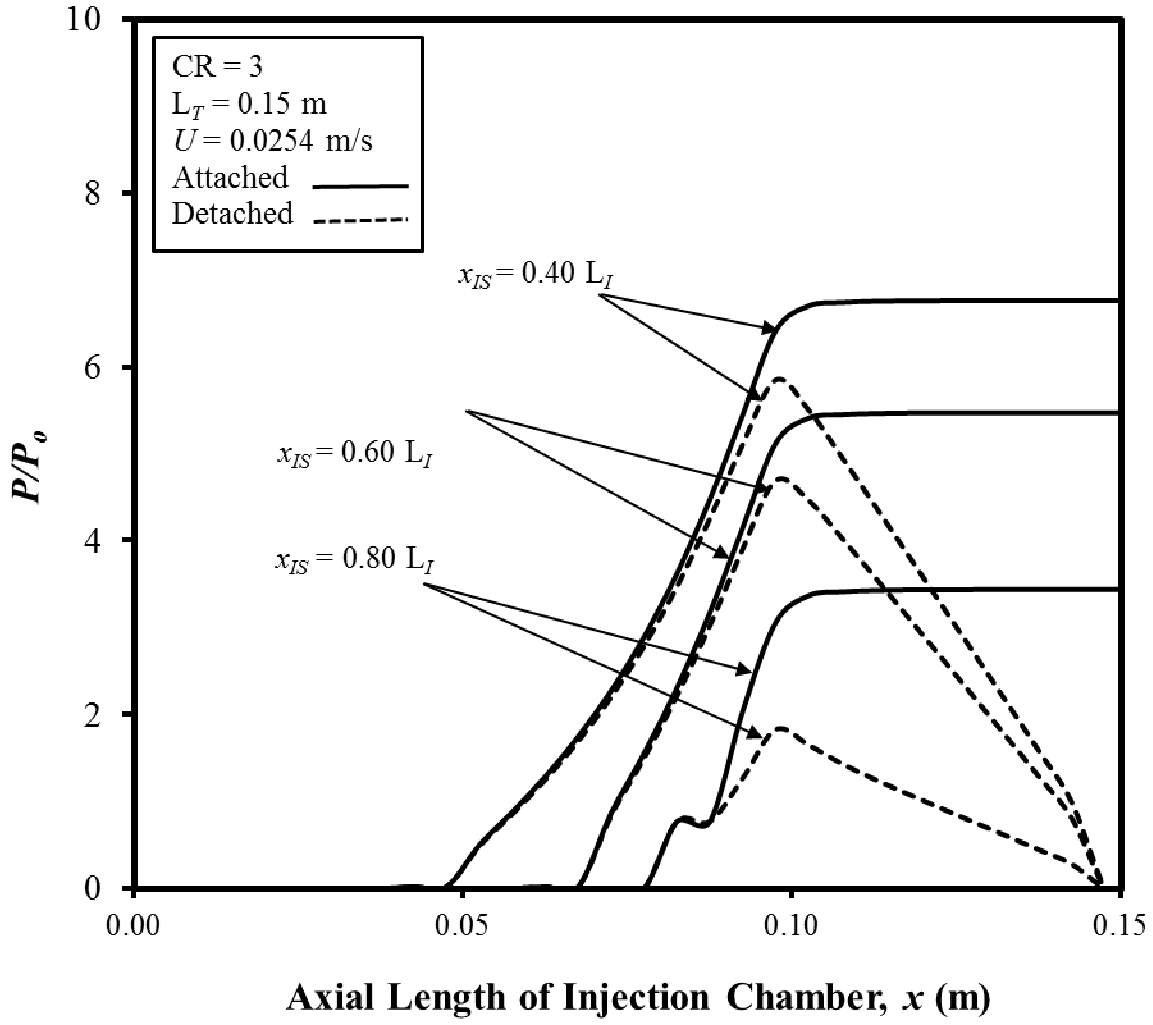


**Figure 4-7. Chamber Wall Axial Pressure Profiles for Attached-Die and Detached-Die Configurations for Injection Chamber Length of $L_T$ = 0.15 m, CR = 3, and $U$ = 0.0254 m/s at Different Injection Slot Locations ($x_{IS}$).**

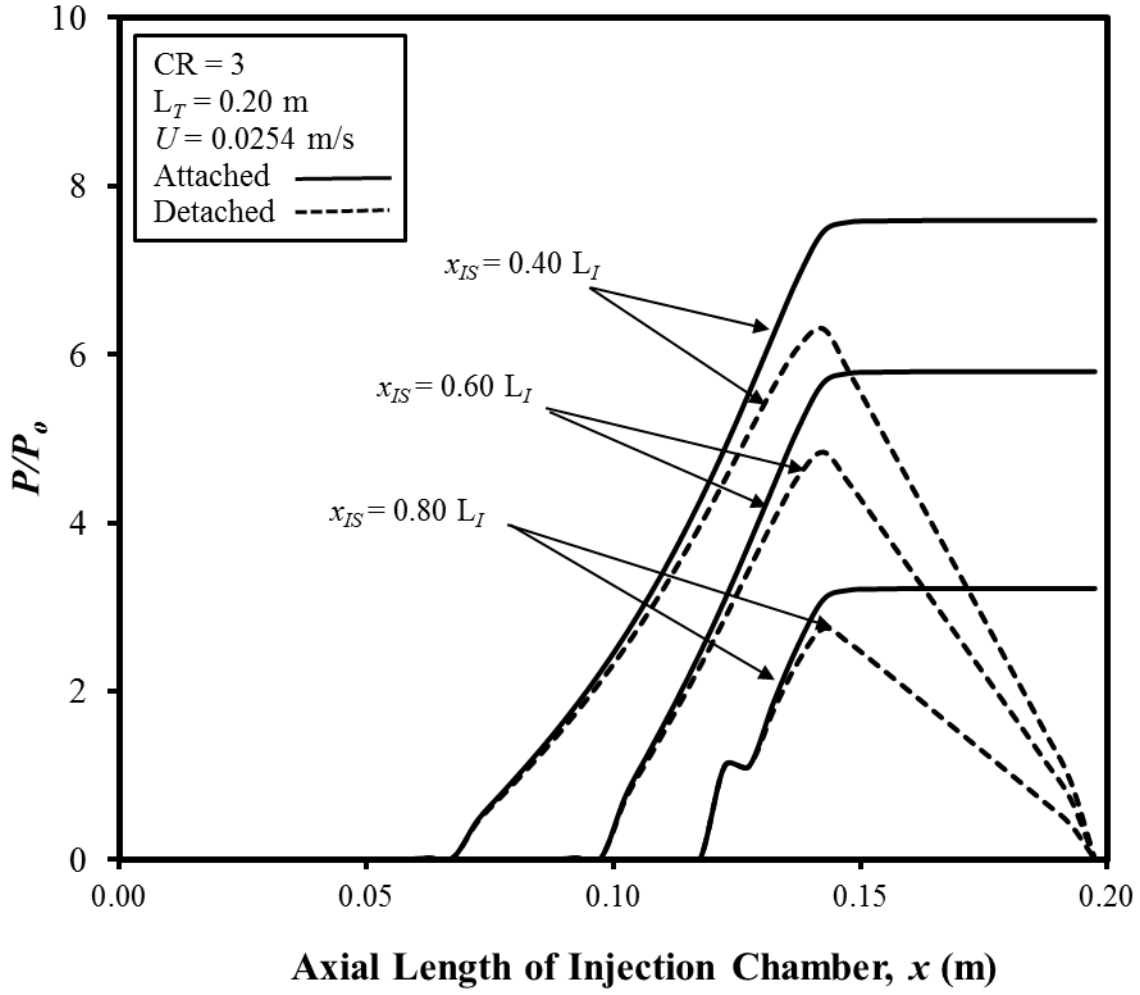


**Figure 4-8. Chamber Wall Axial Pressure Profiles for CR = 3 and $U$ = 0.0254 m/s at Different Injection Locations ($x_{IS}$).**

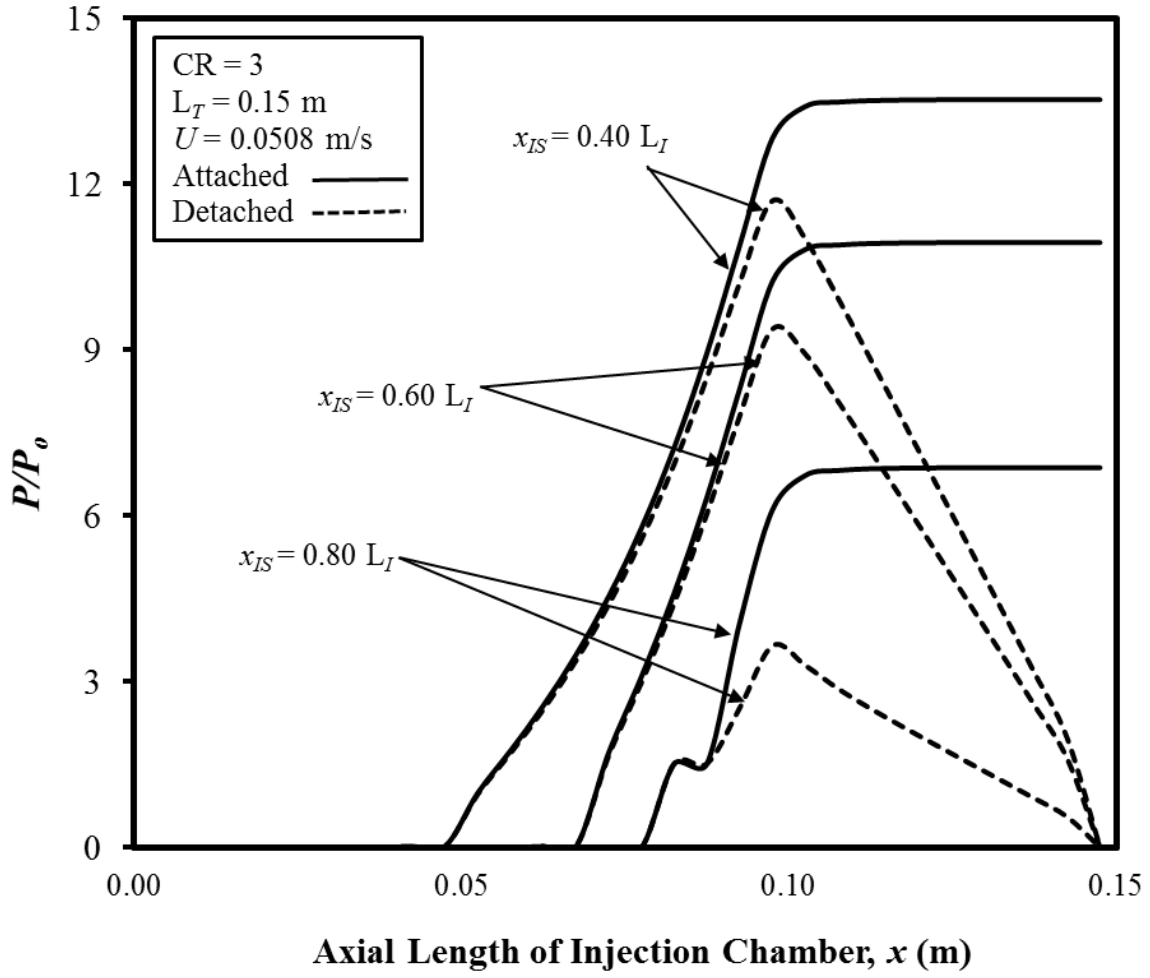


**Figure 4-9. Die Wall Axial Pressure Profiles for CR = 3.0 and $U$ = 0.0254 m/s at Different Injection Locations ($x_{IS}$).**

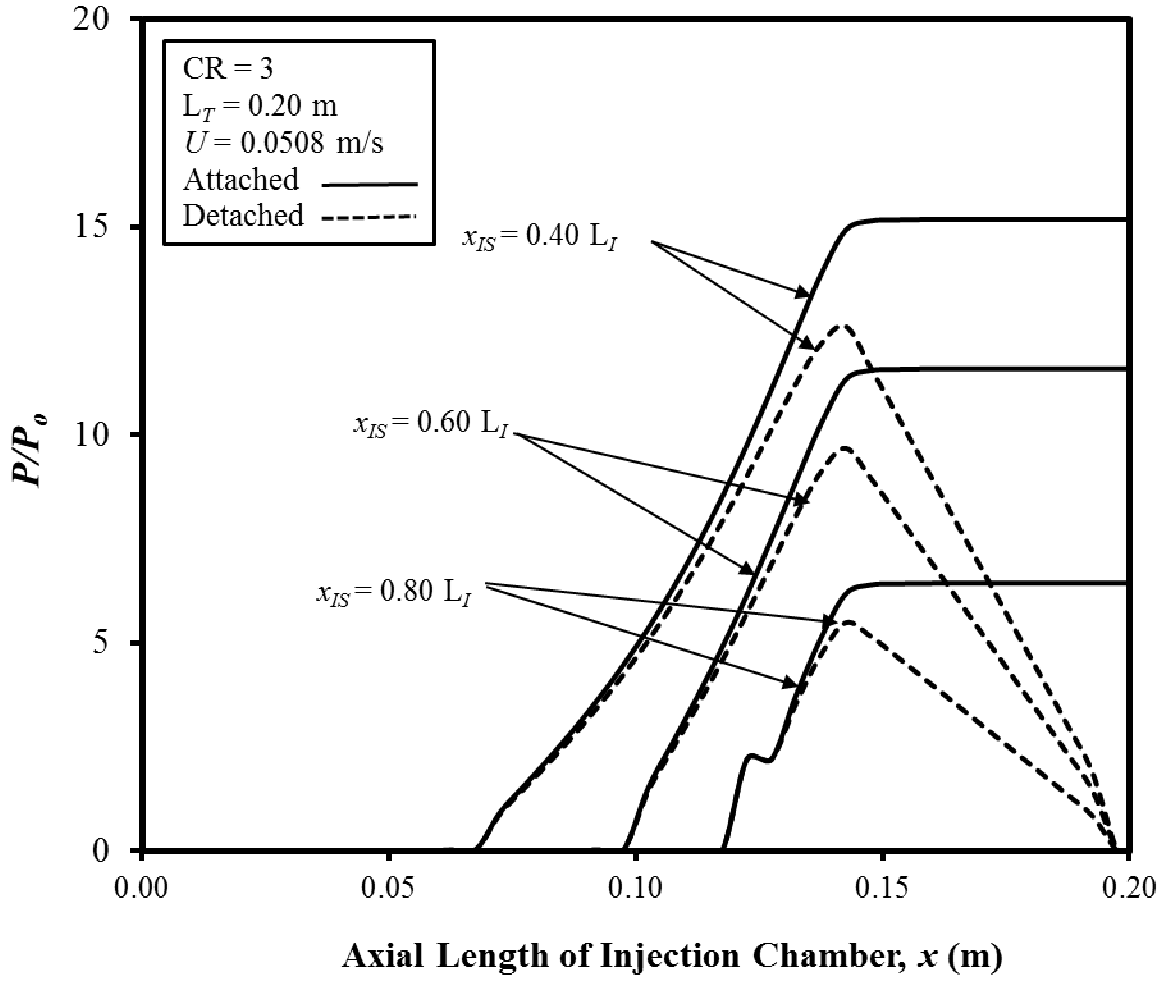


**Figure 4-10. Die Wall Axial Pressure Profiles for CR = 3.0 and U = 0.0508 m/s at Different Injection Locations ($x_{IS}$).**

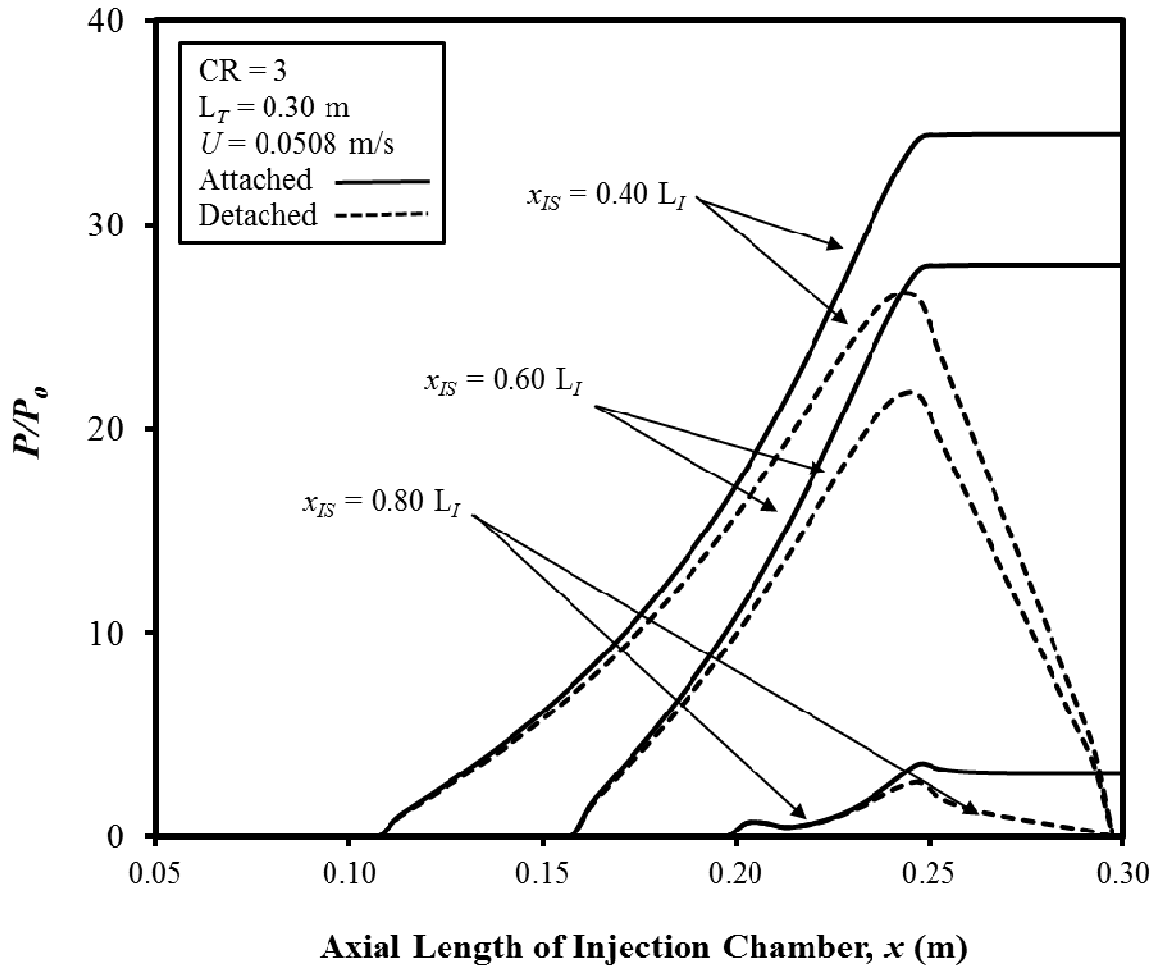


**Figure 4-11. Chamber Wall Axial Pressure Profiles for CR = 3.0 and U = 0.0508 m/s at Different Injection Locations ($x_{IS}$).**

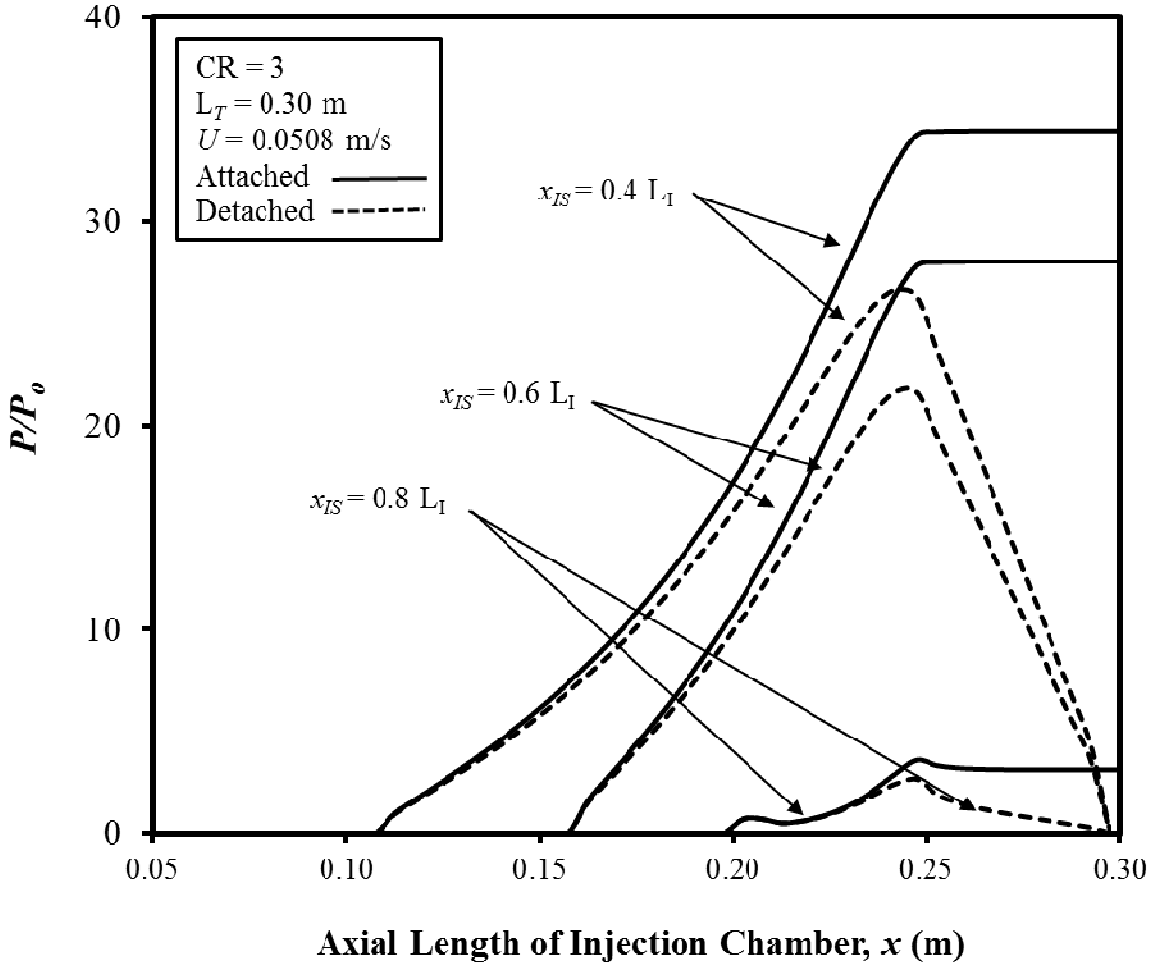


**Figure 4-12. Chamber Wall Axial Pressure Profiles for CR = 3.0 and U = 0.0508 m/s at Different Injection Locations ($x_{IS}$).**

chamber exit; whereas, for the detached-die configuration the pressure rises to a maximum gauge pressure and then decreases to zero gauge pressure at the chamber exit gap. There is a slight change in behavior for the axial location of the injection slot at 0.80 $L_I$, as observed in Figs. 4-7 through 4-12. From Figs. 4-7 through 4-12, it is observed that, for the location of injection slot at 0.80 $L_I$, in attached-die configuration, the chamber wall pressure increases to the injection pressure then decreases slightly after the injection port and again increases to a maximum value and then remains constant to the chamber exit; whereas, in detached-die configuration, the chamber wall pressure increases to injection pressure then decreases slightly after the injection port and again increases to maximum value and then decreases to zero gauge pressure at the chamber exit gap. From Figs. 4-7 through 4-12, it is illustrated that, as the length of the injection chamber increases, the maximum interior chamber wall pressure values for the both attached-die and detached-die configurations increase, and it can also be observed that when the location of the injection slot ($x_{IS}$) is upstream the maximum wall pressure is greater than when the location of the injection slot ($x_{IS}$) is downstream in the injection chamber. For the same proportional location, the general behavior of the wall pressure is observed to be about same when the pull speed is increased from 0.0254 m/s to 0.0508 m/s, but the maximum pressure is observed to be significantly increased when the pull speed is doubled.

Figures 4-13 through 4-15 show the steady-state liquid resin flow front and the isopressure contours within the liquid resin wetout region at CR = 4 with the injection slot location at 0.40 $L_I$ (Fig. 4-13), 0.60 $L_I$ (Fig. 4-14) and 0.80 $L_I$ (Fig. 4-15) of Region I ($L_I$) and pull speed of 0.0254 m/s for $L_T$ = 0.15 m. Figure 4-16 shows the steady-state liquid resin flow front and the isopressure contours within the liquid resin wetout region and for CR = 4, $x_{IS}$ = 0.60 $L_I$ for $L_T$ = 0.30 m and $U$ = 0.0254 m/s. The first dark contour represents the liquid resin flow

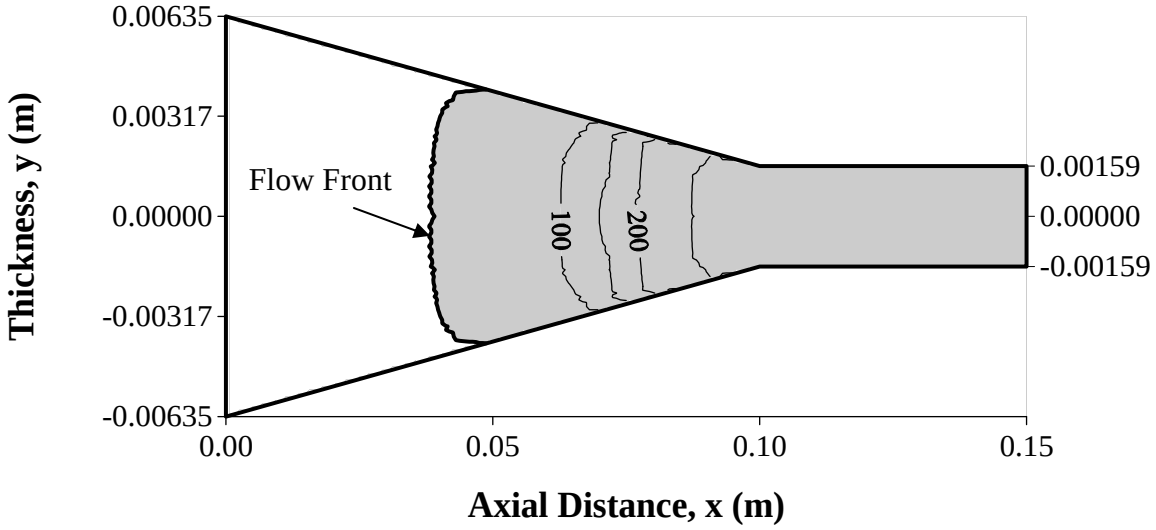


**a. Attached Die Configuration**

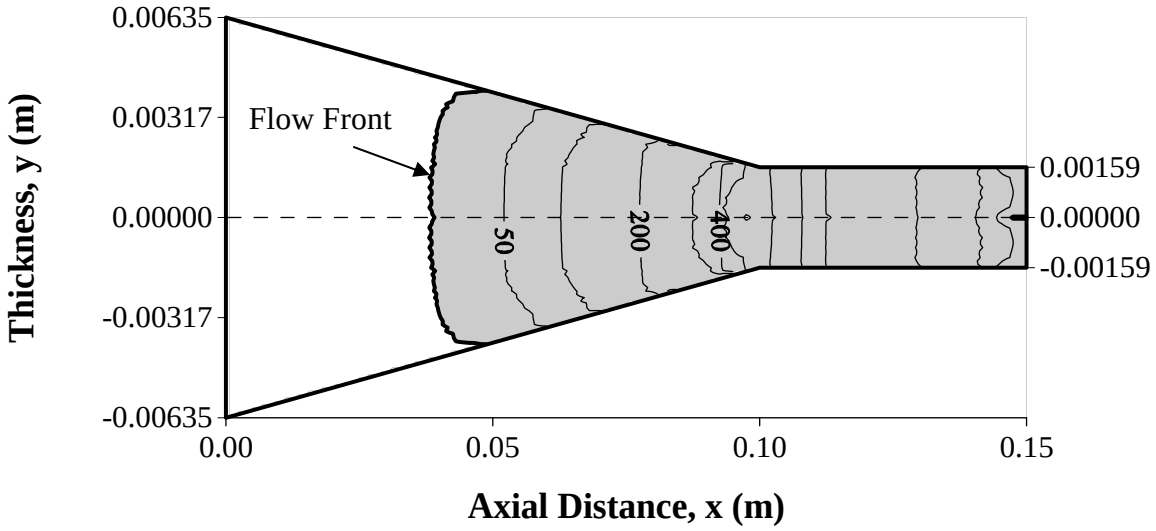


**b. Detached Die configuration**

**Figure 4-13. Flow Front Profile and Gauge Isopresure (KPa) Contours for Case A7, Table 4-1 for $L_T$ = 0.15 m, $x_{IS}$ = 0.4 $L_I$, CR = 4, $V_{fo}$ = 0.68, μ = 0.75 Pa.s with $U$ = 0.0254 m/s (Not to Scale).**

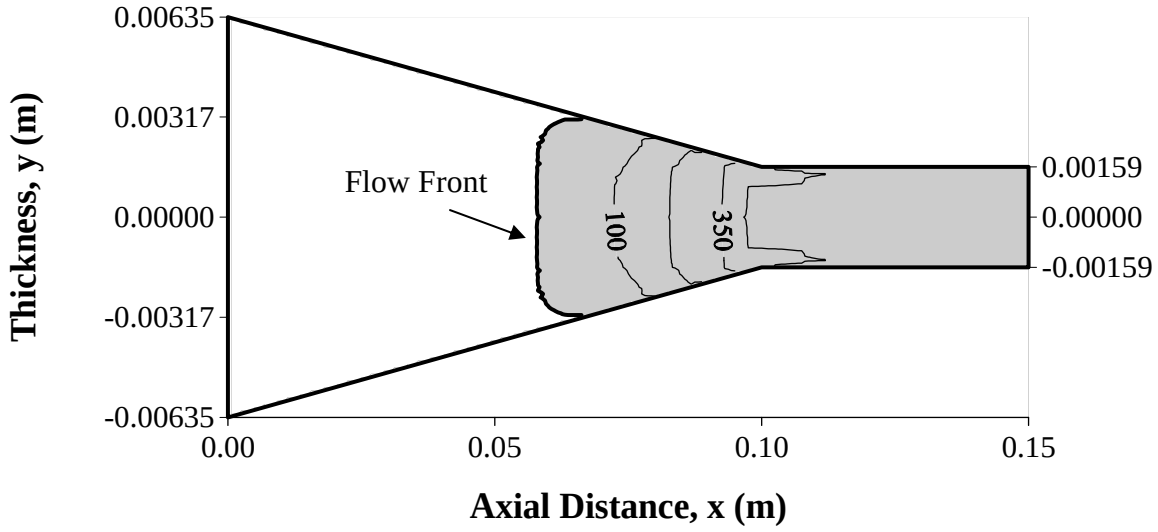


**a. Attached Die Configuration**

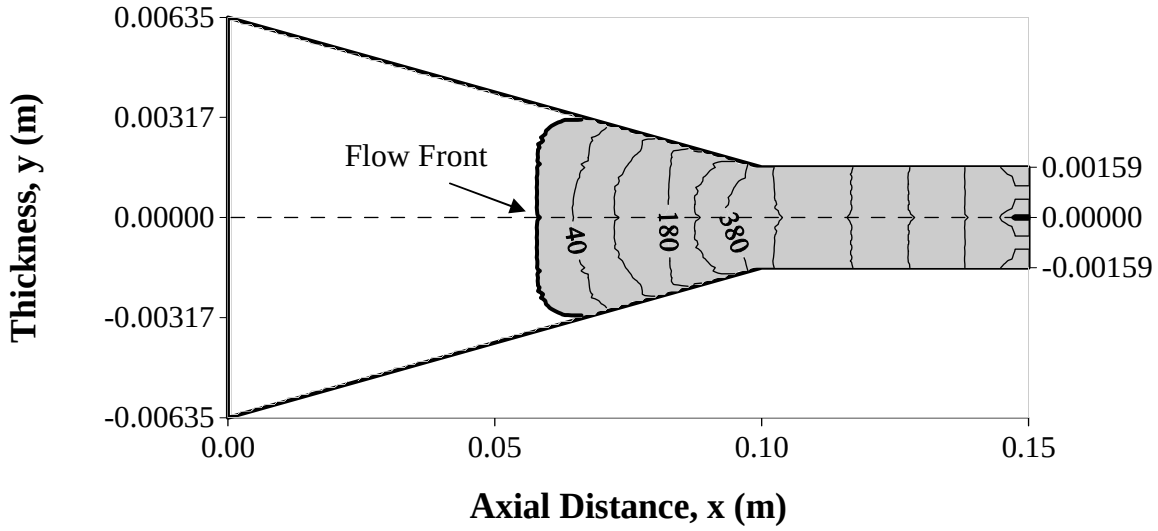


**b. Detached Die Configuration**

**Figure 4-14. Flow Front Profile and Gauge Isopresure (KPa) Contours for Case A8, Table 4-1 for $L_T$ = 0.15 m, $x_{IS}$ = 0.6 $L_I$, CR = 4, $V_{fo}$ = 0.68, μ = 0.75 Pa.s with $U$ = 0.0254 m/s (Not to Scale).**

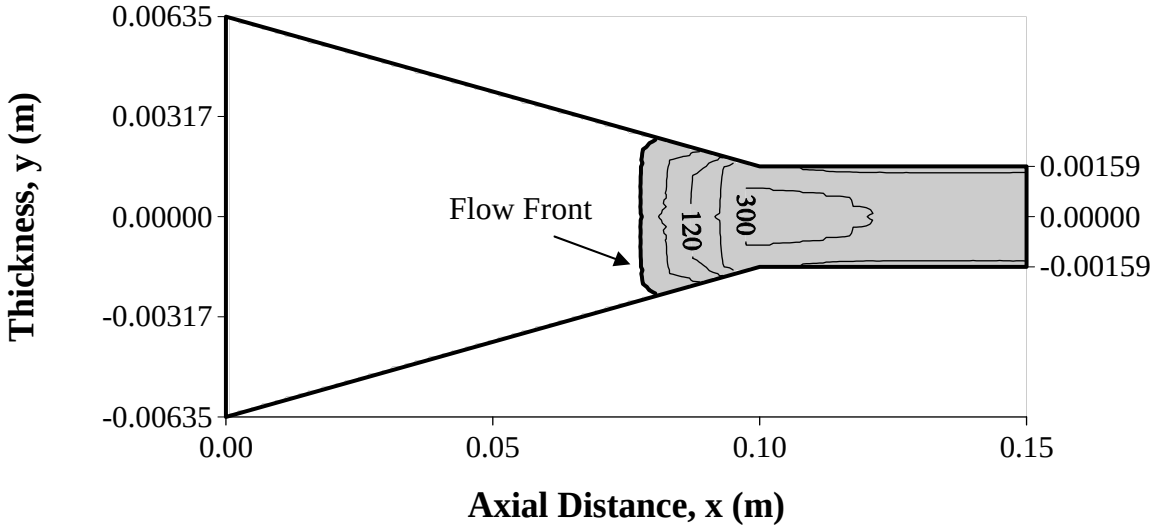


**a. Attached Die Configuration**

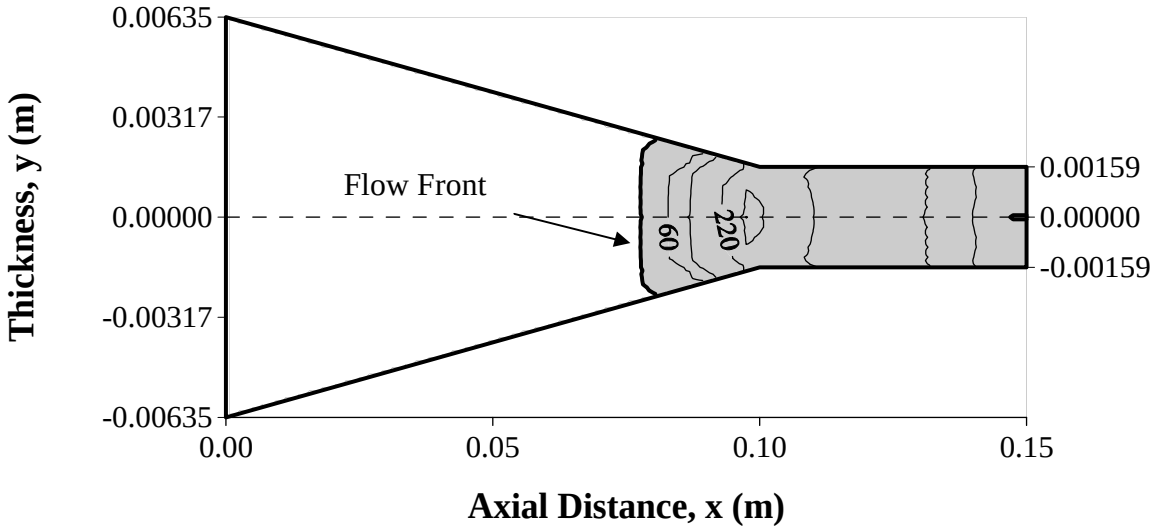


**b. Detached Die Configuration**

**Figure 4-15. Flow Front Profile and Gauge Isopresure (KPa) Contours for Case A9, Table 4-1 for $L_T$ = 0.15 m, $x_{IS}$ = 0.8 $L_I$, CR = 4, $V_{fo}$ = 0.68, μ = 0.75 Pa.s with $U$ = 0.0254 m/s (Not to Scale).**

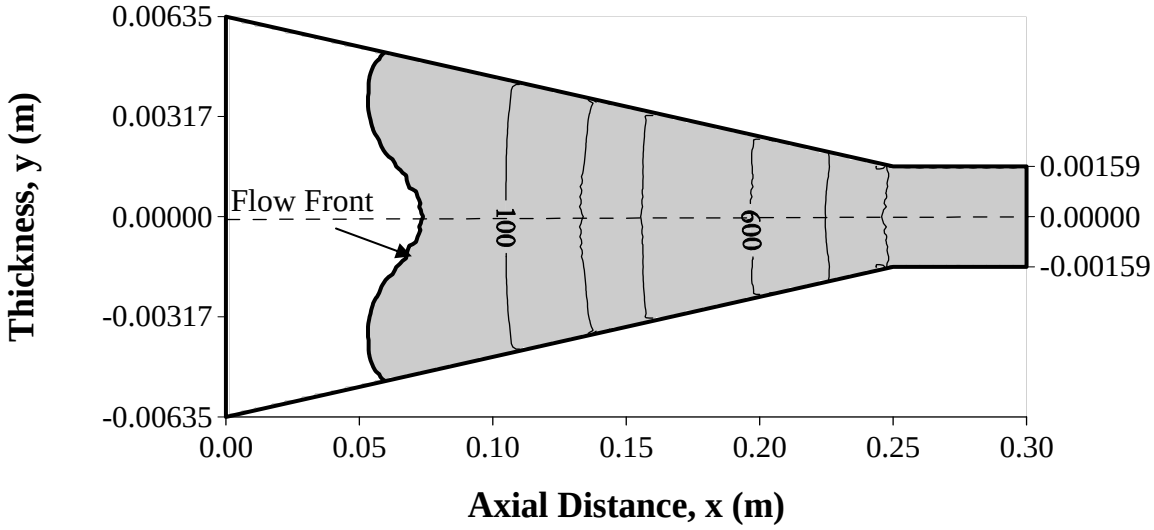


**a. Attached Die Configuration**

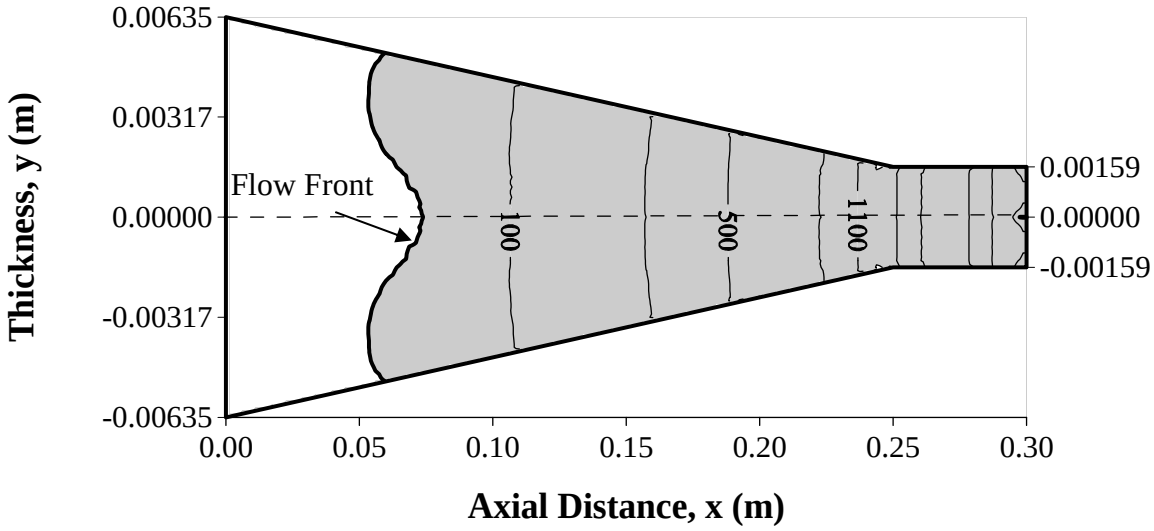


**b. Detached Die Configuration**

**Figure 4-16. Flow Front Profile and Gauge Isopresure (kPa) Contours for Case A27, Table 4-1 for $L_T$ = 0.30 m, $x_{IS}$ = 0.6 $L_I$, CR = 4, $V_{fo}$ = 0.68, μ = 0.75 Pa.s with $U$ = 0.0254 m/s (Not to Scale).**

front and the thin contour lines represent the isopressure curves in kPa. The resin flow front and the pressure values for the attached-die and the detached-die configurations can be readily compared from these figures. The chamber pressure values are always lower for the detached-die configuration system as compared to the attached-die configuration which can be observed from Figs. 4-13 through 4-15. In the detached–die configuration, the isopressure contour can be seen in Region II of the injection chamber due to the decreasing chamber pressure in the Region II and this pressure corresponds to the same pressure contours as depicted in Region I of the injection chamber. Figures 4-13 through 4-16 are displayed not to scale; this was done in order to make the results more viewable and understandable.

### *4. 2 Width of the single injection slot*

In this section, the impact of the injection slot width ($\Delta x$) on the injection pressure necessary to achieve complete wetout of the fiber reinforcement as well as the corresponding maximum resin pressure inside the injection chamber was studied for both the attached-die and detached-die configurations. The study was carried out for the single injection slot width ($\Delta x$) of 0.005 m, 0.010 m and 0.015 m, placed at 60% of the axial distance ($x_{IS}$ = 0.60 $L_I$) for total injection chamber lengths ($L_T$) of 0.15 m, 0.20 m and 0.30 m at compression ratios of 2, 3 and 4 and compared at two different pull speeds, $U$ = 0.0254 m/s and 0.0508 m/s. For a particular slot width the other parameters were hold at their nominal values. Tables 4-3 and 4-4 show the impact of single injection slot width for the pull speeds 0.0254 m/s (Table 4-3) and 0.0508 m/s (Table 4-4) respectively. In Tables 4-3 and 4-4, the minimum injection pressure required for the complete wetout of the reinforcement fiber for both the attached-die and detached-die configurations is shown in column 6 and the corresponding maximum chamber wall pressure are shown in columns 7 and 8 respectively. In Table 4-3 and Table 4-4 the bolded pressure values are unsuitable for commercial pultrusion manufacturing since these values do not satisfy the feasible manufacturing pressure range of the resin injection pressure not being greater than 0.42 MPa (60 psi), and for the resin maximum chamber pressure not being greater than 2.07 MPa (300 psi).

From Tables 4-3 and 4-4 it is observed that when the width of the injection slot ($\Delta x$) is increased with its location at location $x_{IS}$ = 0.60 $L_I$ and for all other parameters fixed, the injection pressure decreases. Similarly, the corresponding maximum chamber wall pressure inside the injection chamber of both the attached-die and detached-die configurations decreases with an

**Table 4-3. Minimum Injection Pressure Required for Complete Wetout for a Single Slot Placed at 60 % of Region I ($L_I$) for Different Slot Widths with $U$ = 0.0254 m/s, $V_{fo}$ = 0.68, $\mu$ = 0.75 Pa·s, $H_D$ = 0.003175 m, $W_D$ = 0.0635 m.**

| Case* | CR | Slot Width ($\Delta x$) (m) | Total Length ($L_T$) (m) | Location of Injection Slot ($x_{IS}$) (m) | Minimum Injection Pressure (Gauge) (MPa) | Maximum Pressure (Gauge) (MPa) | Maximum Pressure (Gauge) (MPa) |
|---|---|---|---|---|---|---|---|
| | | | | | | Attached | Detached |
| C1 | 2 | 0.005 | 0.15 | 0.06 | 0.099 | 0.73 | 0.60 |
| C2 | 2 | 0.010 | 0.15 | 0.06 | 0.077 | 0.70 | 0.58 |
| C3 | 2 | 0.015 | 0.15 | 0.06 | 0.065 | 0.64 | 0.53 |
| C4 | 3 | 0.005 | 0.15 | 0.06 | 0.002 | 0.57 | 0.49 |
| C5 | 3 | 0.010 | 0.15 | 0.06 | 0.002 | 0.55 | 0.48 |
| C6 | 3 | 0.015 | 0.15 | 0.06 | 0.002 | 0.53 | 0.45 |
| C7 | 4 | 0.005 | 0.15 | 0.06 | 0.002 | 0.46 | 0.38 |
| C8 | 4 | 0.010 | 0.15 | 0.06 | 0.002 | 0.45 | 0.38 |
| C9 | 4 | 0.015 | 0.15 | 0.06 | 0.002 | 0.44 | 0.37 |
| C10 | 2 | 0.005 | 0.2 | 0.09 | 0.113 | 0.84 | 0.64 |
| C11 | 2 | 0.010 | 0.2 | 0.09 | 0.085 | 0.81 | 0.62 |
| C12 | 2 | 0.015 | 0.2 | 0.09 | 0.064 | 0.75 | 0.56 |
| C13 | 3 | 0.005 | 0.2 | 0.09 | 0.002 | 0.60 | 0.50 |
| C14 | 3 | 0.010 | 0.2 | 0.09 | 0.002 | 0.59 | 0.49 |
| C15 | 3 | 0.015 | 0.2 | 0.09 | 0.002 | 0.56 | 0.46 |
| C16 | 4 | 0.005 | 0.2 | 0.09 | 0.002 | 0.45 | 0.38 |
| C17 | 4 | 0.010 | 0.2 | 0.09 | 0.002 | 0.44 | 0.38 |
| C18 | 4 | 0.015 | 0.2 | 0.09 | 0.002 | 0.43 | 0.37 |
| C19 | 2 | 0.005 | 0.3 | 0.15 | 0.099 | 1.78 | 1.22 |
| C20 | 2 | 0.010 | 0.3 | 0.15 | 0.051 | 1.74 | 1.19 |
| C21 | 2 | 0.015 | 0.3 | 0.15 | 0.044 | 1.65 | 1.13 |
| C22 | 3 | 0.005 | 0.3 | 0.15 | 0.002 | 1.44 | 1.11 |
| C23 | 3 | 0.010 | 0.3 | 0.15 | 0.002 | 1.42 | 1.10 |
| C24 | 3 | 0.015 | 0.3 | 0.15 | 0.002 | 1.39 | 1.07 |
| C25 | 4 | 0.005 | 0.3 | 0.15 | 0.002 | 1.16 | 0.96 |
| C26 | 4 | 0.010 | 0.3 | 0.15 | 0.002 | 1.16 | 0.96 |
| C27 | 4 | 0.015 | 0.3 | 0.15 | 0.002 | 1.14 | 0.95 |

* Bold font indicates non-acceptable manufacturing solutions for an injection pressure ≥ 0.42 MPa (60 psi) and/or with an associated maximum pressure for attached or detached ≥ 2.07 MPa (300 psi).

**Table 4-4. Minimum Injection Pressure Required for Complete Wetout for a Single Slot Placed at 60 % of Region I ($L_I$) for Different Slot Widths with $U$ = 0.0508 m/s, $V_{fo}$ = 0.68, $\mu$ = 0.75 Pa·s, $H_D$ = 0.003175 m, $W_D$ = 0.0635 m.**

| Case* | CR | Slot Width ($\Delta x$) (m) | Total Length ($L_T$) (m) | Location of Injection Slot ($x_{IS}$) (m) | Injection Pressure (Gauge) (MPa) | Exit Pressure (Gauge) (MPa) | Maximum Pressure (Gauge) (MPa) |
|---|---|---|---|---|---|---|---|
| | | | | | | Attached | Detached |
| D1 | 2 | 0.005 | 0.15 | 0.06 | 0.196 | 1.46 | 1.20 |
| D2 | 2 | 0.010 | 0.15 | 0.06 | 0.161 | 1.40 | 1.15 |
| D3 | 2 | 0.015 | 0.15 | 0.06 | 0.120 | 1.27 | 0.98 |
| D4 | 3 | 0.005 | 0.15 | 0.06 | 0.002 | 1.14 | 0.98 |
| D5 | 3 | 0.010 | 0.15 | 0.06 | 0.002 | 1.11 | 0.95 |
| D6 | 3 | 0.015 | 0.15 | 0.06 | 0.002 | 1.05 | 0.90 |
| D7 | 4 | 0.005 | 0.15 | 0.06 | 0.002 | 0.91 | 0.77 |
| D8 | 4 | 0.010 | 0.15 | 0.06 | 0.002 | 0.90 | 0.76 |
| D9 | 4 | 0.015 | 0.15 | 0.06 | 0.002 | 0.88 | 0.74 |
| D10 | 2 | 0.005 | 0.20 | 0.09 | 0.230 | 1.67 | 1.28 |
| D11 | 2 | 0.010 | 0.20 | 0.09 | 0.168 | 1.61 | 1.24 |
| D12 | 2 | 0.015 | 0.20 | 0.09 | 0.120 | 1.49 | 1.12 |
| D13 | 3 | 0.005 | 0.20 | 0.09 | 0.002 | 1.21 | 1.01 |
| D14 | 3 | 0.010 | 0.20 | 0.09 | 0.002 | 1.17 | 0.98 |
| D15 | 3 | 0.015 | 0.20 | 0.09 | 0.002 | 1.10 | 0.92 |
| D16 | 4 | 0.005 | 0.20 | 0.09 | 0.002 | 0.90 | 0.77 |
| D17 | 4 | 0.010 | 0.20 | 0.09 | 0.002 | 0.89 | 0.76 |
| D18 | 4 | 0.015 | 0.20 | 0.09 | 0.002 | 0.86 | 0.73 |
| D19 | 2 | 0.005 | 0.30 | 0.15 | 0.195 | **3.57** | **2.44** |
| D20 | 2 | 0.010 | 0.30 | 0.15 | 0.099 | **3.47** | **2.37** |
| D21 | 2 | 0.015 | 0.30 | 0.15 | 0.091 | **3.31** | **2.26** |
| D22 | 3 | 0.005 | 0.30 | 0.15 | 0.002 | **2.88** | **2.23** |
| D23 | 3 | 0.010 | 0.30 | 0.15 | 0.002 | **2.84** | **2.20** |
| D24 | 3 | 0.015 | 0.30 | 0.15 | 0.002 | **2.78** | **2.13** |
| D25 | 4 | 0.005 | 0.30 | 0.15 | 0.002 | **2.33** | 1.93 |
| D26 | 4 | 0.010 | 0.30 | 0.15 | 0.002 | **2.31** | 1.92 |
| D27 | 4 | 0.015 | 0.30 | 0.15 | 0.002 | **2.28** | 1.89 |

* Bold font indicates non-acceptable manufacturing solutions for an injection pressure ≥ 0.42 MPa (60 psi) and/or with an associated maximum pressure for attached or detached ≥ 2.07 MPa (300 psi).

increase of the injection slot width ($\Delta x$). This is because for a wider injection slot there is less resistance of the flow of liquid resin in to the fiber reinforcement, thus, a lower minimum resin injection pressure is required to achieve complete wetout; whereas, when the injection slot width is narrow there is more resistance to resin flow through the fiber matrix and thus a higher injection pressure is required to achieve complete wetout. The maximum interior pressure for the detached-die configuration is significantly lower than the corresponding attached-die configuration because of the gap at the exit of the detached-die configuration. Similarly, it is observed from Table 4-3 and Table 4-4 that for a particular length of injection chamber, for the same width of the injection slot ($x_{IS}$), the minimum injection pressure necessary to achieve complete wetout and the associated maximum interior pressure for both the attached-die and detached-die configurations both decrease with an increase of CR values. Tables 4-3 and 4-4, show that for the same length ($L_T$) of the injection chamber, the minimum pressure required for the complete wetout for CR values of 2 decreases with increase in the width of the injection slot; however, for CR values 3 and 4 the injection pressure remains slightly above atmospheric pressure in all cases even when the width of the slot width is varied for both pull speeds. The local fiber volume fraction at the injection slot for CR value of 2 is greater than for CR value of 3 and 4; this greater local fiber volume fraction causes more resistance to the resin flow and thus a higher injection pressure is required to push the resin through the fiber reinforcement to achieve complete wetout. For all cases, as observed from Tables 4-3 ($U$ = 0.0254 m/s) and Table 4-4 ($U$ = 0.0508 m/s), the minimum injection pressure for CR = 2 is doubled when the pull speed is doubled; however, for CR values 3 and 4, the injection pressure remains slightly atmospheric pressure for both pull speed. For all cases, the corresponding maximum interior pressure for

both the attached-die and detached-die configurations are approximately doubled when the pull speed is doubled.

The impact of injection slot width ($\Delta x$) at different chamber lengths ($L_T$) on the minimum injection pressure required to achieve complete wetout along with the associated maximum interior chamber resin pressure of the attached-die and detached-die configurations are shown in Figs. 4-17 through 4-22. Figures 4-17, 4-18 and 4-19 are for a pull speed of 0.0254 m/s at CR values 2, 3 and 4 respectively and Figs. 4-20, 4-21 and 4-22 are for a pull speed of 0.0508 m/s at CR values 2, 3 and 4 respectively. The lower horizontal line corresponding to $P$ = 0.42 MPa and the upper horizontal line corresponding to $P$ = 2.07 MPa represent the limits for the acceptable manufacturing solutions for the resin injection pressure and maximum chamber wall pressure. If the minimum injection pressure to achieve complete wetout is both below the lower horizontal line and the maximum chamber wall pressure is below the upper line simultaneously, then this is an acceptable set of parameters for pultrusion manufacturing. The gauge pressures are non-dimensionlized by taking atmospheric pressure $P_o$ = 0.1013 MPa as a reference pressure.

From Figs. 4-17 through 4-22, it can be illustrated that for particular length of the injection chamber ($L_T$), the maximum pressure for the attached-die and detached-die configurations decreases when the injection slot width ($\Delta x$) is increased as 0.005 m, 0.010 m and 0.015 m. Similarly, the injection pressure also decreases when the width of the injection slot is increased for CR = 2; however for higher CR values 3 and 4, the injection pressure values are approximately 0.002 MPa; hence are difficult to see in figures. From Figs. 4-17 through 4-22, the maximum interior chamber wall pressure for the attached-die configuration is observed to be higher than the corresponding detached-die configuration. In Fig. 4-17 and 4-20, for CR = 2 and pull speeds of 0.0254 m/s and 0.0508 m/s, respectively, it can be observed that the injection

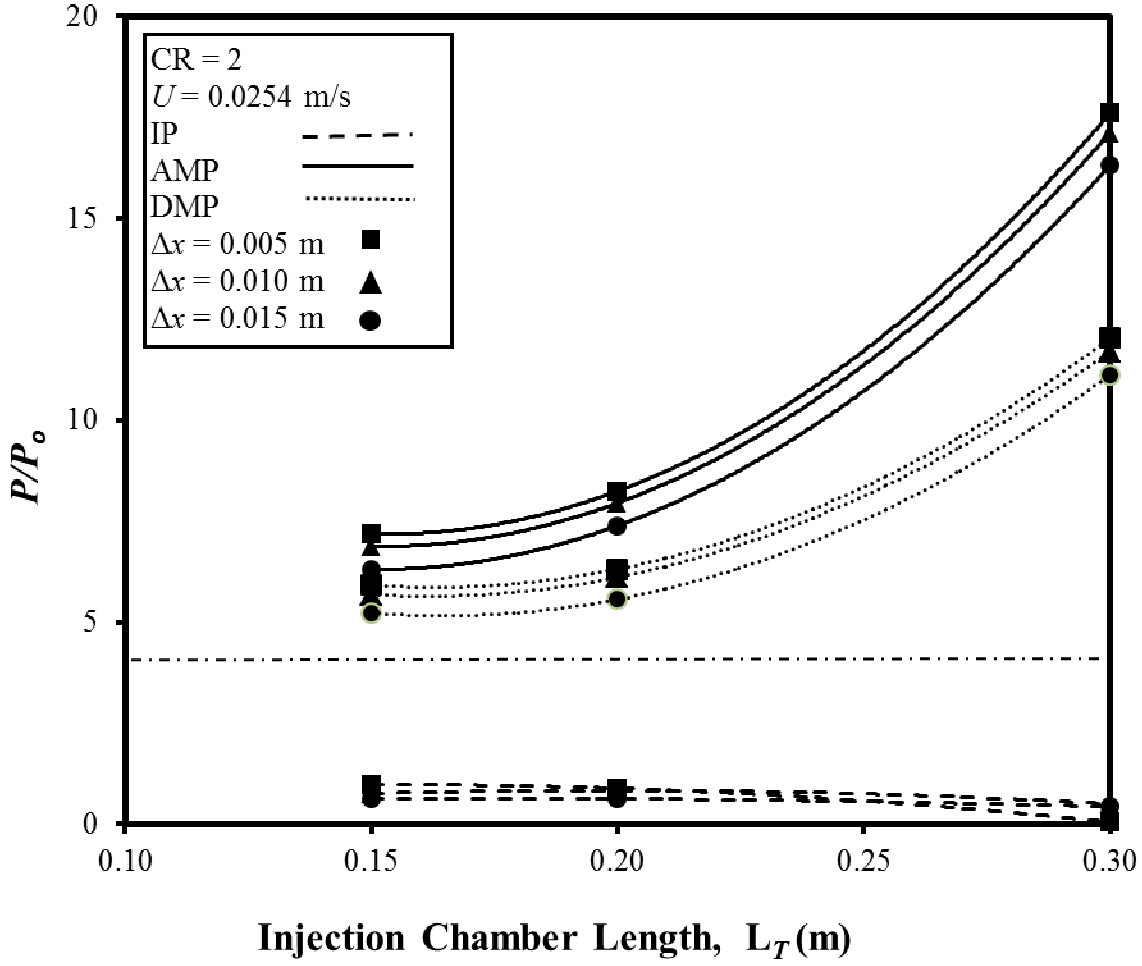


**Figure 4-17. Injection Pressure (IP) and Attached Maximum Pressure (AMP) and Detached Maximum Pressure (DMP) for Different Injection Chamber Lengths and Different Slot Widths at CR = 2, $U$ = 0.0254 m/s, $H_D$ = 0.003175 m, $W_D$ = 0.0635 m, $V_{fo}$ = 0.68, μ = 0.75 Pa·s.**

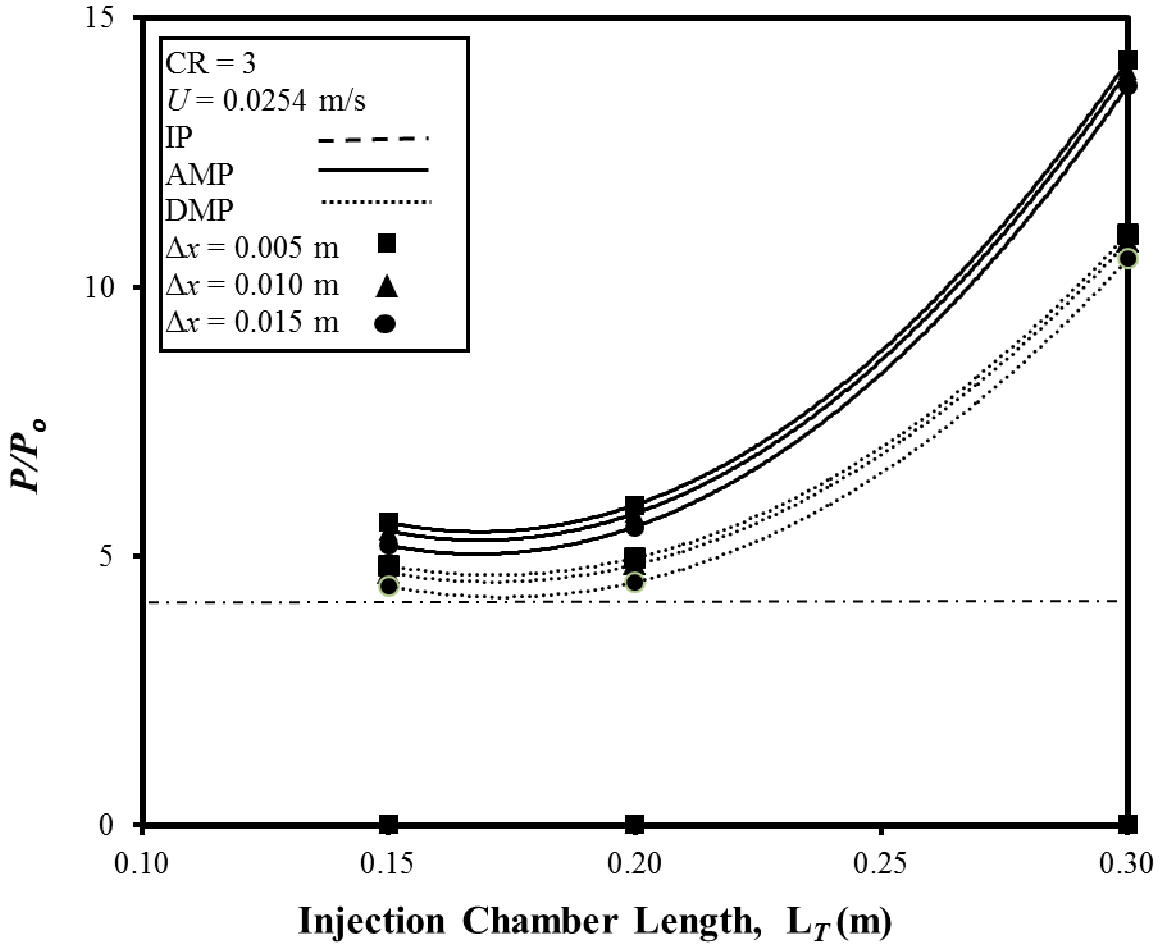


**Figure 4-18. Injection Pressure (IP) and Attached Maximum Pressure (AMP) and Detached Maximum Pressure (DMP) for Different Injection Chamber Lengths and Different slot widths at CR = 3, $U$ = 0.0254 m/s, $H_D$ = 0.003175 m, $W_D$ = 0.0635 m, $V_{fo}$ = 0.68, μ = 0.75 Pa·s.**

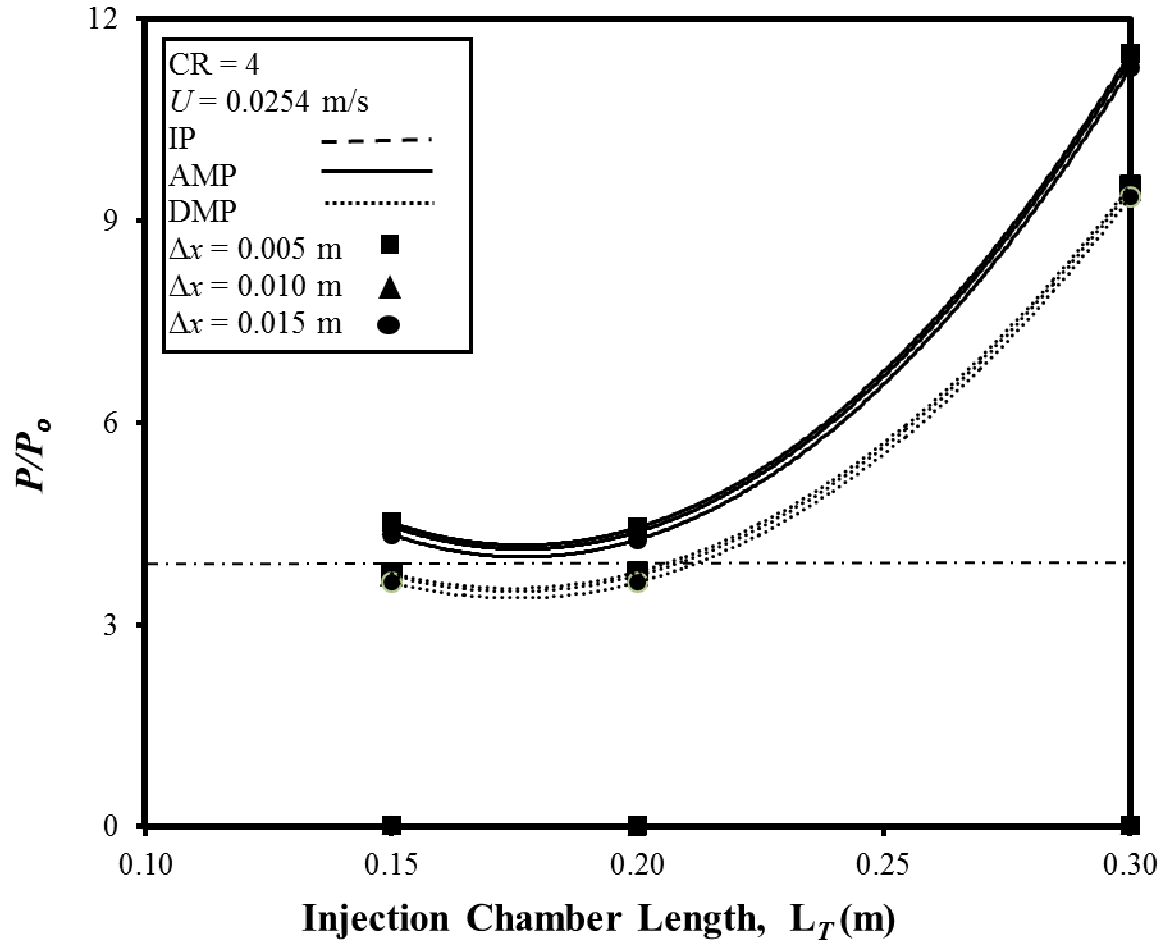


**Figure 4-19. Injection Pressure (IP) and Attached Maximum Pressure (AMP) and Detached Maximum Pressure (DMP) for Different Injection Chamber Lengths and Different slot widths at CR = 4, $U$ = 0.0254 m/s, $H_D$ = 0.003175 m, $W_D$ = 0.0635 m, $V_{fo}$ = 0.68, μ = 0.75 Pa·s.**

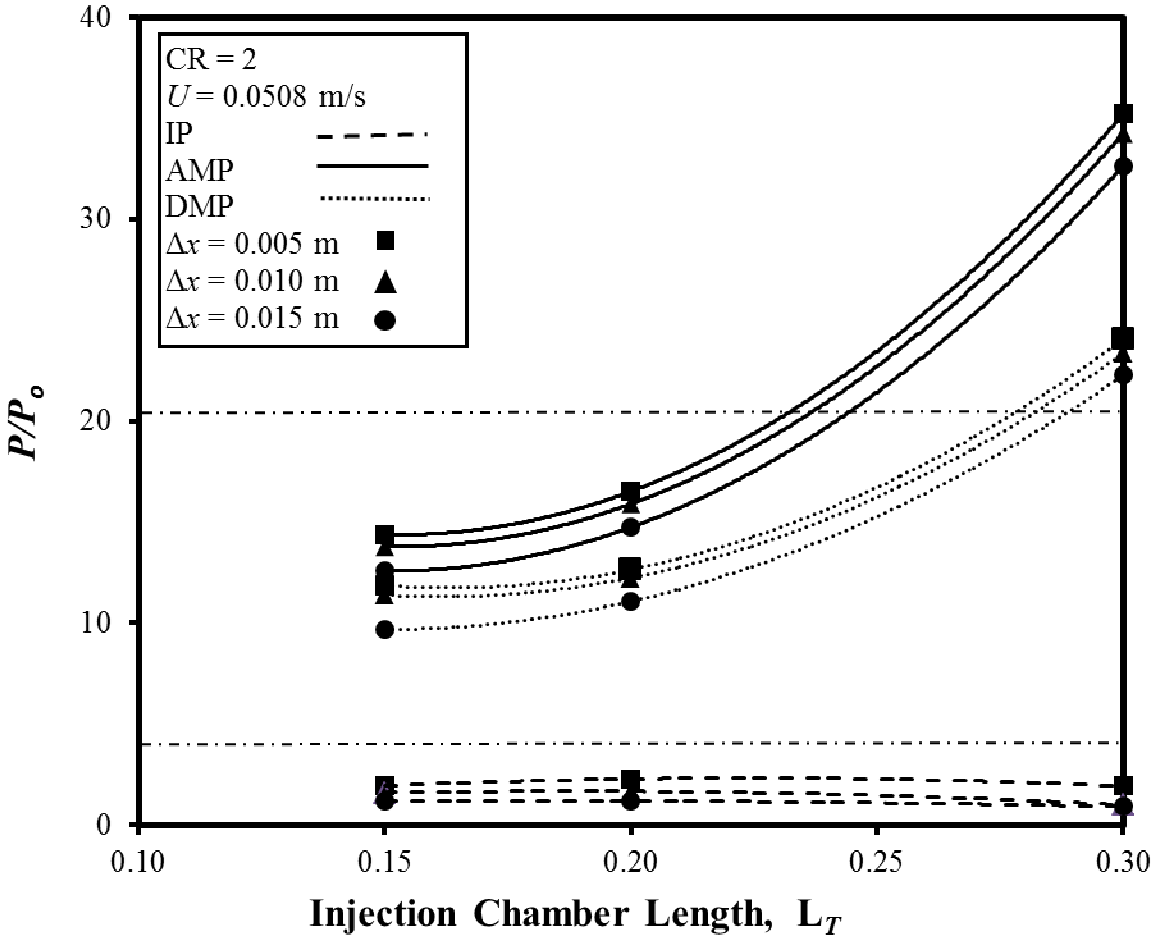


**Figure 4-20. Injection Pressure (IP) and Attached Maximum Pressure (AMP) and Detached Maximum Pressure (DMP) for Different Injection Chamber Lengths and Different slot widths at CR = 2, $U$ = 0.0508 m/s, $H_D$ = 0.003175 m, $W_D$ = 0.0635 m, $V_{fo}$ = 0.68, μ = 0.75 Pa·s.**

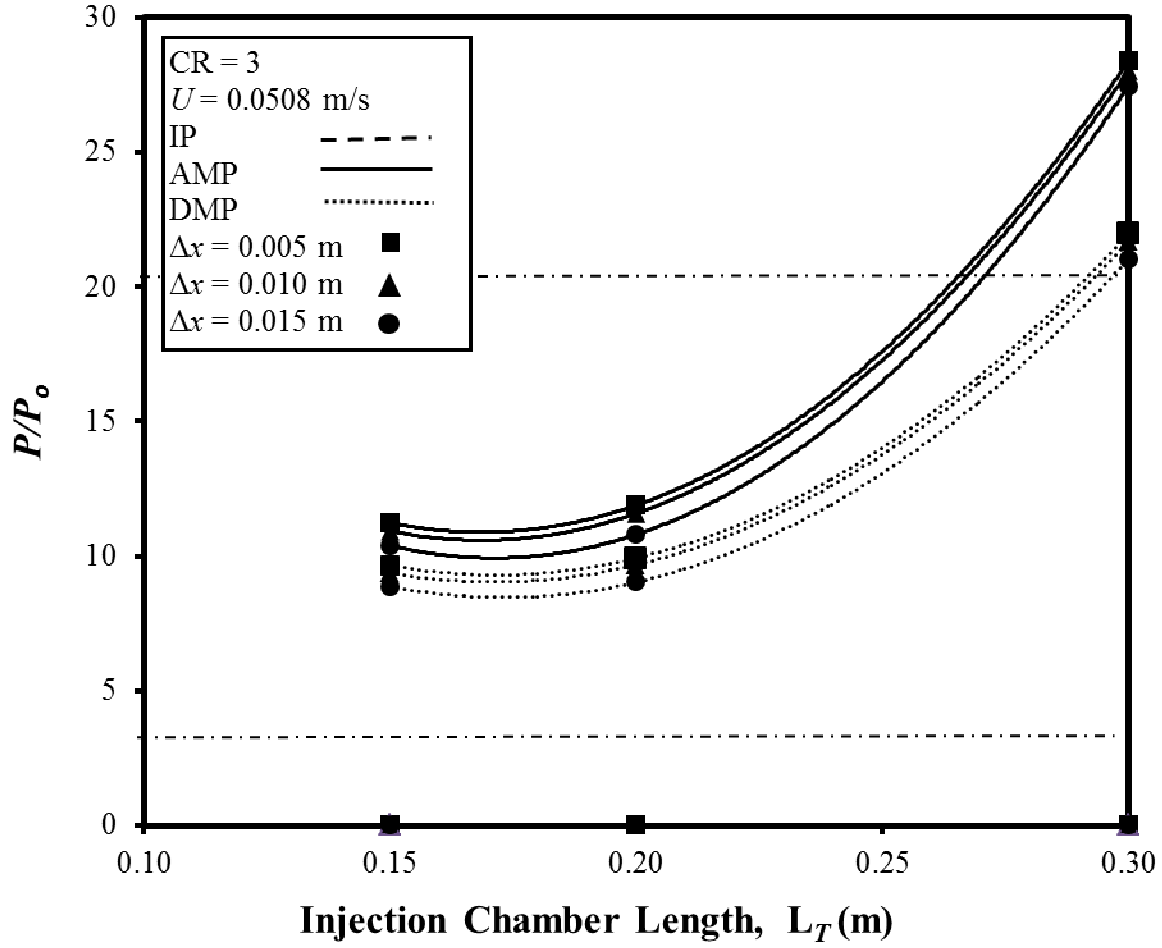


**Figure 4-21. Injection Pressure (IP) and Attached Maximum Pressure (AMP) and Detached Maximum Pressure (DMP) for Different Injection Chamber Lengths and Different slot widths at CR = 3, $U$ = 0.0508 m/s, $H_D$ = 0.003175 m, $W_D$ = 0.0635 m, $V_{fo}$ = 0.68, μ = 0.75 Pa·s.**

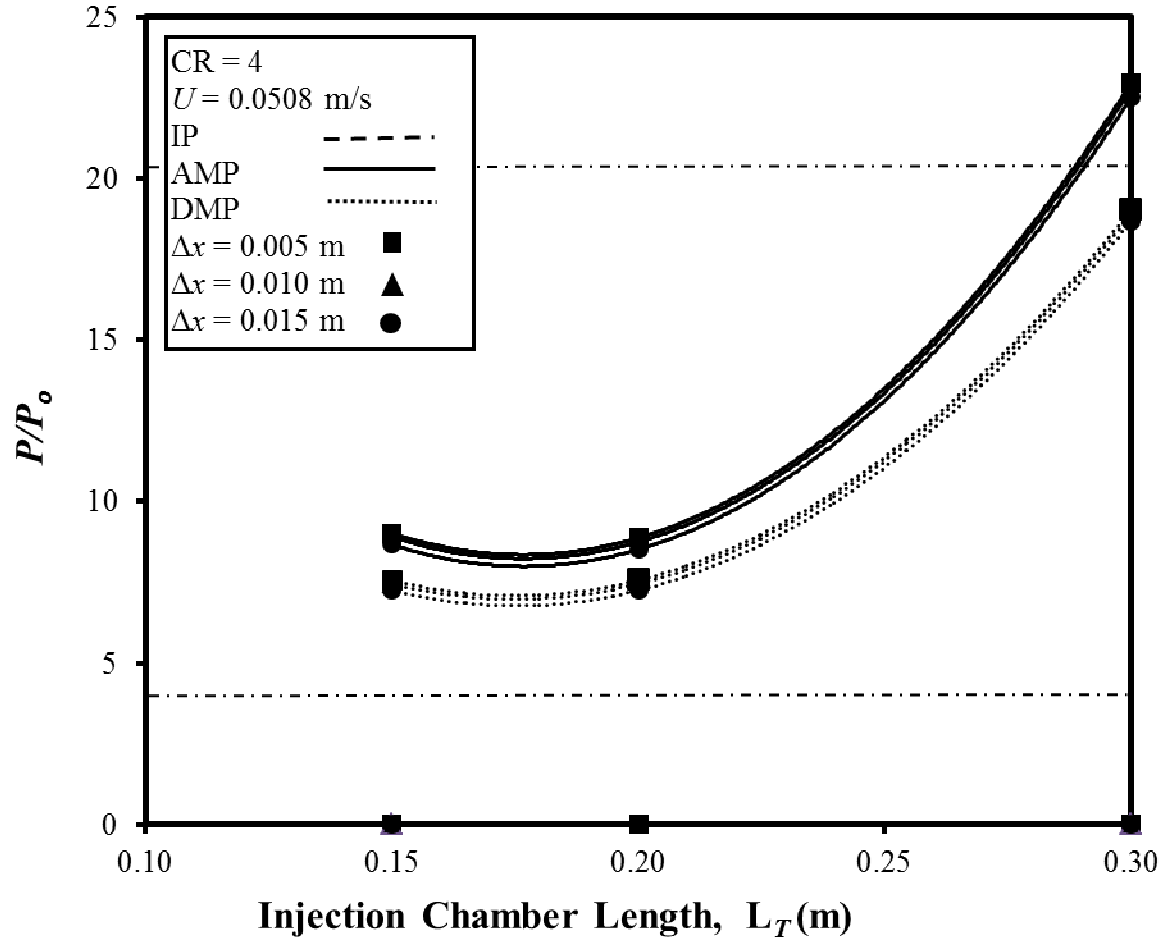


**Figure 4-22. Injection Pressure (IP) and Attached Maximum Pressure (AMP) and Detached Maximum Pressure (DMP) for Different Injection Chamber Lengths and Different slot widths at CR = 4, $U$ = 0.0508 m/s, $H_D$ = 0.003175 m, $W_D$ = 0.0635 m, $V_{fo}$ = 0.68, μ = 0.75 Pa·s.**

pressure remains approximately same for the width of the injection slot ($\Delta x$) 0.005 m, 0.010 m and 0.015 m, even though the length of the injection chamber ($L_T$) is increased from 0.15 m to 0.30 m. The maximum interior pressure for both the attached-die and detached-die configurations increases with an increase of the injection chamber length ($L_T$) for the width of the injection slot ($\Delta x$) 0.005 m, 0.010 m and 0.015 m. In Figs. 4-18 and 4-21, for CR value 3 and pull speeds of 0.0254 m/s and 0.0508 m/s, respectively, and in Figs. 4-19 and 4-22, for CR value 4 and pull speeds of 0.0254 m/s and 0.0508 m/s, respectively, the maximum interior chamber wall pressure for both the attached-die and detached-die configurations, for the width of the injection slot ($\Delta x$) 0.005 m, 0.010 m and 0.015 m, show almost the same kind of behavior when the length of the injection chamber ($L_T$) is increased, where the maximum interior chamber wall pressure for both the attached-die and detached-die configurations for a given injection slot width remains almost the same when the injection chamber length ($L_T$) increases from 0.15 m to 0.20 m and then both increase when the length of the injection chamber is increased from 0.20 m to 0.30 m because of the increased tapered length of the injection chamber. Similarly, the injection pressure also shows similar behavior where it remains essentially atmospheric at all length of injection chamber length ($L_T$) even when the width of the injection slot ($\Delta x$) is varied. However, for CR = 4, the maximum interior chamber wall pressure for both the attached-die and detached-die configurations remains approximately same for the different slot width ($\Delta x$) of 0.005 m, 0.010 m and 0.015 m as shown if Figs. 4-19 and 4-22, for pull speeds of 0.0254 m/s and 0.0508 m/s respectively. From Figs 4-17 through 4-19 for pull speed of 0.0254 m/s and from Figs. 4-20 through 4-22 for pull speed of 0.0508 m/s, it is observed that the general behavior of the injection pressure and maximum chamber wall pressure for both the attached-die and detached-configurations remain the same even when the speed is doubled from 0.0254 m/s

to 0.0508 m/s; however the maximum pressure is observed to be significantly increased when the pull speed is doubled. Hence, for the doubled pull speed of 0.0508 m/s as observed from Figs. 4-20, 4-21 and 4-22, the maximum interior chamber wall pressure for both the attached-die and detached-die configurations may lie in the non-feasible manufacturing region above the upper horizontal line corresponding to 2.07 MPa at large chamber lengths ($L_T$).

The progression of interior chamber wall resin pressure profiles inside the injection chamber of both the attached-die and detached-die configurations for the different widths of the injection slot $\Delta x$ = 0.005 m, 0.010 m, and 0.015 for the various lengths ($L_T$ = 0.15 m, 0.20 m and 0.30 m) of the injection chamber with CR = 3 are illustrated in Figs. 4-23, 4-24 and 4-25 for pull speed $U$ = 0.0254 m/s and in Figs. 4-26, 4-27 and 4-28 for pull speed $U$ = 0.0508m/s. For a given width of the injection slot ($\Delta x$), the chamber wall pressure of the attached-die configuration rises to the injection pressure at the location of the injection slot and continues to rise and reaches a maximum gauge pressure value at the beginning of Region II and maintains the same pressure value through to the chamber exit; whereas, for the detached-die configuration the pressure rises to the injection pressure at the location of the injection slot and then increases to the to a maximum gauge pressure and then finally decreases to zero gauge pressure at the chamber exit gap. It is observed from the Figs. 4-23 through 4-28, that when the width of the injection slot ($\Delta x$) is increased the maximum interior chamber wall pressure decreases. It is also seen from Figs. 4-23 through 4-28, that the general behavior of the maximum interior chamber wall pressure is similar when the pull speed is increased from 0.0254 m/s to 0.0508 m/s, however the maximum interior pressure is observed to be significantly increased. For higher CR = 4, as observed in Figs. 4-25 and 4-28, the maximum interior pressure of both the attached-die and detached-die configuration are approximately same even though the slot width are varied, hence,

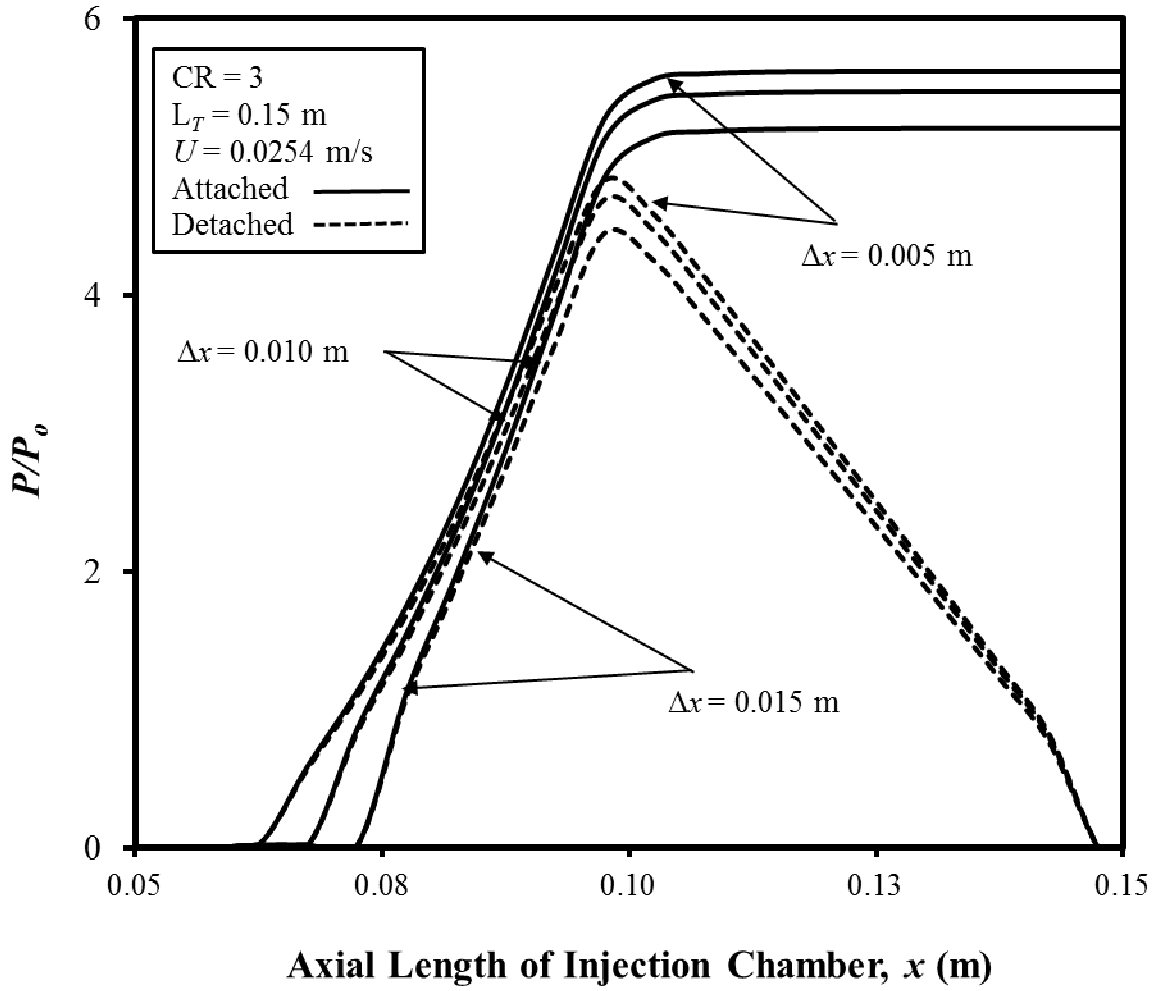


**Figure 4-23. Chamber Wall Axial Pressure Profiles for Attached-Die and Detached-Die Configurations for Injection Chamber Length of $L_T$ = 0.15 m, CR = 3, and $U$ = 0.0254 m/s at Different Width of Single Injection Slot ($\Delta x$).**

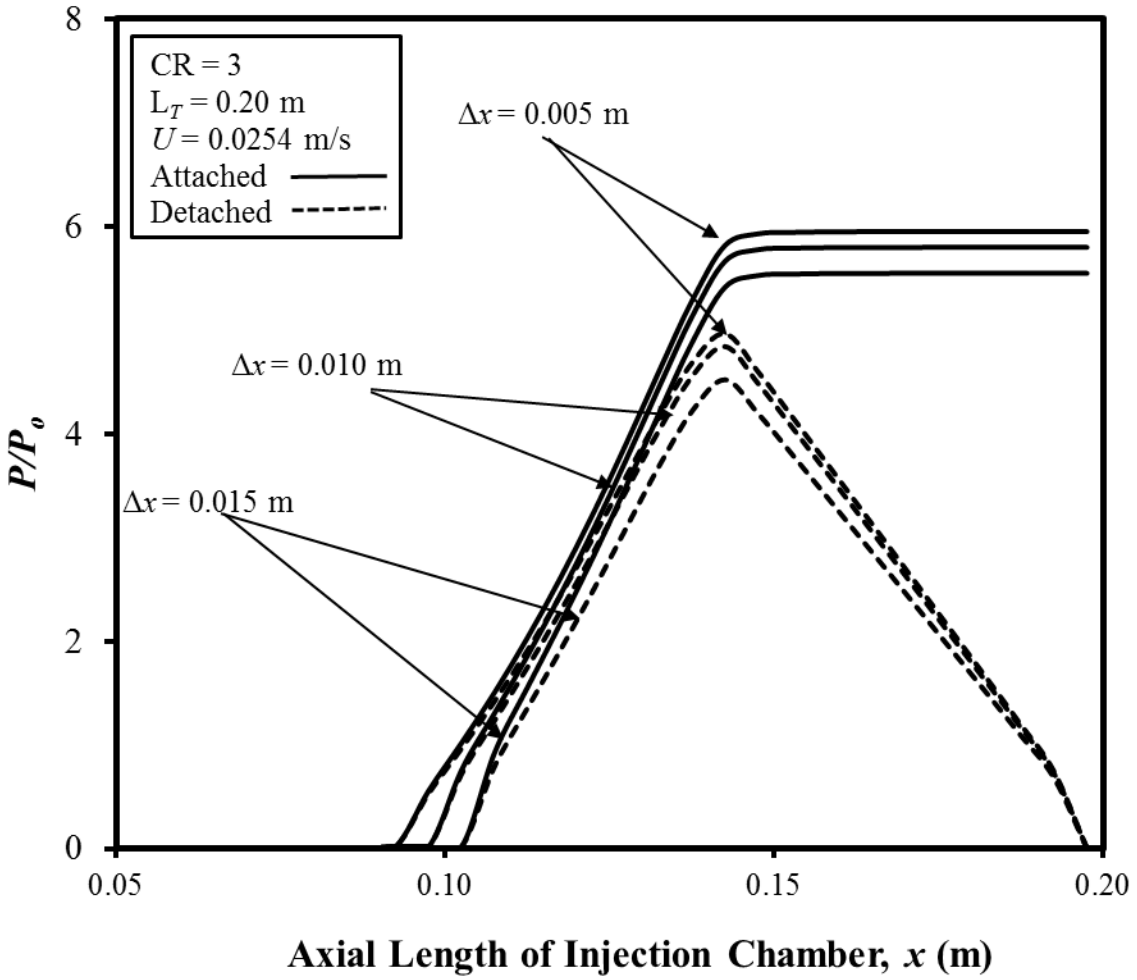


**Figure 4-24. Chamber Wall Axial Pressure Profiles for Attached-Die and Detached-Die Configurations for Injection Chamber Length of $L_T$ = 0.20 m, CR = 3, and $U$ = 0.0254 m/s at Different Width of Single Injection Slot ($\Delta x$).**

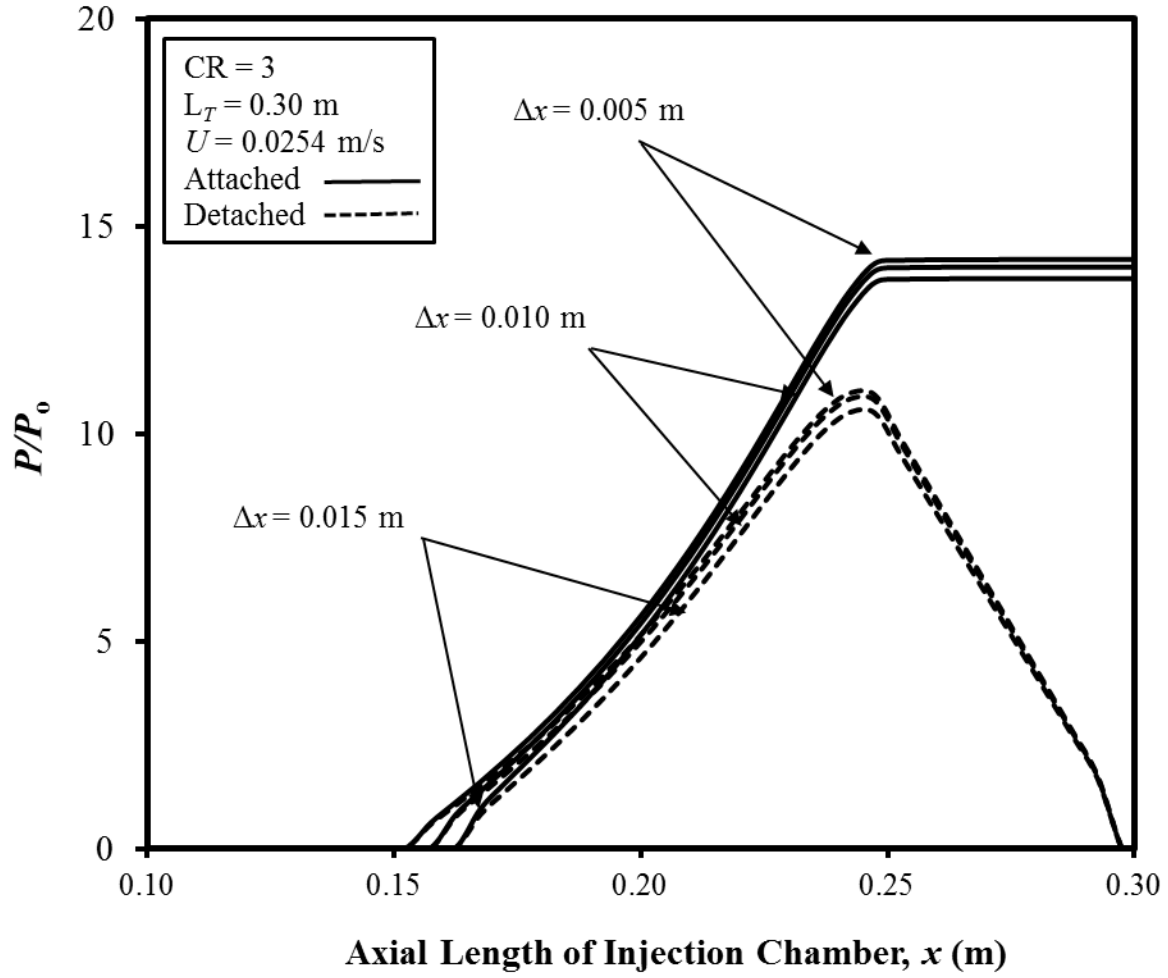


**Figure 4-25. Chamber Wall Axial Pressure Profiles for Attached-Die and Detached-Die Configurations for Injection Chamber Length of $L_T$ = 0.30 m, CR = 3, and $U$ = 0.0254 m/s at Different Width of Single Injection Slot ($\Delta x$).**

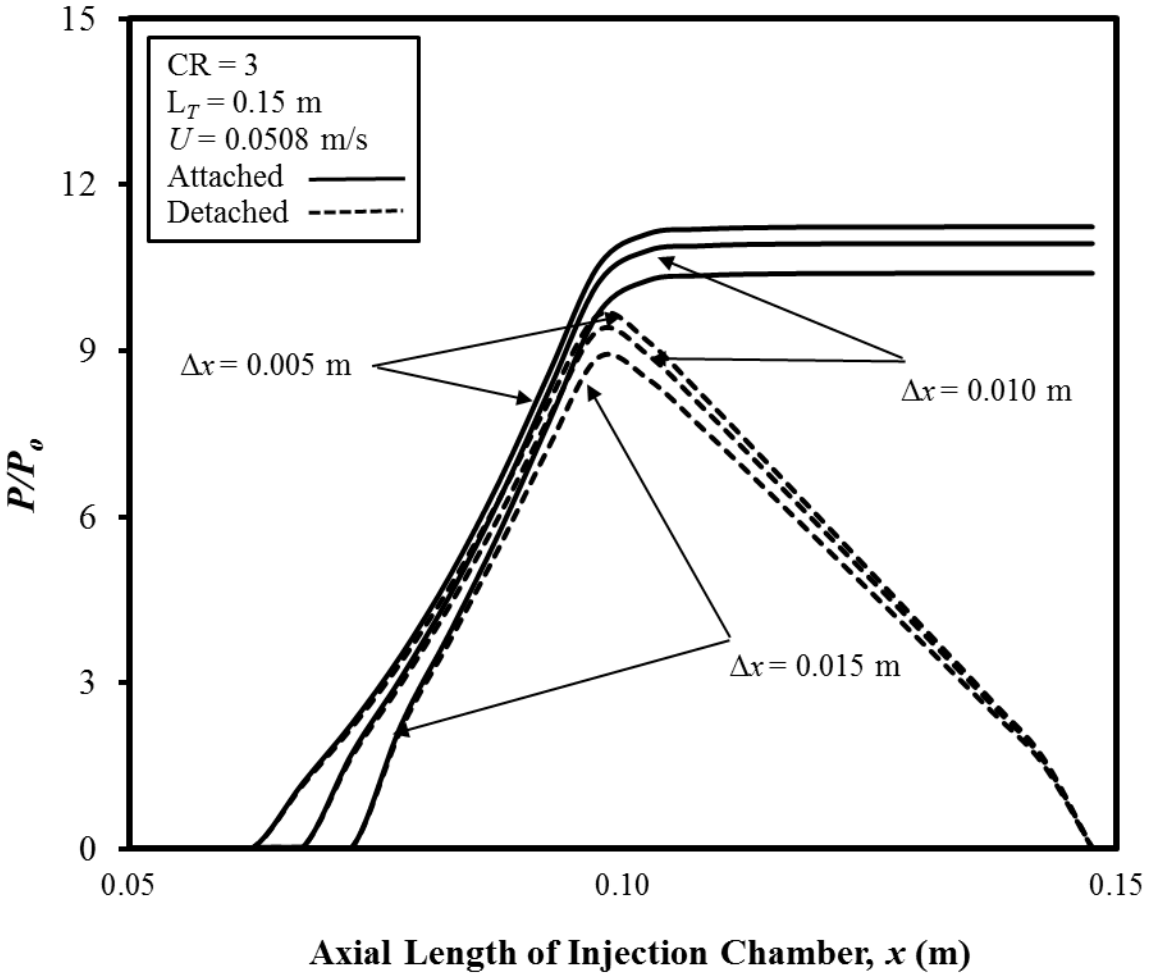


**Figure 4-26. Chamber Wall Axial Pressure Profiles for Attached-Die and Detached-Die Configurations for Injection Chamber Length of $L_T$ = 0.15 m, CR = 3, and $U$ = 0.0508 m/s at Different Width of Single Injection Slot ($\Delta x$).**

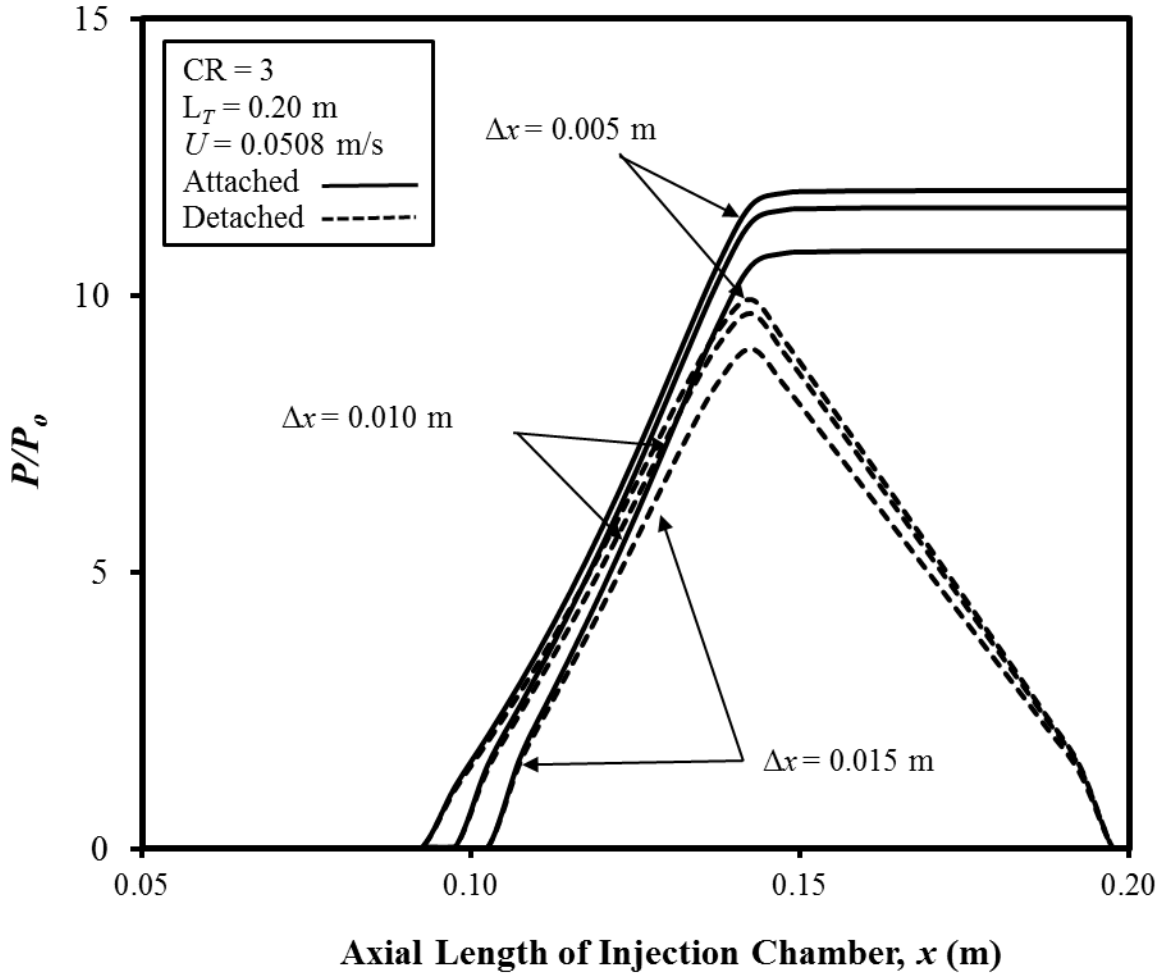


**Figure 4-27. Chamber Wall Axial Pressure Profiles for Attached-Die and Detached-Die Configurations for Injection Chamber Length of $L_T$ = 0.20 m, CR = 3, and $U$ = 0.0508 m/s at Different Width of Single Injection Slot ($\Delta x$).**

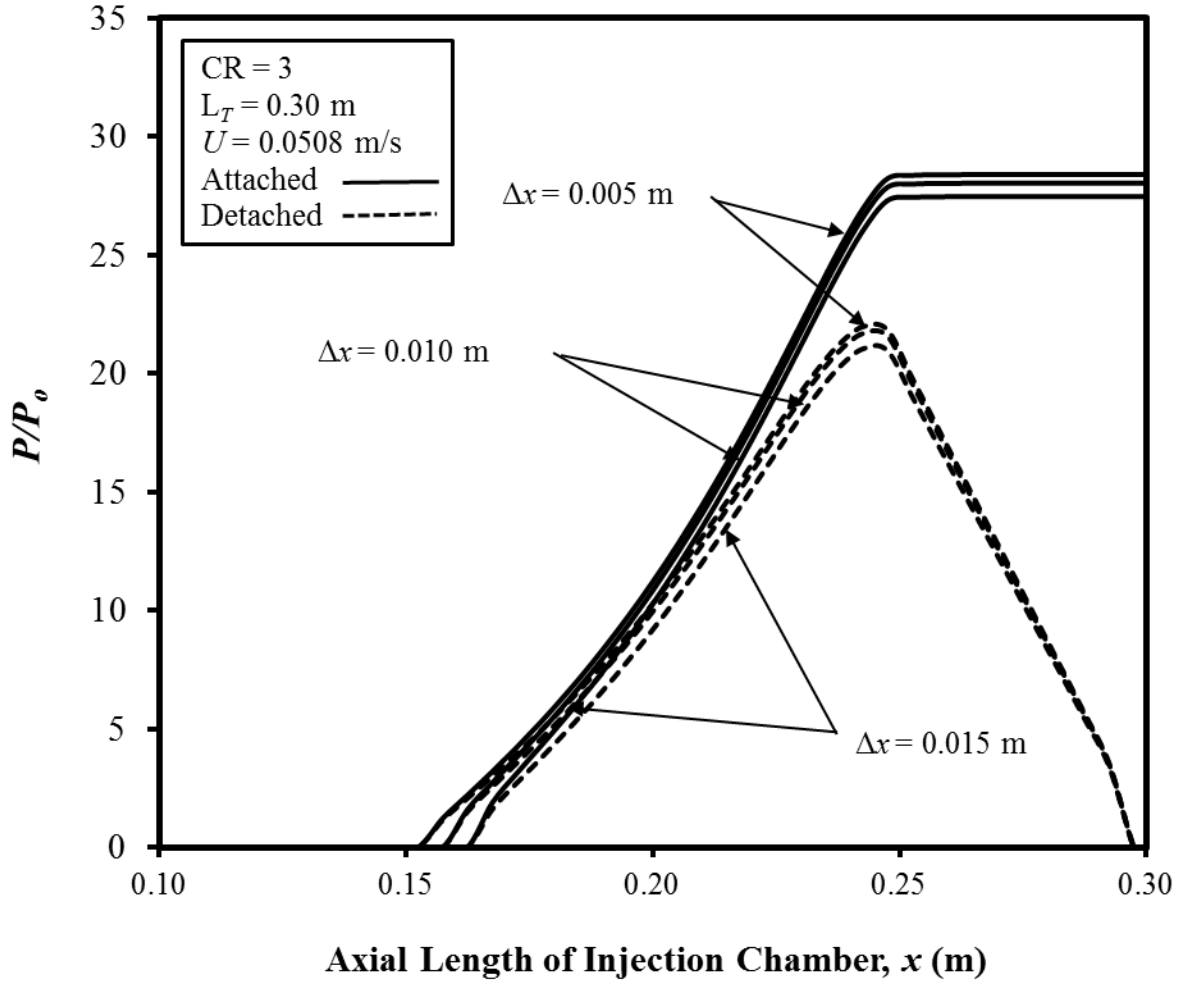


**Figure 4-28. Chamber Wall Axial Pressure Profiles for Attached-Die and Detached-Die Configurations for Injection Chamber Length of $L_T$ = 0.30 m, CR = 3, and $U$ = 0.0508 m/s at Different Width of Single Injection Slot ($\Delta x$).**

it can be concluded that for higher CR value the maximum interior chamber wall pressure is not the function of slot width ($\Delta x$).

Figures 4-29 through 4-31 show the steady-state liquid resin flow front and the isopressure contours (kPa), within the liquid resin wetout region at CR = 4 and pull speed of 0.0254 m/s. with the injection slot width at 0.60 $L_I$ (Region I). For injection chamber length $L_T$ = 0.15 m Figs. 4-29 and 4-30 show the steady-state liquid resin flow front and the isopressure contours within the liquid resin wetout region with injection slot width $\Delta x$ = 0.005 m and $\Delta x$ = 0.010 m respectively and Fig. 4-31 shows the steady-state liquid resin flow front and the isopressure contours within the liquid resin wetout region with injection slot width $\Delta x$ = 0.005 m and for $L_T$ = 0.30 m. The resin flow front and the pressure values for the attached-die and the detached-die configurations can be readily compared from these figures. The chamber pressure values for attached-die configuration are higher than the detached-die configuration as observed in Figs. 4-29 through 4-31. Figures 4-29 through 4-31 are displayed not to scale; this was done in order to make the results more viewable and understandable.

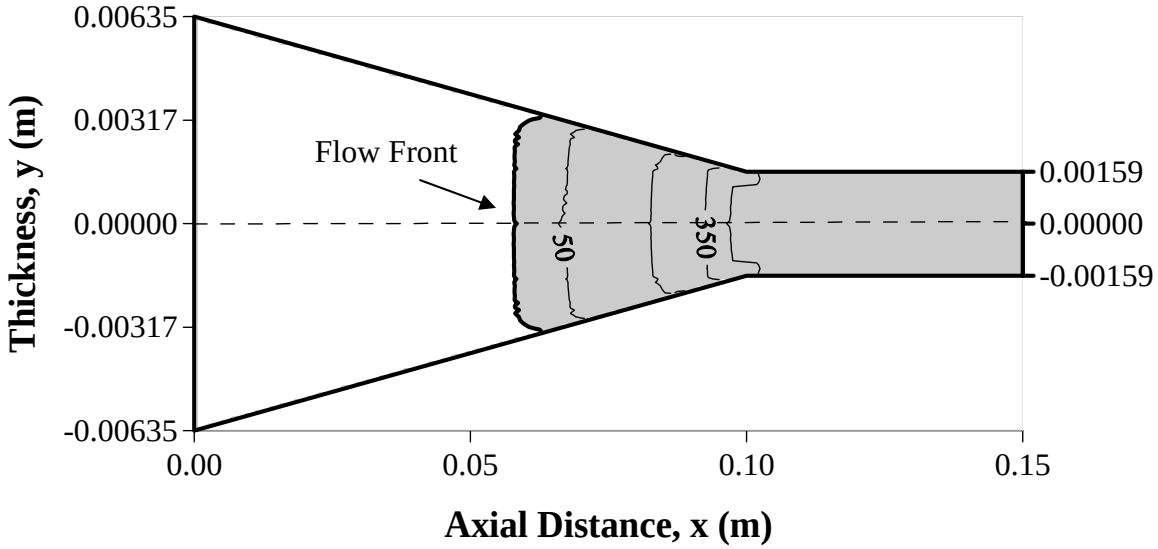


**a. Attached Die Configuration**

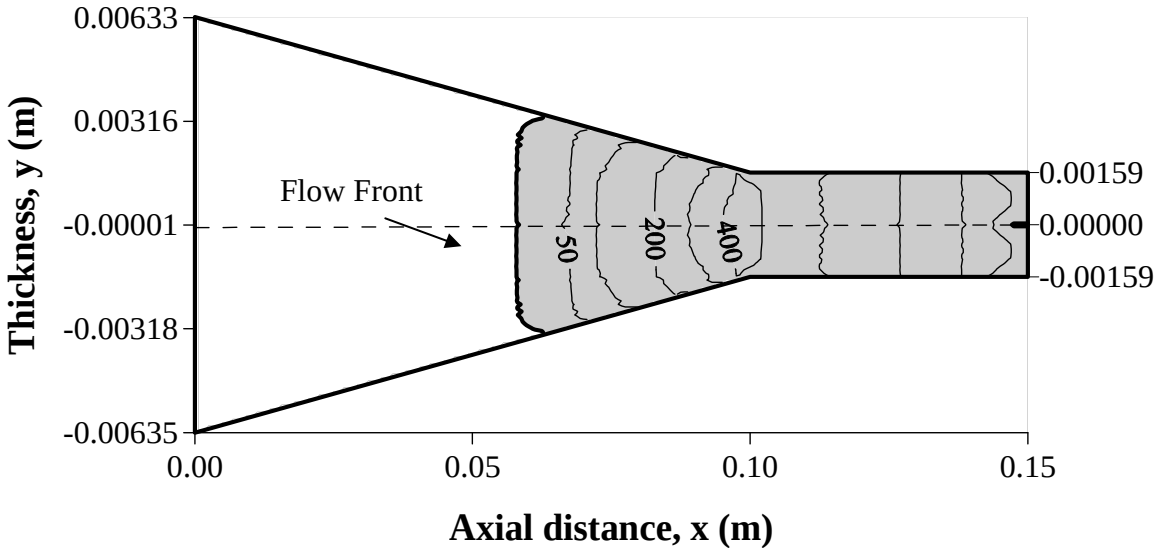


**b. Detached Die configuration**

**Figure 4-29. Flow Front Profile and Gauge Isopresure (KPa) Contours for Case C7, Table 4-3 for $L_T$ = 0.15 m, $\Delta x$ = 0.005 m, $x_{IS}$ = 0.60 $L_I$, CR = 4, $V_{fo}$ = 0.68, μ = 0.75 Pa·s with $U$ = 0.0254 m/s (Not to Scale).**

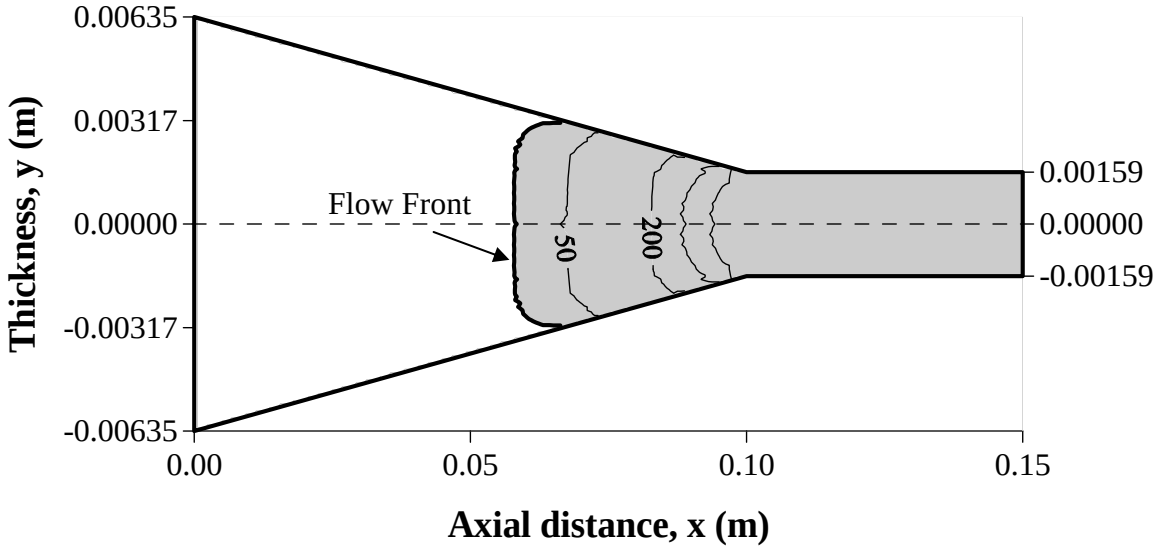


**a. Attached Die Configuration**

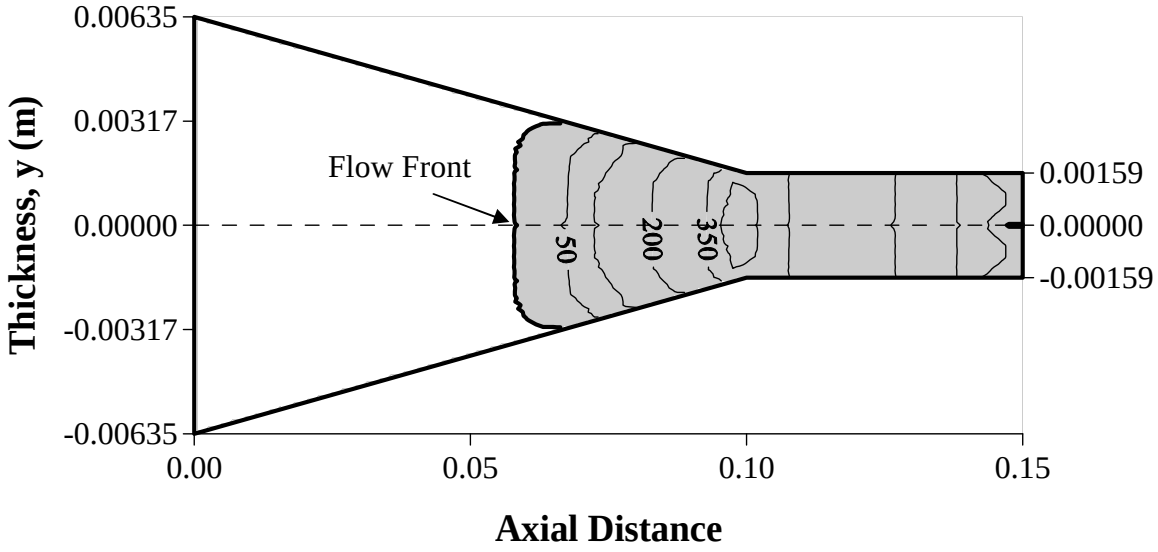


**b. Detached Die Configuration**

**Figure 4-30. Flow Front Profile and Gauge Isopresure (KPa) Contours for Case C8, Table 4-3 for $L_T$ = 0.15 m, $\Delta x$ = 0.010 m, $x_{IS}$ = 0.60 $L_I$ CR = 4, $V_{fo}$ = 0.68, μ = 0.75 Pa·s with $U$ = 0.0254 m/s (Not to Scale).**

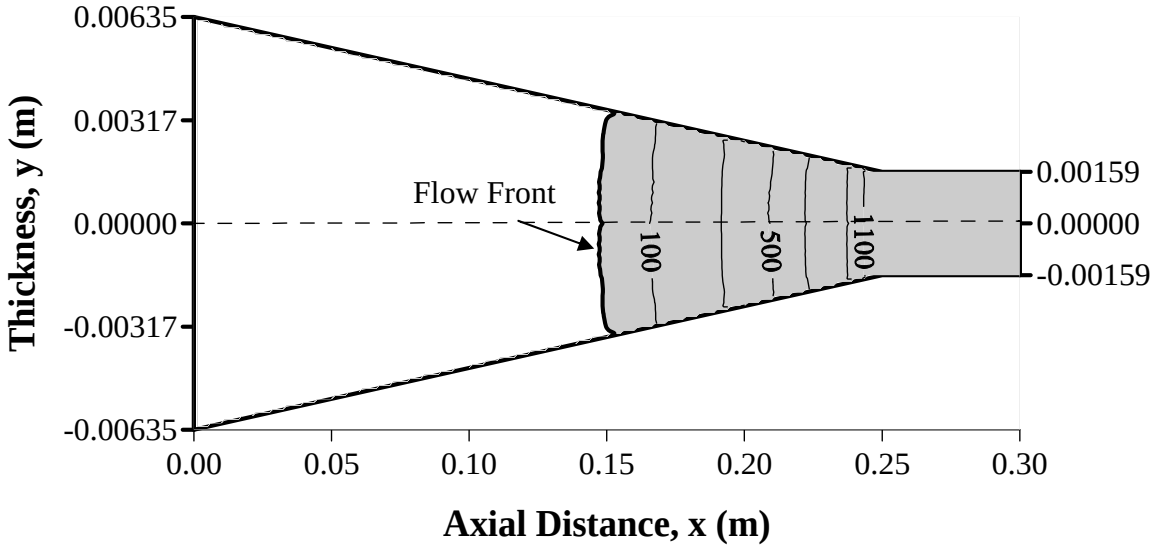


**a. Attached Die Configuration**

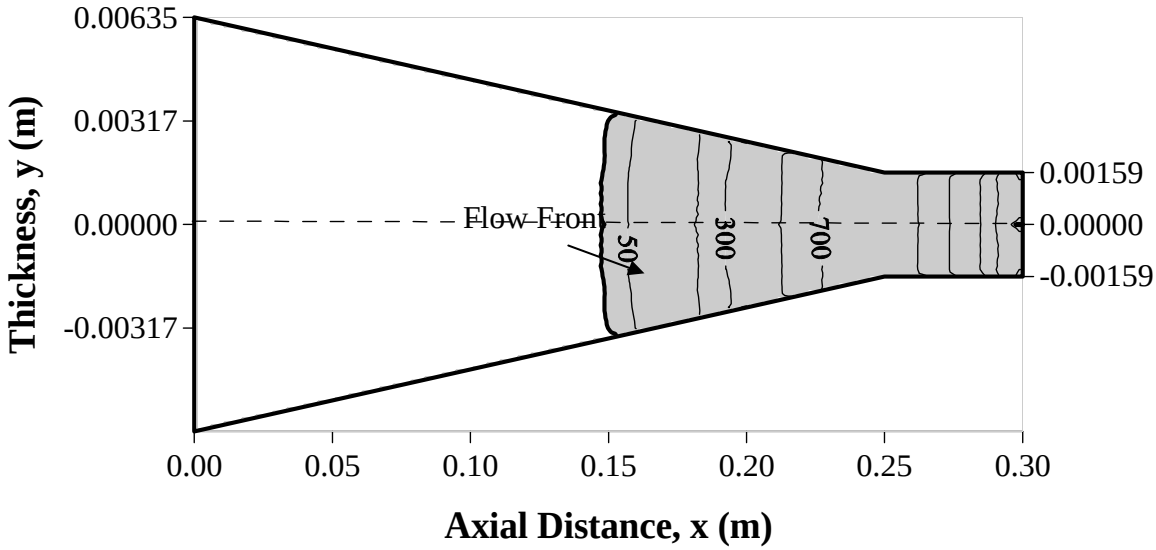


**b. Detached Die Configuration**

**Figure 4-31. Flow Front Profile and Gauge Isopresure (kPa) Contours for Case C25, Table 4-3 for $L_T$ = 0.30 m, $\Delta x$ = 0.005 m, $x_{IS}$ = 0.60 $L_I$, CR = 4, $V_{fo}$ = 0.68, μ = 0.75 Pa·s with $U$ = 0.0254 m/s (Not to Scale).**

### *4.3 Multiple injection slots and axial locations*

In this section, the impact of multiple axial injection slots on the minimum injection pressure necessary to achieve complete wetout of the fiber reinforcement as well as the corresponding maximum resin pressure inside the injection chamber were investigated for both the attached-die and the detached-die configurations. The study was conducted for total injection chamber lengths ($L_T$) of 0.15 m, 0.20 m and 0.30 at compression ratios of 2, 3 and 4 and compared at two different pull speeds, $U$ = 0.0254 m/s and 0.0508 m/s. Multiple resin injection slots, two at the top and two at bottom side of the injection chamber, are placed at 0.20 $L_I$, 0.40 $L_I$ and 0.60 $L_I$ of the axial distance in Region I for the injection chamber of length $L_T$ = 0.15 m and 0.20 m; whereas, for the injection chamber of length $L_T$ = 0.30 m, the injection slots are placed at 0.20 $L_I$, 0.40 $L_I$, 0.60 $L_I$ and 0.80 $L_I$ of the axial distance in Region I. For a particular location of the multiple injection slots, the other parameters, both processing and geometric, were hold at their nominal values.

The impact of multiple injection slots is shown in Table 4-5 for the pull speed 0.0254 m/s and in Table 4-6 for the pull speed of 0.0508 m/s. The minimum injection gauge pressure required for the complete wetout of the reinforcement fiber for both the attached-die and the detached-die configurations is shown in column 6 and the corresponding maximum chamber wall gauge pressure is shown in columns 7 and 8 respectively in Tables 4-5 and 4-6. The bolded pressure values do not satisfy the feasible manufacturing pressure range: this means the resin injection pressure not being greater than 0.42 MPa (60 psi), and simultaneously for the resin maximum chamber pressure not being greater than 2.07 MPa (300 psi). Resin pressures not satisfying these constraints

**Table 4-5. Effect of Multiple Injection Slots on Minimum Injection Pressure for Complete Wetout at Proportional Locations for U = 0.0254 m/s, $V_{fo}$ = 0.68, μ = 0.75 Pa·s, $W_D$ = 0.0635, $H_D$ = 0.003175 m and Slot Width $\Delta x$ = 0.01m.**

| Case* | CR | Injection Chamber Length ($L_T$) (m) | Location of Injection Slots ($x_L$) (m) | | Injection Pressure (Gauge) Mpa | Maximum Pressure (Guage) Mpa | Maximum Pressure (Gauge) (MPa) |
|---|---|---|---|---|---|---|---|
| | | | I | II | | Attached | Detached |
| E1 | 2 | 0.15 | 0.02 | 0.05 | 0.002 | 0.85 | 0.68 |
| E2 | 2 | 0.15 | 0.04 | 0.07 | 0.016 | 0.51 | 0.39 |
| E3 | 2 | 0.15 | 0.06 | 0.09 | 0.078 | 0.23 | 0.17 |
| E4 | 3 | 0.15 | 0.02 | 0.05 | 0.002 | 0.68 | 0.58 |
| E5 | 3 | 0.15 | 0.04 | 0.07 | 0.002 | 0.52 | 0.44 |
| E6 | 3 | 0.15 | 0.06 | 0.09 | 0.002 | 0.26 | 0.19 |
| E7 | 4 | 0.15 | 0.02 | 0.05 | 0.002 | 0.53 | 0.45 |
| E8 | 4 | 0.15 | 0.04 | 0.07 | 0.002 | 0.45 | 0.37 |
| E9 | 4 | 0.15 | 0.06 | 0.09 | 0.002 | 0.26 | 0.19 |
| E10 | 2 | 0.20 | 0.03 | 0.06 | 0.002 | 1.16 | 0.88 |
| E11 | 2 | 0.20 | 0.06 | 0.09 | 0.016 | 0.78 | 0.57 |
| E12 | 2 | 0.20 | 0.09 | 0.12 | 0.071 | 0.24 | 0.17 |
| E13 | 3 | 0.20 | 0.03 | 0.06 | 0.002 | 0.81 | 0.67 |
| E14 | 3 | 0.20 | 0.06 | 0.09 | 0.002 | 0.63 | 0.57 |
| E15 | 3 | 0.20 | 0.09 | 0.12 | 0.023 | 0.36 | 0.30 |
| E16 | 4 | 0.20 | 0.03 | 0.06 | 0.002 | 0.58 | 0.50 |
| E17 | 4 | 0.20 | 0.06 | 0.09 | 0.002 | 0.48 | 0.41 |
| E18 | 4 | 0.20 | 0.09 | 0.12 | 0.002 | 0.30 | 0.25 |
| E19 | 2 | 0.30 | 0.05 | 0.08 | 0.002 | **2.61** | 1.74 |
| E20 | 2 | 0.30 | 0.10 | 0.13 | 0.002 | 1.98 | 1.36 |
| E21 | 2 | 0.30 | 0.15 | 0.18 | 0.037 | 1.17 | 0.83 |
| E22 | 2 | 0.30 | 0.20 | 0.23 | 0.147 | 0.15 | 0.15 |
| E23 | 3 | 0.30 | 0.05 | 0.08 | 0.002 | 1.87 | 1.43 |
| E24 | 3 | 0.30 | 0.10 | 0.13 | 0.002 | 1.61 | 1.24 |
| E25 | 3 | 0.30 | 0.15 | 0.18 | 0.002 | 1.14 | 0.89 |
| E26 | 3 | 0.30 | 0.20 | 0.23 | 0.071 | 0.11 | 0.11 |
| E27 | 4 | 0.30 | 0.05 | 0.08 | 0.002 | 1.41 | 1.16 |
| E28 | 4 | 0.30 | 0.10 | 0.13 | 0.002 | 1.28 | 1.06 |
| E29 | 4 | 0.30 | 0.15 | 0.18 | 0.002 | 1.01 | 0.84 |
| E30 | 4 | 0.30 | 0.20 | 0.23 | 0.030 | 0.42 | 0.34 |

* Bold font indicates non-acceptable manufacturing solutions for an injection pressure ≥ 0.42 MPa (60 psi) and/or with an associated maximum pressure for attached or detached ≥ 2.07 MPa (300 psi).

**Table 4-6. Effect of Multiple Injection Slots on Minimum Injection Pressure for Complete Wetout at Proportional Locations for U = 0.0254 m/s, $V_{fo}$ = 0.68, μ = 0.75 Pa·s, $W_D$ = 0.0635 m, $H_D$ = 0.003175 m and Slot Width $\Delta x$ = 0.01m.**

| Case* | CR | Injection Chamber Length $L_T$ (m) | Location of Injection Slots ($x_L$) (m) | | Injection Pressure (Gauge) Mpa | Maximum Pressure (Guage) Mpa | Maximum Pressure (Gauge) (MPa) |
|---|---|---|---|---|---|---|---|
| | | | I | II | | Attached | Detached |
| F1 | 2 | 0.15 | 0.02 | 0.05 | 0.002 | 1.67 | 1.36 |
| F2 | 2 | 0.15 | 0.04 | 0.07 | 0.023 | 0.93 | 0.78 |
| F3 | 2 | 0.15 | 0.06 | 0.09 | 0.161 | 0.47 | 0.34 |
| F4 | 3 | 0.15 | 0.02 | 0.05 | 0.002 | 1.35 | 1.17 |
| F5 | 3 | 0.15 | 0.04 | 0.07 | 0.002 | 1.04 | 0.88 |
| F6 | 3 | 0.15 | 0.06 | 0.09 | 0.002 | 0.53 | 0.38 |
| F7 | 4 | 0.15 | 0.02 | 0.05 | 0.002 | 1.07 | 0.91 |
| F8 | 4 | 0.15 | 0.04 | 0.07 | 0.002 | 0.89 | 0.74 |
| F9 | 4 | 0.15 | 0.06 | 0.09 | 0.002 | 0.52 | 0.38 |
| F10 | 2 | 0.20 | 0.03 | 0.06 | 0.002 | **2.29** | 1.73 |
| F11 | 2 | 0.20 | 0.06 | 0.09 | 0.03 | 1.49 | 0.57 |
| F12 | 2 | 0.20 | 0.09 | 0.12 | 0.147 | 0.49 | 0.33 |
| F13 | 3 | 0.20 | 0.03 | 0.06 | 0.002 | 1.61 | 1.34 |
| F14 | 3 | 0.20 | 0.06 | 0.09 | 0.002 | 1.26 | 1.05 |
| F15 | 3 | 0.20 | 0.09 | 0.12 | 0.044 | 0.72 | 0.60 |
| F16 | 4 | 0.20 | 0.03 | 0.06 | 0.002 | 1.16 | 0.99 |
| F17 | 4 | 0.20 | 0.06 | 0.09 | 0.002 | 0.97 | 0.83 |
| F18 | 4 | 0.20 | 0.09 | 0.12 | 0.002 | 0.60 | 0.49 |
| F19 | 2 | 0.30 | 0.05 | 0.08 | 0.002 | **5.20** | **3.48** |
| F20 | 2 | 0.30 | 0.10 | 0.13 | 0.002 | **3.96** | **2.68** |
| F21 | 2 | 0.30 | 0.15 | 0.18 | 0.071 | **2.34** | 1.65 |
| F22 | 2 | 0.30 | 0.20 | 0.23 | 0.292 | 0.29 | 0.29 |
| F23 | 3 | 0.30 | 0.05 | 0.08 | 0.002 | **3.74** | **2.87** |
| F24 | 3 | 0.30 | 0.10 | 0.13 | 0.002 | **3.21** | **2.49** |
| F25 | 3 | 0.30 | 0.15 | 0.18 | 0.002 | **2.27** | 1.77 |
| F26 | 3 | 0.30 | 0.20 | 0.23 | 0.113 | **0.22** | 0.22 |
| F27 | 4 | 0.30 | 0.05 | 0.08 | 0.002 | **2.82** | 2.33 |
| F28 | 4 | 0.30 | 0.10 | 0.13 | 0.002 | **2.56** | 2.12 |
| F29 | 4 | 0.30 | 0.15 | 0.18 | 0.002 | 2.02 | 1.68 |
| F30 | 4 | 0.30 | 0.20 | 0.23 | 0.057 | 0.84 | 0.68 |

* Bold font indicates non-acceptable manufacturing solutions for an injection pressure ≥ 0.42 MPa (60 psi) and/or with an associated maximum pressure for attached or detached ≥ 2.07 MPa (300 psi).

are considered as unsuitable for commercial pultrusion manufacturing. From Tables 4-5 and 4-6 it is observed that when the location of multiple injection slots ($x_{IS}$) are moved downstream, the minimum injection pressure required to achieve complete wetout increases, similar to the effect for the single injection slot case. This is because as the injection chamber becomes more tapered downstream, the local fiber volume fraction increases at the location of the injection slots, and this increased local fiber volume fraction offers more resistance to the flow of resin into the fiber reinforcement. Similarly, the corresponding maximum interior chamber wall pressure inside the injection chamber for both the attached-die and the detached-die configurations decreases due the shorter distance over which the resin is compressed inside the injection chamber. The maximum interior pressure values for the detached-die configuration are observed to be lower than the corresponding attached-die configuration because of the gap (see Fig. 2-1) in Chapter 2 at the exit of the detached-die injection chamber. It is also observed from Tables 4-5 and 4-6 that for the particular length of injection chamber ($L_T$), for the same location of the multiple injection slot ($x_{IS}$), the minimum injection pressure necessary to achieve complete wetout and the associated maximum interior chamber wall pressure for both the attached-die and the detached-die configuration both decrease with an increase of CR values (tapering of the injection chamber). This is because for higher CR values, the local fiber volume fraction at the injection slot is lower, which causes less resistance to the resin flow and thus a lower injection pressure is required to push the resin through the fiber to achieve complete wetout. From Tables 4-5 and 4-6, it is observed that, for CR values of 3 and 4, the injection pressure remains slightly above atmospheric pressure except for case E15, E26 and E30 due to the far downstream location of the injection slots where there is higher resin injection flow resistance from the increased local fiber volume fraction. It can be observed from the Tables 4-5 ($U$ = 0.0254 m/s) and Table 4-6 ($U$ =

0.0508 m/s), that the minimum injection pressure for complete wetout is essentially doubled when the pull speed is doubled; however, when the injection pressure is slightly above atmospheric pressure, it remains about the same even when the pull speed is doubled. For all cases, the corresponding maximum interior pressure for both the attached-die and the detached-die are also approximately doubled when the pull speed is doubled. Comparing Tables 4-1 and 4-5 ($U$ = 0.0254 m/s) and comparing Tables 4-2 and 4-6 ($U$ = 0.0508 m/s) for the same location of the injection slot with all other parameters held at their nominal values, the multiple injection slots configuration yields significantly lower minimum injection pressures as well as lower corresponding maximum interior chamber wall pressures for both the attached-die and the detached-die configurations.

It is more discernable in Fig. 4-32 and Fig 4-33 that the pressure values are significantly lower for multiple injection slots configurations than single injection slot configuration at the same location. From Section 4.1.2 it is also seen that the minimum injection pressure decreases with the increase of the width of the injection slot; for the multiple injection slots configuration the resin is injected into the fiber reinforcement through two injection slots which acts somewhat as the wide injection slot which causes the decrease in the minimum injection pressure to achieve complete wetout.

Figures 4-34 through 4-39 show the impact of location ($x_{IS}$) of multiple injection slots at different chamber lengths ($L_T$) on the minimum injection pressure required to achieve complete wetout along with the corresponding maximum interior chamber resin wall pressure of the attached-die and the detached-die configurations. Figures 4-34, 4-35 and 4-36 are for a pull speed of 0.0254 m/s at CR values 2, 3 and 4 respectively and Figs. 4-37, 4-38 and 4-39 are for a pull speed of 0.0508 m/s at CR values 2, 3 and 4 respectively. The vertical axis is the non-

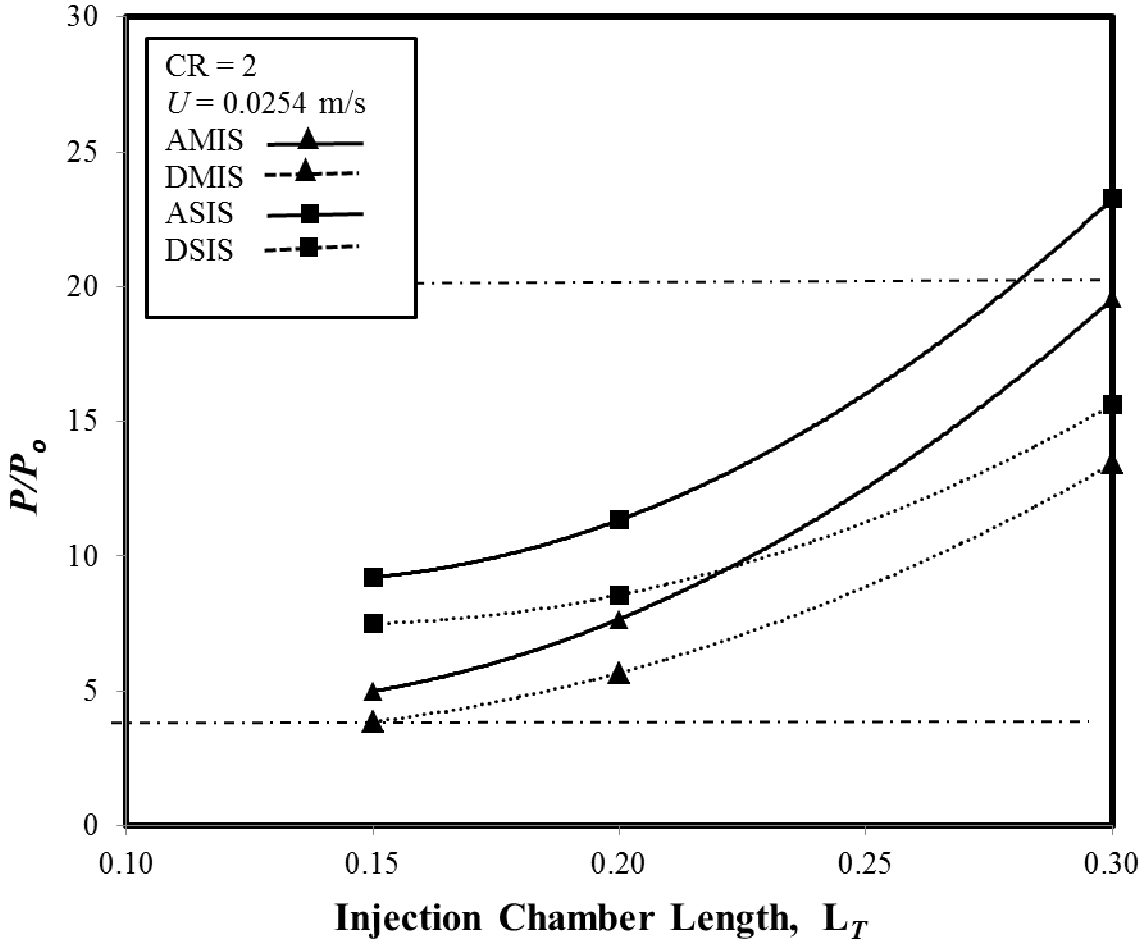


**Figure 4-32. Comparison of Attached-Die Maximum Pressure for Single Injection Slot (ASIS) and Detached-Die Maximum Pressure for Single Injection Slot (DSIS) and Attached-Die Maximum Pressure for Multiple Injection Slot (AMIS) and Detached-Die Maximum Pressure for Multiple Injection Slot (DMIS) for Different Injection Chamber Lengths at CR = 2, $x_{IS}$ = 0.40 $L_I$, $U$ = 0.0254 m/s, $H_D$ = 0.003175 m, $W_D$ = 0.0635 m, $V_{fo}$ = 0.68, μ = 0.75 Pa·s.**

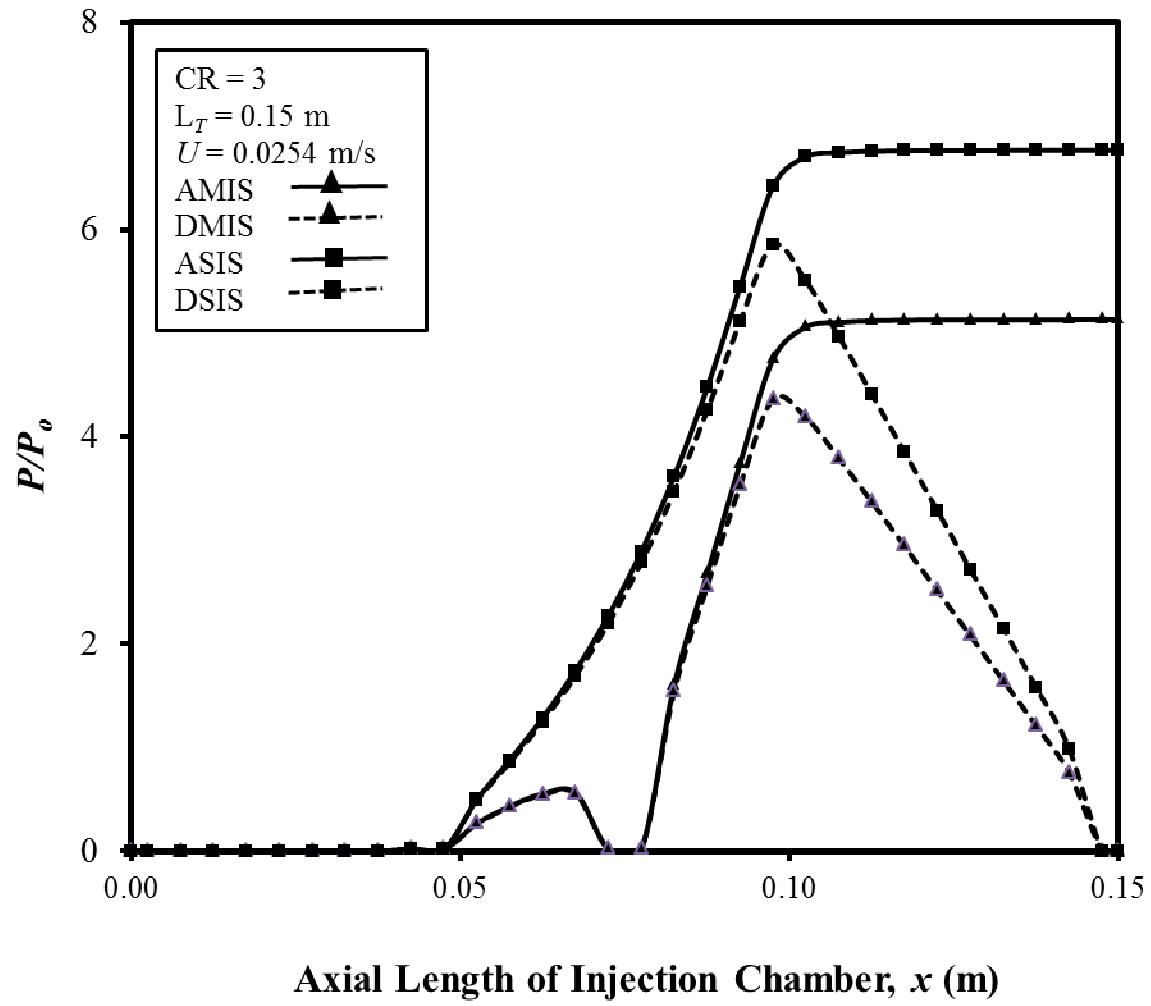


**Figure 4-33. Comparison of Chamber Wall Axial Pressure Profiles of Attached-Die Single Injection Slot (ASIS) and Detached-Die Single Injection Slot (DSIS) configurations and Attached-Die Multiple Injection Slot (AMIS) and Detached-Die Multiple Injection Slot (DMIS) configurations for for Injection Chamber Length of $L_T$ = 0.15 m, at CR = 2, $x_{IS}$ = 0.4 $L_I$, $U$ = 0.0254 m/s, $H_D$ = 0.003175 m, $W_D$ = 0.0635 m, $V_{fo}$ = 0.68, μ = 0.75 Pa·s.**

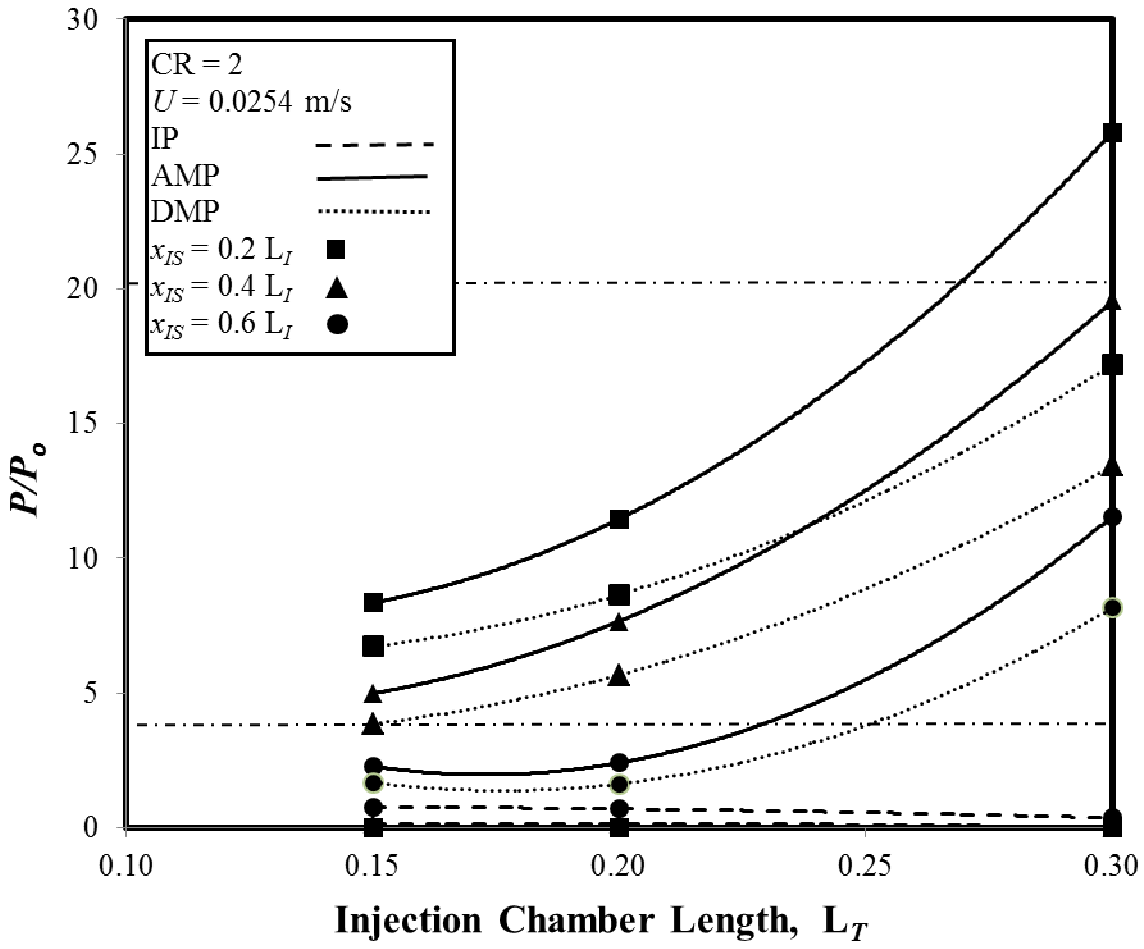


**Figure 4-34. Injection Pressure (IP) and Attached-Die Maximum Pressure (AMP) and Detached-Die Maximum Pressure (DMP) for Different Injection Chamber Lengths and Different Multiple Injection Slot Locations ($x_{IS}$) at CR = 2, $U$ = 0.0254 m/s, $H_D$ = 0.003175 m, $W_D$ = 0.0635 m, $V_{fo}$ = 0.68, μ = 0.75 Pa·s.**

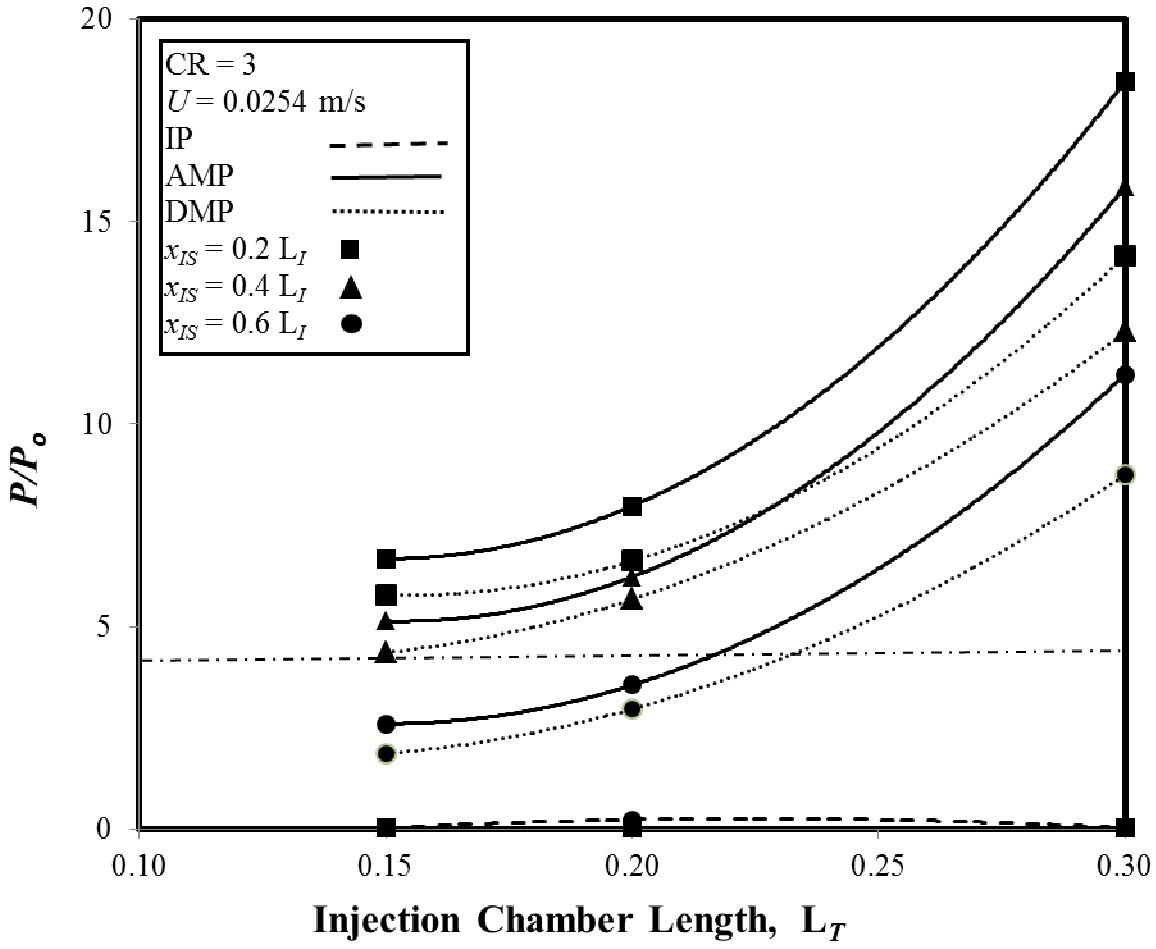


**Figure 4-35. Injection Pressure (IP) and Attached-Die Maximum Pressure (AMP) and Detached-Die Maximum Pressure (DMP) for Different Injection Chamber Lengths and Different Multiple Injection Slot Locations ($x_{IS}$), at CR = 3, $U$ = 0.0254 m/s, $H_D$ = 0.003175 m, $W_D$ = 0.0635 m, $V_{fo}$ = 0.68, μ = 0.75 Pa·s.**

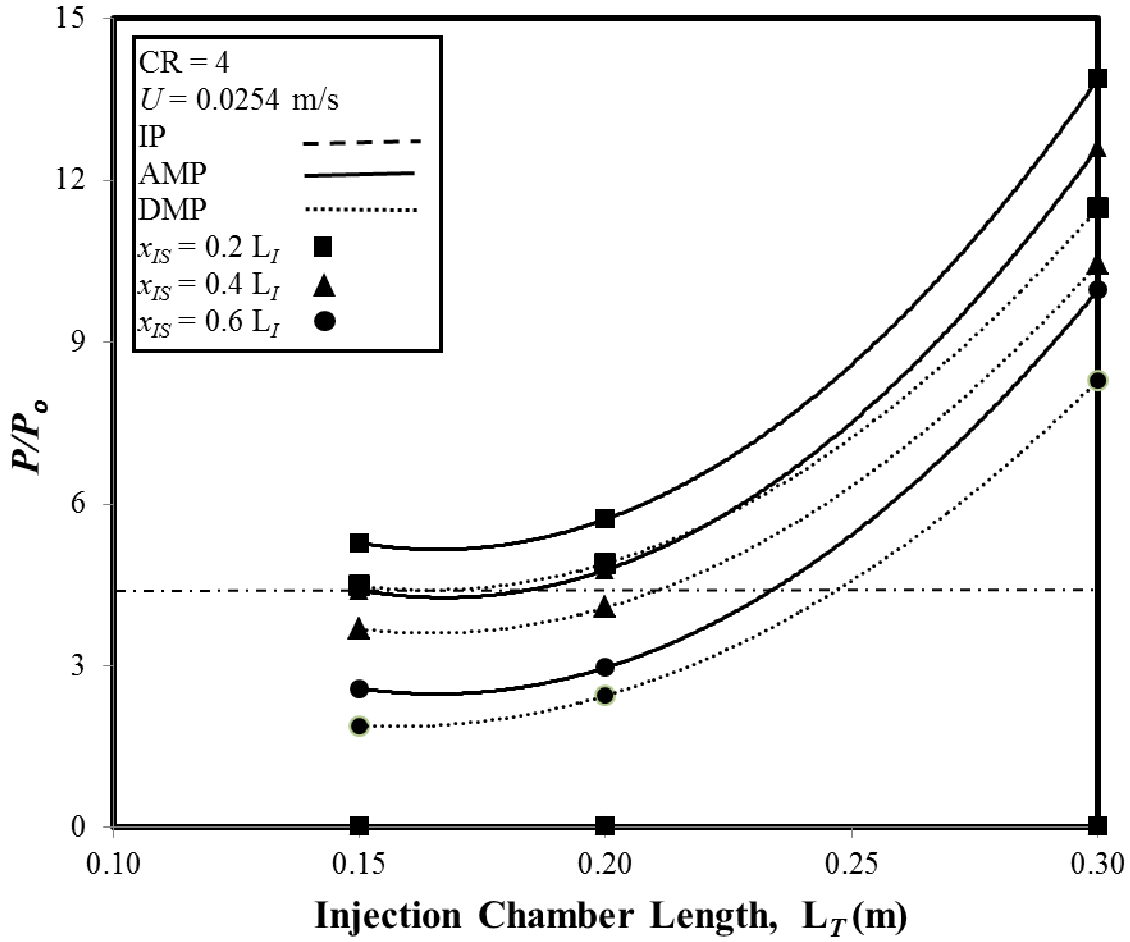


**Figure 4-36. Injection Pressure (IP) and Attached-Die Maximum Pressure (AMP) and Detached-Die Maximum Pressure (DMP) for Different Injection Chamber Lengths and Different Multiple Injection Slot Locations ($x_{IS}$), at CR = 4, $U$ = 0.0254 m/s, $H_D$ = 0.003175 m, $W_D$ = 0.0635 m, $V_{fo}$ = 0.68, μ = 0.75 Pa·s.**

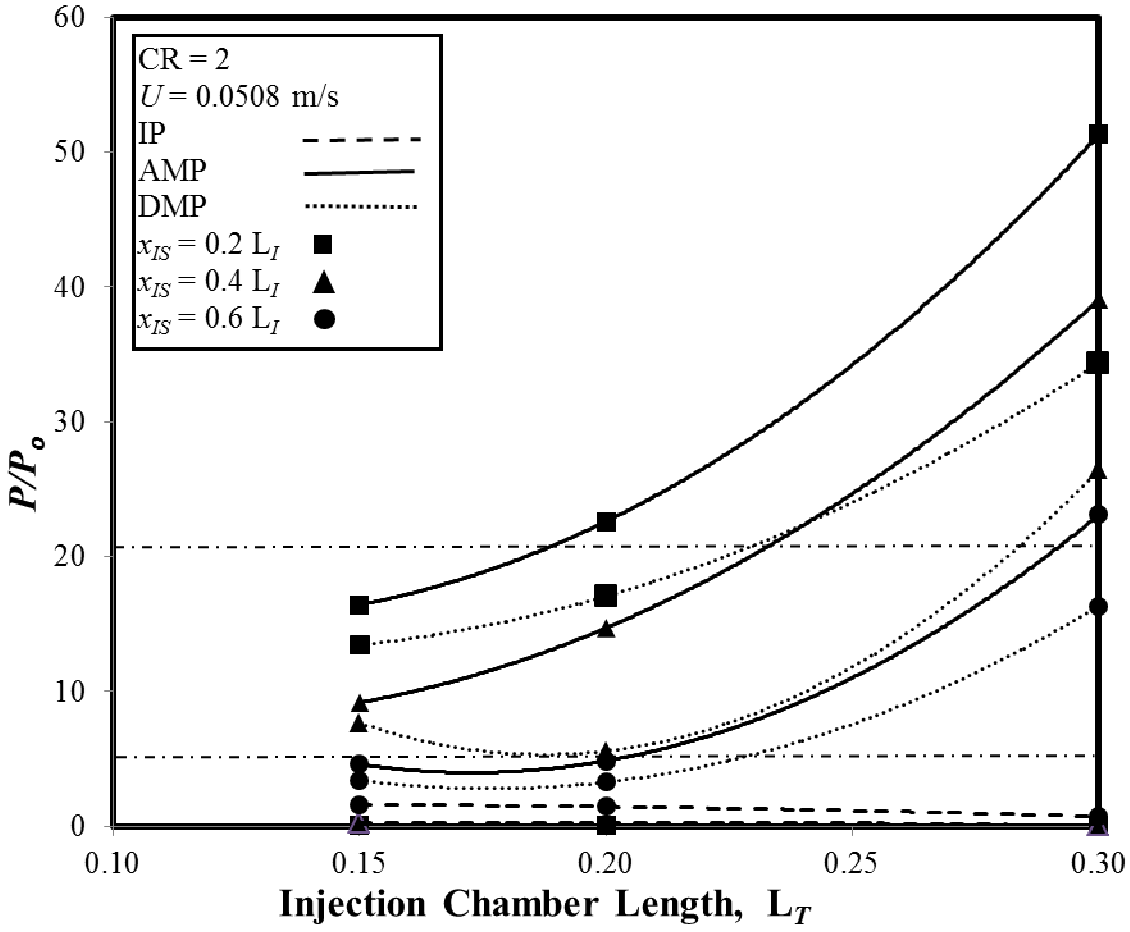


**Figure 4-37. Injection Pressure (IP) and Attached-Die Maximum Pressure (AMP) and Detached-Die Maximum Pressure (DMP) for Different Injection Chamber Lengths and Different Multiple Injection Slot Locations ($x_{IS}$), at CR = 2, $U$ = 0.0508 m/s, $H_D$ = 0.003175 m, $W_D$ = 0.0635 m, $V_{fo}$ = 0.68, μ = 0.75 Pa·s.**

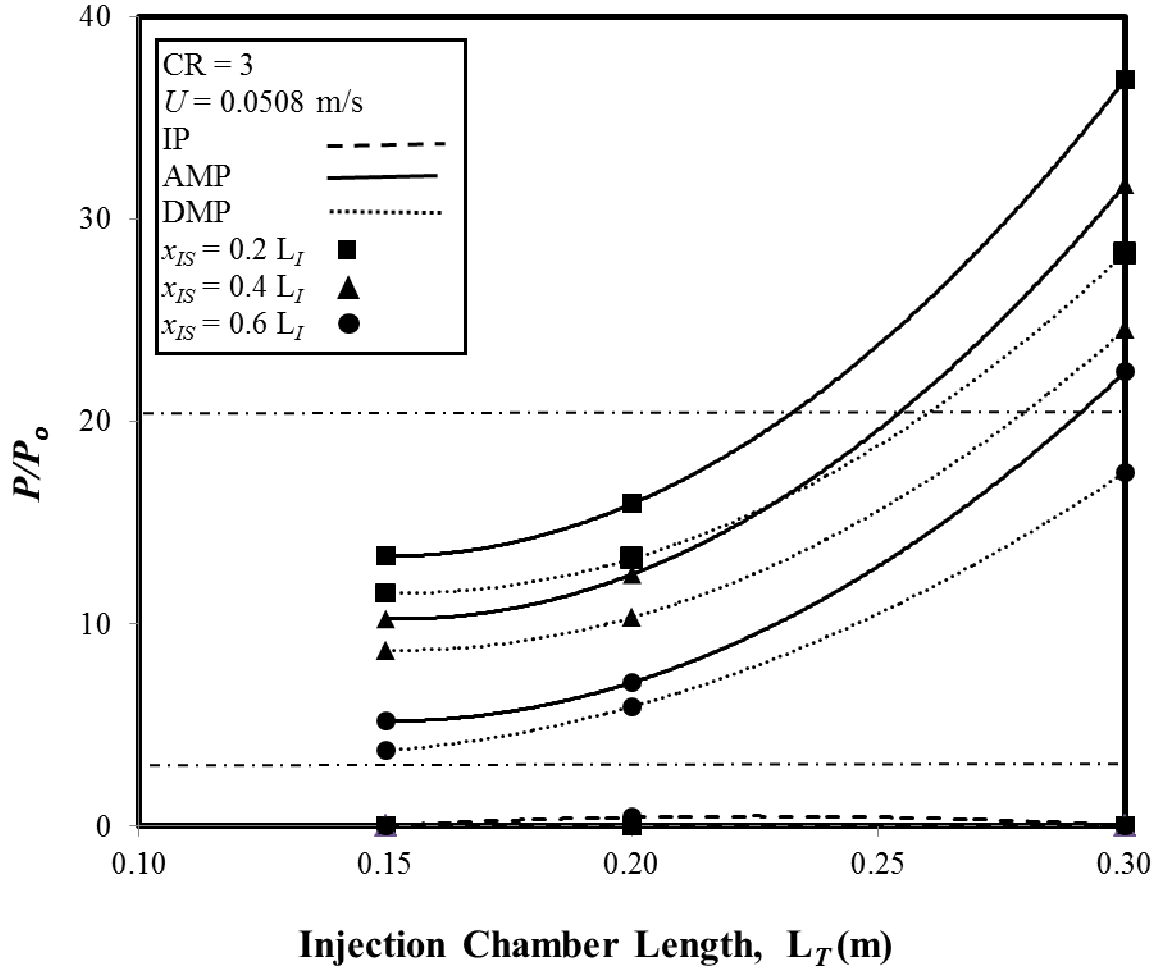


**Figure 4-38. Injection Pressure (IP) and Attached-Die Maximum Pressure (AMP) and Detached-Die Maximum Pressure (DMP) for Different Injection Chamber Lengths and Different Multiple Injection Slot Locations ($x_{IS}$), at CR = 3, $U$ = 0.0508 m/s, $H_D$ = 0.003175 m, $W_D$ = 0.0635 m, $V_{fo}$ = 0.68, μ = 0.75 Pa·s.**

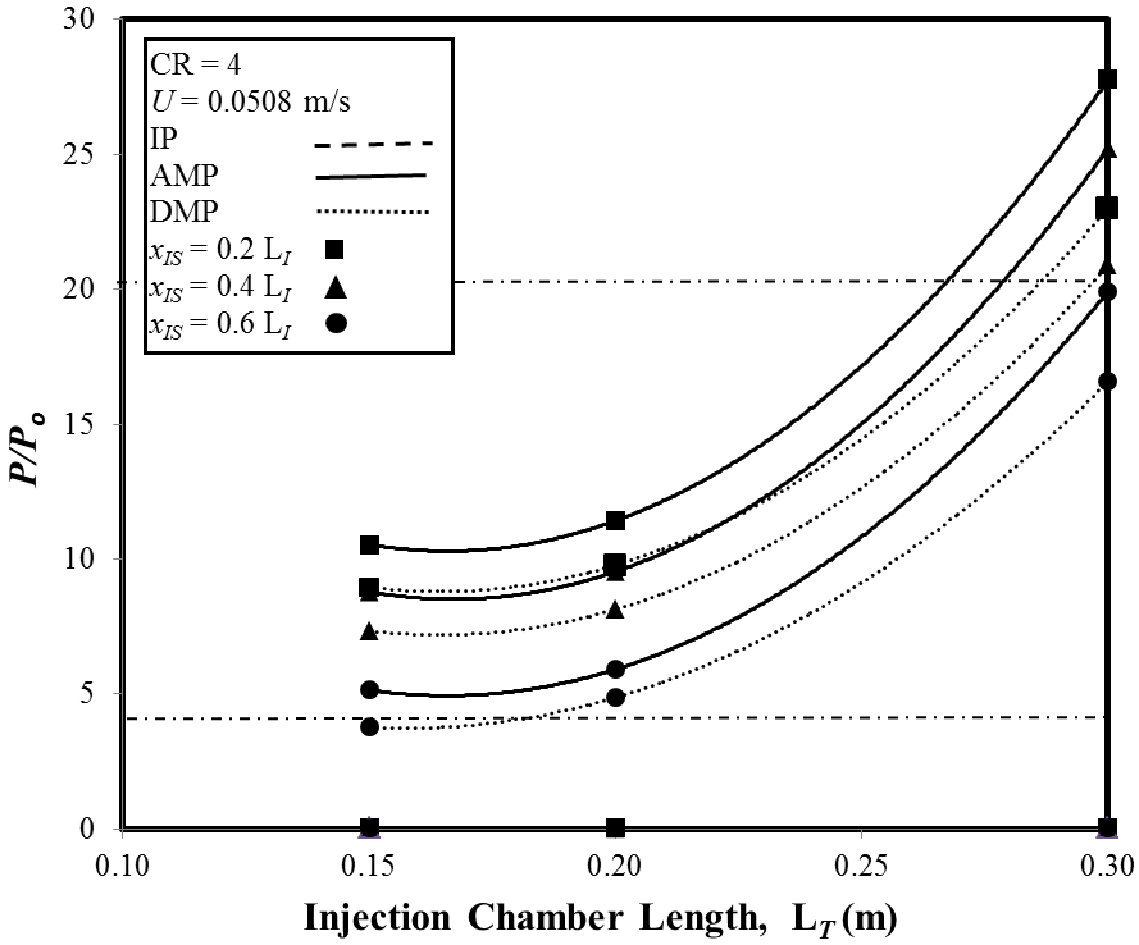


**Figure 4-39. Injection Pressure (IP) and Attached-Die Maximum Pressure (AMP) and Detached-Die Maximum Pressure (DMP) for Different Injection Chamber Lengths and Different Multiple Injection Slot Locations ($x_{IS}$), at CR = 4, $U$ = 0.0508 m/s, $H_D$ = 0.003175 m, $W_D$ = 0.0635 m, $V_{fo}$ = 0.68, μ = 0.75 Pa·s.**

dimentionlized gauge pressure, taking atmospheric pressure ($P_o$ = 0.1013 MPa) as the reference pressure. The lower horizontal line in the plots corresponds to $P$ = 0.42 MPa and the upper horizontal line in the plots corresponds to $P$ = 2.07 MPa, which represent the limits for the acceptable manufacturing solutions for the minimum resin injection pressure and the maximum interior chamber wall pressure. If the minimum injection pressure to achieve complete wetout is both below the lower horizontal line and the maximum chamber wall pressure is below the upper horizontal line simultaneously, then this is an acceptable set of parameters for pultrusion manufacturing.

Figures 4-34 through 4-39, illustrate that for particular length of the injection chamber ($L_T$), the maximum pressure for both the attached-die and detached-die configurations decreases when the location of multiple injection slot width is moved downstream from $x_{IS}$ = 0.20 $L_I$ to 0.60 $L_I$. From Fig. 4-34 for pull speed of 0.0254 m/s and Fig. 4-37 for pull speed of 0.0508 m/s, it can be observed for CR = 2 the minimum injection pressure required to achieve complete wetout remains about the same even when the length of the injection chamber is increased as long as the location of multiple injection slots is at the same percentage location. However, for higher CR values of 3 and 4, the injection pressure values are essentially atmospheric (0.002 MPa) at all lengths of the injection chamber ($L_T$); hence they lie essentially on the $x$-axis. The maximum interior chamber wall pressure for the attached-die configuration is higher than the corresponding detached-die configuration as observed from Figs. 4-34 through 4-39. The maximum interior pressure for both the attached-die and the detached-die configurations increases with an increase of the injection chamber length ($L_T$) for the given multiple injection slot location; however, for CR = 2, with the multiple injection slots at location 0.6 $L_I$, the maximum pressure for both the attached-die and the detached-die configurations remain about

the same when the length of the injection chamber ($L_T$) increases from 0.15 m to 0.2 m and then the pressure increases when $L_T$ is increased from 0.2 m to 0.3 m. Since the maximum interior chamber wall pressure is lower for multiple injection slots configuration, as observed from Figs. 4-34 through 4-36, almost all cases are within the feasible manufacturing range; however, for CR = 2, and when the location of multiple injection slots is at 0.2 $L_I$ of injection chamber length $L_T$ = 3 m, the maximum pressure is not at feasible for manufacturing. From Figs. 4-34 through 4-36 for $U$ = 0.0254 m/s and from Figs. 4-37 through 4-39 for $U$ = 0.0508 m/s, it is observed that, the injection pressure and maximum interior chamber wall pressure of both the attached-die and the detached-configurations have the same trend-wise behavior even when the pull speed is doubled from 0.0254 m/s to 0.0508 m/s; however the maximum pressure is increased significantly when the pull speed is doubled. Hence, for the doubled pull speed of 0.0508 m/s as observed from Figs. 4-37, 4-38 and 4-39, the maximum interior chamber wall pressure for both the attached-die and detached-die configurations may lie in the non-feasible manufacturing region above the upper horizontal line corresponding to 2.07 MPa at large chamber lengths ($L_T$). The multiple injection slot configuration has both more favorable minimum injection pressures and maximum chamber wall pressures for both the attached-die and the detached-die configuration than the corresponding single injection slot location configuration.

Figures 4-40, 4-41 and 4-42 for pull speed $U$ = 0.0254 m/s and Figs. 4-43, 4-44 and 4-45 for pull speed $U$ = 0.0508 m/s illustrate the behavior of chamber wall resin pressure profiles inside the injection chamber of both the attached-die and the detached-die configurations for the different location of multiple slots ($x_{IS}$ = 0.20 $L_I$, 0.40 $L_I$ and 0.60 $L_I$) for the various lengths ($L_T$ = 0.15 m, 0.20 m and 0.30 m) of the injection chamber with CR = 3. As observed from these figures, for all chamber lengths and pull speeds, at a given location of the multiple injection slots

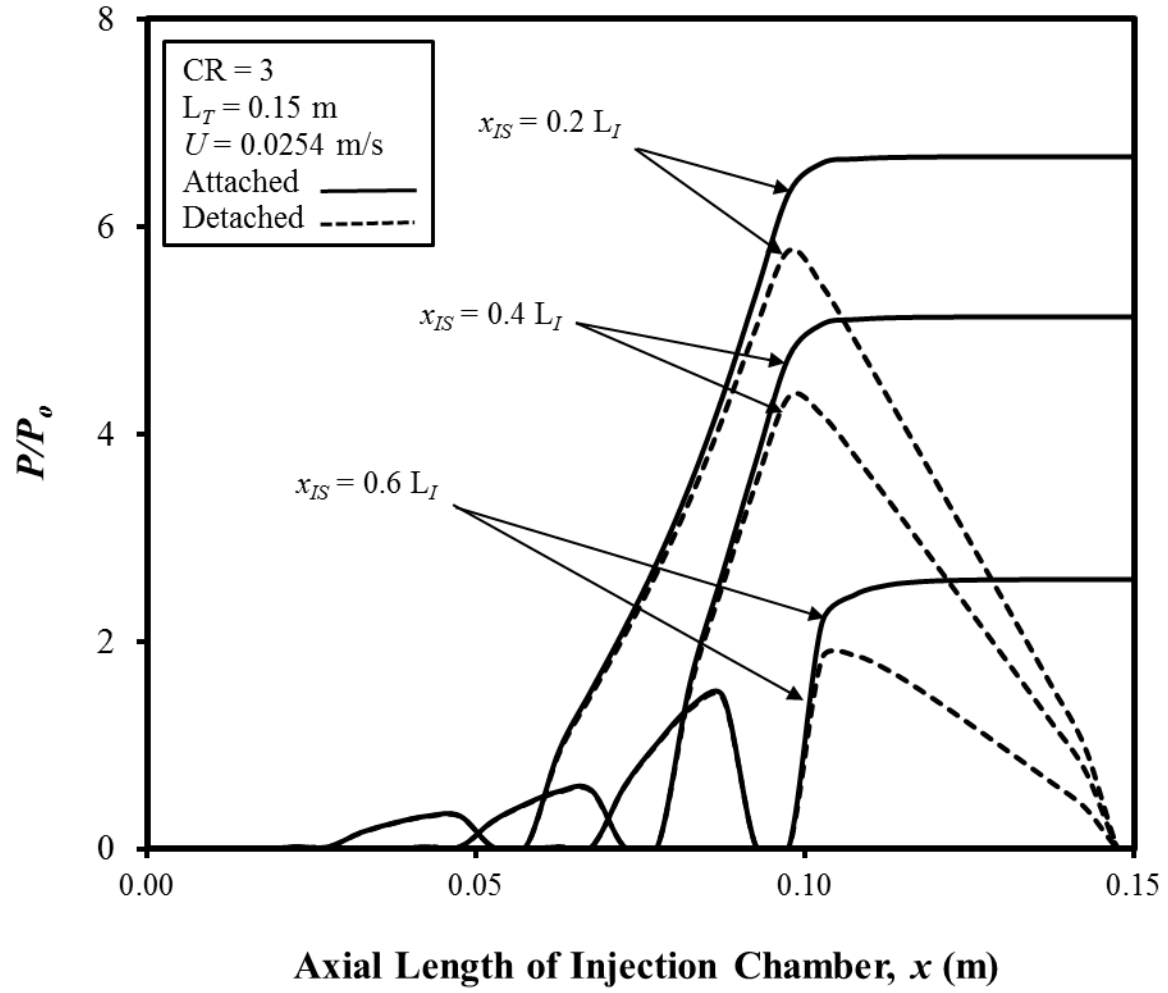


**Figure 4-40. Chamber Wall Axial Pressure Profiles for Attached-Die and Detached-Die Configurations for Injection Chamber Length of $L_T$ = 0.15 m, CR = 3, and $U$ = 0.0254 m/s at Different Multiple Injection Slot Locations ($x_{IS}$).**

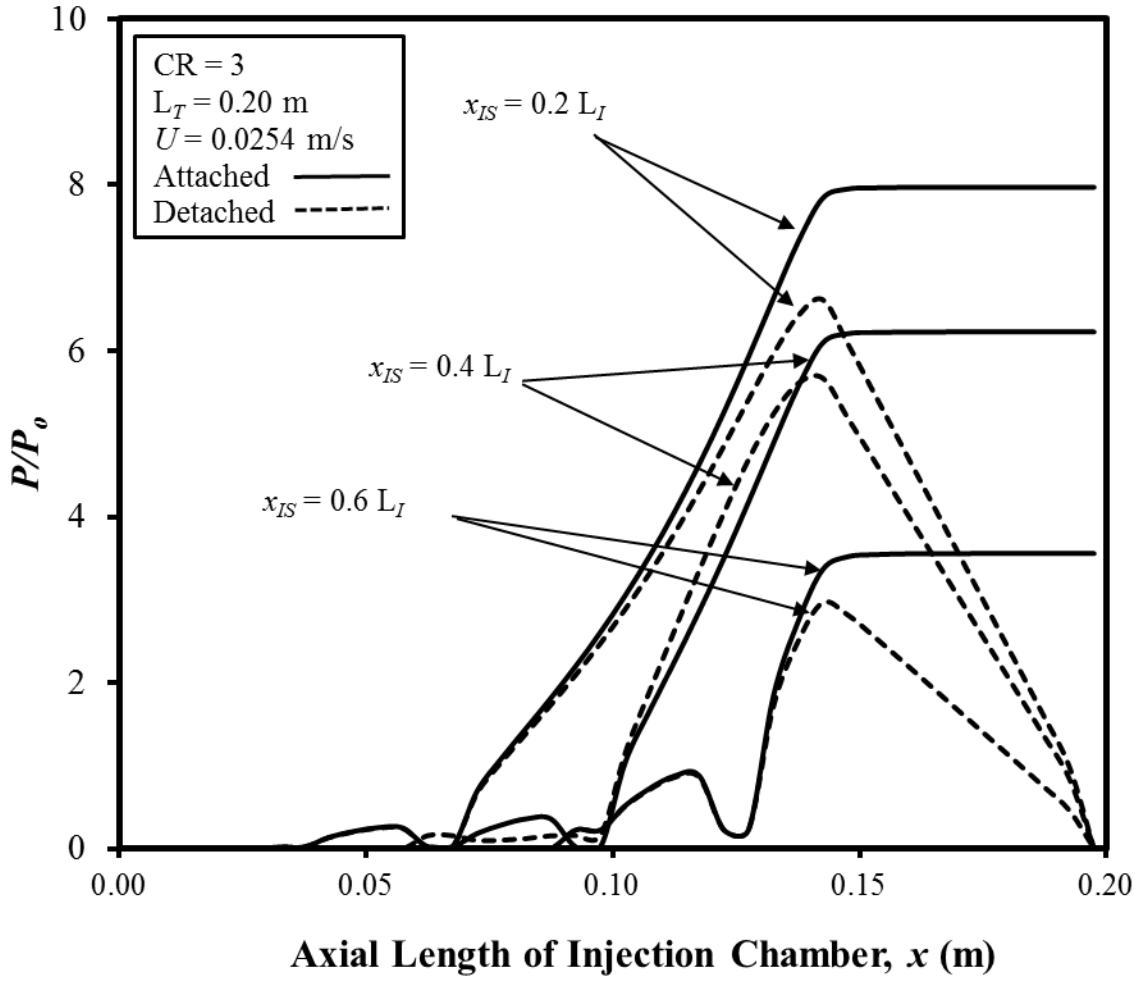


**Figure 4-41. Chamber Wall Axial Pressure Profiles for Attached-Die and Detached-Die Configurations for Injection Chamber Length of $L_T$ = 0.20 m, CR = 3, and $U$ = 0.0254 m/s at Different Multiple Injection Slot Locations ($x_{IS}$).**

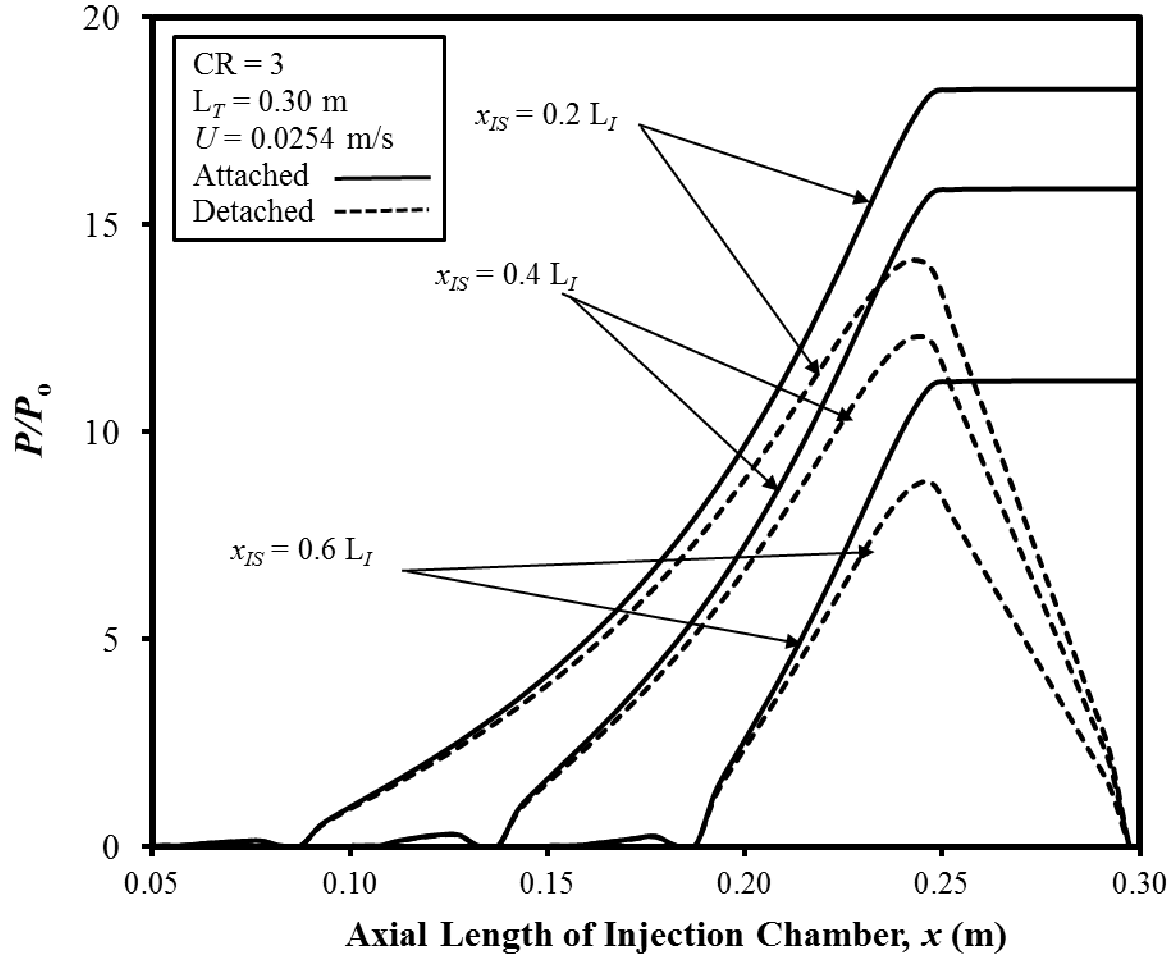


**Figure 4-42. Chamber Wall Axial Pressure Profiles for Attached-Die and Detached-Die Configurations for Injection Chamber Length of $L_T$ = 0.30 m, CR = 3, and $U$ = 0.0254 m/s at Different Multiple Injection Slot Locations ($x_{IS}$).**

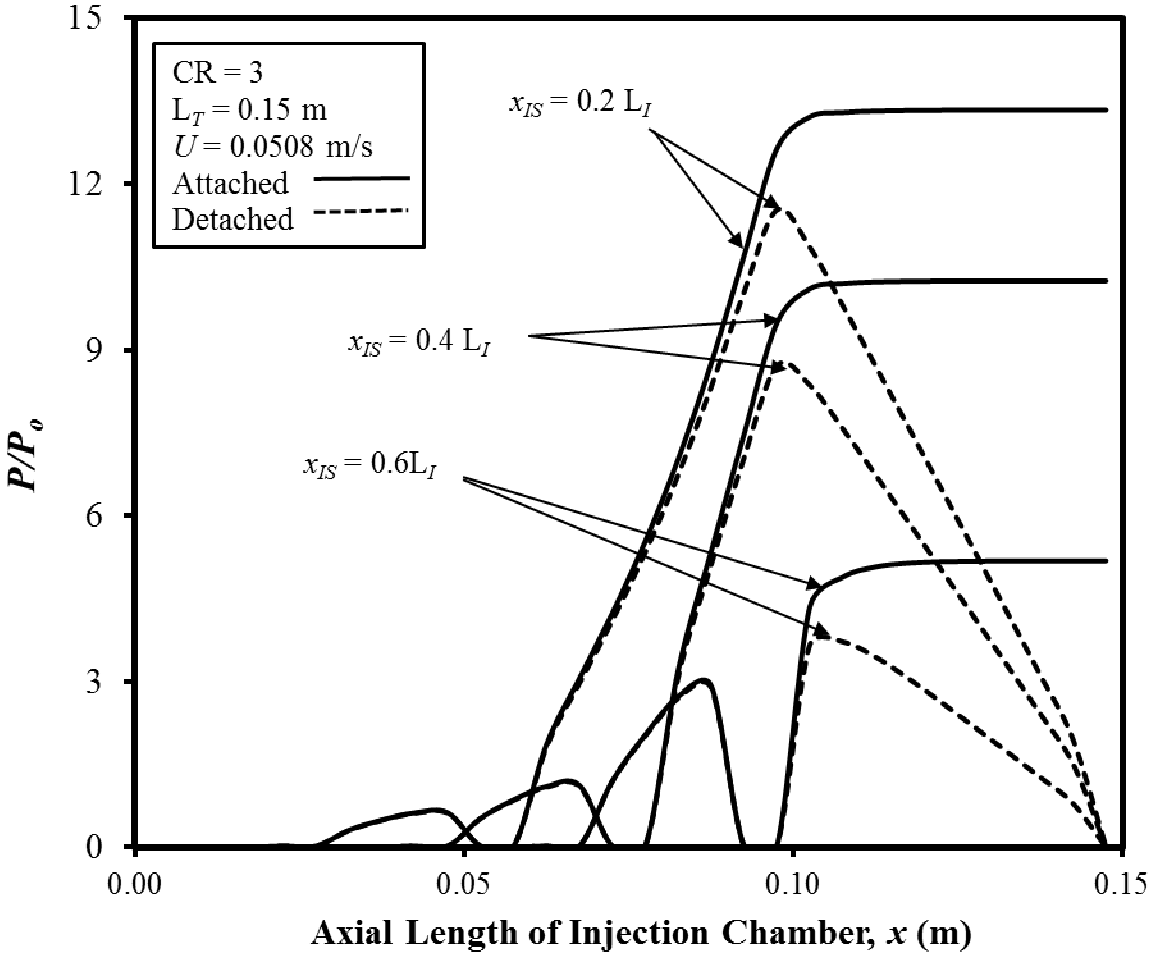


**Figure 4-43. Chamber Wall Axial Pressure Profiles for Attached-Die and Detached-Die Configurations for Injection Chamber Length of $L_T$ = 0.15 m, CR = 3, and $U$ = 0.0508 m/s at Different Multiple Injection Slot Locations ($x_{IS}$).**

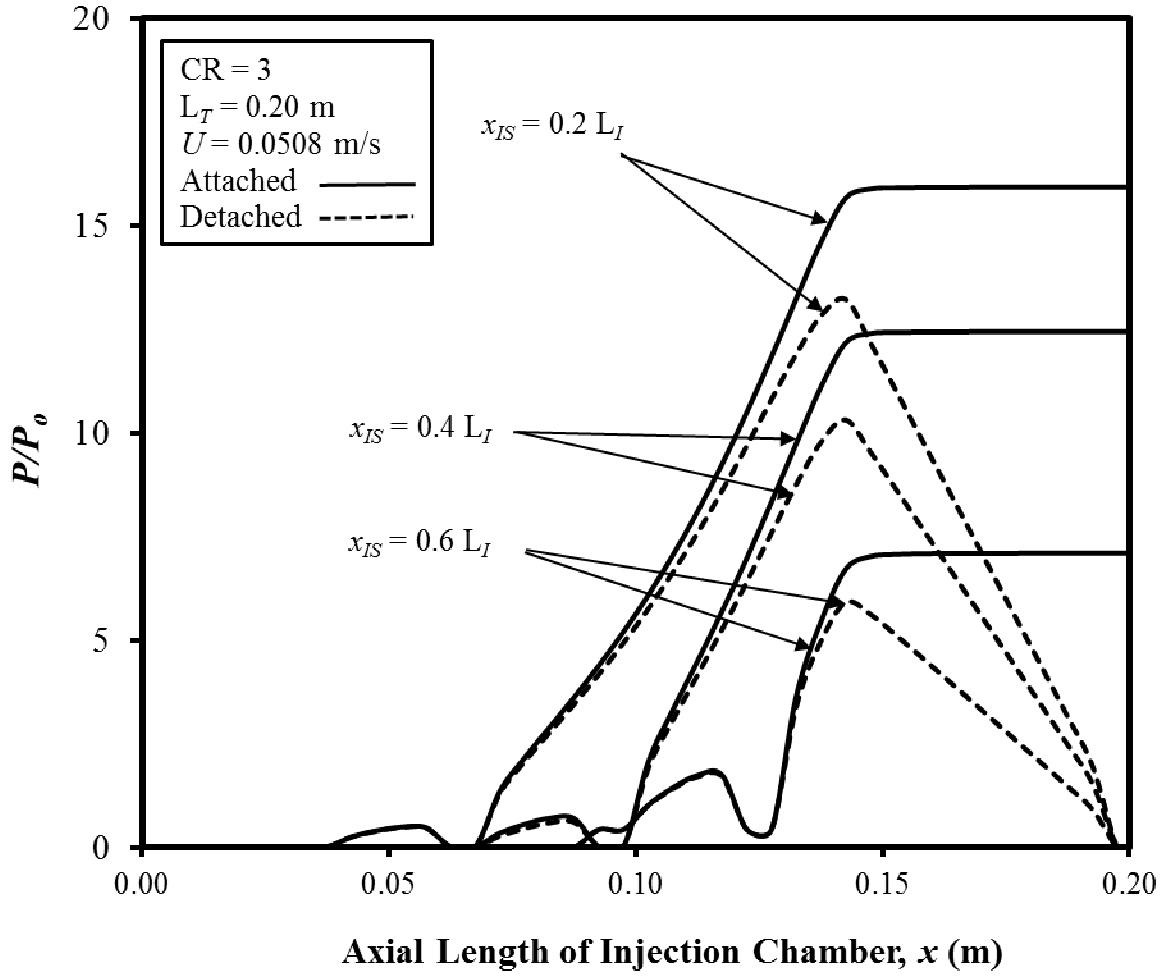


**Figure 4-44. Chamber Wall Axial Pressure Profiles for Attached-Die and Detached-Die Configurations for Injection Chamber Length of $L_T$ = 0.20 m, CR = 3, and $U$ = 0.0508 m/s at Different Multiple Injection Slot Locations ($x_{IS}$).**

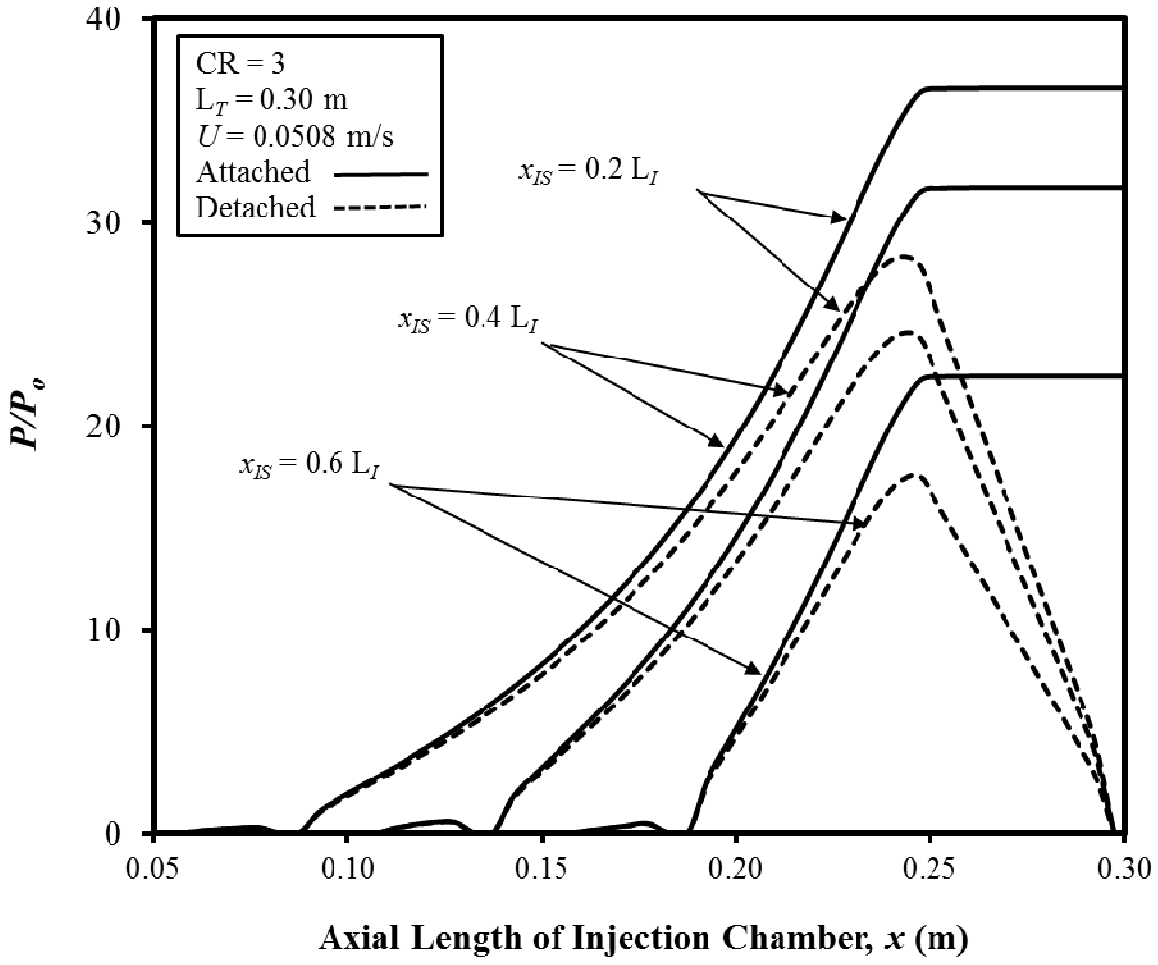


**Figure 4-45. Chamber Wall Axial Pressure Profiles for Attached-Die and Detached-Die Configurations for Injection Chamber Length of $L_T$ = 0.30 m, CR = 3, and $U$ = 0.0508 m/s at Different Multiple Injection Slot Locations ($x_{IS}$).**

($x_{IS}$), the chamber wall pressure of the attached-die configuration initially rises to the injection pressure at the first slot, then decreases, and then rises back to injection pressure at the second injection slot, and then increases to the maximum gauge pressure value near the end of Region I and maintains the same pressure value through Region II to the chamber exit; whereas, for the detached-die configuration the pressure rises to the injection pressure at the first slot, then decreases, and then rises back to injection pressure at the second injection slot, and then increases to the maximum gauge pressure value near the end of Region I and then finally decreases to zero gauge pressure at the chamber exit gap. From Figs. 4-40 through 4-45, it can be observed that, the maximum interior chamber wall pressure for the attached-die is greater than the corresponding detached-die configuration and the maximum pressure of both configurations is greater when the location of the multiple injection slots ($x_{IS}$) are upstream than when the location of the injection slots ($x_{IS}$) are downstream in the injection chamber. It can also be observed that as $L_T$ increases, the maximum interior chamber wall pressure values for the both attached-die and the detached-die configurations increase. For the same proportional location, the trend-wise behavior of the wall pressure is observed to be about the same when the pull speed is increased from 0.0254 m/s to 0.0508 m/s, but the maximum pressure is observed to be significantly increased when the pull speed is doubled.

Figures 4-46 through 4-48 show the steady-state liquid resin flow front and gauge isopressure contours within the liquid resin wetout region at CR = 4 with the injection slot location at 0.20 $L_I$ (Fig. 4-46), 0.40 $L_I$ (Fig. 4-47) 0.60 $L_I$ (Fig. 4-48) of Region I ($L_I$) and pull a speed of 0.0254 m/s for $L_T$ = 0.15 m. Figure 4-49 shows the steady-state liquid resin flow front and the isopressure contours within the liquid resin wetout region and for CR = 4, $x_{IS}$ = 0.20 $L_I$ for $L_T$ = 0.30 m and $U$ = 0.0254 m/s. The first dark contour represents the liquid resin flow front

and the thin contour lines represent the isopressure contours in kPa. The resin flow front and the pressure values for the attached-die and the detached-die configurations can be readily compared from these figures. The chamber pressure values are always lower for the detached-die configuration system as compared to the attached-die configuration which can be observed from Figs. 4-46 through 4-49. In the detached–die configuration, the isopressure contour can be seen in Region II of the injection chamber due to the decreasing chamber pressure in the Region II and this pressure corresponds to the same pressure contours as depicted in Region I of the injection chamber. Figures 4-46 through 4-49 are displayed not to scale; this was done in order to make the results more viewable and understandable.

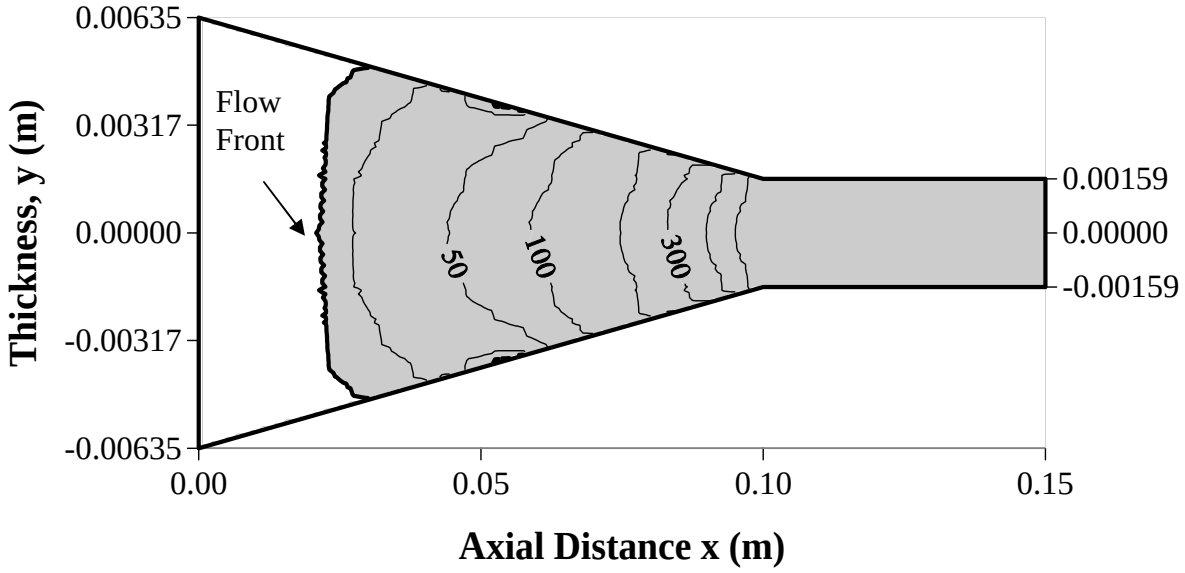


**a. Attached-Die Configuration**

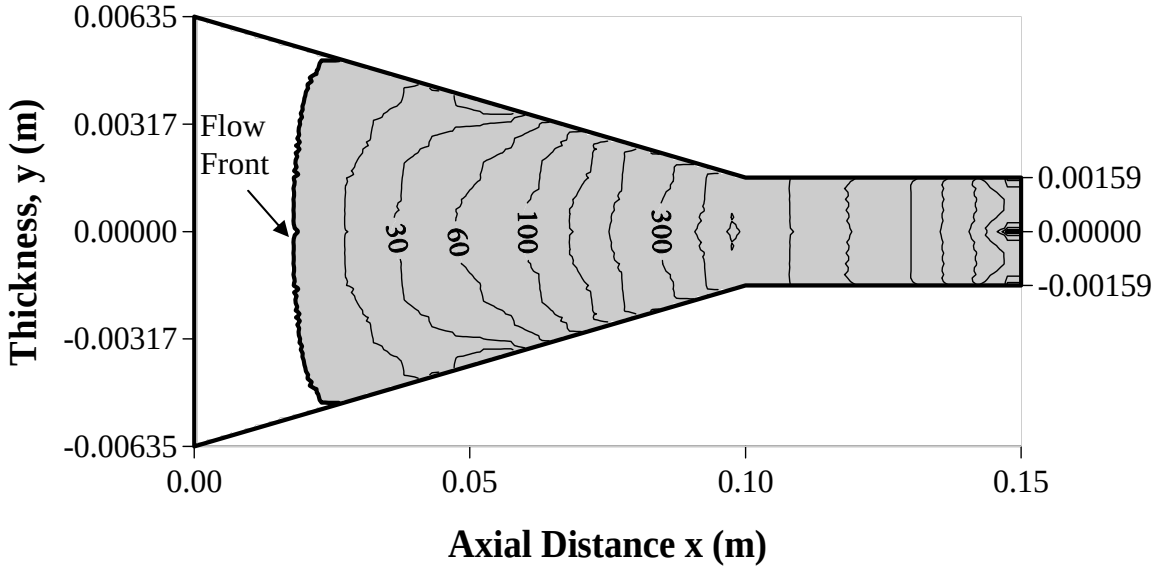


**b. Detached-Die configuration**

**Figure 4-46. Flow Front Profile and Gauge Isopresure (kPa) Contours for Case E7, Table 4-5 for $L_T$ = 0.15 m, $x_{IS}$ = 0.2 $L_I$, CR = 4, $V_{fo}$ = 0.68, μ = 0.75 Pa·s with $U$ = 0.0254 m/s (Not to Scale).**

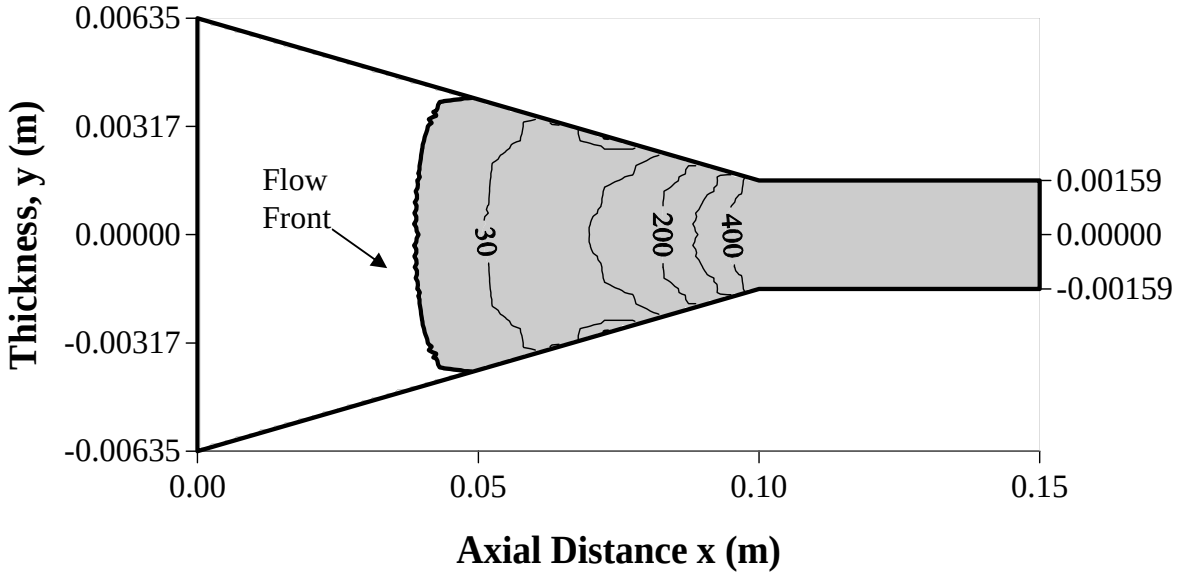


**a. Attached Die Configuration**

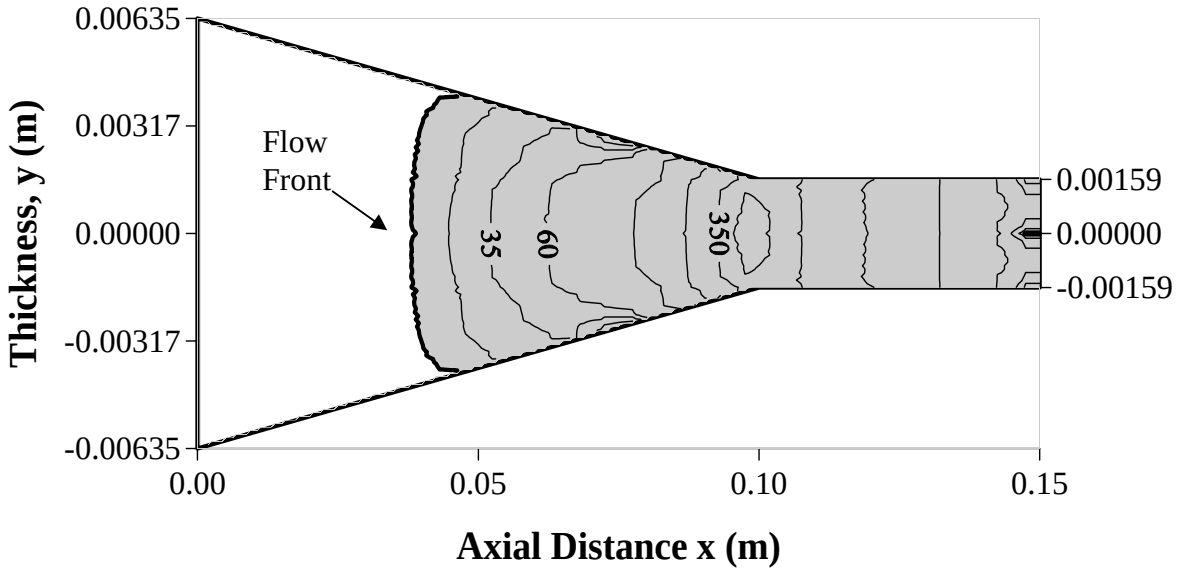


**b. Detached Die Configuration**

**Figure 4-47. Flow Front Profile and Gauge Isopresure (kPa) Contours for Case E8, Table 4-5 for $L_T$ = 0.15 m, $x_{IS}$ = 0.4 $L_I$, CR = 4, $V_{fo}$ = 0.68, μ = 0.75 Pa·s with $U$ = 0.0254 m/s (Not to Scale).**

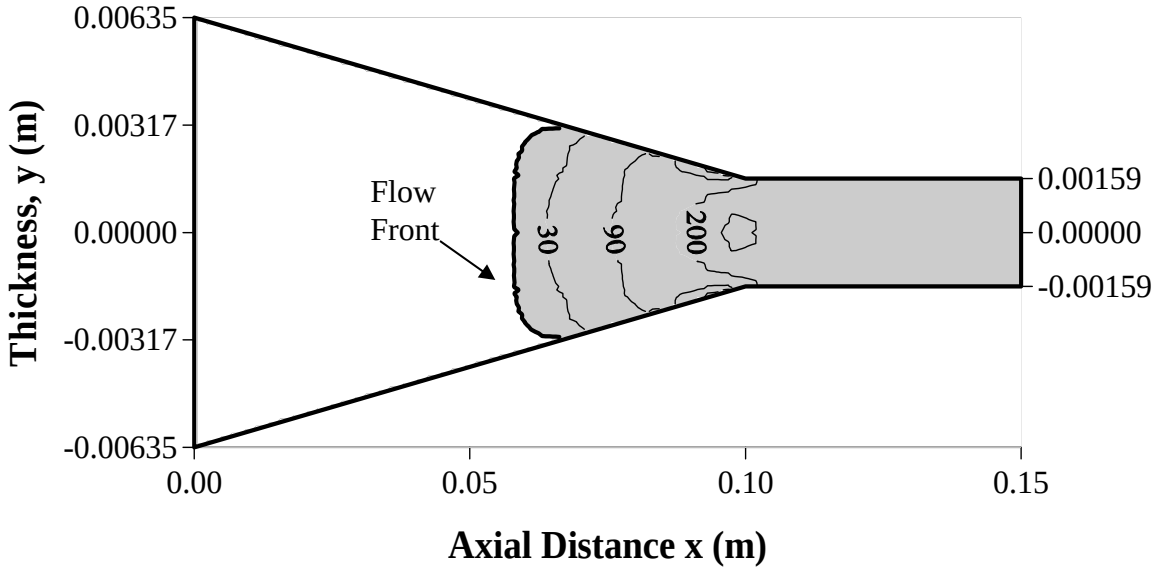


**a. Attached Die Configuration**

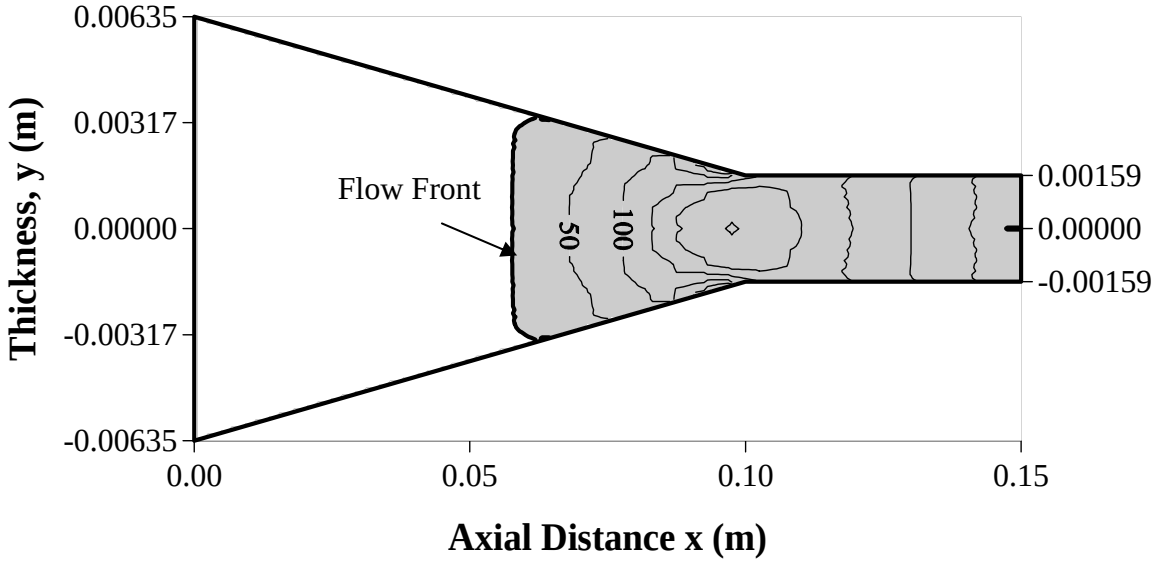


**b. Detached Die Configuration**

**Figure 4-48. Flow Front Profile and Gauge Isopresure (kPa) Contours for Case E9, Table 4-5 for $L_T$ = 0.15 m, $x_{IS}$ = 0.6 $L_I$, CR = 4, $V_{fo}$ = 0.68, μ = 0.75 Pa·s with $U$ = 0.0254 m/s (Not to Scale).**

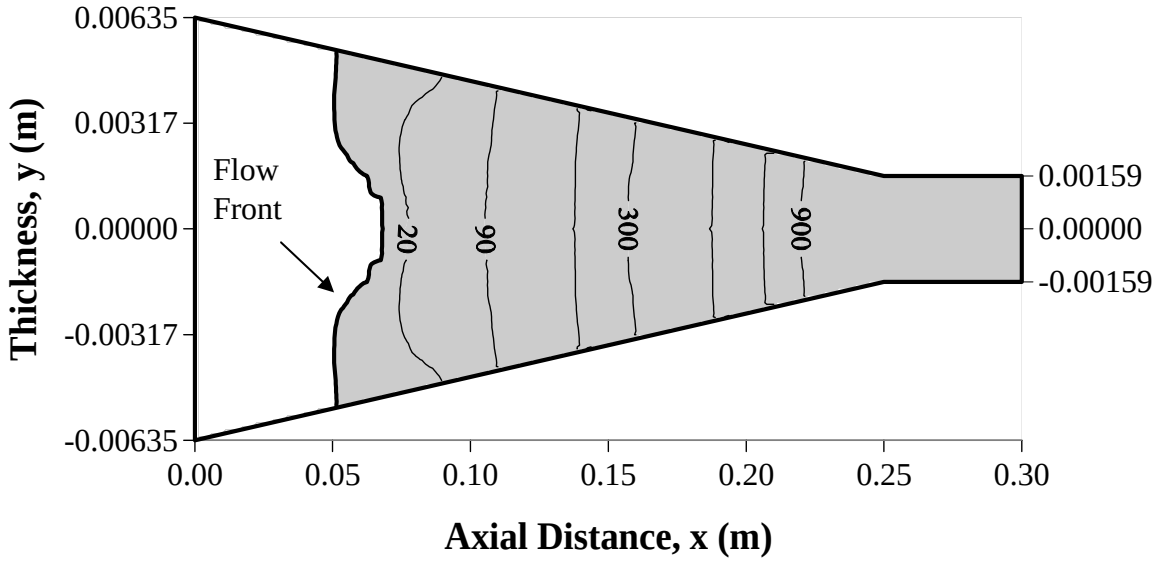


**a. Attached Die Configuration**

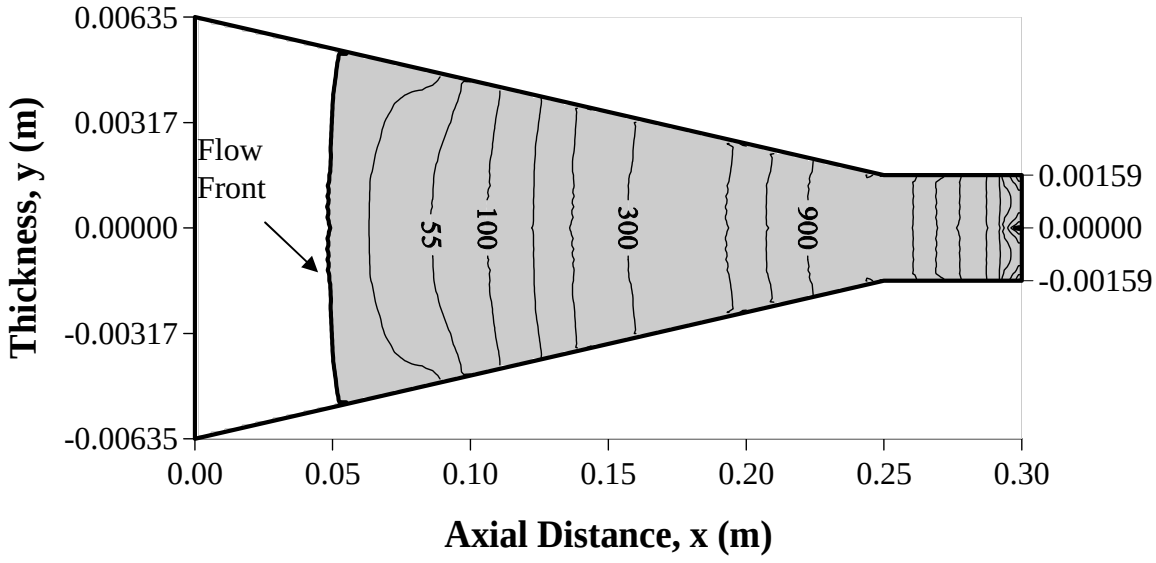


**b. Detached Die Configuration**

**Figure 4-49. Flow Front Profile and Gauge Isopresure (kPa) Contours for Case E27, Table 4-5 for $L_T$ = 0.30 m, $x_{IS}$ = 0.2 $L_I$, CR = 4, $V_{fo}$ = 0.68, μ = 0.75 Pa·s with $U$ = 0.0254 m/s (Not to Scale).**

### *4.4 Final Composite Thickness*

In this section, the impact of part thickness, $H_D$ (nominal thickness of final composite) on the minimum injection pressure necessary to achieve complete wetout of the fiber reinforcement inside the injection chamber as well as the corresponding maximum interior chamber wall pressure for both the attached-die and the detached-die configurations were studied. The part thicknesses ($H_D$) used for this study are 0.003175 m, 0.006350 m and 0.012700 m at different injection chamber lengths ($L_T$) with compression ratios of 2, 3 and 4; the results were compared at two different pull speeds, $U$ = 0.0254 m/s and 0.0508 m/s. The injection slot was placed at 0.60 $L_I$ of the axial distance in Region I of the injection chamber. For a particular part thickness of the injection chamber ($H_D$) the other parameters, both processing and geometric, were hold at their nominal values.

Table 4-7 and Table 4-8 show the minimum injection gauge pressure required for the complete wetout of the fiber reinforcement as well as the corresponding maximum gauge pressure for both the attached-die and the detached-die configurations for the pull speeds of 0.0254 m/s and 0.0508 m/s, respectively. As observed from the tables in column 6, the minimum injection pressure to achieve complete wetout for both the attached-die and the detached-die configurations increases with an increase in the part thickness and it decreases with an increase in CR value. As the part thickness increases, it becomes difficult for the liquid resin to flow completely through fiber reinforcement; hence, the injection pressure must increase to achieve complete wetout. With the increasing tapering of the injection chamber (increasing of CR values), the local fiber volume fraction at the injection slot decreases causing less resistance to the liquid resin flow through the fiber reinforcement as explained in Section 4.1.1. At higher CR values as observed from Tables 4-7 and 4-8, the injection pressure remains essentially atmospheric except for CR = 3 in cases G6, G14, and G15; however, for CR = 4, the injection

**Table 4-7. Minimum Injection Pressure Required for Complete Wetout for a Single Slot Placed at 60 % of Region I for Different Part Thicknesses With $U$ = 0.0254 m/s, $V_{fo}$ = 0.68, μ = 0.75 Pa·s, Slot Width $\Delta x$ = 0.01 m, and $W_D$ = 0.0635 m.**

| Case | CR | Part Thickness $H_D$ (m) | Total Length $L_T$ (m) | Injection Slot Location (m) | Injection Pressure (Gauge) MPa | Maximum Pressure (Gauge) MPa | Maximum Pressure (Gauge) (MPa) |
|---|---|---|---|---|---|---|---|
| | | | | | | Attached | Detached |
| G1 | 2 | 0.003175 | 0.15 | 0.06 | 0.077 | 0.70 | 0.58 |
| G2 | 2 | 0.006350 | 0.15 | 0.06 | 0.223 | 0.53 | 0.38 |
| G3 | 2 | 0.012700 | 0.15 | 0.06 | 0.698 | 0.70 | 0.70 |
| G4 | 3 | 0.003175 | 0.15 | 0.06 | 0.002 | 0.55 | 0.48 |
| G5 | 3 | 0.006350 | 0.15 | 0.06 | 0.002 | 0.60 | 0.48 |
| G6 | 3 | 0.012700 | 0.15 | 0.06 | 0.064 | 0.68 | 0.39 |
| G7 | 4 | 0.003175 | 0.15 | 0.06 | 0.002 | 0.45 | 0.38 |
| G8 | 4 | 0.006350 | 0.15 | 0.06 | 0.002 | 0.56 | 0.45 |
| G9 | 4 | 0.012700 | 0.15 | 0.06 | 0.002 | 0.66 | 0.56 |
| G10 | 2 | 0.003175 | 0.20 | 0.09 | 0.085 | 0.81 | 0.62 |
| G11 | 2 | 0.006350 | 0.20 | 0.09 | 0.258 | 0.93 | 0.43 |
| G12 | 2 | 0.012700 | 0.20 | 0.09 | 0.898 | 1.02 | 0.90 |
| G13 | 3 | 0.003175 | 0.20 | 0.09 | 0.002 | 0.59 | 0.49 |
| G14 | 3 | 0.006350 | 0.20 | 0.09 | 0.009 | 0.62 | 0.50 |
| G15 | 3 | 0.012700 | 0.20 | 0.09 | 0.065 | 0.37 | 0.36 |
| G16 | 4 | 0.003175 | 0.20 | 0.09 | 0.002 | 0.44 | 0.38 |
| G17 | 4 | 0.006350 | 0.20 | 0.09 | 0.002 | 0.47 | 0.38 |
| G18 | 4 | 0.012700 | 0.20 | 0.09 | 0.002 | 0.51 | 0.43 |
| G19 | 2 | 0.003175 | 0.30 | 0.15 | 0.051 | 1.74 | 1.19 |
| G20 | 2 | 0.006350 | 0.30 | 0.15 | 0.196 | 1.05 | 0.77 |
| G21 | 2 | 0.012700 | 0.30 | 0.15 | **0.581** | 0.58 | 0.61 |
| G22 | 3 | 0.003175 | 0.30 | 0.15 | 0.002 | 1.42 | 1.10 |
| G23 | 3 | 0.006350 | 0.30 | 0.15 | 0.002 | 1.45 | 1.15 |
| G24 | 3 | 0.012700 | 0.30 | 0.15 | 0.002 | 1.50 | 1.22 |
| G25 | 4 | 0.003175 | 0.30 | 0.15 | 0.002 | 1.16 | 0.96 |
| G26 | 4 | 0.006350 | 0.30 | 0.15 | 0.002 | 1.19 | 0.98 |
| G27 | 4 | 0.012700 | 0.30 | 0.15 | 0.002 | 1.35 | 1.03 |

* Bold font indicates non-acceptable manufacturing solutions for an injection pressure ≥ 0.42 MPa (60 psi) and/or with an associated maximum chamber pressure for attached or detached ≥ 2.07 MPa (300 psi).

**Table 4-8. Minimum Injection Pressure Required for Complete Wetout for a Single Slot Placed at 60 % of Region I for Different Part Thicknesses With $U$ = 0.0508 m/s, $V_{fo}$ = 0.68, μ = 0.75 Pa·s, Slot Width $\Delta x$ = 0.01 m, and $W_D$ = 0.0635 m**

| Case | CR | Part Thickness $H_D$ (m) | Total Length $L_T$ (m) | Injection Slot Location (m) | Injection Pressure (Gauge) MPa | Maximum Pressure (Gauge) MPa | Maximum Pressure (Gauge) (MPa) |
|---|---|---|---|---|---|---|---|
| | | | | | | Attached | Detached |
| H1 | 2 | 0.003175 | 0.15 | 0.06 | 0.161 | 1.40 | 1.15 |
| H2 | 2 | 0.006350 | 0.15 | 0.06 | **0.444** | 1.05 | 0.76 |
| H3 | 2 | 0.012700 | 0.15 | 0.06 | **1.388** | 1.39 | 1.39 |
| H4 | 3 | 0.003175 | 0.15 | 0.06 | 0.002 | 1.11 | 0.95 |
| H5 | 3 | 0.006350 | 0.15 | 0.06 | 0.002 | 1.19 | 0.97 |
| H6 | 3 | 0.012700 | 0.15 | 0.06 | 0.119 | 1.35 | 1.14 |
| H7 | 4 | 0.003175 | 0.15 | 0.06 | 0.002 | 0.90 | 0.76 |
| H8 | 4 | 0.006350 | 0.15 | 0.06 | 0.002 | 1.11 | 0.91 |
| H9 | 4 | 0.012700 | 0.15 | 0.06 | 0.002 | 1.33 | 1.13 |
| H10 | 2 | 0.003175 | 0.20 | 0.09 | 0.168 | 1.61 | 1.24 |
| H11 | 2 | 0.006350 | 0.20 | 0.09 | 0.513 | 1.85 | 0.85 |
| H12 | 2 | 0.012700 | 0.20 | 0.09 | **1.795** | **2.01** | 1.59 |
| H13 | 3 | 0.003175 | 0.20 | 0.09 | 0.002 | 1.17 | 0.98 |
| H14 | 3 | 0.006350 | 0.20 | 0.09 | 0.009 | 1.24 | 0.98 |
| H15 | 3 | 0.012700 | 0.20 | 0.09 | 0.12 | 1.39 | 0.97 |
| H16 | 4 | 0.003175 | 0.20 | 0.09 | 0.002 | 0.89 | 0.94 |
| H17 | 4 | 0.006350 | 0.20 | 0.09 | 0.002 | 0.95 | 0.77 |
| H18 | 4 | 0.012700 | 0.20 | 0.09 | 0.002 | 1.01 | 0.85 |
| H19 | 2 | 0.003175 | 0.30 | 0.15 | 0.099 | **3.47** | **2.37** |
| H20 | 2 | 0.006350 | 0.30 | 0.15 | 0.382 | **2.10** | 1.54 |
| H21 | 2 | 0.012700 | 0.30 | 0.15 | **1.167** | **1.16** | 1.22 |
| H22 | 3 | 0.003175 | 0.30 | 0.15 | 0.002 | **2.84** | **2.20** |
| H23 | 3 | 0.006350 | 0.30 | 0.15 | 0.002 | **2.91** | **2.29** |
| H24 | 3 | 0.012700 | 0.30 | 0.15 | 0.002 | **3.00** | **2.43** |
| H25 | 4 | 0.003175 | 0.30 | 0.15 | 0.002 | **2.31** | 1.86 |
| H26 | 4 | 0.006350 | 0.30 | 0.15 | 0.002 | **2.38** | 1.97 |
| H27 | 4 | 0.012700 | 0.30 | 0.15 | 0.002 | **2.71** | 2.05 |

* Bold font indicates non-acceptable manufacturing solutions for an injection pressure ≥ 0.42 MPa (60 psi) and/or with an associated maximum chamber pressure for attached or detached ≥ 2.07 MPa (300 psi).

pressure remains nearly atmospheric for all cases. For a particular value of part thickness and compression ratio, the minimum injection pressure tends to increase with increase in injection chamber length as observed in Tables 4-7 and 4-8 which is because of the longer distance at which the fiber resin compresses as explained in Section 4.1.1. The corresponding maximum chamber wall pressure tends to increase with an increase of part thickness and decreases with increase of CR values; however, the regular pattern is not seen for low CR values. With all other parameters held at their nominal values, the injection pressure along with the corresponding maximum pressure for both the attached-die and the detached-die configurations as observed in Table 4-7 ($U$ = 0.0254 m/s) and Table 4-8 ($U$ = 0.0508 m/s) are approximately doubled when the pull speed is increased from 0.0254 m/s to 0.508 m/s. However, for those injection pressures that are approximately atmospheric at different combinations of part thickness ($H_D$), injection chamber length ($L_T$), and CR values also remain essentially the atmospheric even when the pull speed is doubled. For all cases, the maximum interior pressure for the detached-die configuration is significantly lower than the corresponding attached-die configuration because of the exit gap (see Fig. 2.1 in Chapter 2) in the detached-die configuration. The un-bolded pressure values lie within the feasible manufacturing pressure range of the resin injection pressure being less than 0.42 MPa (60 psi), and the resin maximum chamber pressure being less than 2.07 MPa (300 psi) simultaneously. Resin pressures not satisfying these constraints are bolded and are considered as unsuitable for commercial pultrusion manufacturing.

Figures 4-50 through 4-55 show the impact of part thickness ($H_D$) on the minimum injection pressure required to achieve complete wetout along with the associated maximum interior chamber wall pressure for chamber lengths ($L_T$) of 0.15 m, 0.20m and 0.30 m of the attached-die and the detached-die configurations. The non-dimensionalized gauge pressure

values ($P/P_o$) taking atmospheric pressure ($P_o$ = 0.1013 MPa) as the reference pressure for minimum injection resin pressure and associated maximum interior chamber wall pressure for both attached-die and detached-die configurations are plotted at different injection chamber length ($L_T$). Figures 4-49, 4-50 and 4-52 are for a pull speed of 0.0254 m/s at CR values 2, 3 and 4 respectively and Figs. 4-53, 4-54 and 4-55 are for a pull speed of 0.0508 m/s at CR values 2, 3 and 4 respectively. The lower horizontal line in the plots corresponds to $P$ = 0.42 MPa and the upper horizontal line in the plots corresponds to $P$ = 2.07 MPa, show the ranges within which the minimum resin injection pressure and the maximum interior chamber wall pressure are acceptable for pultrusion manufacturing. For an acceptable set of parameters for pultrusion manufacturing, the minimum injection pressure to achieve complete wetout must be below the lower horizontal line and simultaneously the maximum chamber wall pressure must be below the upper horizontal line.

From Fig. 4-50 through Fig. 4-55 it can be observed that when the part thickness increases then the injection pressure to achieve complete wetout increases and it decreases with increasing CR values, and for higher CR values the injection pressure values are just above atmospheric gauge pressure. In Fig. 4-50 for CR = 2, the injection pressure for part thickness ($H_D$) of 0.003175 m remains essentially the same in the injection chamber even though the length of the injection chamber ($L_T$) is increased; while for part thickness ($H_D$) of 0.00635 m, the minimum injection pressure remains almost the same for injection chamber lengths except for 0.20 m. The injection pressure for the part thickness ($H_D$) is 0.0127 m is too high to lie in the feasible manufacturing range and the injection pressure increases when the injection chamber length ($L_T$) increases from 0.15 m to 0.20 m and then it decreases when the injection chamber length ($L_T$) is increased from 0.20 m to 0.30 m. In Fig. 4-51 the injection pressures for the part

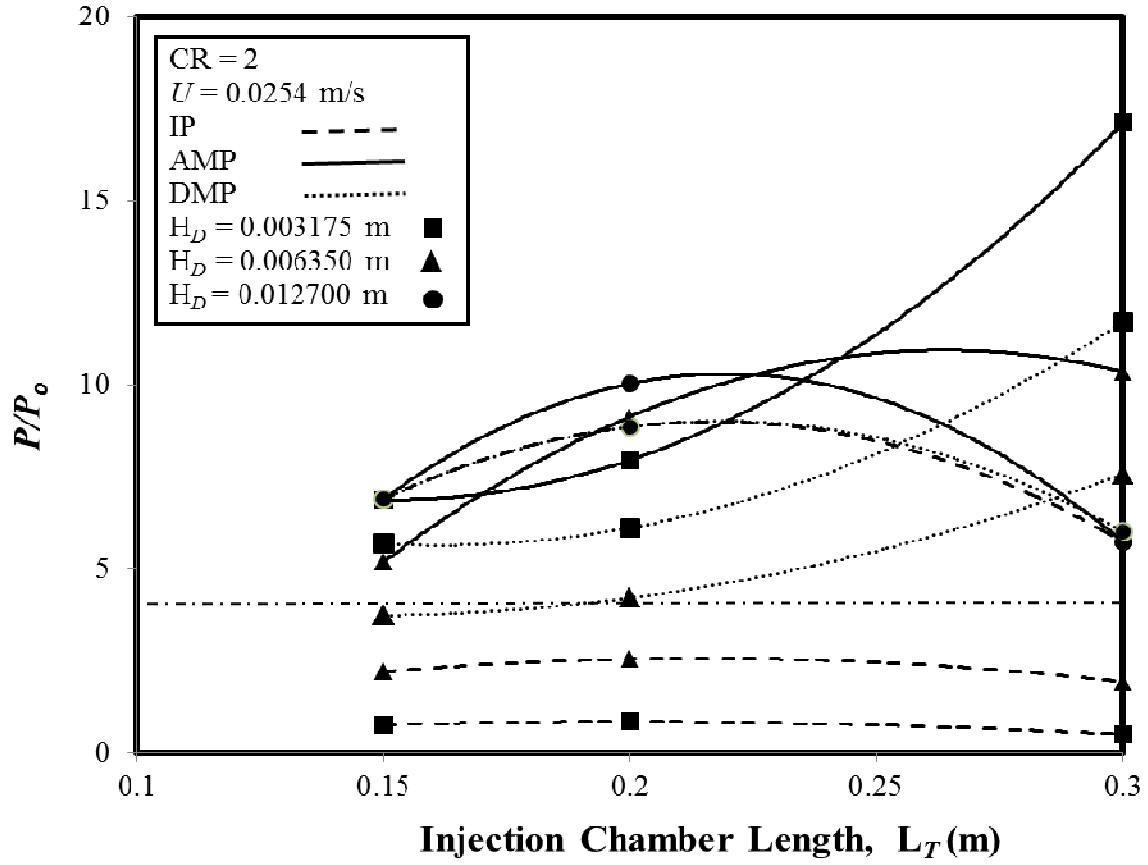


**Figure 4-50. Injection Pressure (IP) and Attached Maximum Pressure (AMP) and Detached Maximum Pressure (DMP) for Different Injection Chamber Lengths at $x_{IS}$ = 0.6 $L_I$, CR = 2, $U$ = 0.0254 m/s, $W_D$ = 0.0635 m, $V_{fo}$ = 0.68, μ = 0.75 Pa·s.**

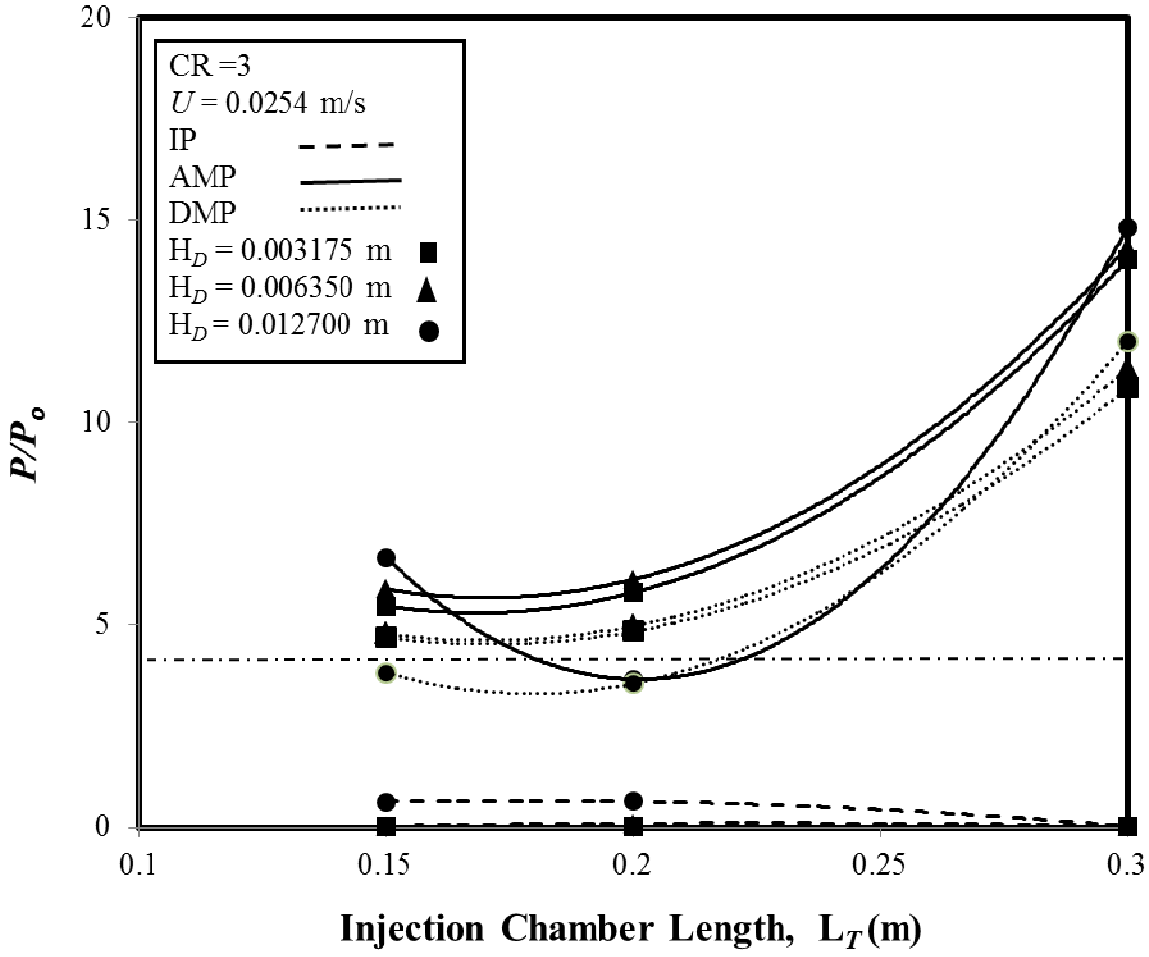


**Figure 4-51. Injection Pressure (IP) and Attached Maximum Pressure (AMP) and Detached Maximum Pressure (DMP) for Different Injection Chamber Lengths at $x_{IS}$ = 0.6 $L_I$, CR = 3, $U$ = 0.0254 m/s, $W_D$ = 0.0635 m, $V_{fo}$ = 0.68, μ = 0.75 Pa·s.**

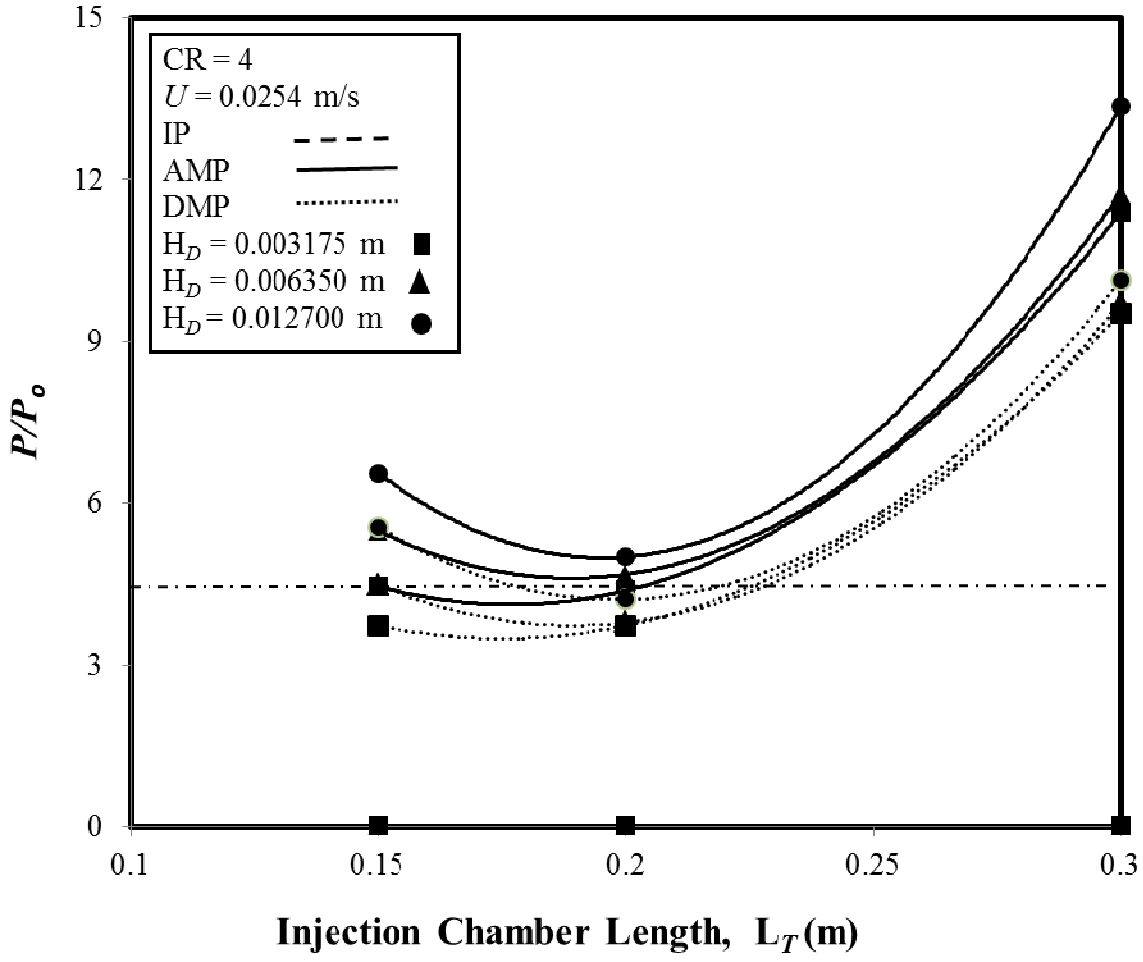


**Figure 4-52. Injection Pressure (IP) and Attached Maximum Pressure (AMP) and Detached Maximum Pressure (DMP) for Different Injection Chamber Lengths at $x_{IS}$ = 0.6 $L_I$, CR = 4, $U$ = 0.0254 m/s, $W_D$ = 0.0635 m, $V_{fo}$ = 0.68, μ = 0.75 Pa·s.**

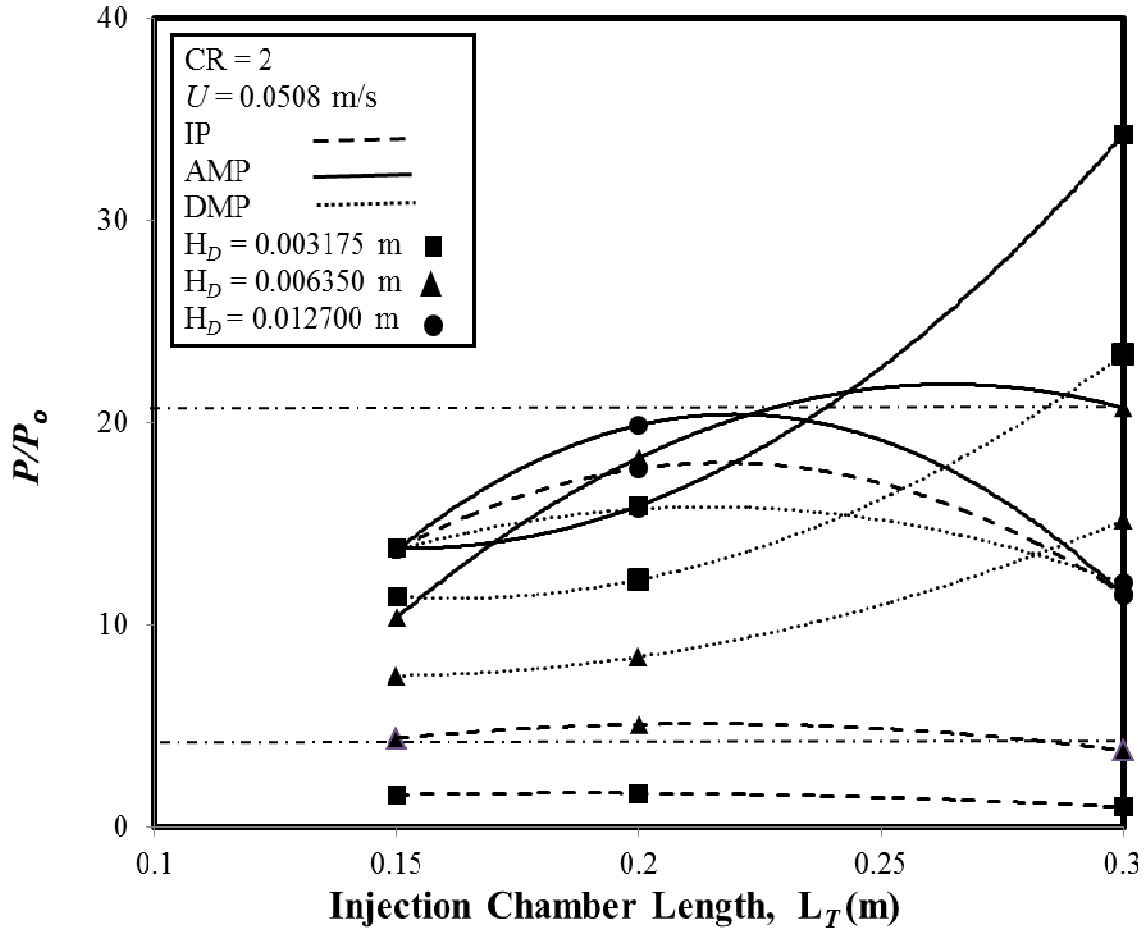


**Figure 4-53. Injection Pressure (IP) and Attached Maximum Pressure (AMP) and Detached Maximum Pressure (DMP) for Different Injection Chamber Lengths at $x_{IS}$ = 0.6 $L_I$, CR = 2, $U$ = 0.0508 m/s, $W_D$ = 0.0635 m, $V_{fo}$ = 0.68, μ = 0.75 Pa·s.**

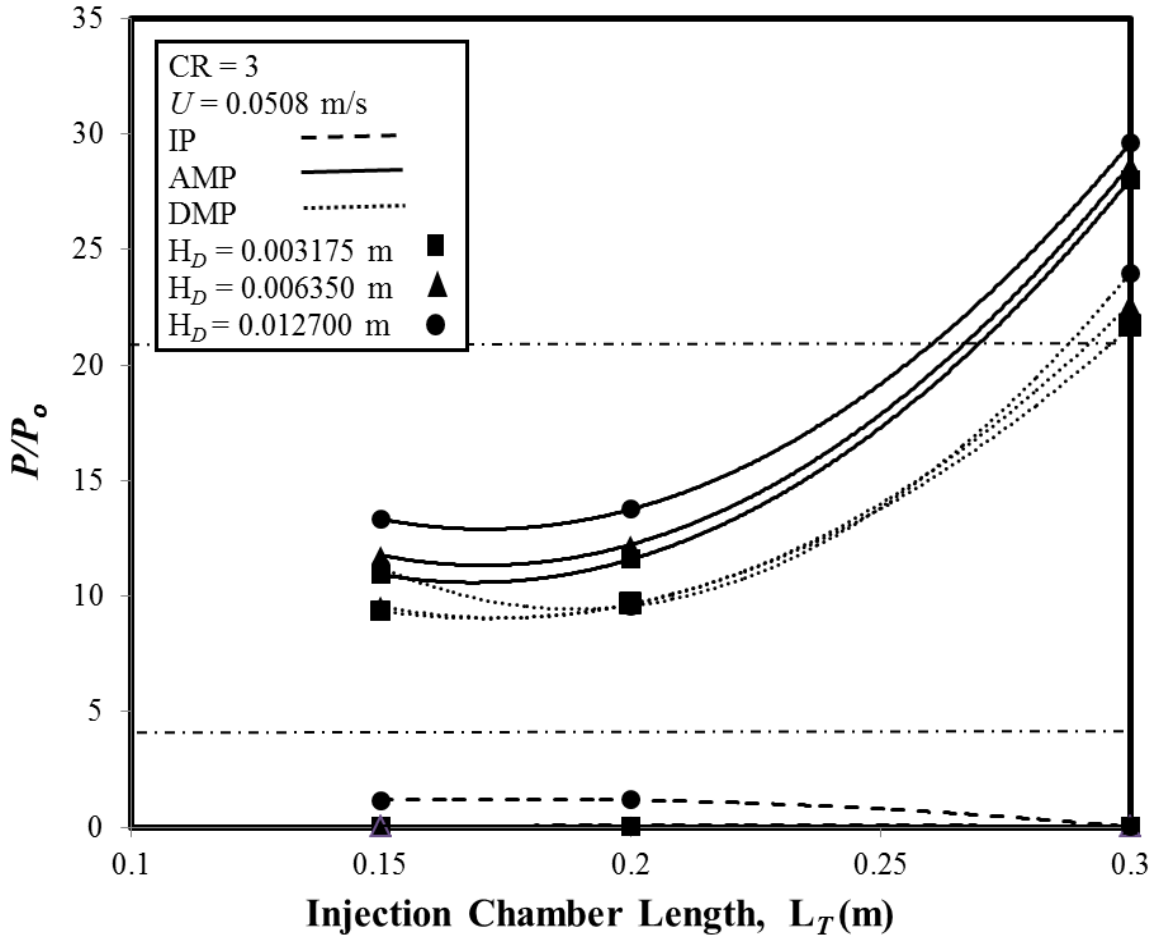


**Figure 4-54. Injection Pressure (IP) and Attached Maximum Pressure (AMP) and Detached Maximum Pressure (DMP) for Different Injection Chamber Lengths at $x_{IS}$ = 0.6 $L_I$, CR = 4, $U$ = 0.0508 m/s, $W_D$ = 0.0635 m, $V_{fo}$ = 0.68, μ = 0.75 Pa·s.**

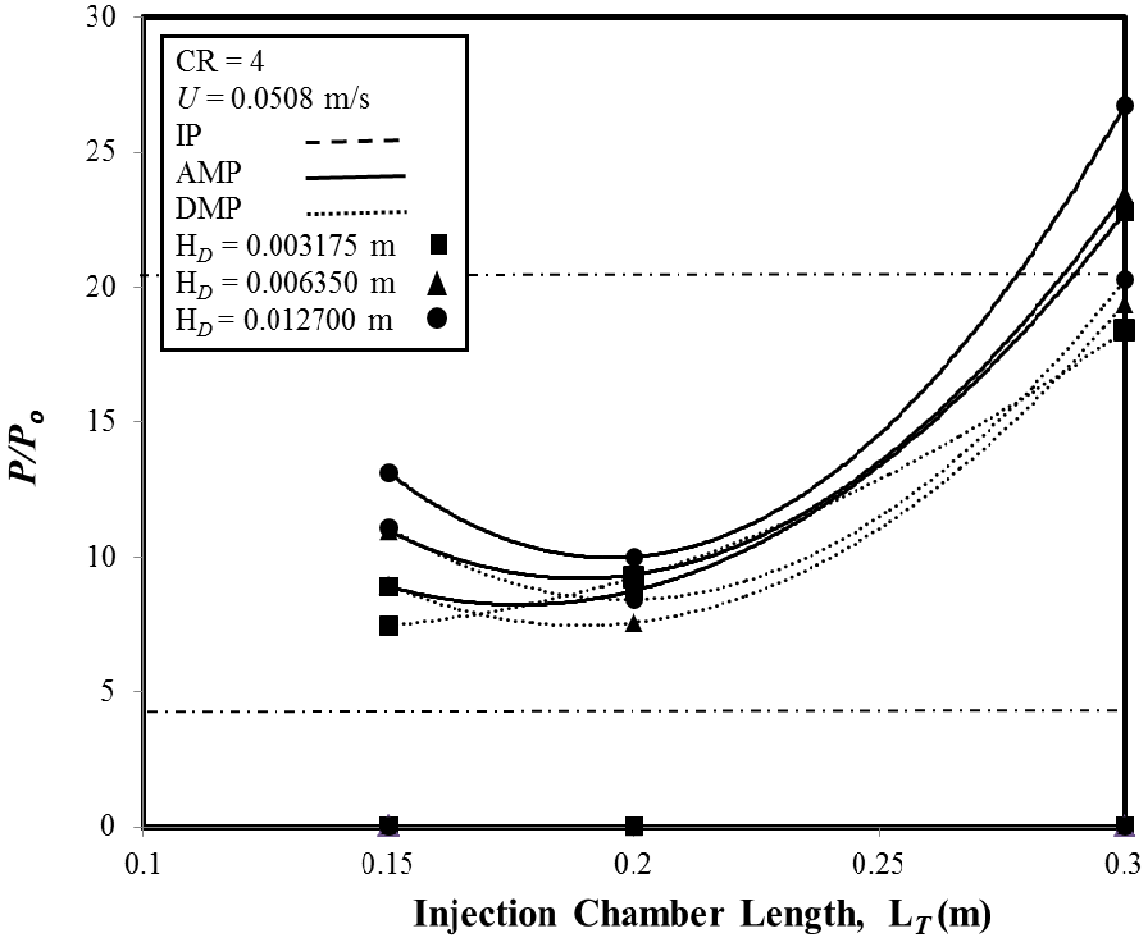


**Figure 4-55. Injection Pressure (IP) and Attached Maximum Pressure (AMP) and Detached Maximum Pressure (DMP) for Different Injection Chamber Lengths at $x_{IS}$ = 0.6 $L_I$, CR =4, $U$ = 0.0508 m/s, $W_D$ = 0.0635 m, $V_{fo}$ = 0.68, μ = 0.75 Pa·s.**

thicknesses ($H_D$) of 0.003175 m and 0.00635 m are essentially atmospheric, while the injection pressure for the part thickness ($H_D$) of 0.0127 m, remains approximately the same when the injection chamber length increases from 0.15 m to 0.20 m and it decreases when the injection chamber length is increased from 0.20 m to 0.30 m.

In Fig. 4-50, for part thickness of 0.003175 m, the maximum chamber wall pressure remains almost the same when the length of the injection chamber ($L_T$) increases from 0.15 m to 0.20 m and then increases when the length of the injection chamber is increased from 0.20 m to 0.30 m; while for part thickness of 0.00635 m, the maximum chamber wall pressure increases when the injection chamber length ($L_T$) is increased. For part thickness of 0.0127 m, as seen in Fig. 4-50, the maximum chamber wall pressures increases when the injection chamber length ($L_T$) is increased from 0.15 m to 0.20 m and it decreases when the injection chamber length ($L_T$) is increased from 0.20 m to 0.30 m. In Fig 4-51, for part thickness ($H_D$) of 0.003175 m and 0.00635 m, the maximum chamber wall pressure for both the attached-die and the detached-die configurations remain almost the same when the length of the injection chamber ($L_T$) increases from 0.15 m to 0.20 m and then increases rapidly when the length of the injection chamber is increased from 0.20 m to 0.30 m. For part thickness of 0.0127 m the maximum chamber wall pressure for the attached-die configuration decreases at $L_T$ = 0.20 m while the maximum chamber wall pressure for the detached-die configuration remains essentially constant until the injection chamber is 0.20 m, then both increase as the length of the injection chamber Length ($L_T$) increases to 0.30 m. In Fig. 4-52, for part thickness ($H_D$) of 0.003175 m, the maximum pressure for both the attached-die and detached-die configurations remain almost constant when the length of the injection chamber ($L_T$) increases from 0.15 m to 0.20 m and then both increase as the length of the injection chamber is increased from 0.20 m to 0.30 m; whereas, for part

thicknesses of 0.00635 m and 0.00127 m, the maximum chamber wall pressures for both the attached-die and detached-die configurations decrease when the injection chamber length ($L_T$) is increased from 0.15 m to 0.20 m and then both increase when the injection chamber length ($L_T$) is increased from 0.20 m to 0.30 m. The injection pressure and maximum chamber wall pressure of both the attached-die and detached-configurations show the same trend-wise behavior even when the speed is doubled from 0.0254 m/s to 0.0508 m/s which can be observed by comparing Figs. 4-50, 4-51, and 4-52 consecutively with Figs. 4-503, 4-54, and 4-55; however, since the pressures are approximately doubled at large chamber lengths ($L_T$), the chamber wall pressure rises into the non-feasible region above the upper horizontal line corresponding to 2.07 MPa.

Figures 4-56, 4-57, and 4-58 ($U$ = 0.0254 m/s) and Figs. 4-59, 4-60, and 4-61 ($U$ = 0.0508 m/s) illustrate the progression of chamber wall resin pressure profiles of both the attached-die and the detached-die configurations along the axial length ($x$) inside the injection chamber for the different part thicknesses ($H_D$ = 0.003175 m, 0.00635 m and 0.0127 m) for the various lengths ($L_T$ = 0.15 m, 0.20 m and 0.30 m) of the injection chamber with CR = 3. For a given part thickness ($H_D$), the chamber wall interior pressure of the attached-die configuration rises at the location of the injection slot and continues to rise and reaches a maximum gauge pressure value within Region II and remains constant till the chamber exit; whereas, for the detached-die configuration the pressure rises to a maximum gauge pressure and then decreases to the zero gauge pressure at the chamber exit gap. This behavior is more discernable at part

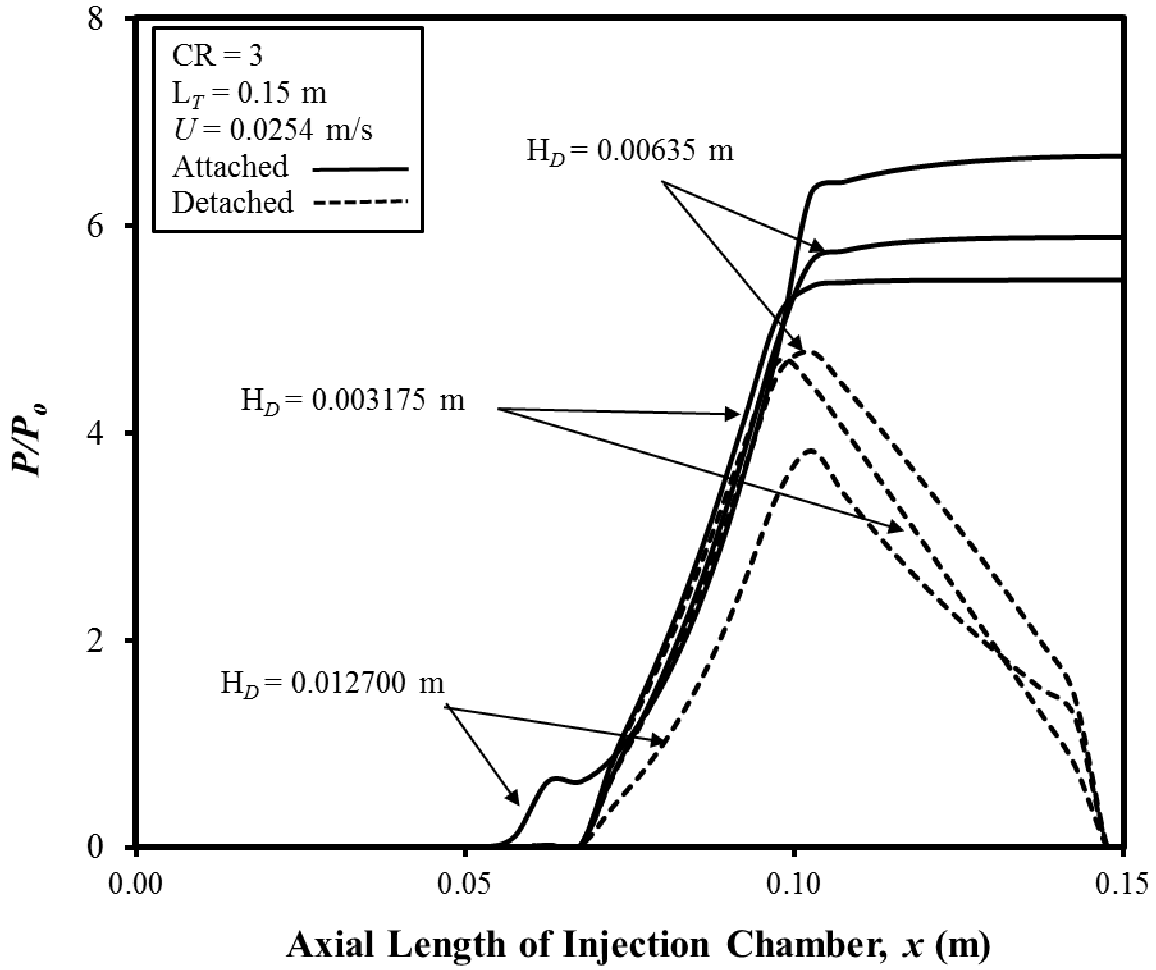


**Figure 4-56. Chamber Wall Axial Pressure Profiles for Attached-Die and Detached-Die Configurations for Injection Chamber Length of $L_T$ = 0.15 m, CR = 3, and $U$ = 0.0254 m/s at Different Part Thicknesses ($H_D$).**

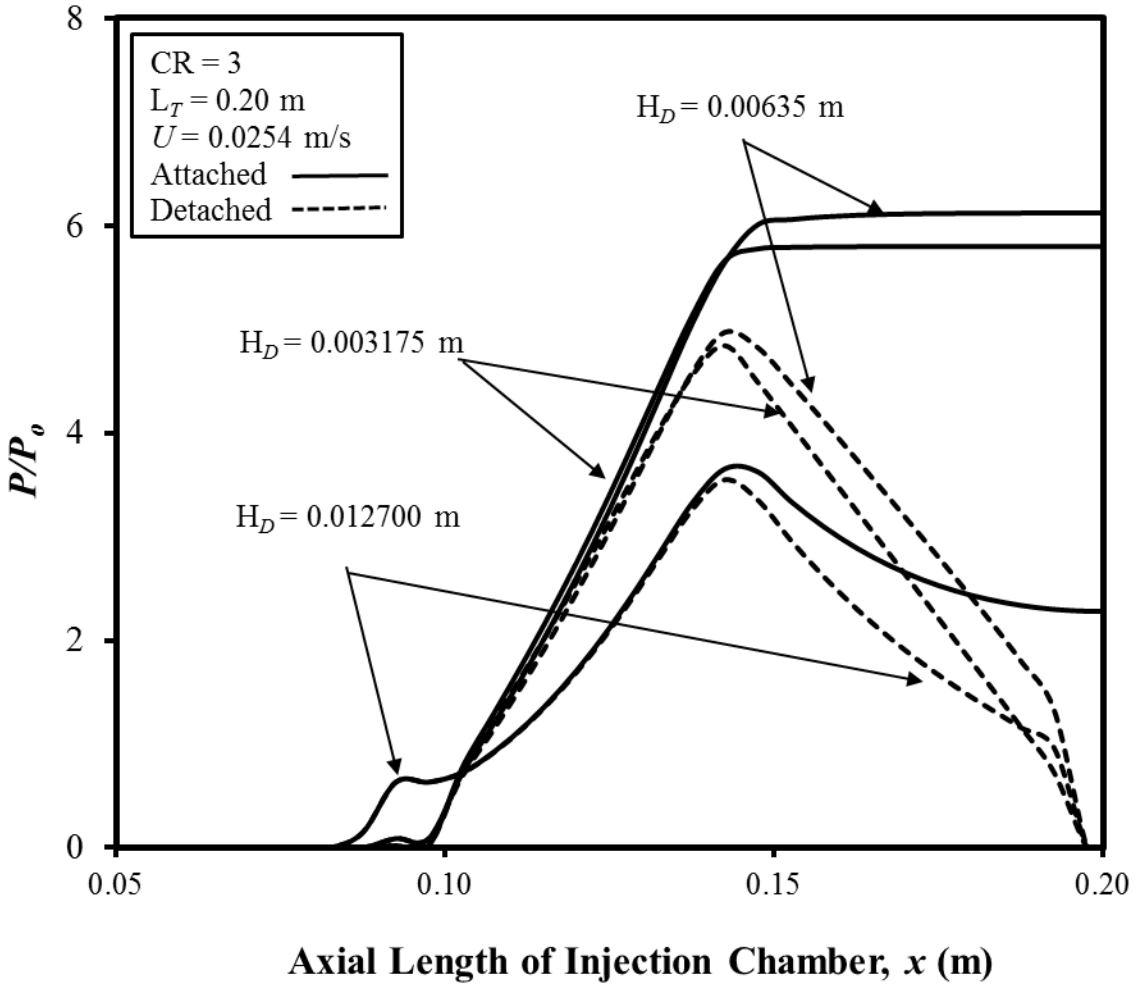


**Figure 4-57. Chamber Wall Axial Pressure Profiles for Attached-Die and Detached-Die Configurations for Injection Chamber Length of $L_T$ = 0.20 m, CR = 3, and $U$ = 0.0254 m/s at Different Part Thicknesses ($H_D$).**

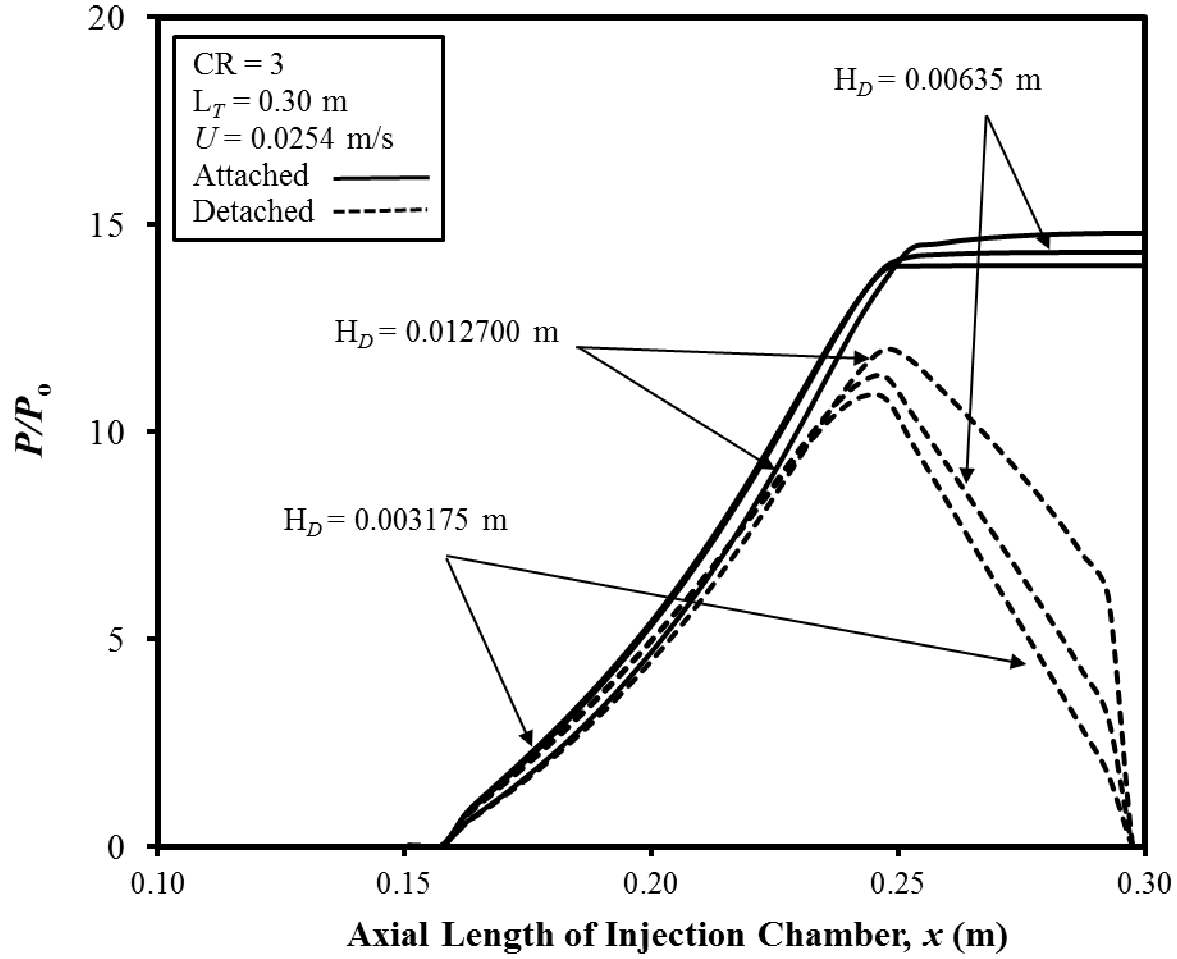


**Figure 4-58. Chamber Wall Axial Pressure Profiles for Attached-Die and Detached-Die Configurations for Injection Chamber Length of $L_T$ = 0.30 m, CR = 3, and $U$ = 0.0254 m/s at Different Part Thicknesses ($H_D$).**

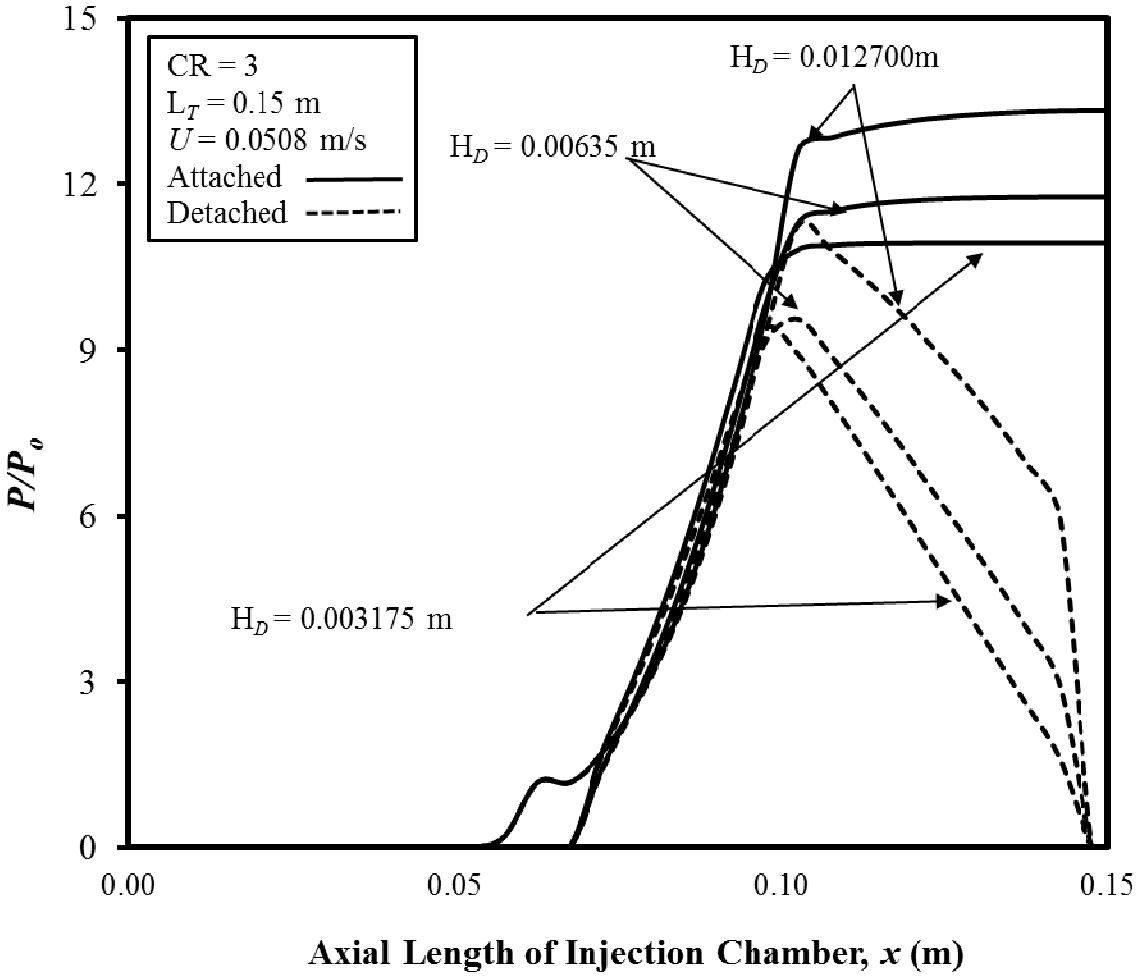


**Figure 4-59. Chamber Wall Axial Pressure Profiles for Attached-Die and Detached-Die Configurations for Injection Chamber Length of $L_T$ = 0.15 m, CR = 3, and $U$ = 0.0508 m/s at Different Part Thicknesses ($H_D$).**

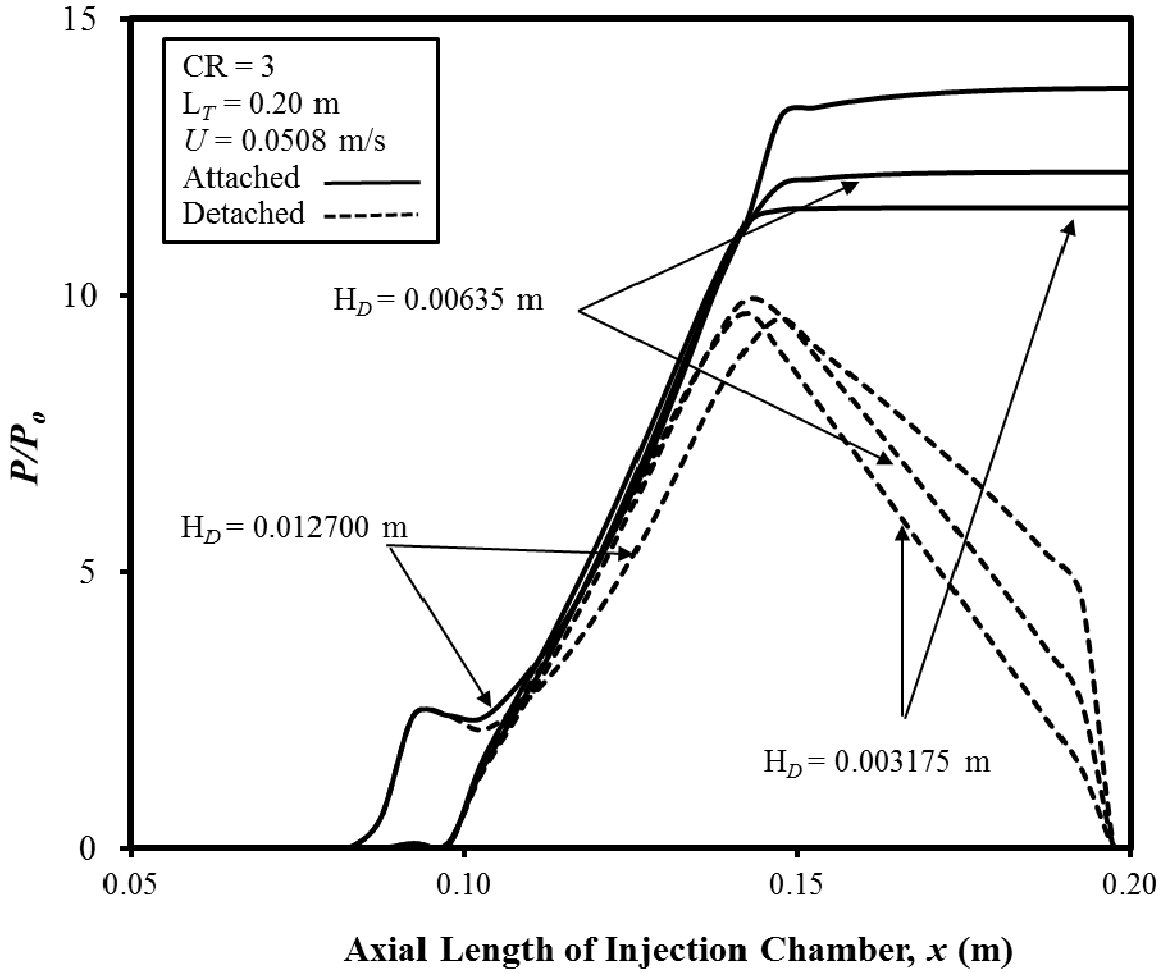


**Figure 4-60. Chamber Wall Axial Pressure Profiles for Attached-Die and Detached-Die Configurations for Injection Chamber Length of $L_T$ = 0.20 m, CR = 3, and $U$ = 0.0508 m/s at Different Part Thicknesses ($H_D$).**

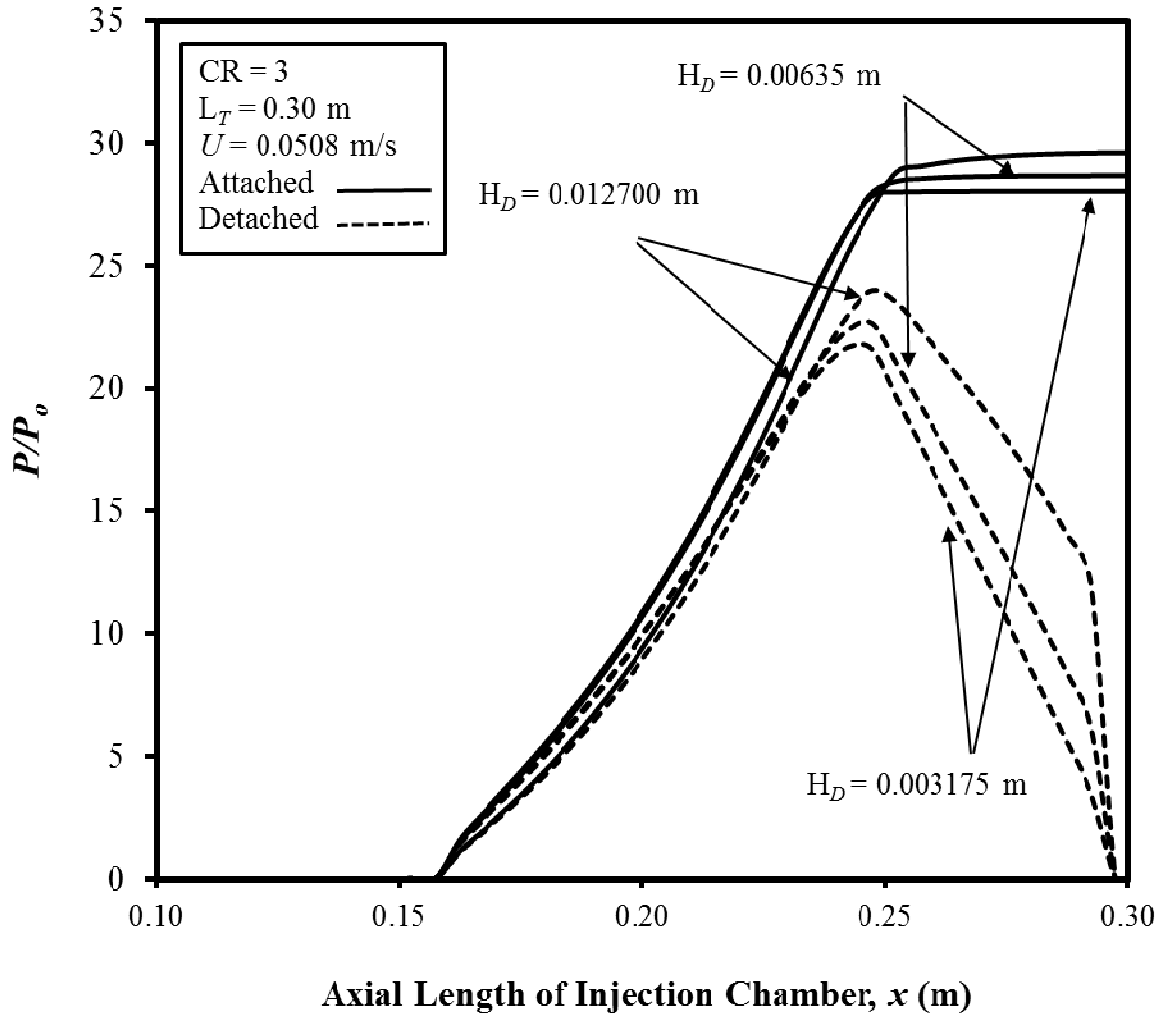


**Figure 4-61. Chamber Wall Axial Pressure Profiles for Attached-Die and Detached-Die Configurations for Injection Chamber Length of $L_T$ = 0.30 m, CR = 3, and $U$ = 0.0508 m/s at Different Part Thicknesses ($H_D$).**

thickness of 0.0127 m. But there is a slight change in behavior for the part thickness of 0.00127 m as observed in Figs. 4-56 ($U$ = 0.0254 m/s) and Fig. 4-59 ($U$ = 0.0508 m/s), in the attached-die configuration, the chamber wall pressure increases to the injection pressure then decreases slightly then again rises to a maximum value and then slightly increases after Region I till the chamber exit. It can be seen from Fig. 4-56 through Fig. 4-58 ($U$ = 0.0254 m/s) and Fig 4-59 through Fig. 4-61 ($U$ = 0.0508 m/s) that the chamber wall pressure has the same trend-like behavior when the pull speed is increased from 0.0254 m/s to 0.0508 m/s, but the maximum pressure is observed to be significantly increased when the pull speed is doubled.

Figures 4-62 shows the steady-state liquid resin flow front and gauge isopressure contours within the liquid resin wetout region for $L_T$ = 0.20 m at CR = 3 with the injection slot location ($x_{IS}$) at 0.60 $L_I$ and pull a speed of 0.0254 m/s for part thickness $H_D$ = 0.0127 m. Figures 4-63 through 4-65 show the steady-state liquid resin flow front and gauge isopressure contours within the liquid resin wetout region at CR = 4 with the injection slot location at 0.60 $L_I$ and pull a speed of0.0254 m/s for $L_T$ = 0.15 m for different part thicknesses $H_D$ = 0.003175 m (Fig. 4-63), $H_D$ = 0.00635 m (Fig. 4-64) and $H_D$ = 0.0.0127 m (Fig. 4-65). Figure 4-66 shows the liquid resin flow front and gauge isopressure contours at $L_T$ = 0.30 m for part thickness $H_D$ = 0.00635 m with all other parameter at their nominal values. The first dark contour represents the liquid resin flow front and the thin contour lines represent the isopressure contours in kPa. Figures 4-61 through 4-66 are not displayed to scale; this was done in order to make the results more viewable and comprehensible.

The resin flow front and the pressure values for the attached-die and the detached-die configurations can be compared from these figures. The chamber pressure values are always lower for the detached-die configuration system as compared to the attached-die configuration

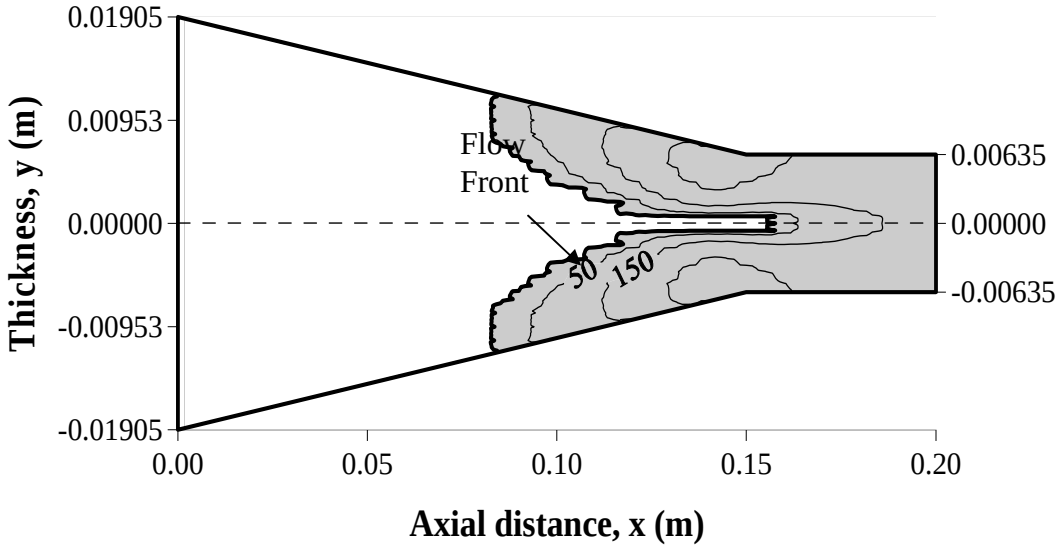


**a. Attached-Die Configuration**

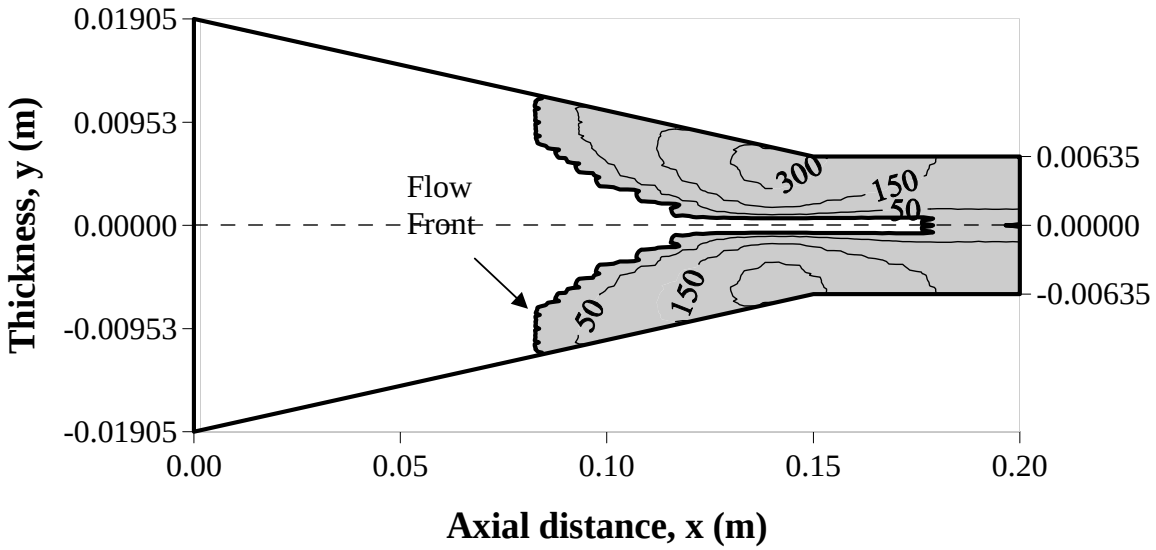


**b. Detached-Die configuration**

**Figure 4-62. Flow Front Profile and Gauge Isopresure (kPa) Contours for Case G15, Table 4-7 for $L_T$ = 0.20 m, $x_{IS}$ = 0.60 $L_I$, CR = 3, $V_{fo}$ = 0.68, μ = 0.75 Pa·s with $U$ = 0.0254 m/s and $H_D$ = 0.0127 m (Not to Scale).**

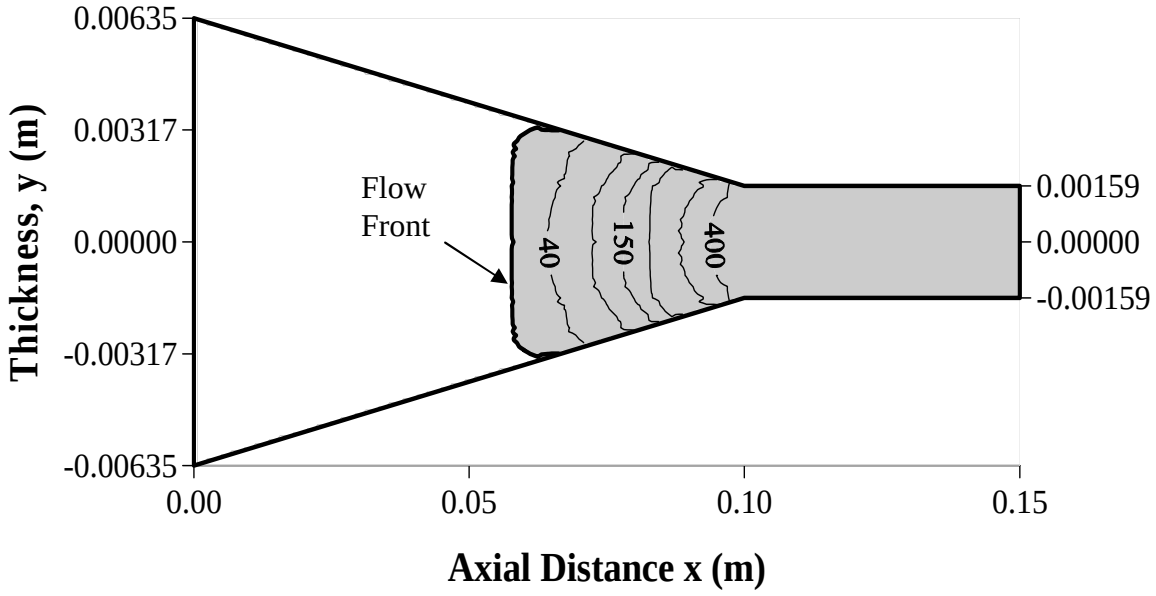


**a. Attached-Die Configuration**

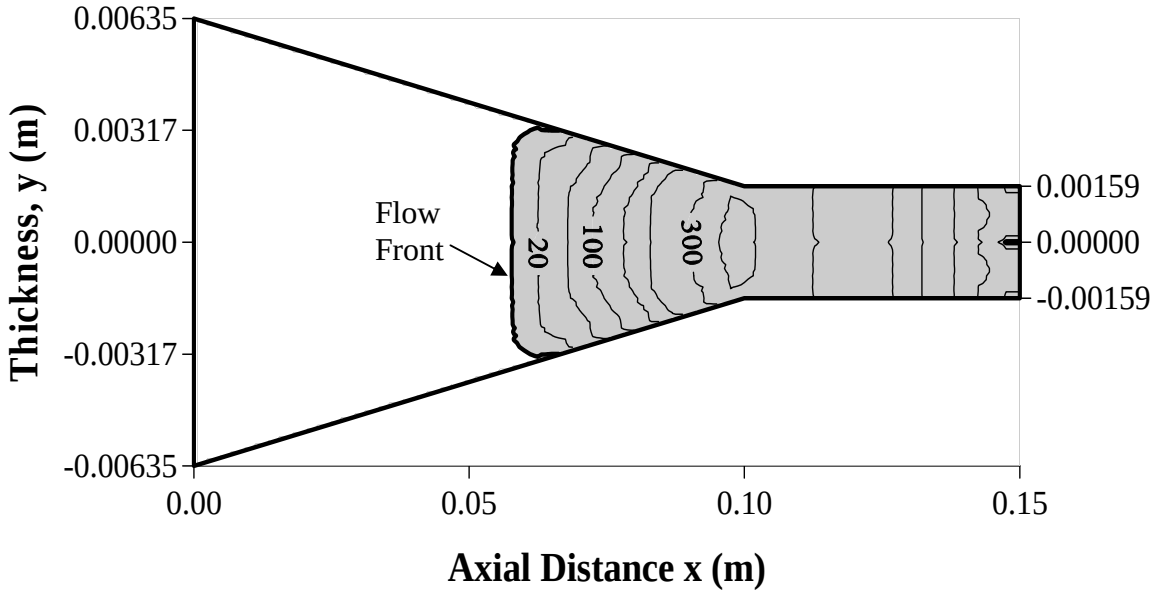


**b. Detached-Die configuration**

**Figure 4-63. Flow Front Profile and Gauge Isopresure (kPa) Contours for Case G7, Table 4-7 for $L_T$ = 0.15 m, $x_{IS}$ = 0.60 $L_I$, CR = 4, $V_{fo}$ = 0.68, μ = 0.75 Pa·s with $U$ = 0.0254 m/s and $H_D$ = 0.003175 m (Not to Scale).**

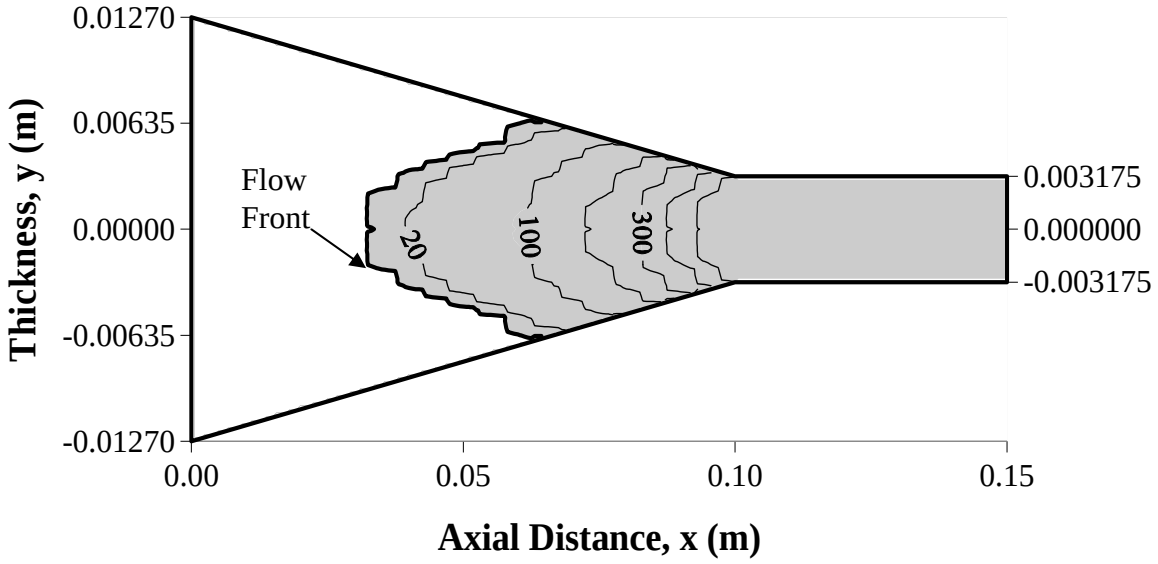


**a. Attached Die Configuration**

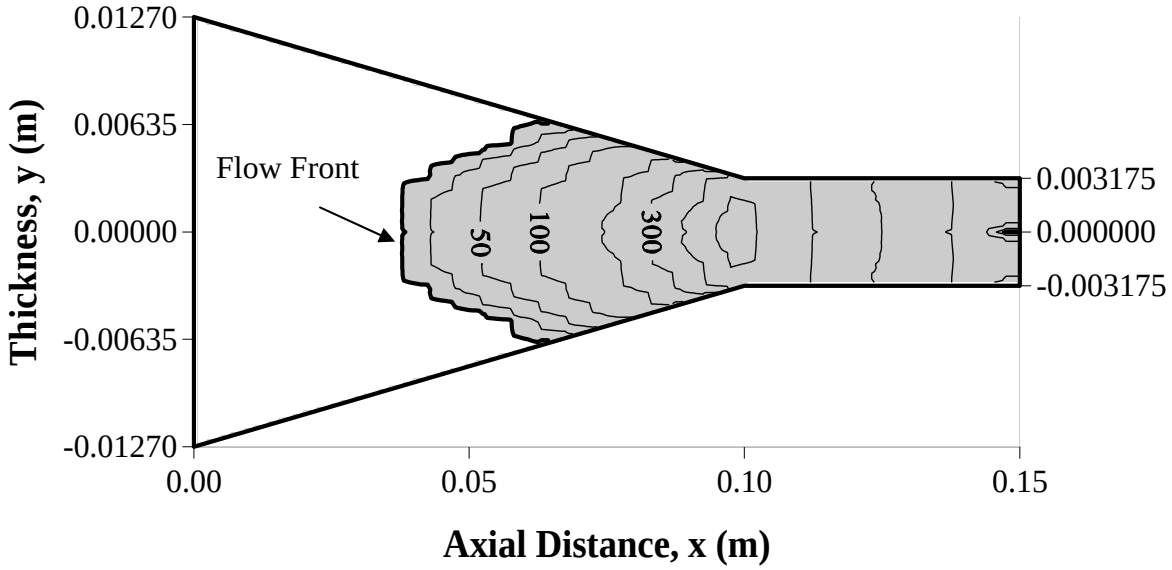


**b. Detached Die Configuration**

**Figure 4-64. Flow Front Profile and Gauge Isopresure (kPa) Contours for Case G8, Table 4-7 for $L_T$ = 0.15 m, $x_{IS}$ = 0.60 $L_I$, CR = 4, $V_{fo}$ = 0.68, μ = 0.75 Pa·s with $U$ = 0.0254 m/s and $H_D$ = 0.006315 m (Not to Scale).**

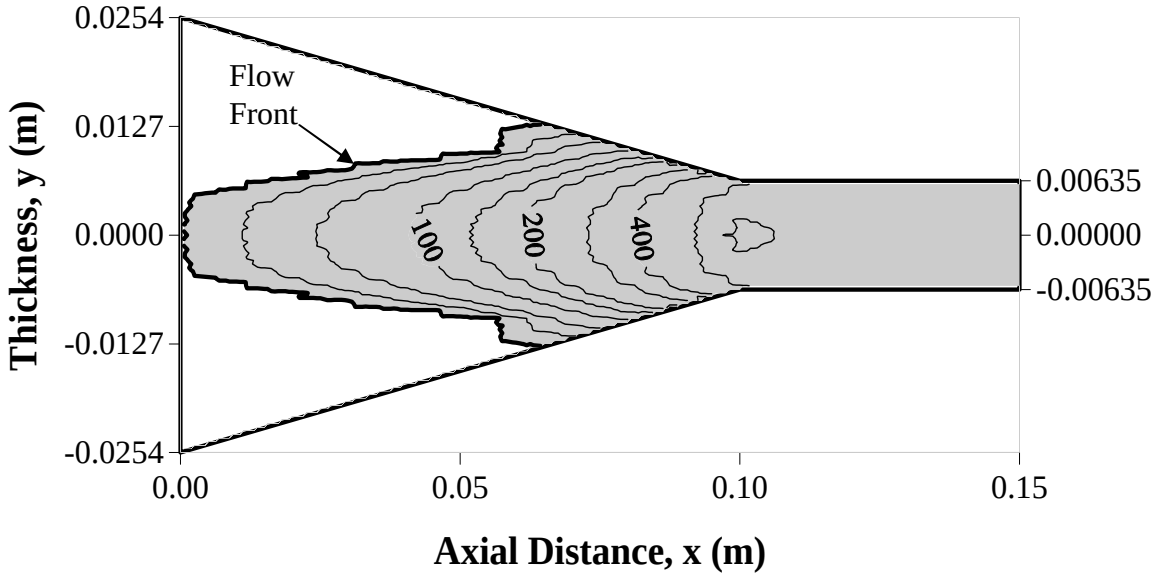


**a. Attached Die Configuration**

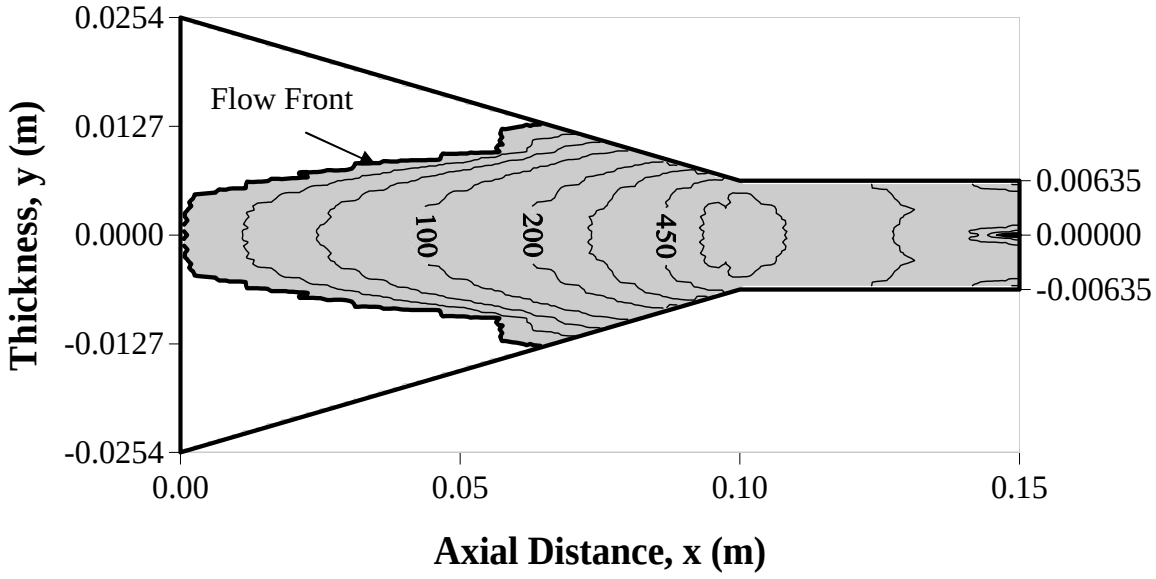


**b. Detached Die Configuration**

**Figure 4-65. Flow Front Profile and Gauge Isopresure (kPa) Contours for Case G9, Table 4-7 for $L_T$ = 0.15 m, $x_{IS}$ = 0.60 $L_I$, CR = 4, $V_{fo}$ = 0.68, μ = 0.75 Pa·s with $U$ = 0.0254 m/s and $H_D$ = 0.0127 m (Not to Scale).**

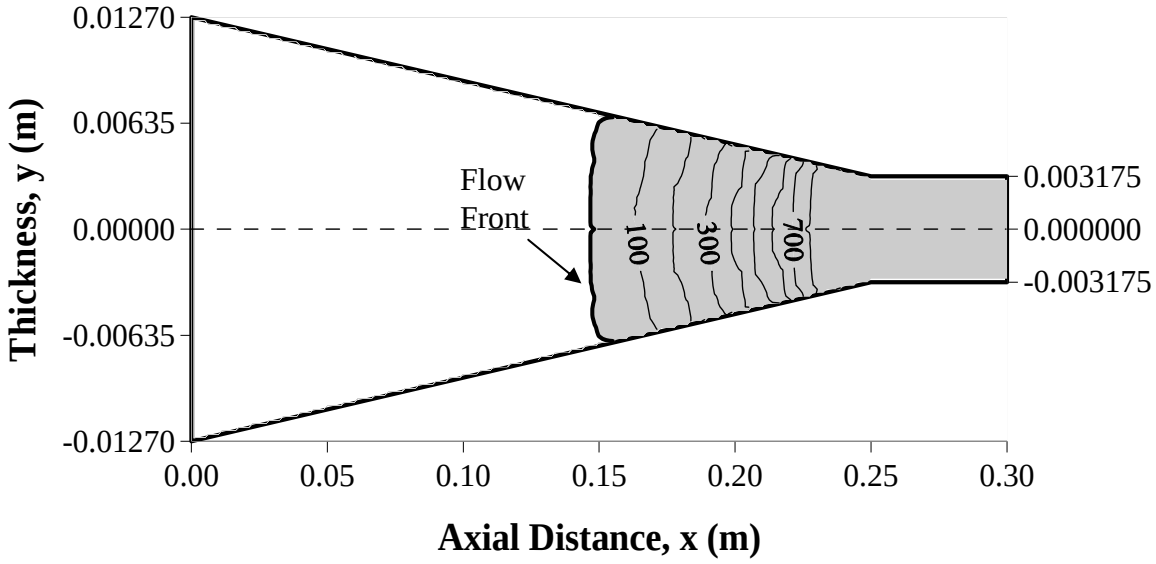


**a. Attached Die Configuration**

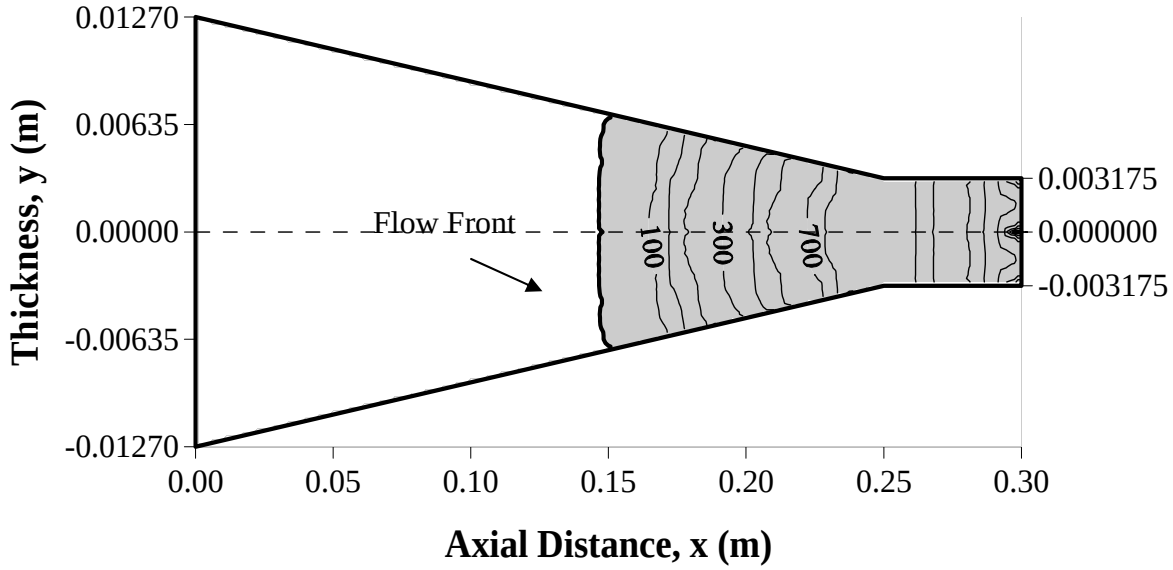


**b. Detached Die Configuration**

**Figure 4-66. Flow Front Profile and Gauge Isopresure (kPa) Contours for Case G26, Table 4-7 for $L_T$ = 0.30 m, $x_{IS}$ = 0.60 $L_I$, CR = 4, $V_{fo}$ = 0.68, μ = 0.75 Pa·s with $U$ = 0.0254 m/s and $H_D$ = 0.00635 m (Not to Scale).**

which can be observed from Figs. 4-62 through 4-66. In the detached–die configuration, the isopressure contours can be seen in Region II of the injection chamber due to the decreasing chamber pressure in the Region II and this pressure corresponds to the same pressure contours as depicted in Region I of the injection chamber. In Fig 4-63 the injection slot is slightly viewable while it is not viewable in other figures.

# CHAPTER 5

# CONCLUSION

This work investigates and compares the impact of compression ratios and injection chamber lengths on minimum resin injection pressure needed to achieve complete wetout and the associated maximum interior chamber wall pressure and to predict the liquid resin flow front location for both the attached-die and detached-die configurations for various geometric design parameters such as location of the injection slot, width of the injection slot, location of multiple injection slots, and part thickness. A 3-D finite volume model was employed to simulate the flow of liquid resin through the fiber reinforcement in the resin injection pultrusion process. The CR values considered for this work are 2, 3 and 4; whereas, the injection chamber lengths considered for this work are 0.15 m, 0.20 m and 0.30 m. The processing parameters are held at nominal values which are $V_{fo}$ = 0.68, μ = 0.75 Pa·s, $\Delta x$ = 0.01 m, $W_D$ = 0.0635 m, $H_D$ = 0.00635 m, and $U$ = 0.0254 m/s or 0.0508 m/s. From the results obtained the acceptable manufacturing criteria for pultrusion process are set as an injection pressure not greater than 60 psi (0.414 MPa), and the maximum interior chamber wall pressure less than 300 psi (2.07 MPa).

Following are the key conclusions made with respect to various geometric parameters:

## A. Axial Location of the Single Injection Slot

- Finding (Tables 4-1 and 4-2) show there are fewer number of unacceptable solutions when the for the pull speed of 0.0254 m/s as compared with the pull speed of 0.0508 m/s. Most

of the unfeasible solutions are obtained for CR = 2 and when the length of the injection chamber length ($L_T$) is 0.03 m.

- The minimum injection pressure required to achieve complete wetout for both the attached-die and the detached-die configurations remains approximately the same for the same proportional location of the injection slot ($x_{IS}$) at different injection chamber lengths ($L_T$) and it (injection pressure) decreases with an increase in CR value; whereas, the associated maximum interior chamber wall pressure increases with an increase in the length of the injection chamber and decreases with the increase in CR value. Similarly, the minimum injection pressure required to achieve complete wetout for both the attached-die and the detached-die configurations increases when the injection slot is moved downstream into the injection chamber; however, the corresponding maximum interior pressure decreases.
- When the pull speed is doubled almost all minimum injection pressures are doubled except for those which are essentially atmospheric. Likewise, the corresponding maximum interior chamber wall pressure for both the attached-die and detached-die configurations are also doubled when the pull speed is doubled.

**B. Width of the Injection Slot**

- Results (Tables 4-3 and 4-4) show that the minimum injection pressure for complete wetout for both the attached-die and detached-die configurations decrease with the increase in the slot width ($\Delta x$). Similarly, the corresponding maximum interior chamber wall pressure decreases with an increase in the slot width ($\Delta x$); however, at higher CR values the maximum interior chamber wall pressure is not the function of slot width ($\Delta x$) since the maximum pressures are approximately the same for all slot width ($\Delta x$).

- For a particular slot width ($\Delta x$), the minimum injection pressure for complete wetout for both the attached-die and detached-die configurations remains the same with an increase of injection chamber length. However, the maximum the corresponding maximum chamber pressure increases with an increase in the injection chamber length ($L_T$).

**C. Multiple Injection Slots and Axial Locations**

- From the results (Tables 4-5 and 4-6) it is clear that for the "multiple injection slot configuration" the minimum injection pressures required to achieve complete wetout are essentially half of the minimum injection pressures for the "single injection slot configuration". The corresponding maximum pressures for both the attached-die and detached-die configurations are lower than the "single injection slot configuration" at the same percentage location of the various injection chamber lengths.

**D. Final Composite Thickness**

- Results (Tables 4-7 and 4-8), show that both the minimum injection pressure required to achieve complete wetout of fiber reinforcement for both the attached-die and detached-die configurations and the corresponding maximum interior chamber wall pressure increases with an increase in the part thickness ($H_D$).
- For the particular part thickness ($H_D$), the minimum injection pressure required to achieve complete wetout of the fiber reinforcement for both the attached-die and detached-die configurations almost remains the same; whereas, the corresponding maximum interior chamber wall pressure increases with an increase in the injection chamber lengths.

Finally, from the results obtained from the simulation model, the overall conclusion is that in the pultrusion process the injection chamber length and the compression ratio both have significant impacts in the minimum injection pressure

required to achieve complete wetout of the fiber reinforcement and the associated maximum interior chamber wall pressure of both the attached-die and detached-die configurations. In general, it is clear that higher CR values at shorter injection chamber lengths ($L_T$) provide more favorable solutions for the pultrusion manufacturing process. The detached-die configuration is better than attached-die configuration since the maximum interior chamber wall pressure is lower in the detached-die configuration. The multiple injection slots configuration is better than the single injection slot configuration, and the part thickness ($H_D$) should not be high for more feasible manufacturing solutions in the pultrusion process.

# REFERENCES

1. Lackey, E., Vaughan, J.G., and Roux, J.A., "Experimental Development and Evaluation of a Resin Injection System for Pultrusion," *Journal of Advanced Materials*, 1997: 29, pp. 30-37.
2. Roux, J.A., Sharma, D. McCarty, T.A., Vaughan, J.G., "Investigation of Dynamic Behavior in a Pultrusion Die," *Journal of Composite Materials*, Vol. 32, No. 10, July 1998, pp. 929-950.
3. Rahatekar, S.S., and Roux, J.A., "Numerical Simulation of Pressure Variation and Resin Flow in Injection Pultrusion," *Journal of Composites Materials*, Vol. 37; 12:2003, pp. 1067-1082.
4. Jeswani, J.L., and Roux, J.A., "Numerical Modeling of Design Parameters for Manufacturing Polyster/Glass Composites by Resin Injection Pultrusion," *Polymers and Polymer Composites,* Vol. 14, No. 7, 2006, pp. 651-669.
5. Ranga, B.K., *Impact of Chamber Length on Performance of Tapered Resin Injection Pultrusion*, Masters Thesis, University of Mississippi; August 2009.
6. Mitlapalli, R., Roux, J.A. "Chamber Length and Injection Slot Location and Multiple Slot for Tapered Resin Injection Pultrusion," *Journal of Porous Media*, Vol.14, No. 1, 2011; pp. xv-vx.
7. Srinivasagupta, D., and Kardos, J.L., "Rigorous Dynamic Model-based Economic Design of the Injected Pultrusion Process with Controllability Considerations," *Journal of Composite Materials*, Vol. 37, No. 20; 2003, pp. 1851-1888.
8. Srinivasagupta, D., Potaraju, S., Kardos, J.L., and Joseph, B., "Steady State and Dynamic Analysis of a Bench-Scale Injected Pultrusion Process," *Composites Part A: Applied Science and Manufacturing*, Vol. 34; 2003, pp. 835-846.

9. Dube, M. G., Batch, G. L., Vogel, J. H., and Mocosko, C. W., "Reaction Injection Pultrusion of Thermoplastic and Thermoset Composites," *Polymer Composites*, 1995; 16:378-85.
10. Li, S., Xu, L., Ding, Z., and Lee, L.J., "Experimental and Theoretical Analysis of Pulling Force in Pultrusion and Resin Injection Pultrusion (RIP) – Part I: Experimental," *Journal of Composite Materials,* Vol. 37; No.3; 2003, pp. 163-189.
11. Li, S., Xu, L., Ding, Z., and Lee, L.J., "Experimental and Theoretical Analysis of Pulling Force in Pultrusion and Resin Injection Pultrusion (RIP) – Part II: Modeling and Simulation," *Journal of Composite Materials,* Vol. 37; No.3; 2003, pp. 195-216.
12. Mustafa, I., Khomami, B., and Kardos, J.L., "3-D Nonisothermal Flow Simulation Model for Injected Pultrusion Processes," *AIChE journal,* Vol. 45, No.1; 1999, pp. 151-163.
13. Kommu, S., Khomami, B., Kardos, J. L., "Modeling of Injection Pultrusion Processes: A Numerical Approach," *Polymer Composites*, 19: 1998; pp. 335-46.
14. Liu, X.L., "A Finite Element/Nodal Volume Technique for Flow Simulation of Injection Pultrusion," *Composites: Part A,* 34 (2003), pp. 649-661.
15. Liu, X.L., "Iterative and Transient Numerical Models for Flow Simulation of Injection Pultrusion," *Composite Structures:* 66; 1-4, 2003, pp. 175-181.
16. Darcy, H. 1856. *Les fontains publique de la ville de Dijon*. Paris: Dalmont.
17. Gutowski, Tg. Cai, A., Bauer, S., Boucher, D., Kingery, J., and wineman, S., 1987, 'Consolidation experiment for Laminate Composites,' *Journal of Caomposite Materials*, Vol. 21, pp. 650-669
18. Patankar, S. 1980, *Numerical Heat Transfer and Fluid Flow*, Hemisphere Publishing Corporation, New York

## LIST OF APPENDICES

**APPENDIA: A**

## Manual For Creating MS Excel Graphs

This appendix explains how to produce the EXCEL graphs using output files (CL AND DIE WALL PRESSURE.DAT):

1. Open the Microsoft Excel 2003.
2. Click File > Open.
3. In the Open dialog box select the appropriate output file.
4. A wizard opens which will import text to excel format.
5. From Menu-bar select Insert > Chart
6. From chart wizard, select the XY scatter with smooth lines graph.
7. Chart area is displayed on Excel sheet.
8. Click to the right of Data Range from the dialog box.
9. Select the required data from the Excel Sheet.
10. Click Add tab to get Edit series box.
11. Select the X values and Y values from the work sheet and give the series name.
12. Make necessary changes in the graph.
13. Label the parameters (processing/design) with suitable font format.
14. The graph should have the specifications approximately equal to height = 5.37 inch and width = 6.43 inch.

**APPENDIX: B**

## Manual For Creating Surfer Plots

Procedure on how to produce SURFER plots using the output file (PRESSURE.DAT):

1. Open a notepad and enter the required number of nodes and save as BLN file.
2. Open the Golden software which opens to SURFER. Click on it, a dialogue box opens a new plot.
3. Create the base map by selecting Map > Load base Map. Select the BLN file and say Ok. Boundary file is visible in the graphic area but with different scale.
4. Edit > Select All and Map > Scale and then input the scale as 6 and y as 3. By unchecking the proportional XY scale.
5. Edit Base Map for required scaling and format
6. Select Grid > Data > File Name > Ok.
7. A Scattered Data Interpolation dialogue box is shown. Enter the required number of lines in X and Y as 241 and 121 respectively.
8. Enter the For Gridding method, select Krigging, click Options and enter the values of radius 1 as 0.1and radius 2 as 0.001 and scale to 210000.
9. After clicking Ok a Grid file is created.
10. Grid > Blank>Grid file from last step and in next dialogue box select the BLN file. Anew Grid file is created.
11. Map > Contour > select appropriate Grid file (last step) and select proper options for Contour Map. A plot is created.
12. To overlay both the Contour and Boundary file, go to Edit >Select all > Map > Overlay Maps, then both maps are overlayed.
13. Change Scale by going to Map > Scale and input scale as earlier.

14. Select Base Map > Click on line to the left and select Line Attributes from Draw. Input proper options. A boundary is created.
15. For editing contours and flow front Map > Edit Overlays > Contours > Edit
16. Edit by selecting appropriate values until you get the fine plot.

# VITA

Sudip Ranjit, son of Mr. Hari Chandra Das Ranjit and Mrs. Gyani Maiya Ranjit, was born in Kathmandu, Nepal. He completed Bachelor in Mechanical Engineering in March 2008 from Institute of Engineering, Tribhuvan University, Nepal. He earned Master of Science in Mechanical Engineering from The University of Mississippi in July 2012. During his graduate studies, from August 2010 to May 2012, he worked as a Graduate Assistant of Professor Dr. Jeffery A. Roux